Modelling and Autoresonant Control Design of Ultrasonically Assisted Drilling Applications

by

Xuan Li

A Doctoral Thesis

Submitted in partial fulfilment of the requirements for the award of Doctor of Philosophy of Loughborough University

2014

Abstract

The target of the research is to employ the autoresonant control technique in order to maintain the nonlinear oscillation mode at resonance (i.e. ultrasonic vibration at the tip of a drill bit at a constant level) during vibro-impact process. Numerical simulations and experiments have been executed. A simplified Matlab-Simulink model which simulates the ultrasonically assisted machining process consists of two parts. The first part represents an ultrasonic transducer that contains a piezoelectric transducer and a 2-step concentrator (waveguide). The second part reflects the applied load to the ultrasonic transducer due to the vibro-impact process. Parameters of the numerical models have been established based on experimental measurements and the model validity has been confirmed through experiments performed on an electromechanical ultrasonic transducer. The model of the ultrasonic transducer together with the model of the applied load was supplemented with a model of the autoresonant control system. The autoresonant control intends to provide the possibility of self-tuning and self-adaptation mechanism for an ultrasonic transducer to maintain its resonant regime of oscillations automatically by means of positive feedback. This is done through a 'signal to be controlled' (please refer to Figure 7.2 and Figure 7.3) transformation and amplification. In order to examine the effectiveness and the efficiency of the autoresonant control system, three control strategies have been employed depending on the attributes of the 'signals to be controlled'. Mechanical feedback control uses a displacement signal at the end of the 2nd step of the ultrasonic transducer. The other two control strategies are current feedback control and power feedback control. Current feedback control employs the electrical current flowing through the piezoceramic rings (piezoelectric transducer) as the 'signal to be controlled' while power feedback control takes into account both the electrical current and the power of the ultrasonic transducer. Comparison of the results of the ultrasonic vibrating system excitation with different control strategies is presented. It should be noted that during numerical simulation the tool effect is not considered due to the complexity of a drill bit creates during the Ultrasonically Assisted Drilling (UAD) process. An effective autoresonant control system was developed and manufactured for machining experiments. Experiments on Ultrasonically Assisted Drilling (UAD) have been performed to validate and compare with the numerical results. Two sizes of drill bits with diameters 3mm and 6mm were applied in combination with three autoresonant control strategies. These were executed during drilling aluminium alloys with one fixed rotational speed associated with several different feed rates. Vibration levels, control efforts, feed force reduction were monitored during experiments. Holes quality and surface finish examinations supplement analysis of the autoresonant control results. In addition, another interesting research on the investigation of the universal matchbox (transformer) has been carried out. Introducing a varying air gap between two ferrite cores allows the optimization of the ultrasonic vibrating system, in terms of the vibration level, effective matchbox inductance, voltage and current level, phase difference between voltage and current, supplied active power etc (more details please refer to Appendix I).

Keywords: Ultrasonically Assisted Drilling (UAD), vibration control, modelling of ultrasonic transducer, autoresonant control, phase control, vibro-impact, filter design, optimization.

Acknowledgement

I would like to take this opportunity to thank my supervisor Prof. Vladimir Babitsky for his continuous support and guidance through my PhD research for 3 years. His insightful suggestions always helped me walk out of the darkness. He not only supervised me in the detailed work but also remind me to stand at a different angle and observe the whole picture of the general problem which is of great importance. It was a great pleasure for me to spend a week time with prof. Vladimir Babitsky for the 3rd International Centre of VIBRO-IMPACT Systems conference in July 2013 in Germany.

Besides, I am also grateful to the advices in terms of mechatronics from my supervisor Prof. Robert Parkin. His financial support ensures the ultrasonic machining laboratory's equipment updated in time so that experiments could be accomplished smoothly and successfully.

Furthermore, Dr. Alan Meadows who works as a technician in the ultrasonic machining laboratory was always to provide help when I encountered troubles and puzzles. His wittiness and experiences taught me a PhD research should not only focus on theories, books and mathematics but also emphasise the great importance of practical work. I appreciate Dr. Alan Meadows and enjoy the entire working process with him, testing equipments, manufacturing mechatronics circuits etc.

I also want to show my gratitude to the electronics workshop technician Steve Hammond and David King for examining the electrical equipments. I appreciate the main work shop technician Michael Porter to help me machine mechanical parts for experiments, Metrology workshop technician Jagpal Singh to tutor me to perform the surface finish examination in metrology laboratory, Keven Smith to receive numerous equipments, integrated circuits and drill bits I ordered and Miss Mary Treasure for her assistance to fill in the purchase requisition forms for me.

I want to thank my parents for their support, without them I am not able to achieve today's success.

List of Figures

List of Tables

Nomenclature

Roman Letters

a	Acceleration (m/s^2)
A_1	Amplitude of 1st step Concentrator (m)
A_2	Amplitude of 2nd step Concentrator (m)
C_1	Damping Coefficient of 1st Step Concentrator (Ns/m)
C_2	Damping Coefficient of 2nd Step Concentrator (Ns/m)
d	Piezoelectric Charge Constant (m/V)
D	Displacement of the Ultrasonic Transducer (m)
D_{UT}	Energy Dissipation of Ultrasonic Transducer
D^E	Piezo Dielectric Displacement (C/m^2)
E	Young's Modulus (Pa)
f	Frequency (Hz)
f_n	Natural Frequency (Hz)
F	Force (N)
F_0	Force on Piezoceramic Plate from 1st Step Concentrator (N)
G	Transfer Function of Ultrasonic Transducer
h	Piezoelectric Deformation Constant (V/m)
j	Imaginary Number ($j^2 = -1$)
k	Wavenumber of Longitudinal Vibration in Ultrasonic Transducer
K_1	Constant Stiffness of 1st Step Concentrator (N/m)
K_2	Constant Stiffness of 2nd Step Concentrator (N/m)
l_0	Thickness of Piezoceramic Plate (m)

L	Length of Entire Concentrator (m)
L_1	Length of 1st Step Concentrator (m)
L_2	Length of 2nd Step Concentrator (m)
L_{UT}	Lagrangian Product of Ultrasonic Transducer
M	Mass Matrix
M_1	Mass of 1st Step Concentrator (Kg)
M_2	Mass of 2nd Step Concentrator (Kg)
q	Charge of Piezo-electric Transducer (C)
R_1	Radius of 1st step Concentrator Cross Section (m)
R_2	Radius of 2nd step Concentrator Cross Section (m)
s	Laplace Operator ($s = j\omega$)
S_0	Area of Piezo-ceramic Plate (m^2)
S_1	Area of 1st Step Concentrator (m^2)
S_2	Area of 2nd Step Concentrator (m^2)
s^E	Elasticity Compliance at Constant Electric Field (m^2/N)
t	Time (s)
T	Period of Vibration (s)
T_{UT}	Kinetic Energy of Ultrasonic Transducer
u	Voltage Supplied to Piezoceramic Plate (V)
U	Distributed Energy of Ultrasonic Transducer (J)
V_{UT}	Potential Energy of Ultrasonic Transducer
x	Longitudinal Coordinate
x_0	Displacement of a Single Piezoceramic Plate (m)
x_1	Displacement of 1st Step Concentrator (m)
x_2	Displacement of 2nd Step Concentrator (m)

x_j	Junction between 1st Step and 2nd Step Concentrator (m)

Greek Letters

ε	Strain
λ	Eigenvalues Matrix of Resonance Frequencies
ρ	Density of Concentrator Material (kg/m^3)
σ	Stress (Pa)
ω	Frequency (Rad/s)
ω_n	Natural Frequency (Rad/s)
ξ_0	Permittivity of Free Space (F/m)
ξ^s	Permittivity at Constant Strain (F/m)
Σ	Piezoelectric Field Strength (V/m)
Ψ	Eigenvectors Matrix of Normalized Amplitude of Vibration
ψ_1	Normalized Amplitude of Vibration for 1st Resonance Frequency
ψ_2	Normalized Amplitude of Vibration for 2nd Resonance Frequency

Abbreviation

AVC	Active Vibration Control
ASAC	Active Structural Acoustic Control
BLT	Bolt-clamped Langevin Transducer (BLT)
CB	Conventional Boring/Conventional Broaching
CD	Conventional Drilling
CG	Conventional Grinding
CM	Conventional Machining/Conventional Milling
DOF	Degree of Freedom
FEM	Finite Element Modelling
HSS	High Speed Steel
LTI	Linear Time Invariant
LQR	Linear Quadratic Regulator
LQG	Linear Quadratic Gaussian
MOSFET	Metal-Oxide-Semiconductor Field-Effect Transistors
PID	Proportional Integral Differential
RMS	Root Mean Square
RUM	Rotary Ultrasonic Machining
UAB	Ultrasonically Assisted Boring
UAD	Ultrasonically Assisted Drilling
UAG	Ultrasonically Assisted Grinding
UAM	Ultrasonically Assisted Machining/Ultrasonically Assisted Milling
UAT	Ultrasonically Assisted Turning
USM	Ultrasonic Machining

VCA	Voltage-Controlled Amplifier

Publications

1. X.Li, V.Babitsky, R.Parkin and A.Meadows. *Autoresonant Excitation and Control of Nonlinear Mode for Ultrasonically Assisted Drilling.* Zeitschrift für Angewandte Mathematik und Mechanik (Journal of Applied Mathematics and Mechanics). (Accepted for Publication)

2. X.Li, A.Meadows, V.Babitsky and R.Parkin. *Autoresonant Control of Ultrasonically Assisted Drilling: Modelling and Experiments.* Mechatronics. (Submitted)

3. X.Li, A.Meadows, V.Babitsky and R.Parkin. *Optimization of a Universal Matchbox on an Ultrasonic Vibrating System.* Ultrasonics. (Accepted)

Table of Content

Chapter One Introduction

1.1 Problem Formulation and Related Research

Ultrasonic Machining (USM) is a non-conventional mechanical material removal process that is used to erode holes and cavities in hard or brittle work pieces by employing shaped tools, high-frequency mechanical motion and an abrasive slurry, which is generally associated with low material removal rates [49,63]. The history of Ultrasonic Machining (USM) began with a paper by R.W. Wood and A.L. Loomis in 1927 and the first patent was granted to L. Balamuth in 1945 [29,55,69]. Ultrasonic Machining (USM) has been initially and variously categorized into: ultrasonic drilling, ultrasonic cutting, ultrasonic dimensional machining, ultrasonic abrasive machining and slurry drilling [63]. However, from the early 1950s it was commonly known either as ultrasonic impact grinding or Ultrasonic Machining (USM) [63].

It has been reported that variations on either using a magnetostrictive transducer or a piezoelectric transducer with brazed and screwed tooling include [63]: Conventional Ultrasonic Machining (USM), Rotary Ultrasonic Machining (RUM) and Ultrasonically Assisted Machining (UAM). Being different from Conventional Ultrasonic Machining (USM) and Rotary Ultrasonic Machining (RUM), Ultrasonic Assisted Machining (UAM) is claimed to reduce work piece residual stresses, strain hardening and improve work pieces surface quality. This project focuses on the research of Ultrasonically Assisted Machining (UAM) with an application of Ultrasonically Assisted Drilling (UAD). Ultrasonically Assisted Drilling (UAD) happens when ultrasonic vibration is superimposed onto the relative cutting motion between a drill bit and a work piece being drilled [64]. The experimental setup for Ultrasonically Assisted Drilling (UAD) for the application of a 3mm drill bit is illustrated in Figure 1.1.

The Ultrasonically Assisted Drilling (UAD) system mainly consists of: an ultrasonic transducer which is formed by piezorings within a package together with a waveguide (concentrator). During operation, the concentrator is gripped uniformly with a number of bolts through an aluminium tube which is clamped into a three-jaw chuck on a lathe. A drill bit is fixed in the tool holder at the thin end of the concentrator. The work piece is clamped firmly against the vertical plane of a Kistler dynamometer installed on the saddle side. The mechanism of Ultrasonically Assisted Drilling (UAD) is that it begins with the conversion of

a low-frequency electrical energy to a high-frequency electrical energy, which is further fed to a piezoelectric transducer [2,19,28,31,45,63]. Then the piezoelectric transducer converts the high-frequency electrical energy into mechanical vibrations which are transmitted through an energy-focusing device, for instance, a horn or a tool assembly [25,35,37], and therefore leads to the tool to vibrate longitudinally at a high frequency (usually$\geq 20KHz$) [31,63]. The vibration amplitude is only a few micrometres on the tool in a direction parallel to the axis of the tool feed [25,31,37]. Typical power ratings range from $50W$ to $3KW$ [59] and can reach $4KW$ in some machines [57]. However, the active power supplied to an ultrasonic transducer is strongly depended on the process elements, for instance, the amplifier module and the universal matchbox (transformer). It has been experimentally found that for an application of a 6mm drill bit on a 4-ring powerful ultrasonic transducer with a high power amplifier module the active power easily develops nearly $2KW$.

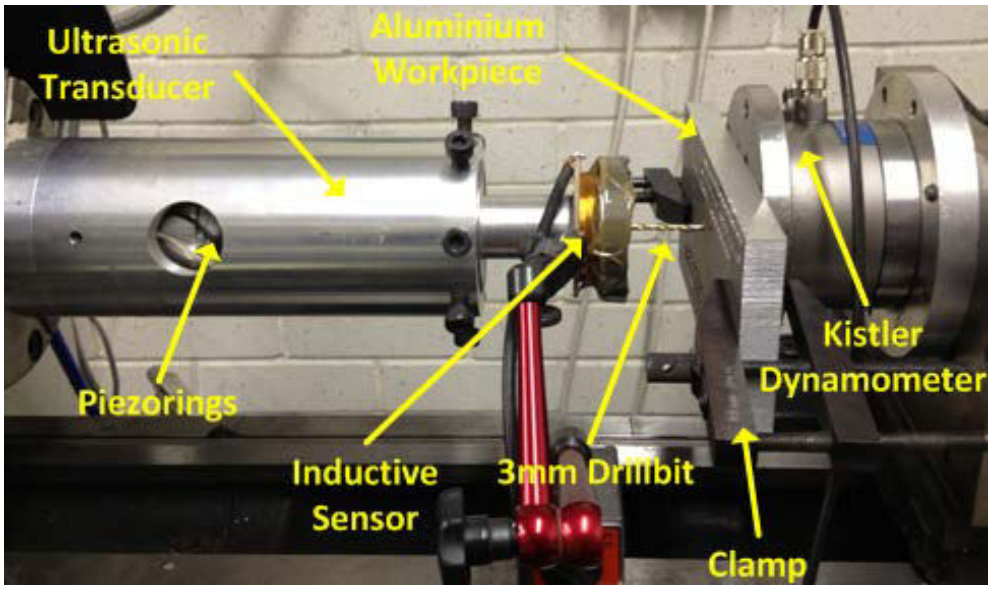

Figure 1.1 : Ultrasonically Assisted Drilling (UAD) experimental setup for a 3mm drill bit application

A research project was previously conducted at Loughborough University on Ultrasonically Assisted Drilling (UAD) [64] and results are shown in Figure 1.2. A standard twist drill bit with diameter 9.5mm and a piece of thin aluminium alloy strip with thickness 0.9mm were employed. Evidently, it can be observed from the upper row in Figure 1.2, the exit faces quality with Ultrasonically Assisted Drilling (UAD) is superior over Conventional Drilling (CD). The lower row illustrates that with a superimposition of ultrasonic vibration it is possible to drill a piece of thin aluminium strip supported just at the end, where using

Conventional Drilling (CD) technique only results in severe deformation of the strip and no penetration. The explanation for this phenomenal effect is the considerable force reduction when the superimposition of the ultrasonic vibration on the tip of a drill bit, which enables the tool to penetrate into the material with less thrust force.

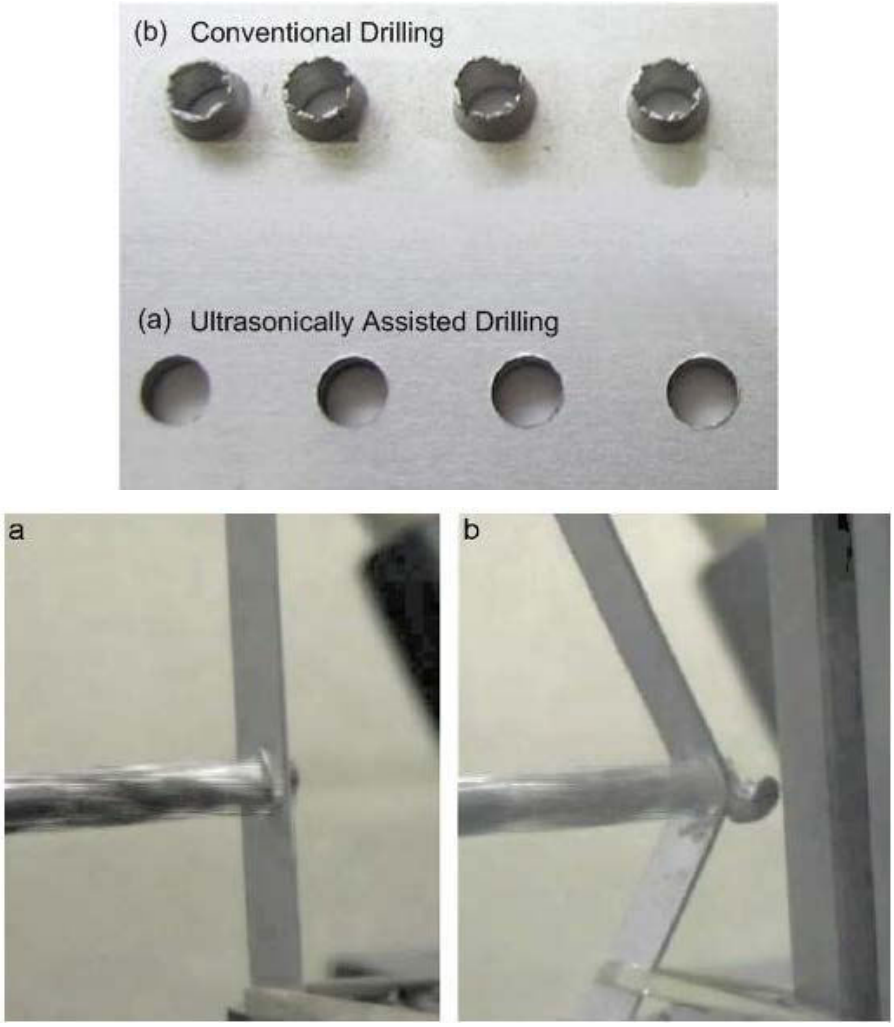

Figure 1.2 : Comparison in drilling flexible aluminium plates and exit faces quality: (a) Ultrasonically Assisted Drilling (UAD), (b) Conventional Drilling (CD)
Reproduced and Revised From [15,64]

Besides the application of Ultrasonic Machining (USM) in drilling, other applications have been performed. Figure 1.3 shows surface finish quality comparison between Conventional Machining (CM) and Ultrasonically Assisted Machining (UAM) which are applied to Ultrasonically Assisted Turning (UAT), Ultrasonically Assisted Milling (UAM), Ultrasonically Assisted Boring (UAB) and Ultrasonically Assisted Grinding (UAG) with different materials as work pieces.

The finish quality improvement in these applications with Ultrasonically Assisted Machining (UAM) and Conventional Machining (CM) technologies is significant. In the case of Ultrasonically Assisted Turning (UAT) of Inconel, the technique produces a smoother surface than Conventional Machining (CM). Similarly, Ultrasonically Assisted Milling (UAM) makes a better quality in contrast to Conventional Milling (CM) which is likely to produce some cracks [68]. For Conventional Boring (CB), there are clear tool marks observed, after the implementation of Ultrasonically Assisted Boring (UAB), however, tool marks are almost undistinguishable [23]. Furthermore, Conventional Grinding (CG) generates cracks and fractures on the surface of work pieces, the grinding grooves are deep and narrow. For the Ultrasonically Assisted Grinding (UAG), the dimensions of grinding grooves are smaller, resulting in a smoother work surface [42].

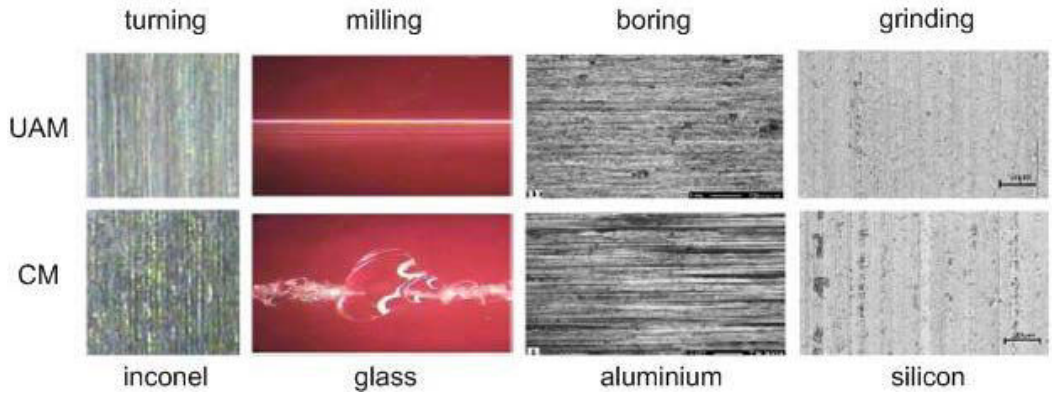

Figure 1.3 : Comparison of Ultrasonically Assisted Machining (UAM) and Conventional Machining (CM)

Reproduced and Revised From [23,42,68]

The significant effects in these applications indicate that Ultrasonically Assisted Machining (UAM) can achieve a number of advantages over Conventional Machining (CM) in industrial applications. Several advantages of introducing ultrasonic vibration in the tool have been reported:

- Ultrasonic Assisted Machining (UAM) has proven to be an efficient technique in improving the machinability of several materials such as aluminium [21] or Inconel 718 [4].

- Ultrasonic Assisted Machining (UAM) can significantly reduce cutting force, tool wear, burr generation in several materials, as well as produce shorter chips [40].

- Ultrasonic Assisted Machining (UAM) improves the surface roughness, roundness [40].

In spite of such advantages, Ultrasonically Assisted Machining (UAM) creates particular problems. One of the essential issues is the proper control of the ultrasonic vibration. The target of the ultrasonic vibration control is to maintain the nonlinear oscillation mode at resonance, or equivalently, to achieve a stable vibration amplitude, in order to make full use of the ultrasonic vibration for machining applications. Nonetheless, during the vibration control process, a number of problems are encountered.

Theoretically, to maintain the ultrasonic vibration at resonant state during machining process, a frequency generator could be used. With a conventional generator system, the horn (waveguide) and tool are set up then mechanically tuned by adjusting their dimensions to achieve resonance [63]. Yet, this traditional tuning method's efficiency and its application feasibility are dependent on the vibrating system's characteristics. For systems which are insensitive to the excitation variation, a conventional frequency generator can be used even though it might not be the optimal option. Nevertheless, as the ultrasonic vibrating systems react drastically and sensitively to the excitation frequency change, this tuning method presents poor control performances which have been proved in experiments.

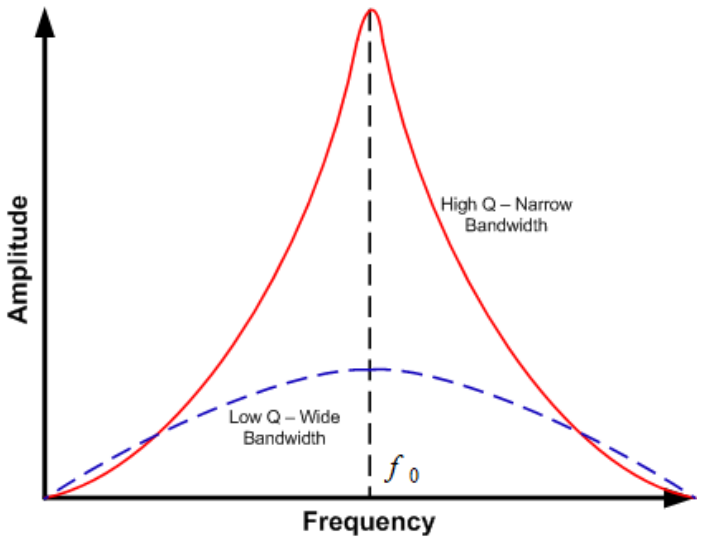

Figure 1.4 : Q factor explanation and illustration

In order to evaluate the sensitivity of the output response with respect to the input, a new dimensionless parameter Q factor is introduced. In physics and engineering the Q factor describes how under-damped an oscillator or resonator is [34], or equivalently, characterises of a resonator's bandwidth relative to its centre frequency [66]. A higher Q value indicates a lower rate of energy loss (lower damping) relative to the stored energy of the oscillator. In other words, oscillation dies out slowly. A high Q factor oscillating system reacts sensitively to the variation in the input signal, which makes the ultrasonic vibration control by adjusting the excitation frequency more difficult. In contrast, for a lower Q factor oscillating system, the energy fades quickly relative to the stored energy, which indicates a moderate response with respect to the variation in input signal. The Q factor illustration is in Figure 1.4.

A high Q factor oscillating system shows a sharp response at resonance frequency f_0 in comparison to the low one, which creates a difficulty to maintain the resonant state. In addition, experiments proved that a high Q oscillating system was sensitive to change in the operating load and the parameters, the vibration amplitude easily falls to an insignificant level. Therefore, resonances following generators have become available which automatically adjust the output high frequency to match the exact resonant frequency of the horn (waveguide) and tool assembly [33]. However, problems transit to a more complicated level when a tool is in contact with a work piece, i.e. nonlinearity occurs in the amplitude-frequency characteristic in the vibrating system because of the vibro-impact nature [18,24,54,60,61].

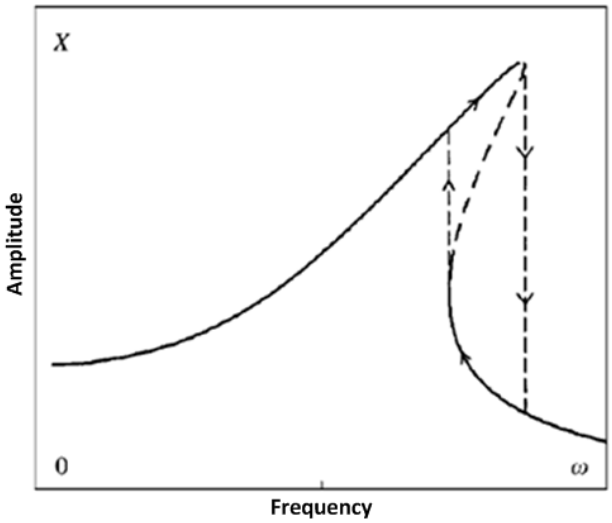

Figure 1.5 : Amplitude-frequency characteristic of a nonlinear system and jump phenomenon Reproduced and Revised From [60]

The amplitude-frequency characteristic of nonlinearity due to vibro-impact is demonstrated in Figure 1.5. One observation is that within a particular frequency range the amplitude-frequency characteristic is not single-valued. In other words, one frequency corresponds to several vibration amplitudes. This is one of the typical properties of the nonlinear oscillating systems. In addition, a drop/jump (both downwards and upwards in this case, shown in arrows) in amplitude at certain frequency is also illustrated, which is well-known as 'jump phenomenon'. The vibrating system's excitation frequency increases gradually along with the curve branch together with the growth of the magnitude to a furthermost point. After this, any slight increase in the excitation frequency will result in a jump of the amplitude to a lower value at its corresponding frequency on the lower branch of the curve. The lower branch will dominate if the excitation frequency is adjusted in the opposite direction, which is undesirable because of the low vibrating amplitude. Obviously, low amplitude in the Ultrasonically Assisted Drilling (UAD) might cause a permanent separation/contact of a drill bit with a work piece which leads to the efficiency loss of the technique [18].

The transition to 'autoresonance' has proven to be able to tackle the nonlinearity problem caused by the vibro-impact effect during machining. The idea of the autoresonant control is to design a resonant vibratory equipment as self-sustaining oscillating systems using electronic and electromechanical positive feedback and a synchronous type actuator for self-excitation of resonant vibration in combination with negative feedback for its stabilisation [11,12]. The term was used later for the concept of vibration excitation in vibratory machines based on the loss of stability due to artificial implementation of positive feedback into design [6,11,18]. 'Autoresonance' was applied to a number of ultrasonic machining processes and machines that were proved to be successful.

For instance, the autoresonant control design has been carried out on the Ultrasonically Assisted Turning (UAT) [68] applications and results were promising. However, Ultrasonically Assisted Turning (UAT) is a simple process in comparison with the Ultrasonically Assisted Drilling (UAD). First of all, a cutter was used in Ultrasonically Assisted Turning (UAT) which is negligible because a cutter has neither a complicated geometry nor a reasonable length that can hardly be considered as an extension of the waveguide. Therefore, the tool effect is insignificant during Ultrasonically Assisted Turning (UAT) which essentially simplifies the machining process and the autoresonant control design. A standard laser vibrometer could be effectively employed because the ultrasonic

transducer is non-rotational during Ultrasonically Assisted Turning (UAT). Therefore a steady, reliable and direct mechanical vibration signal from the cutting zone is captured and used for the feedback control and monitoring. In addition, the constant cutting depth of the Ultrasonically Assisted Turning (UAT) is predefined by the user. This implies a less challenge of the autoresonant control design. No information has been revealed on the autoresonant control efficiency when a cutter is engaged with a variable cutting depth into a work piece. Furthermore, autoresonant control in Ultrasonically Assisted Turning (UAT) employs a limiting element which introduces a strong nonlinearity and brings in a filtering process which complicates the control. However, this limiter has been removed and replaced in the autoresonant control design in Ultrasonically Assisted Drilling (UAD). Last but not least, author who worked on Ultrasonically Assisted Turning (UAT) attributes the low vibration amplitude on the tip of a cutter to the low Q factor of the ultrasonic transducer which is dubious. In Ultrasonically Assisted Drilling (UAD), however, it has been found that the effective inductance of the universal matchbox has a great impact on the ultrasonic vibration amplitude of an ultrasonic vibrating system. In other words, before each application of the Ultrasonically Assisted Machining (UAM), the universal matchbox in the chain should be optimized. This is done through introducing an air gap in the transformer. Details about the optimization of the universal matchbox can be found in Appendix I.

In addition, during Ultrasonically Assisted Drilling (UAD) several drill bits with complicated geometry [15,47,64,65] and different lengths have been employed in order to explore the tools effect on the autoresonant control efficiency. The most challenging point of the Ultrasonically Assisted Drilling (UAD) is the missing knowledge of the mechanical vibration information of the cutting zone (on the tip of a drill bit) during vibro-impact. This certainly complicates the design of the autoresonant control system. Furthermore, an introduction of a drill bit to the ultrasonic transducer needs a proper tuning in order to match the entire ultrasonic vibrating system acoustically because a drill bit cannot be neglected. In addition, the rotational motion of an ultrasonic transducer disables the possibility of employment of a laser vibrometer because no steady signal is captured on the rotating surface of the reflection film. Consequently, a magnetic sensor has to be manufactured and placed at a distance from the cutting zone to record the scaled mechanical vibration signal. Moreover, the drilling depth in Ultrasonically Assisted Drilling (UAD) is a variable which requires the autoresonant control system to be robust in order to deal with the time varying drilling depth.

The basic idea of the autoresonant control is to employ the phase control due to the fact that the amplitude-phase characteristics are single-valued and gently sloping near the resonance for most vibrating systems [60], which are distinct from the amplitude-frequency and the phase-frequency characteristics [18]. The amplitude-phase and the amplitude-frequency characteristics for a nonlinear oscillating system are illustrated in Figure 1.6. The nonlinearity has been shown in the amplitude-frequency characteristic, it can be clearly seen that the peak is sharp and the curve is not single-valued which makes a fixed frequency control insufficient. In contrast, the amplitude-phase characteristic gently slopes near the resonance which is smoother than the amplitude-frequency curve which provides an easier access to the control design. Another observation of the amplitude-phase characteristic is that all points are stable and the curve is single-valued. Therefore, design of an autoresonant system entirely relies on the amplitude-phase characteristic of a vibrating system.

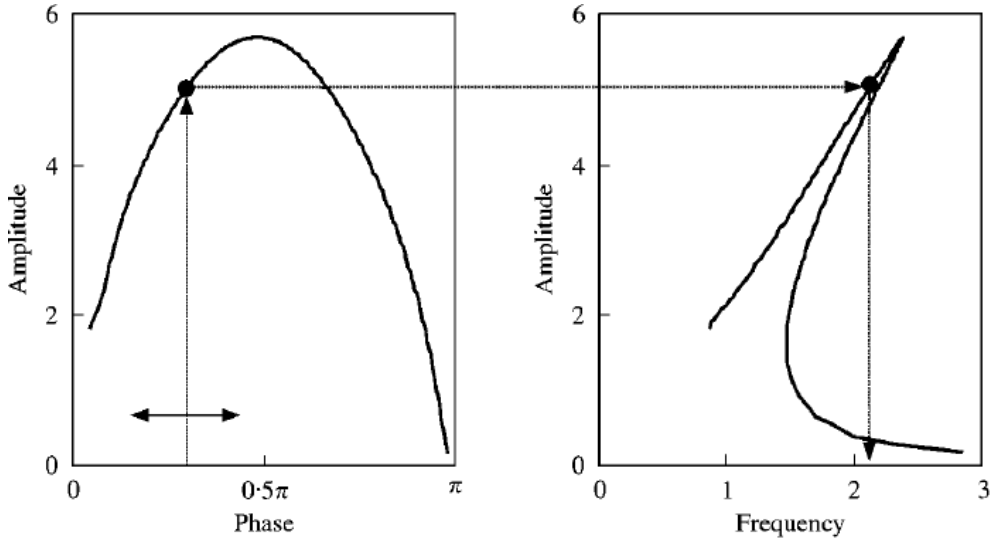

Figure 1.6 : Illustration of amplitude-phase and amplitude-frequency characteristics of nonlinear systems using phase control technique

Reproduced From [60]

The working principle of the autoresonant control is the actuation forms an exciting force F by means of positive feedback based on the transformation of a feedback sensor's signal. The feedback, in its simplest form, shifts the phase of the vibration signal from the sensor and amplifies its magnitude and the produced powerful signal feeds a synchronous actuator which transforms it to the excitation force F. The feedback loop also contains an additional mechanism for the limitation of the excitation force. Hereafter, a synchronous actuator can transform the alternating signal to an alternating excitation force with an exactly same

frequency and a predictable phase shift [18]. In this project, several sensors are available which will be introduced. The synchronous actuator used here is a piezoelectric transducer which can generate an excitation force for the ultrasonic vibrating system. The reason why a piezoelectric transducer is employed over a magnetostrictive transducer is because piezoelectric transducers used for machining applications provide a higher efficiency (lower energy loss) than magnetostrictive transducers due to their higher Q factor value [16]. The schematic of feedback control is shown in Figure 1.7.

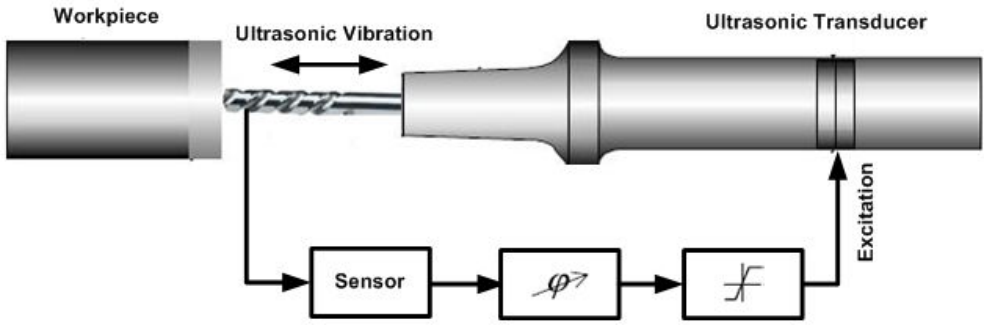

Figure 1.7 : Schematic of feedback of autoresonant control

Reproduced and Revised from [13,18]

Interestingly, an autoresonant system does not have a prescribed frequency of excitation which is contrary to the forced excitation with a prescribed frequency [18]. Frequency and amplitude of the ultrasonic vibration are determined by the parameters of an ultrasonic vibrating system and feedback elements. Parameters of the self-sustained vibration can be controlled by changing the phase shift and/or the limitation level in the feedback circuit. In most cases, autoresonant control is accomplished with a combination of phase control and amplitude control, which will be explained later in Chapter Five. Another important issue which may affect an autoresonant control design is the choice of sensor. Efficiency and accuracy of an autoresonant control system mainly depends on the selection of a sensor. Different selections of sensors have been described in a number of references; however, according to the property of a sensor, there are two types available:

- Mechanical feedback sensor

  A mechanical feedback sensor measures the mechanical displacement of an ultrasonic transducer during the machining process; the outputs of the sensor could be displacement, velocity or acceleration.

- Electrical feedback sensor

  An electrical feedback sensor considers the electrical parameters as feedback signals, which are either current or power of a piezoelectric transducer.

Mechanical feedback sensors and electrical feedback sensors show their advantages and drawbacks in the early research. A mechanical feedback sensor measures the actual vibration of an ultrasonic transducer which means the sensor should be placed at the end face of the ultrasonic transducer along the direction of the ultrasonic vibration [16]. Even though a precise measurement can be achieved by using a mechanical feedback sensor, there are some problems with its permanent fixture to a transducer and some of the mechanical feedback sensors need additional wiring to a control system. In comparison, an electrical feedback sensor has a low cost and a possibility of remote operation; however, an electrical sensor's output reflects the efficiency of the mechanical system oscillations only in an indirect way. In this project, sensor selections and explanations will be introduced and sensor performances will be compared for mechanical feedback and electrical feedback.

1.2 Aims and Objectives

The development of the Ultrasonically Assisted Machining (UAM) has been widely applied to manufacturing in recent years. However, control design of the Ultrasonically Assisted Machining (UAM) remains undeveloped. Autoresonant control has only been applied to the Ultrasonically Assisted Turning (UAT) [68], results were proven promising. However, Ultrasonically Assisted Turning (UAT) is not as challenging as Ultrasonically Assisted Drilling (UAD). Also, no research has been devoted to the investigation of control design on the Ultrasonically Assisted Drilling (UAD). Therefore, a strategy providing an efficient and reliable control of the ultrasonic vibration becomes a challenging and topical engineering problem in the Ultrasonically Assisted Drilling (UAD) process. This is the main concern of the project. In brief, a successful completion of the project will achieve the following targets:

- Establish an accurate numerical model in Matlab-Simulink which simulates the ultrasonic transducer, according to the experimental measurements on an electromechanical ultrasonic transducer. The created model should embrace similar features to the electromechanical ultrasonic transducer.

- Acquire a reliable numerical model which simulates the applied load based on a vibro-impact experiment performed on an electromechanical ultrasonic transducer. The tuned parameters of the applied load model should produce a similar vibration magnitude to the experimental measurements.

- Develop a control system on the principle of autoresonance in Matlab-Simulink. The autoresonant control should be able to deal with different control strategies on an ultrasonic vibrating system. In addition, the control system should be robust to parameter changes in the applied load. Analyse and compare results between different autoresonant control strategies.

- Design and manufacture a prototype autoresonant control system in experiment and evaluate its efficiency and robustness on different control strategies for different performance sensors. Execute autoresonant control experiments on a fixed spindle rotation speed in combination with various feed rates for 3mm and 6mm in diameter drill bits. Compare experimental results with simulation results for both sizes of drill bits and analyse tool effect with different control strategies.

- Examine holes surface roughness produced by different control strategies for both sizes of drill bits.

- Investigate the universal matchbox (transformer) effect on the ultrasonic vibration level for different air gap distance between two ferrite cores and optimize the universal matchbox for an ultrasonic vibrating system.

1.3 Outline of Thesis

The rest of the thesis consists of the following chapters.

Chapter Two is devoted to the literature review study. Ultrasonic Machining (USM) has been overviewed including the descriptions of Conventional Ultrasonic Machining (USM), Rotary Ultrasonic Machining (RUM) and Ultrasonically Assisted Machining (UAM). The working principle of Ultrasonically Assisted Machining (UAM) has been elaborately described.

Advantages and disadvantages of different geometries of waveguides have been analysed and a stepped concentrator has been employed to design an ultrasonic transducer. Vibro-impact mechanism has been described in the application of Ultrasonically Assisted Drilling (UAD) as well as the critical drilling velocity calculation. Ultrasonic vibration direction has been selected as longitudinal due to the special property of the actuation elements (piezoceramic rings) of the Ultrasonically Assisted Drilling (UAD) in this project.

Chapter Three is dedicated to the analysis of vibration control methodologies. Due to the fact that an ultrasonic vibrating system normally shows a high Q factor, a classical control method (frequency control) fails to maintain the nonlinear oscillating mode at resonance during vibro-impact. In comparison, the phase-amplitude characteristic remains linear and gently slopes near the resonance. Therefore, a specific control algorithm 'autoresonance' has been developed to tackle the nonlinearity problem. Autoresonance control principle has been described in details together with possible sensor selections. Two feedback control strategies are available which are mechanical feedback control and electrical feedback control.

Chapter Four focuses on the establishment of a 2-DOF model which is employed to replace the electromechanical ultrasonic transducer used in experiments. Dynamics of a distributed parameter model which resembles the ultrasonic transducer has been analysed and resonant frequencies have been computed. Results have been compared with the resonant frequency measurement in experiments and the difference remains small which implies the validity of the distributed parameter model. A 2-DOF model has been created including a piezoelectric transducer together with a package of two spring-mass-damper sets. This model is used to replace the ultrasonic transducer used in experiment. Parameters of the spring-mass-damper sets have been calculated accordingly. The validity of the 2-DOF model has been confirmed experimentally. An applied load model which consists of an elastic spring and a viscous damper has been designed and model parameters are obtained through a vibro-impact experiment. The loaded ultrasonic transducer model is established for the design and evaluation of an autoresonant control system.

Autoresonant control system design principles and steps are discussed in Chapter Five. Each element in the autoresonant control system and the functions have been thoroughly analysed. Depending on the feedback control strategies, the phase-amplitude characteristics on different observation points are obtained. Proper filters design is consequently required to pick up the

desired vibration regime depending on the feedback control strategies. Amplitude-frequency characteristics of the mechanical parameters and the electrical characteristics in simulation and experiments are obtained and compared. A high similarity between simulation and experiments is confirmed.

Chapter Six is dedicated to the numerical simulation analysis on different control strategies. It should be emphasized that the drill bit effect analysis is not involved in the numerical simulation due to the complexity it creates during vibro-impact process. Frequency control, mechanical feedback control and electrical feedback control are compared during the change of the applied load parameters. Advantages and disadvantages are addressed in simulation for different control strategies which lays a foundation for the autoresonant control system design in experiments.

Chapter Seven concentrates on the analysis of the experimental results. A prototype autoresonant control system has been designed and manufactured. Frequency control, mechanical feedback and electrical feedback have been executed on a 3mm and a 6mm in diameter drill bits together with different feed rates. Tool effect has been explored. Efficiencies of different control strategies have been compared and analysed. Results show consistencies with numerical simulation. Holes finish qualities have been examined.

Chapter Eight consists of the conclusions of the project and recommendations for the future work.

Appendices are comprised of the structures of simulation blocks, equation derivations and some interesting research results on the universal matchbox (transformer).

Chapter Two Literature Review

2.1 Ultrasonic Machining

Unlike other non-traditional processes such as laser beam and electrical discharge machining, Ultrasonic Machining (USM) does not thermally damage the work piece or appear to introduce significant levels of residual stress, which is important for the survival of the brittle materials in service [63]. Ultrasonic Machining (USM) is a non-conventional mechanical material removal process generally associated with low material removal rates. However, its application is not limited by the electrical or chemical characteristics of the work piece materials [63]. For industrial application, it is used for machining both conductive and non-metallic materials, preferably those with low ductility and a hardness above 40 HRC [33,55,62], namely, inorganic glasses, silicon nitride, nickel/titanium alloys. Depending on the type of a transducer employed, the machining process with ultrasound application can be classified into: Conventional Ultrasonic Machining (USM), Rotary Ultrasonic Machining (RUM) and Ultrasonically Assisted Machining (UAM).

2.1.1 Conventional Ultrasonic Machining (USM)

The history of Ultrasonic Machining (USM) can be traced back to the American Engineer, Lewis Balamuth, who discovered ultrasonic cutting in the 1940's [46,58]. The technique was exploited rapidly in industry and between 1953 and 1955 several countries began with the manufacture of industrial prototypes of ultrasonic machine tools [58]. There exists a range of applications where ultrasonic vibration alone is used to assist well known machining operations: grinding, milling, turning, reaming and lapping [46].

The concept of the Conventional Ultrasonic Machining (USM) has been discussed in many references. Basically, Ultrasonic Machining (USM), sometimes called ultrasonic impact grinding, is a mechanical material removal process used to erode holes and cavities in hard or brittle work pieces by using shaped tools, high-frequency mechanical motion and an abrasive slurry [63]. It is effective and practical for all brittle materials, including glass, ceramics, carbide and graphite [32].

Figure 2.1 demonstrates the process of the Conventional Ultrasonic Machining (USM). A tool of desired shape vibrates at an ultrasonic frequency ($19KHz \sim 25KHz$) with a vibration

amplitude around $15\mu m \sim 50\mu m$ at the work piece [44]. Generally the tool is pressed downward with a static feed force driven by an acoustic horn (known as concentrator). The horn can automatically adjust the process output frequency to maintain an acceptable resonant frequency during operation [32]. Between the tool and the work piece, the machining zone is flooded with hard abrasive particles generally in the form of water based slurry. As the tool vibrates over the work piece, the abrasive particles act as the indenters and indent both the work material and the tool. The abrasive particles, as they indent, the work material, would remove the same, particularly if the work material is brittle, due to crack initiation, propagation and brittle fracture of the material [44].

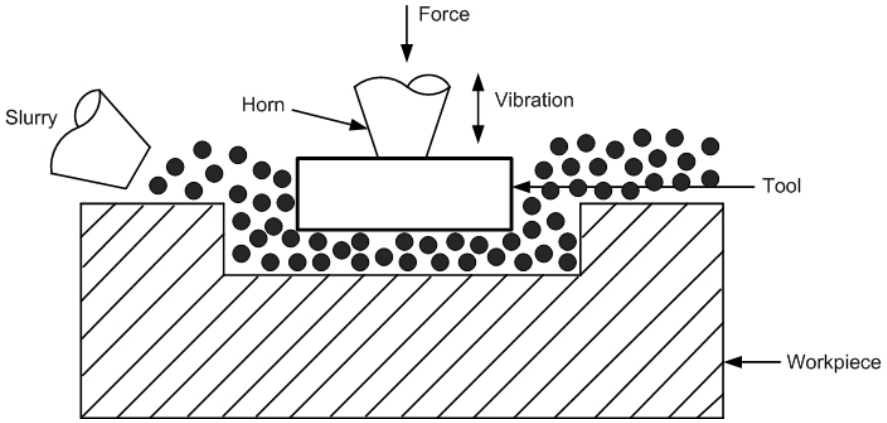

Figure 2.1 : Conventional Ultrasonic Machining (USM) process
Reproduced and Revised from [44]

The Conventional Ultrasonic Machining (USM) process is non-thermal, non-chemical and non-electrical, leaving the chemical and physical properties of the work piece unchanged. In addition, the Conventional Ultrasonic Machining (USM) is a loose abrasive machining process that requires a very low force applied to the abrasive grain, which leads to reduced material requirements and minimal to no damage to the surface of work piece. Extreme hard and brittle materials can be easily machined like glass, semiconductor and ceramics etc [44]. Besides, highly accurate profiles and good surface finish of a work piece can be easily obtained. Another benefit of the Conventional Ultrasonic Machining (USM) is that parts machined ultrasonically often perform better in downstream machining processes than do parts machined using more Conventional Machining (CM) methods. However, the Conventional Ultrasonic Machining (USM) creates minor problems during machining process. For instance, its sonotrode vibration uniformity may limit the process to objects less than 4 inches in diameter and it has a low material-removal rate [32]. The Conventional

Ultrasonic Machining (USM) process is unsuitable for heavy metal removal. Moreover, for soft materials this technique is infeasible.

2.1.2 Rotary Ultrasonic Machining (RUM)

Rotary Ultrasonic Machining (RUM) was invented in 1964 by Percy Legge, a technical officer at United Kingdom Atomic Energy Authority [50]. The Rotary Ultrasonic Machining (RUM) is demonstrated in Figure 2.2. A rotating core drill with metal-bonded diamond abrasives is ultrasonically vibrated in the axial direction and fed towards the work piece at a constant feed rate or constant force. Coolant pumped through the core of the drill washes away the swarf, prevents jamming of the drill, and keeps it cool [41].

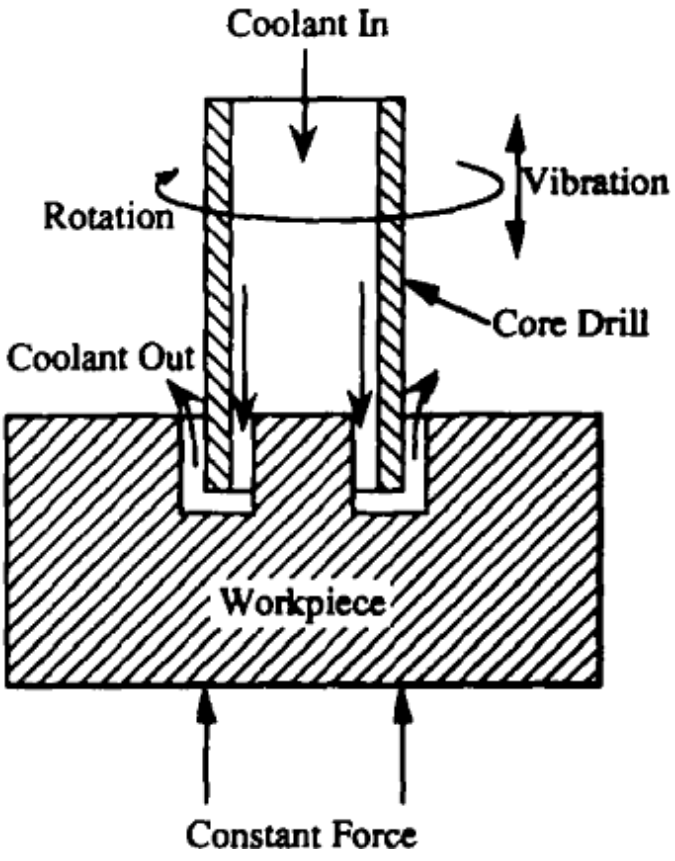

Figure 2.2 : Rotary Ultrasonic Machining (RUM) process
Reproduced From [51]

The Rotary Ultrasonic Machining (RUM) combines the material removal mechanisms of the Ultrasonic Machining (USM) process and the conventional diamond grinding process, which includes hammering, abrasion, and extraction. The combination of these three material

removal mechanisms results in higher material removal rates in the Rotary Ultrasonic Machining (RUM) than those obtained by either the Ultrasonic Machining (USM) process or conventional diamond grinding process [51]. In comparison with the Conventional Ultrasonic Machining (USM), Rotary Ultrasonic Machining (RUM) is about 10 times faster [41]. It is easier to drill deep and small holes with Rotary Ultrasonic Machining (RUM) than with Conventional Ultrasonic Machining (USM) and hole accuracy could be improved [51]. Another difference between Conventional Ultrasonic Machining (USM) and Rotary Ultrasonic Machining (RUM) is that the Conventional Ultrasonic Machining (USM) uses a soft tool, such as stainless steel, brass or mild steel, and slurry loaded with hard abrasive particles, while in Rotary Ultrasonic Machining (RUM) the hard abrasive particles are diamond and are bonded on the tools. Additionally, Rotary Ultrasonic Machining (RUM) tool rotates and vibrates simultaneously, while the Conventional Ultrasonic Machining (USM) tool only vibrates. These differences enable Rotary Ultrasonic Machining (RUM) to provide both speed and accuracy in ceramic and glass machining operations.

Among non-traditional machining processes being currently proposed for machining hard-to-machine materials, Rotary Ultrasonic Machining (RUM) is a relatively low-cost, environment-benign process that easily fits in with the infrastructure of the traditional machining environment. Studies of various material removal processes applicable to advanced ceramics indicate that the Rotary Ultrasonic Machining (RUM) has the potential for high material removal rate while maintaining low machining pressure and resulting in less surface damage [41]. The major limitation of the Rotary Ultrasonic Machining (RUM) is only circular holes or cavities can be machined due to the rotary motion of a tool. Attempts have been made by other researchers to extend rotary ultrasonic machining process to machining flat surfaces or milling slots. However, these extensions either changed the material removal mechanisms or had severe drawbacks [51].

2.1.3 Ultrasonically Assisted Machining (UAM)

The use of ultrasonic vibration in different manufacturing processes is well documented for more than 50 years [40]. Recently, ultrasonic vibration was applied as an assisting technology for Conventional Machining (CM) operations (turning and drilling) which is well-known as Ultrasonically Assisted Machining (UAM) process. Figure 2.3 demonstrates ultrasonically assisted turning. The ultrasonic transducer consists of piezorings clamped together with a

waveguide (concentrator) and a back section. A cutting tip is fixed in the tool holder installed at the narrow end of the waveguide. The transducer is supported and rigidly clamped at its nodal cross-section in a fixture mounted on the saddle of the lathe. The work piece is fixed by a three-jaw spindle chuck and is rotated universally by a lathe drive [16]. When a high-frequency signal from an electronic amplifier is fed to the input of the piezoelectric transducer, it starts to vibrate due to piezoelectric effect. This vibration excites longitudinal waves in the waveguide and through it the vibration can be transferred to the cutting tip.

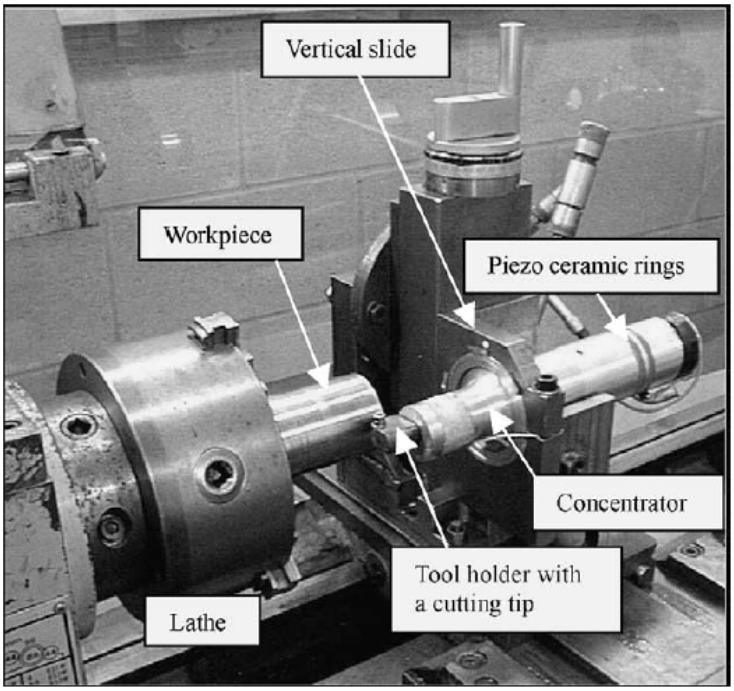

Figure 2.3 : Ultrasonically Assisted Machining (UAM) Process
Reproduced From [16]

The Ultrasonically Assisted Machining (UAM) technique has been used both for high precision machining applications and for difficult-to-cut materials machining such as hardened steels, nickel-based alloys, titanium and aluminium metal matrix composites [40]. In comparison with the Conventional Machining (CM) technology, Ultrasonically Assisted Machining (UAM) process proves to show a considerable decrease in cutting forces and produce shorter chips [67]. Besides, Ultrasonically Assisted Machining (UAM) can provide an improvement of finish quality by up to 50% (surface roughness and roundness). Limitations of the Ultrasonically Assisted Machining (UAM) application are tool use life is a challenging issue since it has to sustain the vibration and cutting of the work piece. Other limitations of the Ultrasonically Assisted Machining (UAM) such as proper control of

vibration at resonance have been solved successfully by applying autoresonant control technique.

2.2 Description of Ultrasonically Assisted Machining (UAM)

Ultrasonically Assisted Machining (UAM) happens when the ultrasonic vibration is superimposed onto the relative cutting motion between the tool and the work piece being machined [6,15,68]. In many industrial applications, Ultrasonically Assisted Turning (UAT) and Ultrasonically Assisted Drilling (UAD) are two most pronounced development using autoresonant control technique. Ultrasonically Assisted Turning (UAT) has been successfully investigated and implemented in [68]. However, Ultrasonically Assisted Turning (UAT) process is quite simple compared to Ultrasonically Assisted Drilling (UAD) process and the proper autoresonant control on Ultrasonically Assisted Drilling (UAD) remains undeveloped due to several limitations. For instance, in Ultrasonically Assisted Turning (UAT), a cutting tool effect (single edge contact) on the process is not as drastic as a drill bit effect (multi edges contact) on Ultrasonically Assisted Drilling (UAD) process since a drill bit creates more complex dynamic behaviour and for larger sized drill bits proper acoustic matching with waveguide is required as an extension of an ultrasonic vibrating system. Moreover, being different from non-rotational ultrasonic transducer in Ultrasonically Assisted Turning (UAT), the ultrasonic transducer rotates during Ultrasonically Assisted Drilling (UAD), which will inevitably introduce torsional behaviours that might demand the autoresonant control to be robust etc.

2.2.1 Working Principle of Ultrasonically Assisted Drilling (UAD)

Figure 2.4 demonstrates the working principles of the Ultrasonically Assisted Drilling (UAD). An ultrasonic transducer is clamped in a three-jaw chuck of the lathe through the intermediate bush and is energised by means of the slip ring assembly fitted to the hollow shaft of the lathe at the end remote from the chuck [15]. Samples to be drilled are clamped firmly by an external holder. In an ultrasonic vibrating system, the electromechanical transducer generates a powerful ultrasonic oscillation due to piezoelectric effect [16], and then the piezoelectric transducer converts high-frequency electrical signals from an electronic amplifier into high-frequency vibrations. The vibration amplitude at the source (piezoelectric transducer), however, is small, which enables the waveguide (concentrator or acoustic horn) to amplify the vibration magnitude to the maximal at the tool tip. Normally, a drill bit

vibrates axially at around $20\,KHz$ with amplitude of a cutting edge about $10\,\mu m$ [2]. However, resonant frequency and vibration amplitude depends on the size of a drill bit and structure of an ultrasonic transducer. A drill bit rotates whilst it vibrates along the axial direction. To achieve a resonant vibration state for a drill bit as well as stabilise the ultrasonic vibration, a feedback control system using autoresonant control is established, which defines a resonant frequency and a driving voltage for the piezoelectric transducer. During vibration propagation, the amplitude depends on the characteristics of the waveguide (concentrator). Proper design of a concentrator enables an ultrasonic vibrating system to work at the most efficient regime.

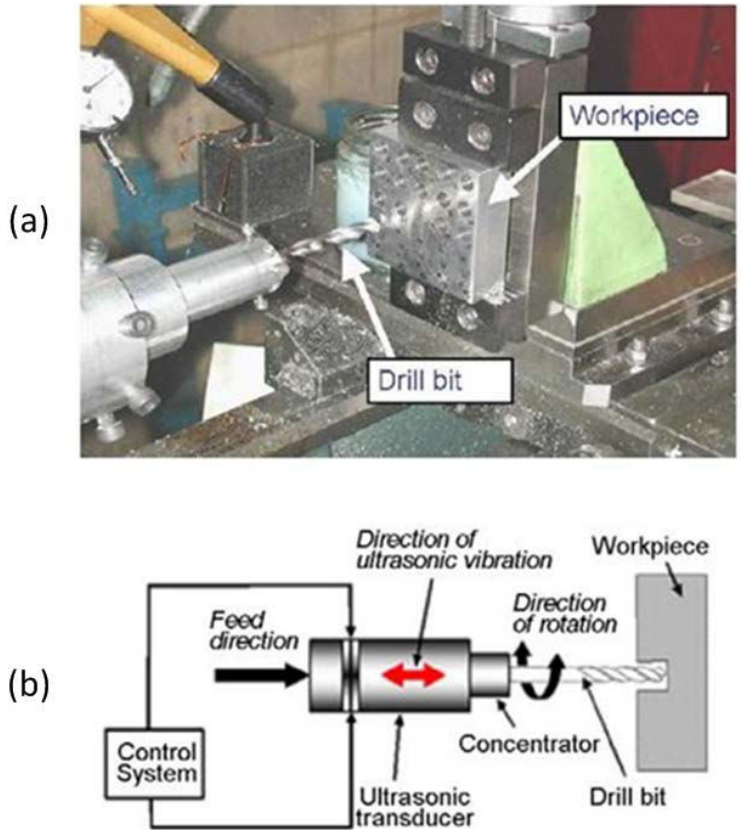

Figure 2.4 : Ultrasonically Assisted Drilling (UAD): (a) UAD experimental setup, (b) Schematic of UAD devices

Reproduced From [2] and [15]

2.2.2 Design of Waveguide (Concentrator)

Generally speaking, there are five types of concentrators available in industrial applications which are shown in Figure 2.5. (a) represents an exponential concentrator, (b) is a catenoidal concentrator, (c) stands for a cosine shape concentrator, (d) is a form of conic shape

concentrator and (e) shows a stepped waveguide which consists of two steps with different cross sectional areas. According to the amplification ratio calculation, the stepped shape waveguide (concentrator) (e) demonstrates the maximum magnitude amplification in all known concentrators given a same difference in cross sectional area [20].

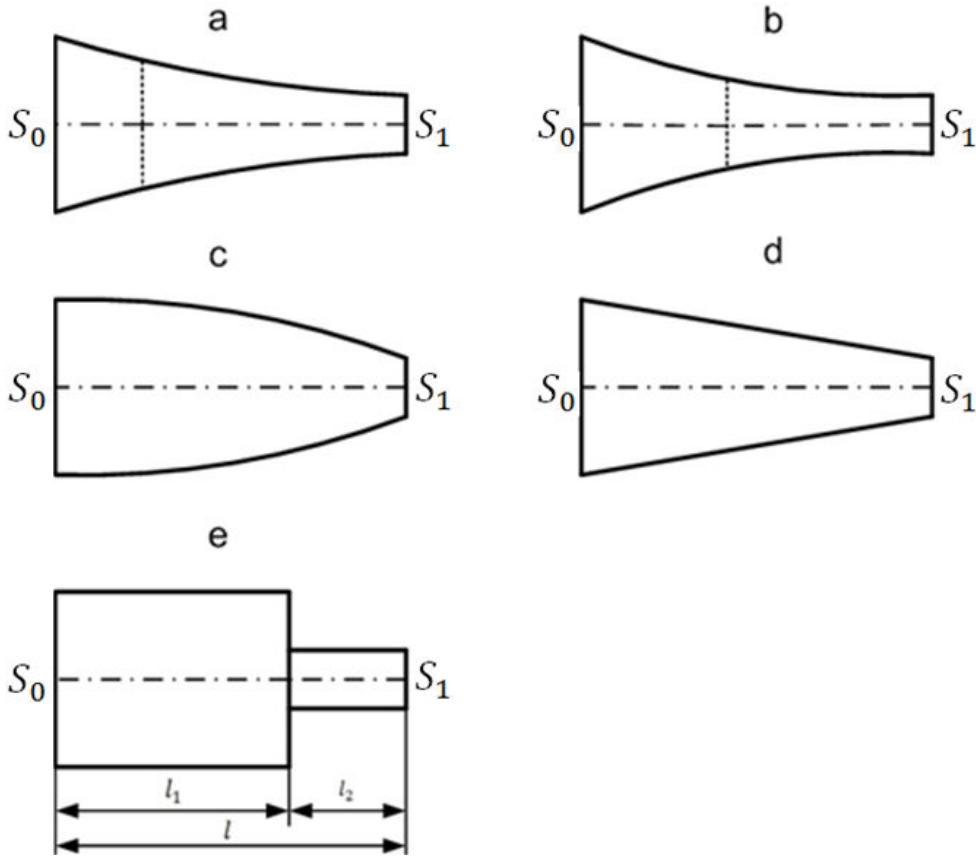

Figure 2.5 : Possible waveguide (concentrator) shapes: (a) exponential, (b) catenoidal, (c) cosine, (d) conic, (e) stepped

Reproduced From [8]

Figure 2.6 shows that for a fixed ratio of cross-sectional areas S_0/S_1, the stepped concentrator presents maximum amplitude amplification K, while the conic shape concentrator has the minimum amplification between all shapes of concentrators. Therefore, the stepped shape concentrator has been selected to design an ultrasonic transducer. In addition, not only the shape of a concentrator determines the amplification ratio, but also a proper length distribution of a 2-step waveguide to contribute vibration amplitude. A well-designed horn not only smoothly transfers and amplifies the ultrasonic amplitude, but also reduces the occurrence of pressure concentrations [39]. To maximise both amplitude of ultrasonic

vibration on a drill bit and work piece removal rate, the resonance of a drill bit and concentrator assembly needs to be within the adjustable frequency range of the Ultrasonically Assisted Drilling (UAD) machine [68].

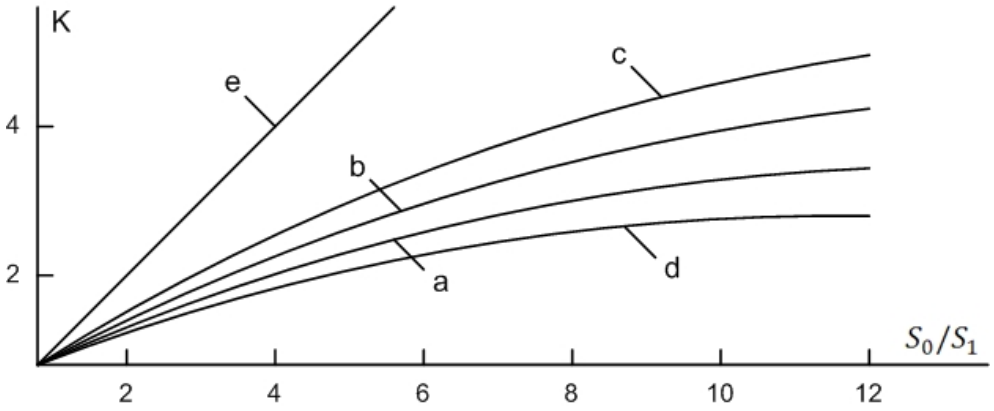

Figure 2.6 : Amplitude amplification for different cross section areas ratio: (a) exponential, (b) catenoidal, (c), cosine, (d) conic, (e) stepped

Reproduced From [8]

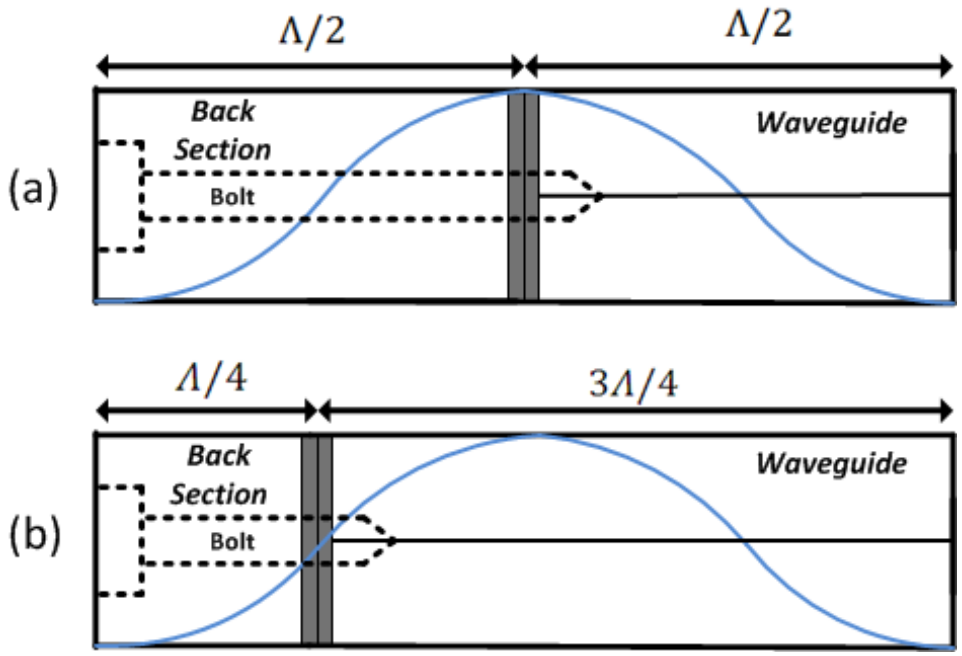

Figure 2.7 : Transducer tuning length for different conditions: (a) $1/2$ wavelength, (b) $3/4$ wavelength

Reproduced and Revised From [64]

Figure 2.7 shows an example of a typical ultrasonic Bolt-clamped Langevin Transducer (BLT). In this ultrasonic transducer, two piezoceramic elements are clamped between a mild

steel back section and an aluminium waveguide by a steel bolt. It has been investigated when a transducer is manufactured with a $n/2$ wavelength of the vibration in concentrator, n is an artificial number, as shown in Figure 2.7 (a) with $1/2$ wavelength for instance, the amplitude amplification ratio of the concentrator can only reach a maximum value of unity, this type of design (tuning) does not significantly amplify the amplitude of the ultrasonic transducer [14]. However, for a concentrator with uniform area in cross-section and length of $n/4$, n here represents an odd number, as shown in Figure 2.7 (b) with $3/4$ wavelength for example, the amplitude amplification is expected to reach a theoretical maximum value of infinity [64]. In this case, the concentrator action is similar to a dynamic absorber 'neutralising' mechanical vibration of the piezo element [14]. However, the infinite amplitude amplification ratio is only a theoretical value where in reality material damping exists which leads to vibration to a limitation.

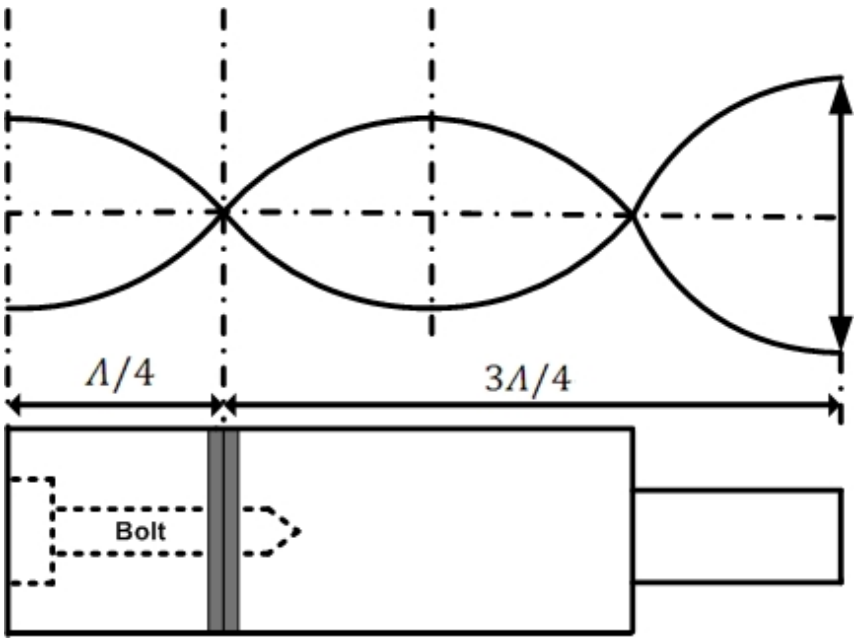

Figure 2.8 : Anti-Node condition of ultrasonic transducer

Reproduced and Revised From [68]

Since the second method of design (tuning) produces the amplitudes of vibration essentially bigger than the first, it has been employed to the design of an ultrasonic transducer. Besides, the ultrasonic transducer needs to be 2-step shape as explained in Figure 2.6. The ultrasonic transducer's structure is illustrated in Figure 2.8 according to the design. The back section length of the 2-step ultrasonic transducer is $1/4$ of the longitudinal wavelength, piezoceramic elements that are used to generate vibration are clamped tightly by a bolt. The piezorings act

as a physical nodal point. The entire length of the concentrator is $3/4$ of the ultrasound wavelength. The connection plane between 1st step and 2nd step is another physical nodal point which has been proved by experiments; Due to the cross section area difference between the 1st step and the 2nd step of concentrator, the vibration amplitude is expected to reach its maximum at the end of the 2nd step concentrator. The longitudinal vibration amplitude has been illustrated in Figure 2.8.

An ultrasonic transducer system generally consists of two parts: a piezoelectric transducer and a 2-step concentrator. The described design principle can only ensure the vibration magnitude to reach certain maximum under ideal condition. In practice, however, all components (tool holder, screws, drill bit etc) within the ultrasonic transducer assembly have to be tuned and designed appropriately so that the energy transfer from the piezoelectric transducer to the waveguide is the most efficient. For effective tuning of an Ultrasonically Assisted Drilling (UAD) system, the matching of the dynamic qualities of a transducer and a drill bit with dynamic load imposed by the cutting process is required [15]. The components comprising the ultrasonic transducer are different in different materials, shapes etc, which generates various resonant frequencies. The tuning rule shown in Figure 2.8 is a starting point, dimensions and design could be slightly different in practice. In addition, for an introduction of a drill bit into the ultrasonic transducer, it has to be treated as an additional step which needs proper acoustic matching with the ultrasonic transducer.

2.2.3 Ultrasonically Assisted Drilling (UAD) Mechanism and Drilling Velocity Analysis

During Ultrasonic Assisted Drilling (UAD), a drill bit vibrates in the axial direction whilst it rotates. A work piece is clamped firmly with a tool holder and fed towards the drill bit. Assuming the drill bit vibrates harmonically without signal distortions, the following motion equation can be obtained:

$$\begin{aligned} x &= a sin\omega t \\ \dot{x} &= a\omega cos\omega t \end{aligned} \tag{2.1}$$

x represents the drill bit vibration displacement, $\dot{x}$ is the vibration velocity of a drill bit, a stands for the vibration magnitude, ω is the natural frequency. The illustration of the

vibration motion process is shown in Figure 2.9. It should be noted that in order to explain the vibro-impact process clearly, the details between the drill bit and the work piece has been enlarged. The drill bit is oscillating whilst rotating around the centre axis. The work piece travels at a feed speed v towards the drill bit. The drill bit has a harmonic vibration with maximum amplitude a around its vibration origin point. During the process, the drill bit contacts with the work piece initially at point A at t_1 and keeps on penetration when it reaches the maximum displacement with velocity 0 then it starts to withdraw. At point B at t_2 the drill bit is separated from the work piece and continues its vibration. The second contact between the drill bit and the work piece takes place at point C at t_3 and the drill bit is separated from the work piece again at point D at t_4.

During the process, it is notable that in time interval t_1 to t_2 as well as t_3 to t_4, the drill bit has a permanent contact with the work piece. In contrast, from t_2 to t_3 the drill bit is separated from the work piece. This is the nature of vibro-impact which is essential in the Ultrasonically Assisted Drilling (UAD). In addition, the work piece's displacement during this process is denoted as x_D while the period of the ultrasonic vibration is T:

$$\begin{aligned} x_D &= v(t_4 - t_1) \\ T &= \frac{2\pi}{\omega} \end{aligned} \tag{2.2}$$

The advantages of the Ultrasonically Assisted Drilling (UAD) root from the nature of the vibro-impact response. In order to maintain the vibro-impact response during Ultrasonically Assisted Drilling (UAD) the relation between feed speed of a work piece v and the vibration velocity of a drill bit need to be precisely adjusted. Interestingly, from Figure 2.9 it can be concluded that at both point B and D, the work piece feed velocity and drill bit vibrating velocity are equivalent since the drill bit is at the edge of leaving the work piece. The existence of vibro-impact is due to the fact that the maximum vibration velocity of a drill bit is essentially greater than the feed speed of a work piece. Consequently, a critical vibration velocity of a drill bit when it equals a work piece feed speed can be obtained:

$$v_c = a\omega \tag{2.3}$$

v_c represents the critical vibration velocity of a drill bit, its value can be calculated from equation (2.1). The vibro-impact response only happens if the maximum vibration velocity of a drill bit is larger than the constant feed speed of the work piece, i.e. $a\omega > v$. In contrast, when $a\omega < v$, the drill bit has a permanent contact with the work piece which indicates a Conventional Drilling (CD) process. However, during Ultrasonically Assisted Drilling (UAD) process, the feed rate of the work piece is considerably smaller than the ultrasonic vibration velocity of the drill bit, i.e. $a\omega \gg v$. Due to the power limitation of piezoelectric transducer, a higher feed rate will normally cause a failure in autoresonant control.

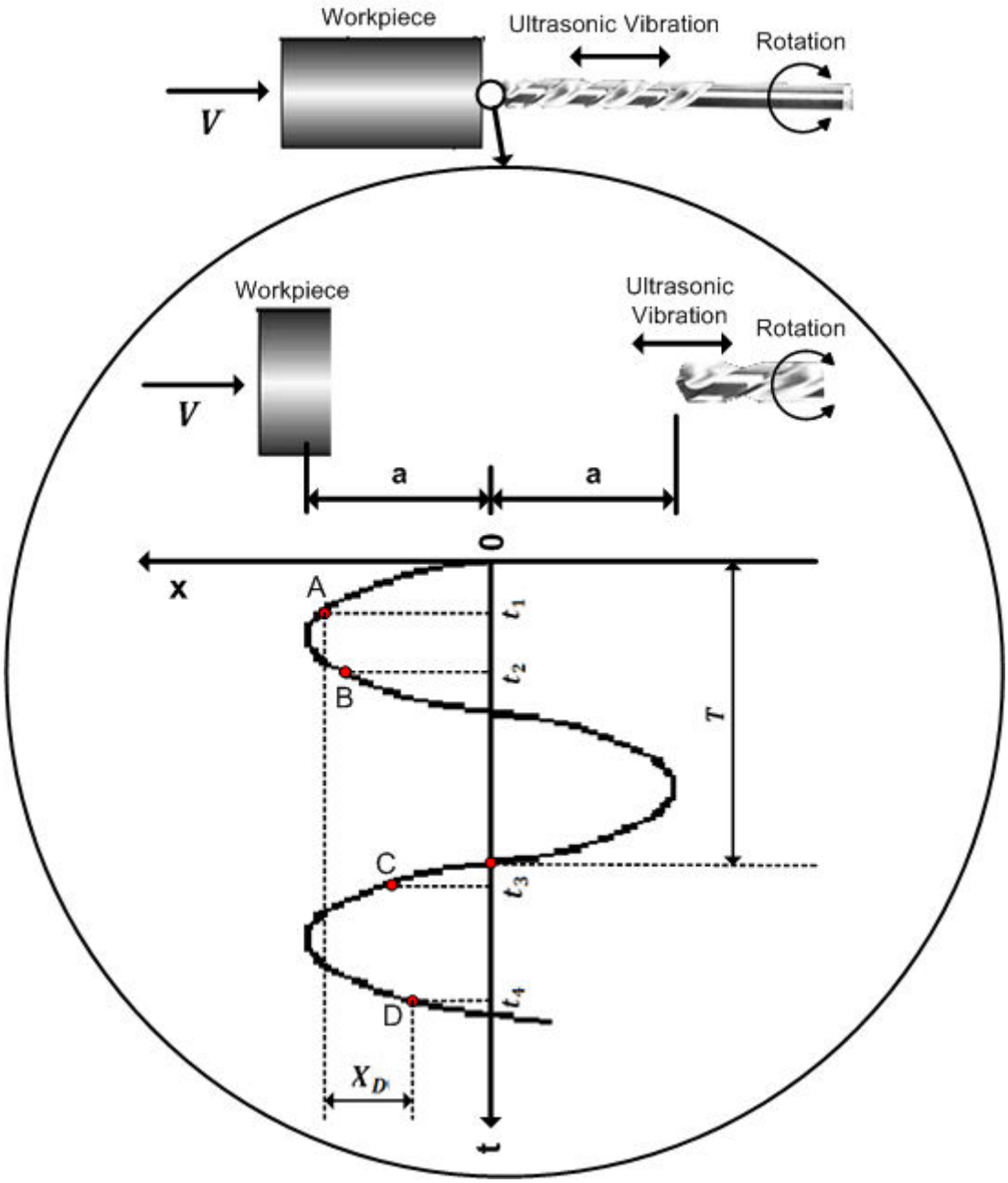

Figure 2.9 : Ultrasonically Assisted Drilling (UAD) mechanism

2.2.4 Ultrasonically Assisted Drilling (UAD) Vibration Direction

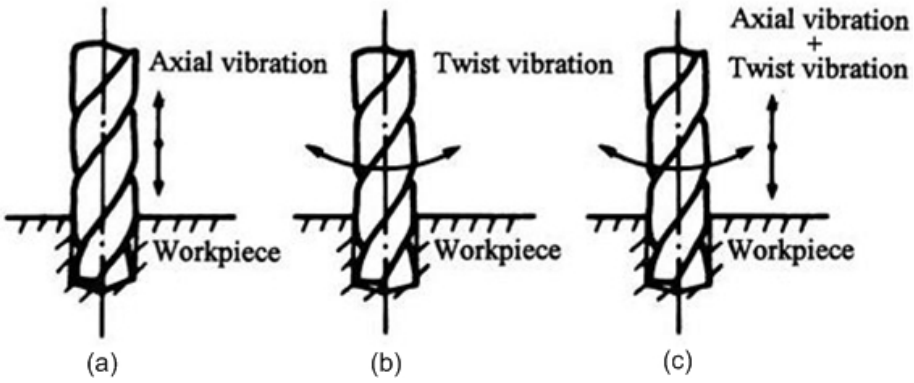

Figure 2.10 : Three possible excitation of drilling vibration: (a) axial excitation, (b) twist (torsional) excitation (c) complex excitation (axial and torsional combination)
Reproduced and Revised From [70]

Another important issue in Ultrasonically Assisted Drilling (UAD) is the vibration excitation direction of a drill bit since it affects the drilled holes quality in terms of surface finish, roughness and roundness etc. In Figure 2.10, three possible vibration excitation directions are demonstrated.

Ultrasonically Assisted Drilling (UAD) could be achieved by applying the excitation of a drill bit vibration twist (torsional) [38,70], axial [27,47,70] or complex (combined torsional vibration and axial vibration) [70]. In many industrial applications the axial excitation takes place most frequently [15] hence will be employed. It also should be noted that the vibration excitation device used in Ultrasonically Assisted Drilling (UAD) is a piezoelectric transducer which consists of piezoceramic rings that can generate axial vibrations shown in Figure 2.10 (a). However, for the torsional vibration generation, it requires different vibration excitation elements also for the combined longitudinal vibration and torsional vibration. As observed in experiments, however, the longitudinal vibration will simultaneously create torsional vibration due to the special geometry of a drill bit. It has been observed from the experiments that with the application of the longitudinal ultrasonic vibration on a drill bit, the torque nearly vanished or sometimes becomes negative in comparison with the Conventional Drilling (CD). This verifies the torsional vibration excitation from longitudinal vibration. In addition, due to the imperfection of the piezoelectric effect (compression and extension in both longitudinal direction and transverse direction), vibration produced from the piezoelectric transducer is not only in axial direction but also slightly in transverse direction

which is strongly undesirable because the lateral vibration will severely worsen the holes finish quality during drilling and sometime damage the drill bit.

2.3 Summary

In this chapter, the description of Conventional Ultrasonic Machining (USM), Rotary Ultrasonic Machining (RUM) and Ultrasonically Assisted Machining (UAM) have been introduced together with their advantages and limitations. Ultrasonically Assisted Machining (UAM) has been widely developed in industrial applications nowadays including Ultrasonically Assisted Turning (UAT) and Ultrasonically Assisted Drilling (UAD).

In addition, the basic working principle of Ultrasonically Assisted Machining (UAM) is explained. Different geometries of waveguides (concentrators) are available and the stepped one shows the maximal amplification therefore is selected to design the ultrasonic transducer. More important issues during Ultrasonically Assisted Drilling (UAD) including mechanism, critical velocity and ultrasonic vibration direction selection are also introduced.

Chapter Three Vibration Control

3.1 Vibration Control Methodology

Traditionally, vibration control refers to Active Vibration Control (AVC) in structures (such as cylinders, pipes and plates etc) which is used to suppress the unwanted vibrations by using an optimal controller such as PID (Proportional Integral Differential) controller, LQR (Linear Quadratic Regulator)/LQG (Linear Quadratic Gaussian) controller, centralized/decentralized gain controller and robust controller etc [30]. During industrial machining processes, undesired vibrations take place frequently such as transverse vibrations in Ultrasonically Assisted Machining (UAM). Such vibrations can damage surface finish quality and holes circularity as well as damage the tool and accelerate machine tool wear. Meanwhile, unwanted vibrations lead to considerable noise pollution. To suppress such vibrations, an active vibration control strategy can be applied. In addition, to suppress the noise, the Active Structural Acoustic Control (ASAC) [30] can be implemented into industrial machining. However, traditional control methodologies have a number of limitations. First of all, traditional control only deals with Linear Time Invariant (LTI) systems. In addition, traditional control methods require considerable amount of power consumption (control efforts) and force a system to function at a designed regime which is against its intention. Furthermore, traditional control methods lack of ability of self-adaption and it is mainly employed to ensure a system's stability which is well known as negative feedback control.

In Ultrasonically Assisted Machining (UAM) process, nonlinearity in frequency-amplitude characteristics will occur due to the vibro-impact nature between a cutting tool and a work piece which suggest an employment of autoresonant control strategy. Being different from the traditional control methodologies, autoresonant control employs the phase-amplitude characteristic of an ultrasonic vibrating system and effectively controls the phase. This phase-amplitude characteristic remains linear even under vibro-impact response. Hence, vibro-impact induced nonlinearity problem can be tackled easily with autoresonance. In addition, autoresonance allows an ultrasonic vibrating system to adapt itself under variant applied load conditions rather than forces it to function. Furthermore, autoresonance normally requires less power than traditional control however achieves a higher efficiency. Autoresonance is devoted to the excitation and maintenance of desired level of ultrasonic vibrations during machining. In other words, it is to keep the ultrasonic vibration amplitude at tip of a cutting

tool to allow it to work at the most efficient state. Obviously, a successful application of autoresonant control during Ultrasonically Assisted Drilling (UAD) brings in a number of benefits including the possibility to machine difficult to cut materials such as hardened steels, nickel-based alloys, titanium and aluminium metal matrix composited [40], exhibition of a considerable decrease in cutting forces and tool wear as well as production of shorter chips [67] and improve surface roughness and roundness.

The application of autoresonant control allows the realisation of the vibration control in Ultrasonically Assisted Machining (UAM) process. Autoresonant control is to keep the ultrasonic vibration amplitude on a tool tip at a desired level so that an ultrasonic transducer can work at resonance regardless of the machining condition (idle or loaded). In other words, autoresonant control ensures that the excitation energy is expended only to overcome an active load of the operating process and dissipative forces leading to the actuation energy being used in the most efficient way [7]. However, during practical applications, autoresonant control encounters a number of difficulties. Several factors of an ultrasonic vibrating system need to be taken into account to design an autoresonant control system properly, such as Q factor, characteristics including frequency-amplitude, amplitude-phase and frequency-phase, proper sensor selections, feedback control strategy etc.

3.2 Quality Factor of Ultrasonic Vibrating System

Quality factor also called Q factor is a dimensionless parameter used to describe how under-damped an oscillator or resonator [34] is or equivalently, characterise a resonator's bandwidth relative to its centre of frequency [66]. This parameter is widely employed in physics and engineering field. A high Q factor oscillation system indicates a lower rate of energy loss relative to the stored energy. In contrast, a low Q factor system's energy dies out faster relative to the stored energy. In Figure 3.1 frequency-amplitude characteristic for a linear vibrating system is demonstrated, f_0 represents the resonant frequency with magnitude A_{max}, f_1 and f_2 are frequency points corresponding to the half power (0.707 maximum magnitude). The bandwidth of the frequency-amplitude characteristic is then defined as $\Delta f = f_2 - f_1$. The Q factor hence can be calculated:

$$Q = \frac{f_0}{\Delta f} = \frac{f_0}{f_2 - f_1} \tag{3.1}$$

If a system has a high Q factor then it means the frequency-amplitude characteristic is sharp at peak and the bandwidth is narrow, and vice versa. A Q factor value determines the sensitivity of a vibrating system to the variation in the change of the excitation frequency; the higher a value is the more sensitive a system reacts. In order to achieve the most efficient operation state, resonant modes of a vibrating system should be used. In order to maintain the ultrasonic vibration at peak, frequency control is employed.

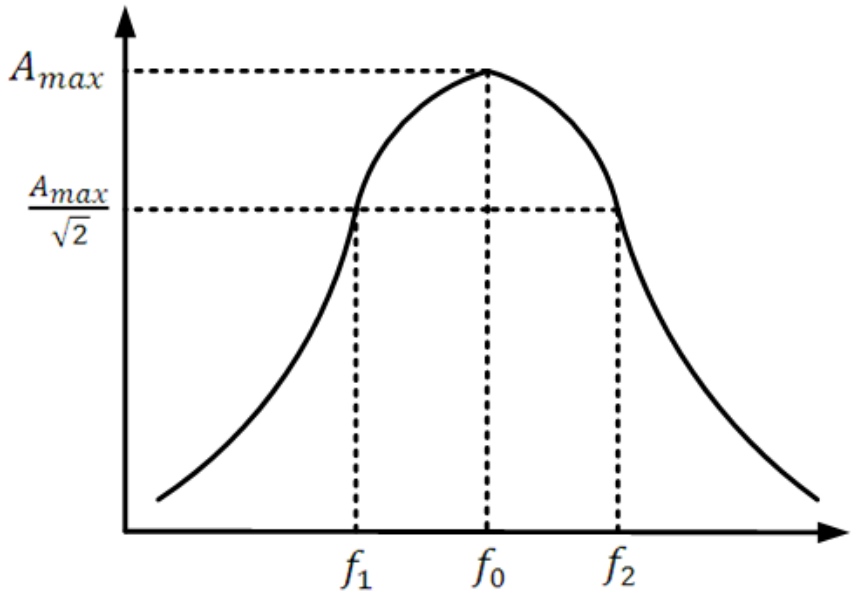

Figure 3.1 : Amplitude-frequency characteristic as a demonstration of Q factor

3.3 Frequency Control of Ultrasonic Vibrating System

A method to maintain a vibrating system's resonance is to adjust its excitation frequency. Normally if a synchronous actuator is employed for a forced excitation, both amplitude A and frequency ω can be tuned respectively and independently in order to enable the vibrating system to work consistently [60]. This is illustrated in Figure 3.2. However, systems with high-Q factors tend to react sensitively to any slight change in the excitation frequency. Therefore, an oscillating system that is sensitive to the applied load will lead to efficiency loss when a load varies or with attachment of different cutting tools [16].

Resonance following generators can be used to automatically adjust the output high frequency to match the exact resonance of an ultrasonic vibrating system, these resonance following generators can also accommodate any small error in setup and tool wear, giving minimum acoustic energy loss and very small heat generation [33]. The working principle of

the resonance following generators is based on minimising the phase difference between voltage and current of the power supply to an ultrasonic transducer [68]. However, drawbacks of such generators appear when an ultrasonic vibrating system suffers from nonlinearity due to vibro-impact. In this case the magnitude response of the system demonstrates ambiguity and jumps at certain frequencies close to the resonance, which makes it difficult to maintain the peak performance. Theoretically, the actual steady state of an ultrasonic vibrating system with frequency control is determined by the history of control, but in no case, can the point of the optimal performance be reached [6]. Therefore, a fixed-frequency or even resonance following generator is insufficient to achieve peak performance, especially for high Q factor vibrating systems.

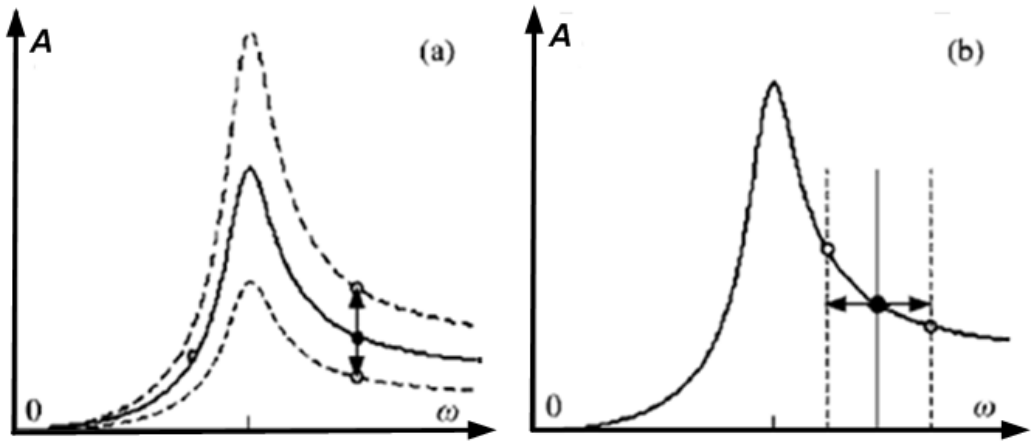

Figure 3.2 : Amplitude and frequency control : (a) amplitude control (b) frequency control Reproduced and Revised From [60]

3.3.1 Vibro-Impact Induced Nonlinearity Nature of Ultrasonic Vibrating System

Ultrasonic vibration is upgraded to a more complicated level when vibro-impact is introduced. Vibro-impact means during ultrasonic machining applications, tools contact the work piece with periodic impacts. In other words, vibro-impact effect has some impulsive property. This effect can significantly change an ultrasonic vibration system's natural frequency and the characteristics of its amplitude-frequency response [7].

Distortion of amplitude-frequency characteristic from a linear system to a nonlinear system is shown in Figure 3.3. Plot (a) presents a hardening nonlinearity that natural frequency increases as vibration amplitude rises. In comparison, picture (b) shows a softening

nonlinearity in which the natural frequency declines as the vibration amplitude increases. The curve line which follows the natural frequency of the vibration system is called the backbone [8]. Hardening nonlinearities generally happen when an additional elastic restoring force is applied to an ultrasonic vibration system. In contrast, a softening nonlinearity occurs when plastic deformation takes place. During Ultrasonically Assisted Machining (UAM) process, hardening nonlinearities happen due to elastic impacts, and softening nonlinearities take place owing to plastic work piece deformation [64]. Another notable point in Figure 3.3 is one frequency corresponds to several vibration amplitudes near the backbone region. Consequently, the direction in which the excitation frequency changes will determine the path (branch) an amplitude-frequency curve follows.

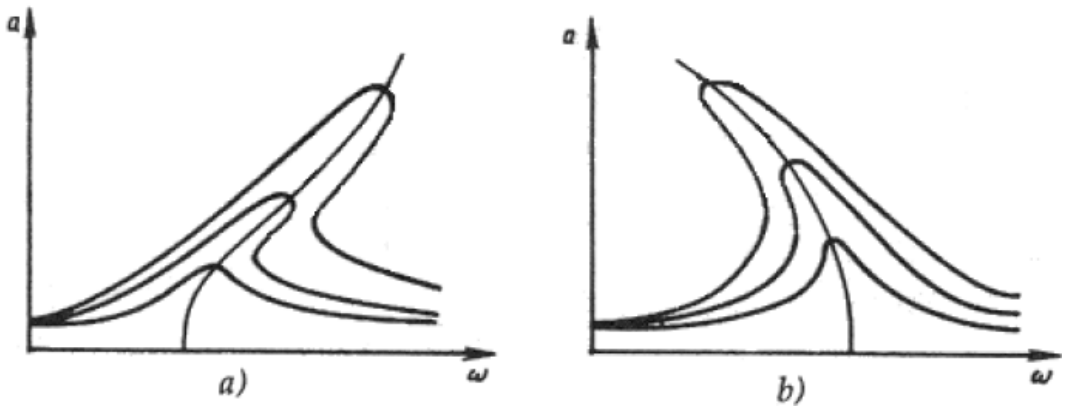

Figure 3.3 : Amplitude-frequency characteristic with nonlinearity

Reproduced From [7]

If the excitation frequency is increased or decreased gradually along one of the amplitude-frequency curves in (a) or (b) in Figure 3.3, the 'jump phenomenon' will occur which will complicate the process. 'Jump phenomenon' happens in amplitude-frequency curve illustrated in Figure 3.4 which is a typical form of the hardening nonlinearity. In the beginning, the excitation frequency continuously increases and the amplitude rises simultaneously along the upper branch of the curve until it arrives at the furthermost point B. Any slight increase in frequency will give rise to a jump of magnitude of a steady-state regime to this frequency's corresponding value on the lower branch of the curve (downward dashed arrows). Further increase in the excitation frequency results in a decrease in amplitude to a lower level. However, if the frequency is reduced from point C, system will not return directly to the resonance, but will take the lower path of the curve and climb from point D to

point A (upwards dashed arrows). Further decrease in the excitation frequency will decrease the vibration amplitude.

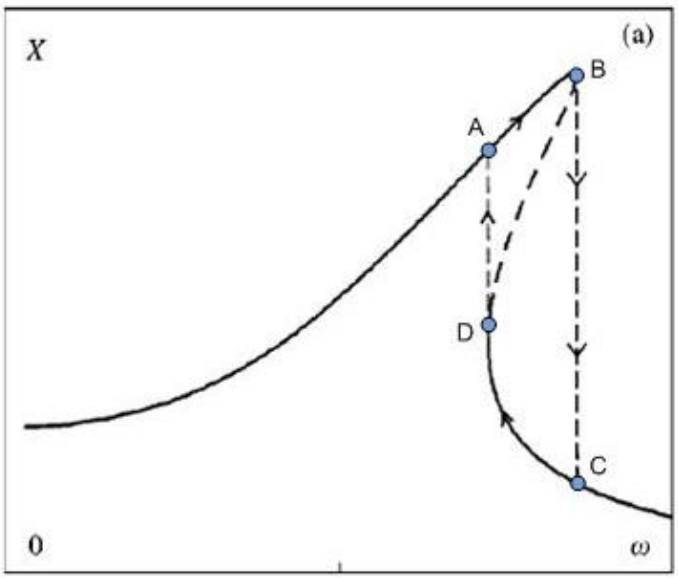

Figure 3.4 : Jump phenomenon illustration

Reproduced and Revised from [60]

It should be noted there is an additional path in Figure 3.4 depicted in dashed curve DB (ambiguity). This dashed curve is the analytically predicted response of the system. It indicates although the path theoretically fulfils the steady state vibration regime, it is unstable and physically unreachable during experiment. Ultrasonic cutting processes are strongly nonlinear especially at high feed rates due to vibro-impact nature. For this reason, when employing frequency control, an ultrasonic vibrating system's optimal performance can never be reached [6].

3.3.2 Phase Control of Ultrasonic Vibrating System

The nature of the vibro-impact response between a tool and a work piece makes frequency control or even resonance following generator insufficient to keep the ultrasonic vibration at resonance. In order to overcome this problem, phase control is employed. The concept of phase control is to control the ultrasonic vibration by means of changing the phase shift between the exciting force and the vibrating system response [60], i.e. changing the phase shift between the input and the output of an ultrasonic vibrating system. For a single-degree-of-freedom system or a simplest two-degree-of-freedom system, resonant regime takes place

when the force is in phase with vibratory velocity (or lags $3\pi/2$ in phase from vibratory displacement), this control system is then designed as an autoresonant system [7,11]. Such a system maintains the resonant regime of oscillations when the natural frequency of a mechanical subsystem changes, as the phase shift changes, the regime of the oscillations (amplitude, frequency) also changes. But basically, amplitude-phase curves determine the system's behaviour when phase shift changes purposely or accidentally [60]. These curves play a same role in phase-controlled systems as traditional resonance curves play in frequency-controlled systems. In Figure 3.5, a 3-D amplitude-phase-frequency characteristic of a single-degree-of-freedom vibrating system is presented together with the projections. It should be noted it is a vibrating system without an external load. Another notable point is that in comparison with the amplitude-frequency characteristic which has a sharp peak at resonance, the amplitude-phase characteristic presents a plainer and gently sloping response around resonance.

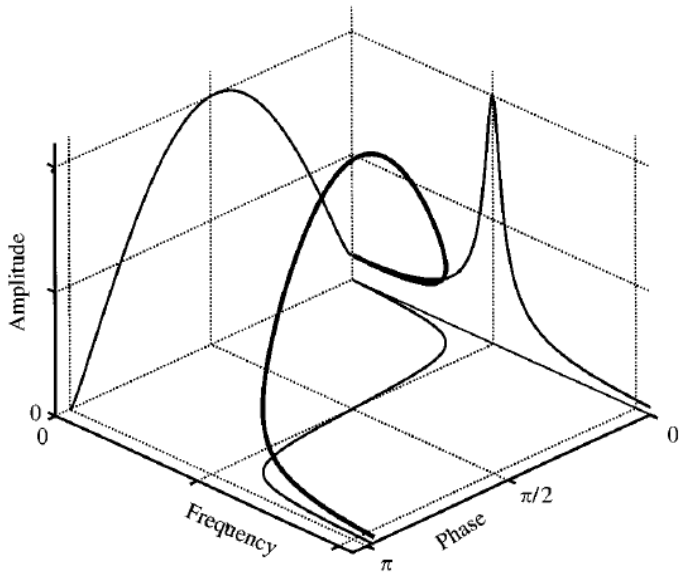

Figure 3.5 : A 3-D amplitude-phase-frequency curve for a single-degree-of-freedom linear vibrating system

Reproduced From [60]

When the ultrasonic vibrating system starts vibro-impact, the amplitude-phase-frequency characteristics of the system will be inevitably altered. In Figure 3.6, the amplitude-phase-frequency characteristics of a single-degree-of-freedom vibrating system with vibro-impact response has been illustrated with projections. Obviously, in the amplitude-frequency characteristic, nonlinearity occurs with 'jump phenomenon'. Due to the nonlinearity of the

amplitude-frequency characteristic, it is difficult to apply frequency control or use resonance following generators. However, even though vibro-impact changes the amplitude-frequency characteristic drastically, the amplitude-phase characteristic remains flat and gently sloping near resonance. In other words, a slight change in the amplitude-phase characteristic will not significantly influence vibration amplitude which indicates phase control method could be effectively employed in vibro-impact induced vibrating systems.

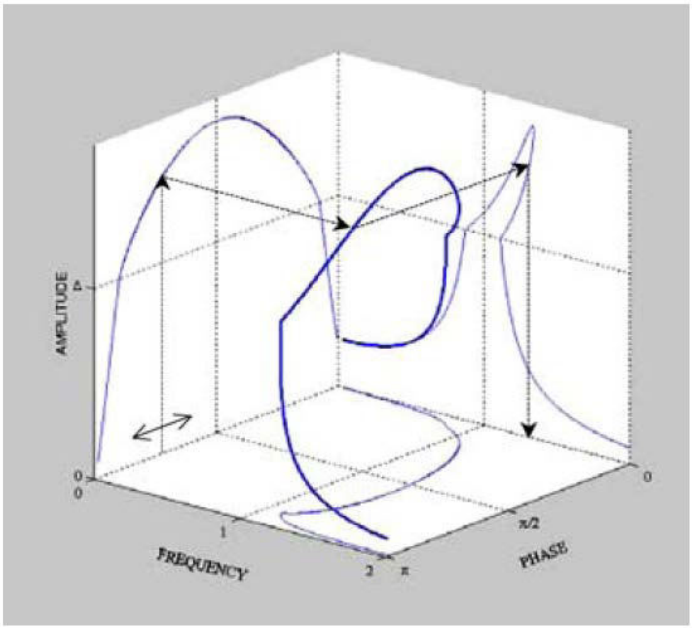

Figure 3.6 : A 3-D amplitude-phase-frequency curve for a single-degree-freedom vibro-impact system

Reproduced From [18]

The phase control technique has been illustrated in Figure 1.6. Apparently, in comparison with the amplitude-frequency response with a sharp peak and non-single-valued feature, the amplitude-phase characteristic shows a smooth and flat peak near resonance as well as its single-valued property. Furthermore, all points on the amplitude-phase characteristic correspond to the stable regimes of vibration [60]. Phase control technique is the essential part of autoresonant control.

3.3.3 Autoresonant Control of Ultrasonic Vibrating System

The fundamental principle of autoresonant control is to maintain the resonant regime of oscillations automatically by means of positive feedback using phase shift and amplification

of a signal obtained from a performance sensor. The idea is that during resonance the phase lag between the vibration of a drill bit and the excitation force applied to an ultrasonic transducer remains constant [67]. Figure 3.7 illustrates the autoresonant control process. In comparison with the traditional forced excitation with a prescribed frequency, autoresonant excitation forms the excitation force by means of positive feedback based on the transformation of either displacement/velocity/acceleration, current or power obtained from a performance sensor. The feedback shifts the phase of the feedback signal from the sensor and amplifies its power, and then the powerful signal feeds a synchronous actuator/motor which transforms it into an excitation force. In the feedback loop, there is an additional mechanism for the limitation of the excitation force, after this the synchronous actuator transforms the alternating signal to an alternating excitation force with an exactly same frequency and a predictable phase shift [18].

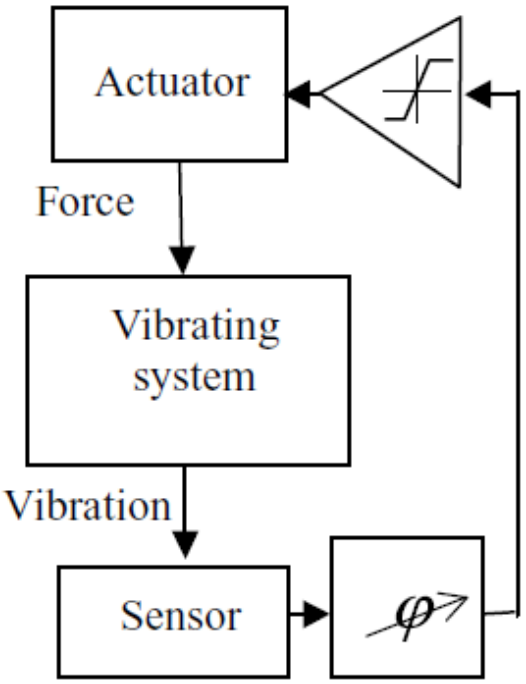

Figure 3.7 : Schematic diagram of autoresonant control

Reproduced From [18]

Autoresonant control provides a possibility of self-tuning and self-adaptation mechanisms for a system to keep the nonlinear resonant mode of oscillation under unpredictable variation of load, structure and parameters which allows a simple regulation of intensity of the process whilst keeping a maximum efficiency at all times [14]. Amplitude-phase characteristic of an ultrasonic vibrating system determines a proper design of an autoresonant control system. In

autoresonant control, positive feedback and negative are combined. Positive feedback often leads a system to exponential divergences or the exponential growth of oscillations. In other words, a system exhibiting positive feedback, in response to external perturbation, acts to increase the magnitude of the perturbation. Consequently, under positive feedback and a lack of stabilising forces, systems will typically accelerate towards a nonlinear region which may stabilise the system or conversely destroy it. In spite of such a risk, autoresonant control system still uses positive feedback so as to generate a self-oscillation for an ultrasonic transducer. Instability as a result of excitation of ultrasonic vibrations in an autoresonant system will be produced by the positive feedback. In this case, positive feedback enables the ultrasonic vibrating system to freely oscillate at its natural frequency. To prevent the possibility of system damage caused by the positive feedback, a limiter is added to the positive feedback loop which acts as a negative feedback. Negative feedback is dedicated to the control of a system's stability, accelerate transient response to steady state response and alleviate the system's sensitivity.

3.4 Autoresonant Control Strategy

Autoresonant control can effectively maintain an ultrasonic vibrating system at a resonance regime by controlling the phase shift and amplification of signal measured by a performance sensor by means of positive feedback. The efficiency and accuracy of a sensor which is shown in Figure 3.7 therefore plays an important role in autoresonant control design. A sensor is a device that measures a physical quantity and converts it into a signal which can be read by an observer or by an instrument. There are various sensors for different engineering fields. For the ultrasonically assisted drilling process, the types of sensors available in measuring ultrasonic vibration are:

- Laser vibrometer
- Accelerometer
- Ultrasonic microphone
- Inductive sensor
- Current sensor
- Power sensor

A laser vibrometer is a precise instrument provided with remote operation, but it is an expensive instrument and not intended for use within an industrial environment [16]. In addition, a laser vibrometer gathers ultrasonic vibration information through reflecting and receiving a signal from a reflection film, due to the rotary motion of the ultrasonic transducer in Ultrasonically Assisted Drilling (UAD), it is impractical to employ a laser vibrometer. A standard instrumental accelerometer, as found during trials, suffered permanent damage and would not withstand the prolonged and high level of vibration necessary for Ultrasonic Machining (USM) [16]. There are also some problems with its permanent fixture to the ultrasonic transducer as well as its influence on a drill bit's performance during machining. An accelerometer is not desirable of use in the Ultrasonically Assisted Drilling (UAD) [16]. In the case of an ultrasonic microphone, the sensor not only measures the ultrasonic vibration but also absorbs noises. The measurement is inaccurate and it has been proved that noise power is not equivalent to vibration amplitude, especially at particular frequencies. Furthermore, the necessity for additional wiring to the control system for the ultrasonic microphone makes it infeasible for industrial use [16]. An inductive sensor also called a magnetic sensor is an electronic proximity sensor, which detects the metallic objects without touching them. The magnetic sensor consists of an induction loop, an alternating current generates a magnetic field which collapses generating a current falls asymptotically toward zero from its initial level when the input electricity ceases. Such a sensor needs to be calibrated before measurements. An inductive sensor is suitable for industrial application therefore will be considered in Ultrasonically Assisted Drilling (UAD). A current sensor is a sensor used to measure the current signal flowing through a piezoelectric transducer and a power sensor is a sensor used to calculate the instantaneous power supplied to a piezoelectric transducer.

The advantage of a mechanical sensor is that it reflects the ultrasonic vibration directly from the cutting zone which provides the opportunity of direct detecting and control. However, normally a mechanical sensor has a high price or needs calibration. In comparison, the advantages of an electrical sensor are its low cost and the possibility of remote operation. However, sensor output reflects the oscillation and efficiency of an ultrasonic vibrating system only in an indirect way. However, due to the advantages electrical sensors will be used. According to the choice of sensors, positive feedback loop in autoresonant control can be generally classified into:

- Mechanical Feedback

  Mechanical feedback employs a mechanical sensor which might be a laser vibrometer, an accelerometer, an ultrasonic microphone or an inductive sensor. Such a sensor measures the mechanical vibration directly.

- Electrical Feedback

  Electrical feedback uses electrical sensors: either a current sensor or a power sensor. Electrical sensors detects the electrical properties of an ultrasonic vibrating system therefore reflects the mechanical vibrations indirectly.

Two types of feedback have their advantages and drawbacks. Electrical feedback sensors are cheaper and their possibility of remote operation is suitable for industrial applications. However, electrical feedback sensors can only measure the mechanical vibrations in an indirect way. In contrary, mechanical feedback sensors detect the ultrasonic vibrations directly from the cutting zone, which provides a direct access to autoresonant control design. In spite of such advantages, mechanical feedback sensors are difficult to be properly fixed in harsh machining conditions and the cost is relatively high. In comparison, electrical feedback sensors are easier to be installed on an ultrasonic transducer and their costs are low.

In addition to a proper sensor selection, other designs such as filters design, amplifier design and limiter design need to be investigated as well. The detailed investigation and comparison between mechanical feedback and electrical feedback on Ultrasonically Assisted Drilling (UAD) are the main task of the project which will be discussed in details in numerical simulation and experiments. A reliable numerical model establishment of an ultrasonic transducer is necessary for autoresonant control design.

3.5 Summary

In this chapter, the possible vibration control methodologies have been introduced. High Q factor values in an ultrasonic vibrating system complicate the control design. However, this can be solved by frequency control method or advanced resonance following generators. Despite such success, the control design is further complicated due to the occurrence of the nonlinearity caused by the vibro-impact nature between a cutting tool and a work piece. The idea of employing the amplitude-phase characteristic in control design will effectively

resolve the ‘jump phenomenon’ and maintain the nonlinear oscillating mode of the ultrasonic vibrating system at the resonance regime. Depending on the sensor selections, mechanical feedback control and electrical feedback control are available which will be implemented and compared in numerical simulations and experiments.

Chapter Four Ultrasonic Vibration System Model

In order to create an efficient and effective autoresonant control system, the establishment of an accurate and simple model to simulate the electromechanical ultrasonic transducer seems crucial. The created model should reflect the features of the electromechanical ultrasonic transducer used in experiments. In literature review, a number of papers are dedicated to the modelling of electromechanical ultrasonic transducers. Unsurprisingly, most descriptions focus on Finite Element Modelling (FEM) [1]. One-dimensional numerical models with nonlinear impact have hardly been investigated. In comparison with Finite Element Modelling (FEM), a simple numerical simulation model provides a faster and easier access to the analysis of an ultrasonic transducer's dynamics and reveals the property of an ultrasonic vibrating system [68]. An autoresonant control system design seems more feasible to be executed on a simple one-dimensional numerical model rather than a complicated FEM model.

This chapter mainly follows the numerical simulation procedures described in [68] together with more thorough investigations. Modelling of the ultrasonic vibrating system in one-dimensional has been presented. Furthermore, parameters calculation for the created model will be included. In the end, vibro-impact model parameters are computed. The simulation results have been verified through experiments on an electromechanical transducer. In Figure 4.1, the transformation from an electromechanical ultrasonic transducer to a 2-DOF model is illustrated. The length of the back section equals a quarter of the wavelength of the ultrasound used and the concentrator has length of three quarters of it. As a result, the transducer has two nodal points: in position of piezorings and between two steps of the concentrator. Due to the existence of the physical nodal point at the piezorings (actuation elements), the back section has been removed during simulation (b). Due to another physical nodal point exists between the 1^{st} step and the 2^{nd} step (which will be proved numerically and experimentally) concentrator, the connection point has been clamped.

Theoretically, a 2-DOF model (c) is sufficient to replace an electromechanical ultrasonic transducer. It represents two experimentally active oscillation modes with two corresponding resonant frequencies. The 1^{st} resonant frequency corresponds to the 1^{st} step and 2^{nd} step concentrator vibrate in same phase. The 2^{nd} resonant frequency shows the 1^{st} step and 2^{nd} step concentrator vibrate in anti-phase. It should be noted that the 2-DOF model shown in (c)

excludes a drill bit due to the complexity that it creates during Ultrasonic Machining (USM). In other words, the 2-DOF model only represents the replacement of an electromechanical ultrasonic transducer itself. Briefly speaking, the 2-DOF system consists of two parts:

- A piezoelectric transducer model
- A 2-step concentrator model shown as two mass-spring-damper sets

Provided the information above, the next step is to calculate the parameters for both the piezoelectric transducer model and the 2-step concentrator model according to the known dimensions and experimental measurements.

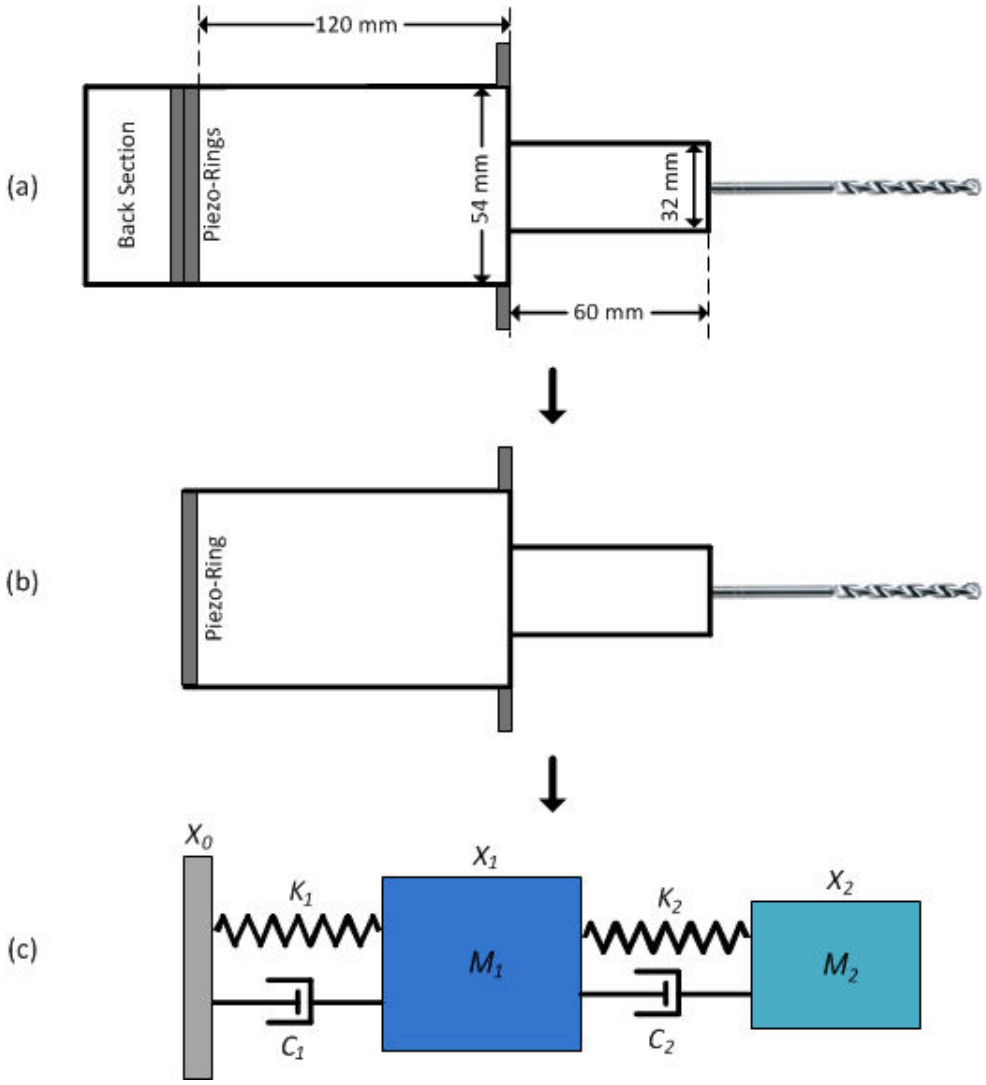

Figure 4.1 : Structure and modelling of an electromechanical ultrasonic transducer: (a) ultrasonic transducer dimensions, (b) transformation of ultrasonic transducer, (c) a 2-DOF model as a placement of ultrasonic transducer

4.1 2-DOF Concentrator Model

In this section, the parameters calculation of the 2-step concentrator will be performed, following the method described in [68], eigenvalues-eigenvectors and the energy conservation law will be used.

4.1.1 Computation of Oscillation Modes and Natural Frequencies of 2-DOF Concentrator Model

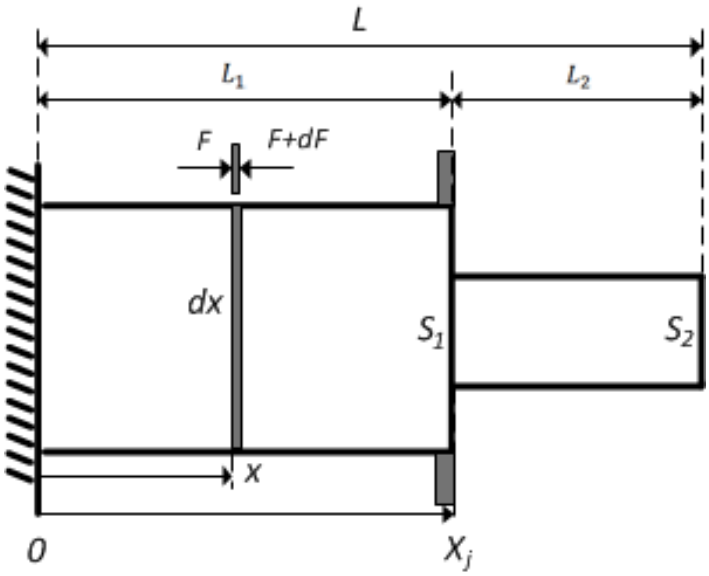

Figure 4.2 : 2-step concentrator structure

The concentrator used is a 2-step aluminium alloy concentric bar with different cross-sectional areas. Figure 4.2 shows the structures and dynamic motion of the 2-step concentrator. Coordinate at the connection between the 1st step and 2nd step is x_j, S_1 and S_2 represent the 1st and 2nd step cross-sectional areas. L_1 and L_2 are the length of the 1st step and 2nd step concentrators. L is the entire length of the 2-step concentrator. The piezoelectric plate is temporarily removed and the left end is considered immovable. In the following sections, the 2-step concentrator model dynamics will be analysed.

Longitudinal waves are characterised by a particle motion which is parallel to the direction of propagation [30]. In order to obtain the differential motion equation of the longitudinal vibration, a small arbitrary section dx is manually defined which is shown in Figure 4.2. The displacement at coordinate x is $D(x,t)$. Applying the Newton second law to this small arbitrary section dx gives:

$$ma = \Delta F \tag{4.1}$$

m represents the mass of the small arbitrary section dx and a is the acceleration produced by the force difference ΔF over section dx. Mass, acceleration and force difference are calculated:

$$m = \rho S_1 dx \tag{4.2}$$

$$a = \frac{\partial^2 D(x,t)}{\partial t^2} \tag{4.3}$$

$$\Delta F = F + dF - F = dF \tag{4.4}$$

ρ is the material density, F is the force at the cross-section x, hence the strain in the concentrator equals [30]:

$$\varepsilon = \frac{\partial D(x,t)}{\partial x} \tag{4.5}$$

Thereafter, the expression of the force F can be further transformed into:

$$F = ES_1\varepsilon = ES_1 \frac{\partial D(x,t)}{\partial x} \tag{4.6}$$

Where E is Young's modulus. As a result, the force difference over the arbitrary section dx becomes:

$$\Delta F = dF = \left[ES_1 \frac{\partial D(x,t)}{\partial x}\right]' dx = ES_1 \frac{\partial^2 \mathrm{D}(x,\mathrm{t})}{\partial x^2} dx \tag{4.7}$$

Combining equation (4.1), (4.2), (4.3) and (4.7), the following motion equation is derived:

$$\rho \frac{\partial^2 \mathrm{D}(x,\mathrm{t})}{\partial t^2} = E \frac{\partial^2 D(x,t)}{\partial x^2} \tag{4.8}$$

Due to the fact that the concentrator has 2-step, equation (4.8) can be transformed into the following form:

$$\rho \frac{\partial^2 D_i(x,t)}{\partial t^2} = E \frac{\partial^2 D_i(x,t)}{\partial x^2} \tag{4.9}$$

Where the subscript $i = 1,2$ represents the step. Assuming the bar vibrates harmonically without any distortions, the displacement of the arbitrary section dx has an expression $D(x,t) = D(x)sin\omega t$. Therefore, equation (4.9) can be revised:

$$\frac{d^2 D_i(x)}{dx^2} + \frac{\rho\omega^2}{E} D_i(x) = 0 \tag{4.10}$$

Observing the 2nd order dynamic differential equation (4.10), a general solution of the 1st step concentrator ($0 < x \leq x_j$) is defined as:

$$D_1\,(x) = A_1 \sin(kx) + A_2 \cos(kx) \tag{4.11}$$

In equation (4.11), A_1 and A_2 are the vibration amplitudes. k stands for the wavenumber of the longitudinal vibration which is:

$$k = \sqrt{\frac{\rho\omega^2}{E}} \tag{4.12}$$

Since the concentrator is fixed at the left end, the boundary condition of the 1st step is:

$$D_1|_{x=0} = 0 \tag{4.13}$$

Substituting the boundary condition (4.13) into equation (4.11) gives $A_2 = 0$; therefore, the displacement of the 1st step concentrator is:

$$D_1(x) = Asin(kx) \tag{4.14}$$

Where $A = A_1$. Similarly, the general solution of equation (4.10) for the 2nd step ($x_j \leq x \leq L$) concentrator is:

$$D_2(x) = B_1 \sin(kx) + B_2 \cos(kx) \tag{4.15}$$

Where B_1 and B_2 are the amplitudes and k is the wavenumber shown in equation (4.12). Due to the fact that the right end of the concentrator vibrates freely, the boundary condition of the 2nd step concentrator is:

$$\left.\frac{dD_2}{dx}\right|_{x=L} = 0 \tag{4.16}$$

Consequently, the expression of the displacement of the 2nd step concentrator can be obtained (detailed derivation from equation (4.16) to equation (4.17) can be found in Appendix II):

$$D_2(x) = Bcos[k(x-L)] \tag{4.17}$$

Where $B = \frac{B_1}{\sin(kL)}$.

Figure 4.3 illustrates the oscillation mode excited by the 2nd resonant frequency of the 2-step concentrator (1st step and 2nd step concentrator vibrate in anti-phase). It can be observed that the vibration amplitude reaches 0 at the 1st and 2nd step connection point x_j (detailed derivation and proof can be found in Appendix II). In other words, point x_j is found to be the vibration nodal point at the resonant frequency in experiment when 1st step and 2nd step concentrator vibrate in anti-phase. On each structure, there are areas or points that have zero-displacement at resonance and these are recognized as nodal points [56]. Nodal point locations are determined by a system's property and resonant frequency rather than a point that is externally clamped or fixed, since the longitudinal wave can propagate in the structure which enables the vibrations to flow internally therefore makes the fixed point vibrations non-zero.

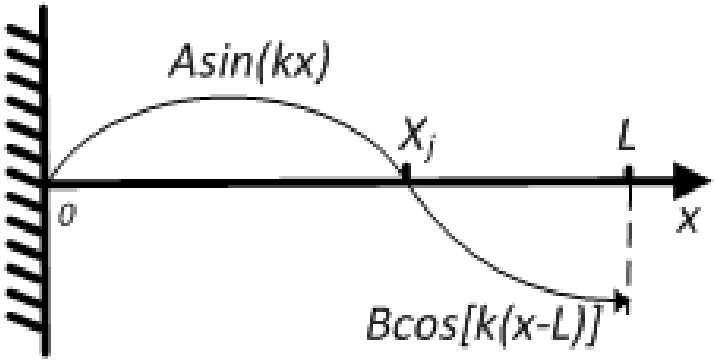

Figure 4.3 : Possible vibration mode of the 2-step concentrator

The nodal point of the 2-step concentrator is experimentally found to be located at the connection point between the 1st step and 2nd step concentrator at resonance (when 1st step and 2nd step concentrator vibrate in anti-phase, experimental proof will be shown later). At the end of the 2nd step concentrator, the vibration amplitude is expected to reach its maximum which will also be experimentally proved. Taking equation (4.14) and (4.17) into account, the longitudinal vibration equations of the 2-step concentrator are:

$$D(x) = \begin{cases} Asin(kx) & 0 < x < x_j \\ Bcos[k(x-L)] & x_j < x < L \end{cases} \tag{4.18}$$

In order to explore the relation between the 1st and 2nd step vibration magnitudes A and B, another equation implies the equality of both steps at the connection point x_j can be written:

$$D_1|_{x=x_j} = D_2|_{x=x_j} \tag{4.19}$$

Substituting this equation into the expression of D_1 in equation (4.14) and D_2 in equation (4.17) gives:

$$Asin(kx_j) = Bcos[k(x_j - L)] \tag{4.20}$$

To search for another relation between A and B, another equality can be employed. At the connection point between the 1st and 2nd step concentrator, the reciprocal force acting on the cross-section is equivalent for both steps:

$$S_1\sigma_1 = S_2\sigma_2 \tag{4.21}$$

Taking the relation of stress and strain $\sigma = E\varepsilon$ into account and assuming the vibration is within the elastic region, the following equation can be derived:

$$\left.\frac{\partial D_2}{\partial x}\right|_{x=x_j} = \frac{S_1}{S_2}\left.\frac{\partial D_1}{\partial x}\right|_{x=x_j} \tag{4.22}$$

By replacing the expression of the displacement $D_1(x)$ in equation (4.14) and $D_2(x)$ in equation (4.17) into equation (4.22) produces another relationship between A and B:

$$-Bsin[k(x_j - L)] = \frac{S_1}{S_2} Acos(kx_j) \tag{4.23}$$

Hence the combination of equation (4.20) with equation (4.23) generates an expression of the distributed parameters model of the 2-step concentrator shown in Figure 4.2:

$$\tan(kx_j)\tan[k(x_j - L)] = -\frac{S_1}{S_2} \tag{4.24}$$

In Table 4.1, the dimensions and material parameters of the 2-step concentrator are illustrated. R_1 and R_2 are the radius of the 1st step and 2nd step concentrator. Using the parameter values shown in Table 4.1, a graphical solution to equation (4.24) can be calculated and shown in Figure 4.4. As can be seen, the red dashed straight line represents the right side value and blue solid curve shows the left side value of equation (4.24). Taking the wavenumber shown in equation (4.12) into account, the natural frequencies of the 2-step distributed parameter model can be calculated:

$$\begin{aligned} f_1 &= 8.8KHz \\ f_2 &= 21.3KHz \end{aligned} \tag{4.25}$$

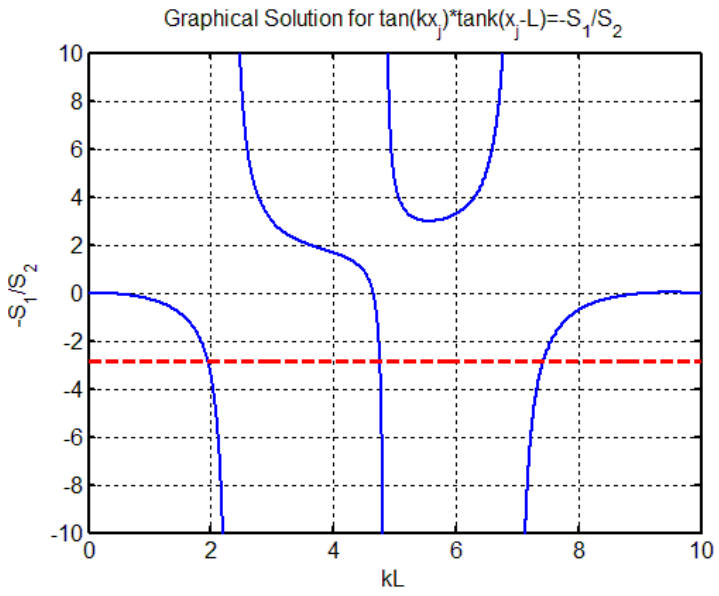

Figure 4.4 : Graphical solution for $tankx_j tank(x_j - L) = -\frac{S_1}{S_2}$

$f_2 = 21.3KHz$ has been chosen as the working frequency for the numerical model creation as it is in the range of ultrasonic frequency (nominally over $20KHz$) as well as the only solution

allows the 1st step and 2nd step concentrators to oscillate in anti-phase (which will be proved later) and this is normally used in practice.

Table 4.1 : Dimensions and material parameters of the 2-step concentrator

Variable	$R_1(m)$	$R_2(m)$	$L_1(m)$	$L_2(m)$	$L(m)$
Value	0.027	0.016	0.12	0.06	0.18
Variable	x_j	$E(N/m^2)$	$\rho(kg/m^3)$	$S_1(m^2)$	$S_2(m^2)$
Value	$0.67L$	0.7×10^{11}	2.7×10^3	0.0023	0.0008

4.1.2 Experimental Verification and Comparison of Oscillation Modes and Natural Frequencies of 2-DOF Model

In order to verify the accuracy of the calculated resonant frequencies shown in (4.25), experiments on a 2-step electromechanical transducer have been executed. Experimental setup is shown in Figure 4.5. Experiments indicated the nodal point was located at the connection between the 1st and 2nd step concentrator. Therefore, the connection point was clamped by an aluminium tube with 8 bolts uniformly and the tube was fixed tightly to the lathe. This ensures the energy propagation within the electromechanical ultrasonic transducer the most efficient. The ultrasonic vibration signal was captured by a laser vibrometer (Manufactured in Polytec Germany, OFV 512 & OFV 3001) and then transferred into a PicoScope (PicoScope 4424 with bandwidth $20MHz$, details in [82]) for data analysis. Frequency-amplitude characteristic over a frequency range is shown in Figure 4.6.

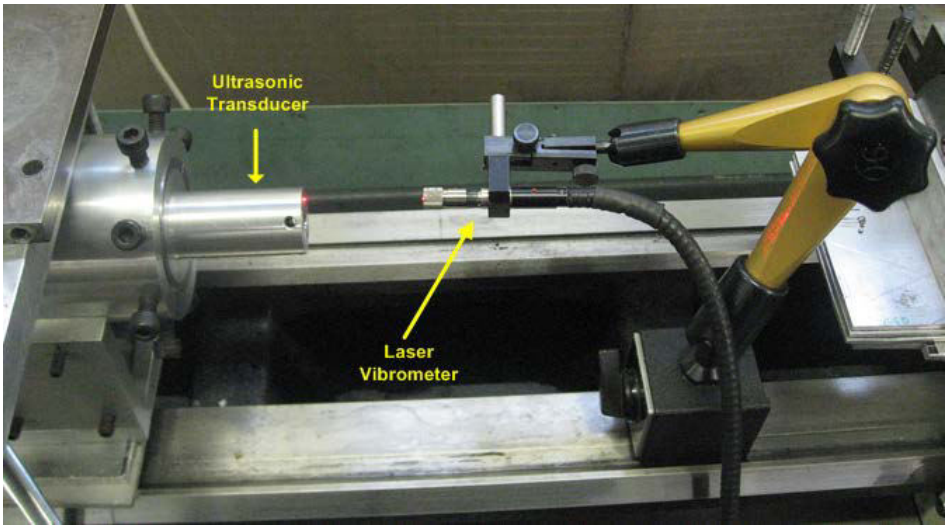

Figure 4.5 : Experimental setup of electromechanical ultrasonic transducer

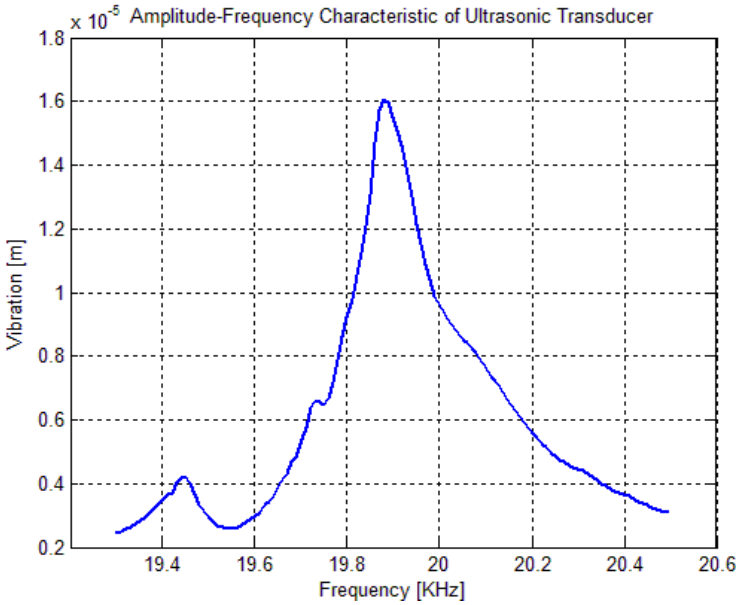

Figure 4.6 : Amplitude-frequency characteristic of electromechanical ultrasonic transducer

The ultrasonic vibration signal was recorded at the end of the electromechanical ultrasonic transducer without any drill bit attached as shown in Figure 4.5. Clearly, the zero-to-peak vibration amplitude at the end of 2nd step is $16\mu m$ with a resonant frequency $19.9KHz$. Taking the resonant frequency value of equation (4.25) into account, the difference between the results of the distributed parameter model shown in Figure 4.2 and the experiment measurement shown in Figure 4.5 is about 6.6%. The contributions to this error could be: in the distributed parameter model shown in Figure 4.2, the concentrator is assumed to be ideal, i.e. completely solid, vibration direction is purely longitudinal etc. However, in experiments, there were several uncertainties; for instance, transverse vibration participation, energy loss, temperature change (which has been proved to shift the resonant frequency) etc. These factors will change the electromechanical transducer's behaviour.

4.1.3 Eigenvalue-Eigenvector Analysis of 2-DOF Model

As introduced before, a 2-DOF model can be a replacement of the electromechanical ultrasonic transducer. The structure of the 2-DOF model is shown in Figure 4.7. K_1 and K_2 represent the stiffness, M_1 and M_2 are the mass, x_1 and x_2 are the absolute displacements of the 1st and 2nd step concentrator. Theoretically, a complete 2-DOF model should consist of damping coefficients too. However, the involvement of the damping coefficients will increase the number of unknown parameters therefore complicate the calculation of the contact stiffness and the mass. More importantly, during ultrasonic vibration, natural

damping of an ultrasonic transducer is negligible because the ultrasonic vibration will not be significantly affected. The damping which affects the ultrasonic vibration is the damping created during ultrasonic machining process.

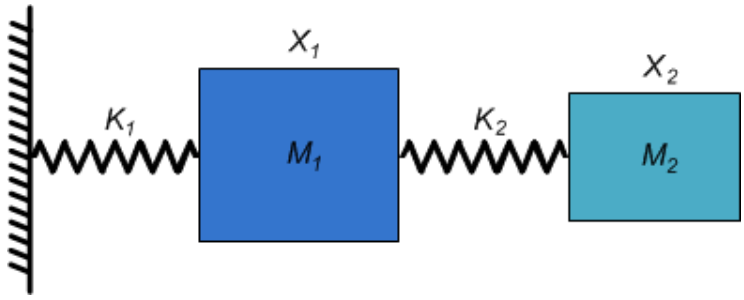

Figure 4.7 : 2-DOF model as a replacement of 2-step concentrator

According to the Euler-Lagrange mechanical motion equation [22]:

$$L_{UT} = T_{UT} - V_{UT} \tag{4.26}$$

L_{UT} represents the Lagrangian product, T_{UT} stands for the kinetic energy and V_{UT} is the potential energy of the 2-DOF model . Each of these energy terms will be calculated:

$$T_{UT} = \frac{1}{2}M_1\dot{x}_1^2 + \frac{1}{2}M_2\dot{x}_2^2 \tag{4.27}$$

$$V_{UT} = \frac{1}{2}K_1x_1^2 + \frac{1}{2}K_2(x_1 - x_2)^2 \tag{4.28}$$

$$L_{UT} = \frac{1}{2}M_1\dot{x}_1^2 + \frac{1}{2}M_2\dot{x}_2^2 - \frac{1}{2}K_1x_1^2 - \frac{1}{2}K_2(x_1 - x_2)^2 \tag{4.29}$$

Where $\dot{x}_1$ and $\dot{x}_2$ are the velocities of the 1st and 2nd mass shown in Figure 4.7. Applying derivative to both variables x_1 and x_2, the following equations are derived:

$$\frac{d}{dt}\left(\frac{\partial L_{UT}}{\partial \dot{x}_1}\right) - \frac{\partial L_{UT}}{\partial x_1} = 0 \tag{4.30}$$

$$\frac{d}{dt}\left(\frac{\partial L_{UT}}{\partial \dot{x}_2}\right) - \frac{\partial L_{UT}}{\partial x_2} = 0 \tag{4.31}$$

After transformation, following equations are derived:

$$M_1\ddot{x}_1 + K_1x_1 + K_2(x_1 - x_2) = 0 \tag{4.32}$$

$$M_2\ddot{x}_2 - K_2(x_1 - x_2) = 0 \tag{4.33}$$

Due to the longitudinal vibration is assumed harmonic, following assumptions are made:

$$x_1 = V_1\sin(\omega t) \tag{4.34}$$
$$x_2 = V_2\sin(\omega t) \tag{4.35}$$

Where V_1 and V_2 are the vibration amplitude of M_1 and M_2 shown in Figure 4.7. V_1 has the same value as A shown in equation (4.14) which is the maximal amplitude of the 1st step concentrator. V_2 has the same value as B shown in equation (4.17) which is the maximal amplitude at the end of the 2nd step concentrator. Substituting equation (4.34) and (4.35) into equation (4.32) and (4.33) gives:

$$(K_1 + K_2 - M_1\omega^2)V_1 - K_2V_2 = 0 \tag{4.36}$$
$$-K_2V_1 + (K_2 - M_2\omega^2)V_2 = 0 \tag{4.37}$$

As shown in equation (4.36) and (4.37), frequency is the only variable therefore is selected as the eigenvalues. Due to the fact that the distributed parameter model shown in Figure 4.2 can be replaced with a 2-DOF model shown in Figure 4.7, only the first two vibration modes' corresponding frequencies participate in the calculation, which are $f_1 = 8.8KHz$ and $f_2 = 21.3KHz$ shown in equation (4.25). Rearranging equation (4.36) and (4.37) into matrix form gives:

$$M\lambda\Psi = K\Psi \tag{4.38}$$

In equation (4.38), M represents the mass matrix, K is the stiffness matrix, λ is the eigenvalues matrix which contains the frequency components, Ψ is the eigenvector matrix with vibration magnitudes. Expressions of these matrices are shown below:

$$M = \begin{bmatrix} M_1 & 0 \\ 0 & M_2 \end{bmatrix} \quad K = \begin{bmatrix} K_1 + K_2 & -K_2 \\ -K_2 & K_2 \end{bmatrix} \quad \lambda = \begin{bmatrix} \omega_1^2 & 0 \\ 0 & \omega_2^2 \end{bmatrix} \quad \Psi = \begin{bmatrix} \psi_1 & \psi_2 \\ 1 & 1 \end{bmatrix} \tag{4.39}$$

In equation (4.39), ψ_1 and ψ_2 are normalised amplitudes of ultrasonic vibration of the 1st mass (ratio between 1st and 2nd step) when 1st and 2nd oscillation mode is excited respectively.

$$\psi_1 = \psi_2 = \frac{V_1}{V_2} \tag{4.40}$$

According to the eigenvalue-eigenvector decomposition [3]:

$$Ax = \lambda x \tag{4.41}$$

Equation (4.38) can be rearranged:

$$M^{-1}K\Psi = \lambda\Psi \tag{4.42}$$

A manual definition can be made that $H = M^{-1}K$, where:

$$H = \begin{bmatrix} h_1 & h_2 \\ h_3 & h_4 \end{bmatrix} = \begin{bmatrix} \frac{K_1+K_2}{M_1} & -\frac{K_2}{M_1} \\ -\frac{K_2}{M_2} & \frac{K_2}{M_2} \end{bmatrix} \tag{4.43}$$

According equation (4.38) to (4.43), the following equations are derived:

$$\begin{cases} h_1\psi_1 + h_2 = \omega_1^2\psi_1 \\ h_3\psi_1 + h_4 = \omega_1^2 \\ h_1\psi_2 + h_2 = \omega_2^2\psi_2 \\ h_3\psi_2 + h_4 = \omega_2^2 \end{cases} \tag{4.44}$$

It should be noted that in equation (4.43), $h_3 = -h_4$. Substituting this equality into (4.44) gives:

$$\omega_1^2 - \omega_2^2 = \omega_1^2\psi_2 - \omega_2^2\psi_1 \tag{4.45}$$

Using equation (4.45), equation (4.44) can be reduced into:

$$\begin{cases} h_1\psi_1 + h_2 = \omega_1^2\psi_1 \\ h_3\psi_1 + h_4 = \omega_1^2 \\ h_1\psi_2 + h_2 = \omega_2^2\psi_2 \end{cases} \tag{4.46}$$

As mentioned in equation (4.20) that as well as equation (4.23))

$$B = \frac{Asinkx_j}{cosk(x_j - L)} \tag{4.47}$$

After arrangement gives:

$$\frac{A}{B} = \frac{cosk(x_j - L)}{sinkx_j} \tag{4.48}$$

In order to obtain vibration amplitude ratio between the 1st mass and 2nd mass at resonant frequency for the 2-DOF model shown in Figure 4.7, an experiment was performed. During experiment, a strip of reflection film was adhered to the longitudinal surface of the electromechanical ultrasonic transducer and the laser beam moved along the length of the strip. Ultrasonic vibrations in the middle of the 1st step and 2nd step concentrator as well as at the connection point between the 1st step and 2nd step concentrator were recorded literally. Results are shown in Figure 4.8.

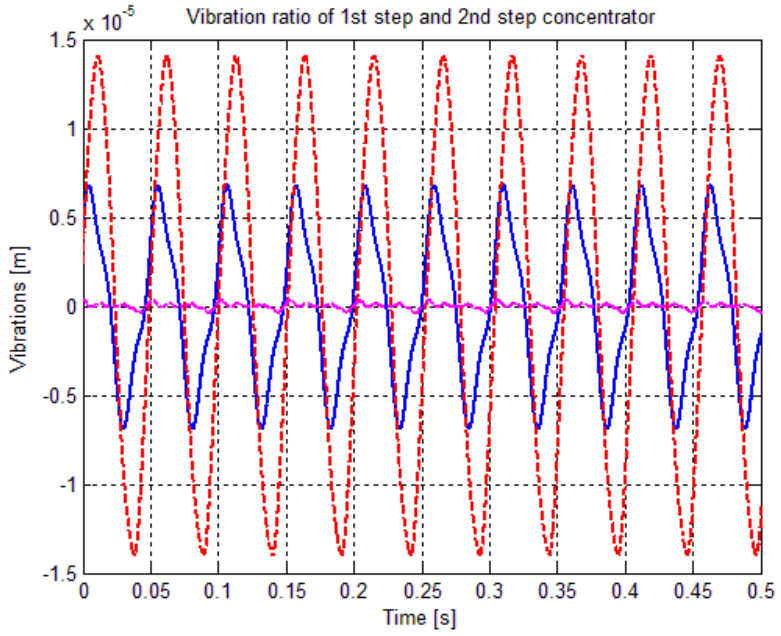

Figure 4.8 : Experiment measurements of electromechanical ultrasonic transducer

Red dashed curve represents the ultrasonic vibration at the end of the 2nd step concentrator. Blue solid curve stands for the vibration measured in the middle of 1st step. Pink dash-dotted curve is ultrasonic vibration signal recorded at the connection point between 1st step and 2nd step which is nearly zero and clearly insignificant in comparison to the other two curves. Therefore, the assumption has been experimentally proved that the physical nodal point is located at the connection between the 1st step and 2nd step concentrator. By clamping this point allows most efficient energy propagation. Another notable point is the ratio between the 1st step and 2nd step is around 0.5 and the vibrations are in anti-phase in experiment (this has been proved experimentally which cannot be observed from Figure 4.8 since data sets were recorded separately).

Therefore, vibration ratio between the 1st step and 2nd step concentrator at resonance is:

$$\psi_2 = \frac{A}{B} = \frac{V_1}{V_2} = -0.5 \tag{4.49}$$

As a result, the eigenvector of the 2nd oscillation mode becomes:

$$\Psi = \begin{pmatrix} -0.5 \\ 1 \end{pmatrix} \tag{4.50}$$

Collectively, the eigenvector (normalized amplitude of vibration) of 1st oscillation mode can be calculated according to equation (4.45):

$$\Psi = \begin{pmatrix} 0.75 \\ 1 \end{pmatrix} \rightarrow \psi_1 = 0.75 \tag{4.51}$$

After substituting the expression of h_1, h_2,h_3 and h_4 shown in equation (4.43) into equation (4.46) produces:

$$\begin{cases} (M_1\omega_1^2 - K_1 - K_2)\psi_1 - K_2 = 0 \\ M_2\omega_1^2 + (\psi_1 - 1)K_2 = 0 \\ (M_1\omega_2^2 - K_1 - K_2)\psi_2 + K_2 = 0 \end{cases} \tag{4.52}$$

However, there are four unknown parameters (K_1, K_2, M_1, M_2) with only three independent equations, solutions hence are in infinite combinations (infinite number of solutions). This could be explained that a number of oscillation regimes develop a same natural frequency for the 2-DOF system shown in Figure 4.7. Consequently, in order to seek for the unique solution of the parameters (K_1, K_2, M_1, M_2), it is suggested to explore the 4th equation related to these unknown parameters. Law of conservation of energy is taken into account [68]. It is assumed that during ultrasonic vibration, there is no energy loss which implies the energy distribution to the 2-DOF model is completely propagated through the 2-step concentrator. The distributed energy for the 2-step concentrator shown in Figure 4.2 is shown in the following:

$$U = \frac{E}{2}\left[S_1 \int_0^{x_j} \left(\frac{dD_1(x)}{dx}\right)^2 dx + S_2 \int_{x_j}^{L} \left(\frac{dD_2(x)}{dx}\right)^2 dx\right] \tag{4.53}$$

After rearrangement using expression of $D_1(x)$ and $D_2(x)$ in equation (4.14) and (4.17), the energy expression is obtained:

$$U = \frac{E}{2}\left[S_1 \int_0^{x_j} A^2k^2 cos^2 kx dx + S_2 \int_{x_j}^{L} B^2k^2 sin^2 k(x-L) dx\right] \tag{4.54}$$

Using the dimensions in Table 4.1 and assuming the 2-step concentrator is working at its 2nd oscillation mode, i.e. $A = V_1 = -0.5$ and $B = V_2 = 1$:

$$U = \frac{E}{2}\left[S_1 A^2k^2 \left(\frac{x}{2} + \frac{sin2kx}{4k}\right)\Big|_0^{x_j} + S_2 B^2k^2 \left(\frac{x}{2} - \frac{sin2[k(x-L)]}{4k}\right)\Big|_{x_j}^{L}\right] = 1.42 \times 10^9 J \tag{4.55}$$

The energy of the 2-DOF model shown in Figure 4.7 can be calculated as the potential energy when it reaches the maximum vibration amplitude (since the velocity is zero when the maximum amplitude is reached which implies zero kinetic energy):

$$U = \frac{1}{2}K_1V_1^2 + \frac{1}{2}K_2(V_2 - V_1)^2 \tag{4.56}$$

According to energy conservation law (Total amount of energy in an isolated system remains constant over time):

$$\frac{1}{2}K_1\psi_2^2 + \frac{1}{2}K_2(1-\psi_2)^2 = 1.42 \times 10^9 \tag{4.57}$$

Taking equation array (4.52) into account, the following equation array is established:

$$\begin{cases} (M_1\omega_1^2 - K_1 - K_2)\psi_1 - K_2 = 0 \\ M_2\omega_1^2 + (\psi_1 - 1)K_2 = 0 \\ (M_1\omega_2^2 - K_1 - K_2)\psi_2 + K_2 = 0 \\ K_1\psi_2^2 + K_2(1-\psi_2)^2 = 2.84 \times 10^9 \end{cases} \tag{4.58}$$

Eventually, the parameters of the 2-DOF model shown in Figure 4.7 are obtained:

$$\begin{gathered} K_1 = 1.145 \times 10^9 N/m \\ K_2 = 1.135 \times 10^9 N/m \\ M_1 = 0.25\ Kg \\ M_2 = 0.1 Kg \end{gathered} \tag{4.59}$$

Interestingly, based on the dimensions of the 2-step concentrator shown in Table 4.1, the calculation of the mass for the 1st and 2nd concentrator gives:

$$\begin{gathered} M_1 = \rho S_1 L_1 = 0.742\ Kg \\ M_2 = \rho S_2 L_2 = 0.130\ Kg \end{gathered} \tag{4.60}$$

Two values shown in equation (4.60) are different from the values calculated from the 2-DOF model shown in equation (4.59). This is due to the limitation of the scope of the 2-step concentrator shown in Figure 4.2 to a 2-DOF system shown in Figure 4.7. In reality, the 2-step concentrator has an infinite number of degree of freedom aggregations. The limited 2-DOF system mass and spring coefficients works as efficiently and accurately as the real electromechanical ultrasonic transducer.

4.2 Piezoelectric Transducer Model

The piezoelectric transducer used in the 2-step ultrasonic transducer is Navy I type, PZT-4 which is manufactured in Morgan Electronics. The material is ideally suited for ultrasonic cleaning, sonar, and other high power-acoustic radiation applications. In addition, it produces large mechanical drive amplitudes while maintaining low mechanical and dielectric losses.

Piezoelectric effect is understood as the linear electromechanical interaction between the mechanical and the electrical states. The piezoelectric transducer can convert electrical energy into vibration mechanical energy. For the 2-step ultrasonic transducer, piezoelectric rings are used to generate ultrasonic vibrations for Ultrasonically Assisted Drilling (UAD) process. A desired piezoelectric transducer model is used to define the interaction between the displacement of piezoelectric transducer, the interaction force with the 2-step concentrator and the voltage that is supplied to the piezoceramic rings.

According to the information in Morgan Electro Ceramic Solutions brochure [83] and the reports in [48], to a good approximation, interaction between electrical and mechanical behaviour of the piezoelectric medium can be described by the following relationships:

$$\begin{aligned} S &= s^E T + dE \\ D &= dT + \varepsilon^T E \\ E &= -gT + \frac{D}{\varepsilon^T} \\ S &= s^D T + gD \\ d &= \varepsilon^r \varepsilon^0 g \end{aligned} \tag{4.61}$$

Where S is strain, T is applied stress, s^E is elastic compliance at constant electric field, d is piezoelectric charge constant, D is dielectric displacement, E is electric field strength, ε^T is permittivity under constant stress, g is voltage constant, s^D is elastic compliance with electrode circuit open, ε^0 is permittivity of free space which is normally $8.85 \times 10^{-12} F/m$. Taking $T = \frac{F_0}{S_0}$, $E = \frac{u}{l_0}$, $D = \frac{q}{S_0}$ into account and substituting them into equation (4.61):

$$\begin{aligned} x_0 &= \frac{S_{33}^E l_0}{S_0} F_0 + d_{33} u \\ q &= d_{33} F_0 + \frac{\varepsilon_{33}^T S_0}{l_0} u \end{aligned} \tag{4.62}$$

Where S_0 is area and l_0 is thickness of a piezoceramic ring, F_0 is the force applied to the piezoelectric transducer from the 2-step concentrator and u is the voltage supplied to the piezoceramic rings, x_0 is the displacement of a piezoceramic ring and q is the electrical charge stored in it. In experiment, parameters of the piezoelectric transducer [26] have been measured and shown in Table 4.2. Observation of equation (4.62) implies that the electrical

charge is related to the interaction force F_0 and the supplied voltage u. Substituting parameters shown in Table 4.2 into (4.62) generates:

$$\begin{aligned} x_0 &= 3.84 \times 10^{-11} F_0 + 3.4 \times 10^{-10} u \\ q &= 3.4 \times 10^{-10} F_0 + 2.1 \times 10^{-9} u \end{aligned} \tag{4.63}$$

Table 4.2 : Parameter of piezoelectric transducer

Variable	$S_0(m^2)$	$l_0(m)$	$s_{33}^E(m^2/N)$	$d_{33}(m/V)$
Value	2.29×10^{-3}	6.11×10^{-3}	14.4×10^{-12}	340×10^{-12}
Variable	$g_{33}(Vm/N)$	$\varepsilon_{33}^T(F/m)$	$s_{33}^D(m^2/N)$	$\xi_0(F/m)$
Value	25×10^{-3}	$635\xi_0$	7.9×10^{-12}	8.85×10^{-12}

Differentiating the charge q shown in equation (4.63) with respect to time develops current flowing through the piezoelectric transducer, which will be further used for the control design based on the current feedback (will be discussed in details).

4.3 Ultrasonic Transducer Model

After the creation of a 2-DOF model shown in Figure 4.7 and a piezoelectric transducer model, the next step is to combine these two models and construct an entire model known as an ultrasonic transducer model; the structure of ultrasonic transducer model is shown in Figure 4.9:

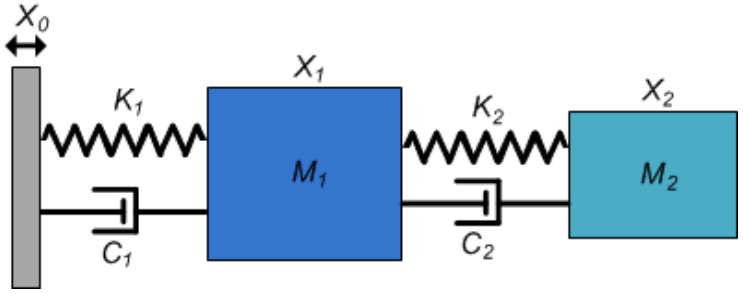

Figure 4.9 : Ultrasonic transducer model

According to the Euler-Lagrange mechanical motion equation [22]:

$$L_{UT} = T_{UT} - V_{UT} \tag{4.64}$$

L_{UT} represents the Lagrangian product, T_{UT} stands for the kinetic energy and V_{UT} is the potential energy of the ultrasonic transducer model. Each of these energy terms can be calculated:

$$T_{UT} = \frac{1}{2}M_1\dot{x}_1^2 + \frac{1}{2}M_2\dot{x}_2^2 \tag{4.65}$$

$$V_{UT} = \frac{1}{2}K_1(x_1 - x_0)^2 + \frac{1}{2}K_2(x_2 - x_1)^2 \tag{4.66}$$

$$L_{UT} = \frac{1}{2}M_1\dot{x}_1^2 + \frac{1}{2}M_2\dot{x}_2^2 - \frac{1}{2}K_1(x_1 - x_0)^2 - \frac{1}{2}K_2(x_2 - x_1)^2 \tag{4.67}$$

K_1 and K_2 represent the stiffness, M_1 and M_2 are the weights, x_1 and x_2 are displacements, C_1 and C_2 represent process damping coefficients, $\dot{x}_1$ and $\dot{x}_2$ are the velocities of the 1st mass and 2nd mass. Being different from the undamped 2-DOF model shown in Figure 4.7, during ultrasonic vibration, the ultrasonic transducer shown in Figure 4.9 creates more process damping which is significant than physical damping of the material. As a result, energy dissipation due to process damping D_{UT} cannot be neglected. Applying derivative to both variables x_1 and x_2, the following equations are produced:

$$\frac{d}{dt}\left(\frac{\partial L_{UT}}{\partial \dot{x}_1}\right) - \frac{\partial L_{UT}}{\partial x_1} + \frac{\partial D_{UT}}{\partial \dot{x}_1} = 0 \tag{4.68}$$

$$\frac{d}{dt}\left(\frac{\partial L_{UT}}{\partial \dot{x}_2}\right) - \frac{\partial L_{UT}}{\partial x_2} + \frac{\partial D_{UT}}{\partial \dot{x}_1} = 0 \tag{4.69}$$

Where D_{UT} represents the energy dissipation in the ultrasonic transducer model which equals:

$$D_{UT} = \frac{1}{2}C_1(\dot{x}_1 - \dot{x}_0)^2 + \frac{1}{2}C_2(\dot{x}_2 - \dot{x}_1)^2 \tag{4.70}$$

After combination and substitution, the following equations are produced:

$$M_1\ddot{x}_1 + C_1(\dot{x}_1 - \dot{x}_0) + K_1(x_1 - x_0) + C_2(\dot{x}_1 - \dot{x}_2) + K_2(x_1 - x_2) = 0 \tag{4.71}$$

$$M_2\ddot{x}_2 - C_2(\dot{x}_1 - \dot{x}_2) - K_2(x_1 - x_2) = 0 \tag{4.72}$$

Due to the interaction force between a piezocerrmic ring and the 1st step concentrator is reciprocal, expression of the applied force between the 2-step concentrator and the piezoceramic ring is:

$$F_0 = C_1(\dot{x}_1 - \dot{x}_0) + K_1(x_1 - x_0) \tag{4.73}$$

x_0 is displacement of a piezoceramic ring. Parameters of the undamped 2-DOF model shown in Figure 4.2 (K_1, K_2, M_1, M_2) have been calculated. Calculation of the damping coefficients C_1 and C_2 is based on the fact that the ultrasonic vibration amplitude of the 2-DOF ultrasonic transducer model shown in Figure 4.9 in simulation equals the amplitude of the electromechanical ultrasonic transducer in experiment. As can be seen in Figure 4.6, the vibration amplitude at the end of the 2nd step concentrator at resonance is $V_2 = 16\mu m$ zero-to-peak. Since $\psi_2 = -0.5$ for the 2nd oscillation mode, vibration amplitude of the 1st step concentrator can be calculated as $V_1 = 8\mu m$ zero-to-peak.

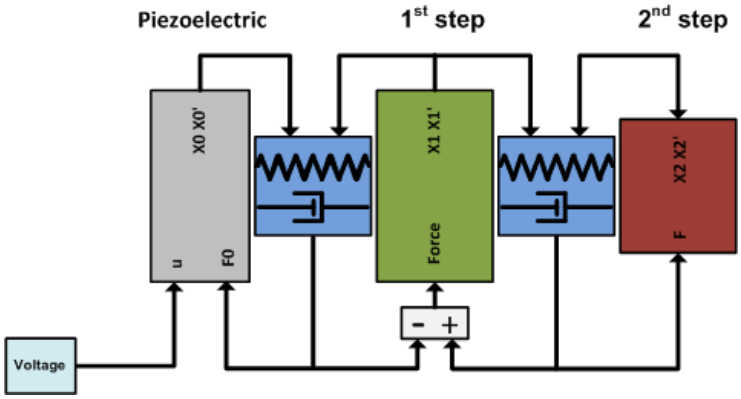

Figure 4.10 : Matlab-Simulink model of ultrasonic transducer in idle condition

In association with the motion equations of the piezoelectric transducer and the 2-DOF ultrasonic transducer model, a prototype Matlab-Simulink model is created and demonstrated in Figure 4.10. u represents voltage applied to a piezoelectric ring. F_0 is interaction force between the piezoelectric ring and the 1st step concentrator. 'Force' stands for resultant force that 1st step concentrator receives (calculated from two sets of spring-damper). F is force acting on the 2nd step concentrator (calculated from the 2nd set of spring-damper). Outputs of the piezoelectric transducer, the 1st step concentrator and 2nd step concentrator are $[x_0\ \dot{x}_0 x_1 \dot{x}_1 x_2\ \dot{x}_2]$. Output of the 1st spring-damper set is F_0. Output of the2nd spring-damper set is F. Zero-to-peak amplitude of the supplied voltage in Matlab-Simulink model was measured experimentally $200V$. Therefore, the harmonic supplied voltage signal in Figure 4.10 can be written as:

$$u = 200\sin(\omega t) \tag{4.74}$$

ω is the natural (resonant) frequency of the ultrasonic transducer shown in Figure 4.9. Taking into account the ultrasonic vibration amplitudes of the 1st step and 2nd step in experiments, the process damping coefficients can be computed by adjusting the ultrasonic vibration in the simulation. Adjustment in Matlab-Simulink produces the following damping coefficients:

$$C_1 = 7.75\ Ns/m$$
$$C_2 = 7.25\ Ns/m \tag{4.75}$$

Ultrasonic vibration of application of the voltage and corresponding parameters to the ultrasonic transducer model shown in Figure 4.9 can be calculated in Matlab-Simulink and results are shown in Figure 4.11. Green curve represents the ultrasonic vibration of the 2nd mass x_2 , pink curve depicts displacement of 1st mass x_1 and central blue curve shows ultrasonic vibration of the piezoceramic ring x_0. It can be clearly observed that the transient response of the ultrasonic vibration lasts 0.06secs and then three curves gradually settle down to their steady states. Steady ultrasonic vibration amplitude of the 1st mass and 2nd mass shown in Figure 4.9 complies with experimental results.

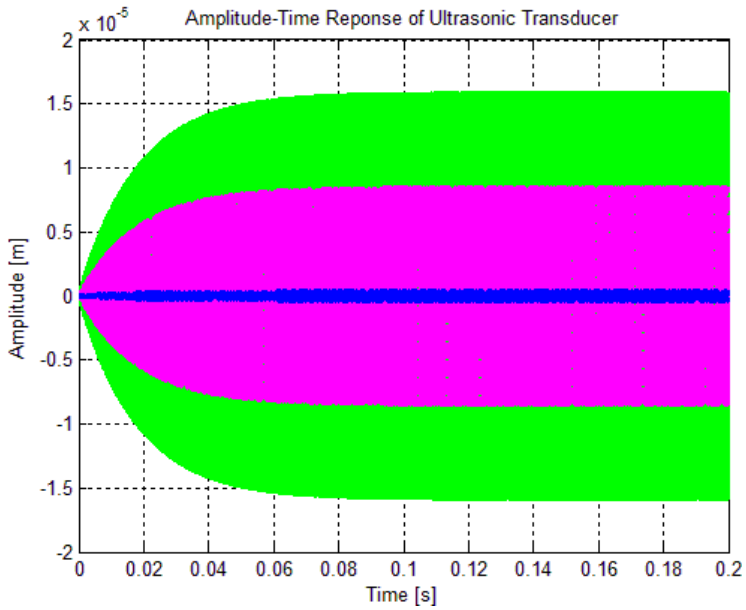

Figure 4.11 : Ultrasonic vibration of ultrasonic transducer model

In order to verify the accuracy and validity of the Matlab-Simulink model, steady state vibration has been enlarged and shown in Figure 4.12. Zero-to-peak vibration amplitude of the 2nd mass (shown in green solid curve) is roughly $16\mu m$, and zero-to-peak displacement of the 1st mass (shown in pink dashed curve) is about $8\mu m$, both coincide with experiment

measurements. The blue dash-dotted curve represents the vibration amplitude of the piezoring x_0 which is insignificant compared with x_1 and x_2. Moreover, the 1st mass and 2nd mass vibrations are in anti-phase which ensures the ultrasonic vibration reaches its maximum amplitude at the end of the 2nd step which also proves ψ_2 shown in (4.49).

In order to analyse the characteristics of the created ultrasonic transducer model in Matlab-Simulink, linearization on the dynamic equation shown in (4.71) and (4.72) on the ultrasonic transducer model shown in Figure 4.9 has been executed on the ultrasonic transducer model's equilibrium point. The input to the linearized model is the supplied voltage u and the output from the linearized model is the 2nd step concentrator (2nd mass) displacement x_2 .

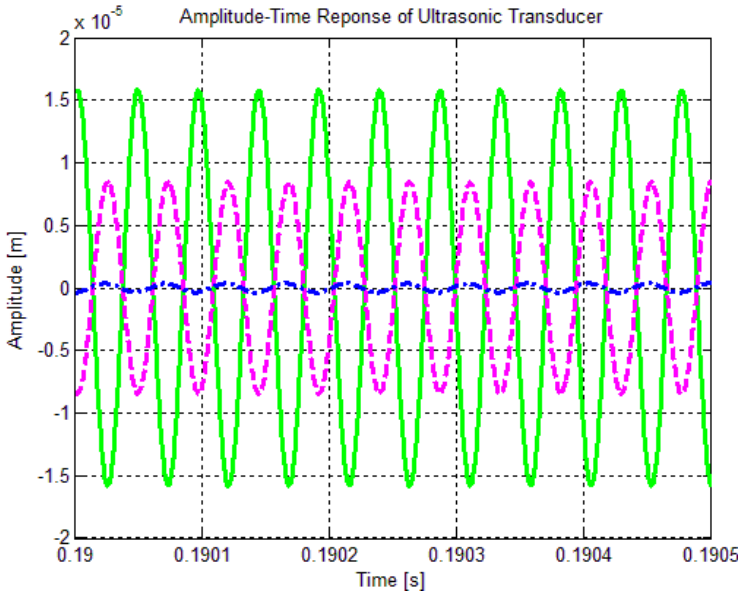

Figure 4.12 : Steady state ultrasonic vibration of ultrasonic transducer model

As a result, the transfer function defines the relation between the input (supplied voltage u) and the output (absolute displacement at the end of 2nd step concentrator x_2) is obtained:

$$G = \frac{x_2}{u} = \frac{108.1s+1.693\times10^{10}}{s^4+131.2s^3+2.028\times10^{10}s^2+6.551\times10^{11}s+4.979\times10^{19}} \tag{4.76}$$

Where s represents the Laplace operator and G is the transfer function. The system poles which can be calculated according to transfer function (4.76) are shown below:

$$
\begin{aligned}
P_1 &= -9.6 + 5.3 \times 10^4 j \\
P_2 &= -9.6 - 5.3 \times 10^4 j \\
P_3 &= -56 + 1.3 \times 10^5 j \\
P_4 &= -56 - 1.3 \times 10^5 j
\end{aligned}
\tag{4.77}
$$

Where j is a complex unit. The system response is stable because all system poles are located in the negative s-plane. Observation of the system poles suggests that there are two resonant frequencies. P_1 and P_2 contribute to the 1st resonant frequency, P_3 and P_4 form the 2nd resonant frequency. These two resonant frequencies are calculated:

$$
\begin{aligned}
f_1 &= 8.5\ KHz \\
f_2 &= 21.0\ KHZ
\end{aligned}
\tag{4.78}
$$

The 2nd resonant frequency f_2 differs from the result in equation (4.25) by only $0.3KHz$. Therefore, it can be claimed that the linearization on the ultrasonic transducer and the graphical solution shown in Figure 4.4 have a close agreement.

4.4 Applied Load Calculation with Vibro-Impact

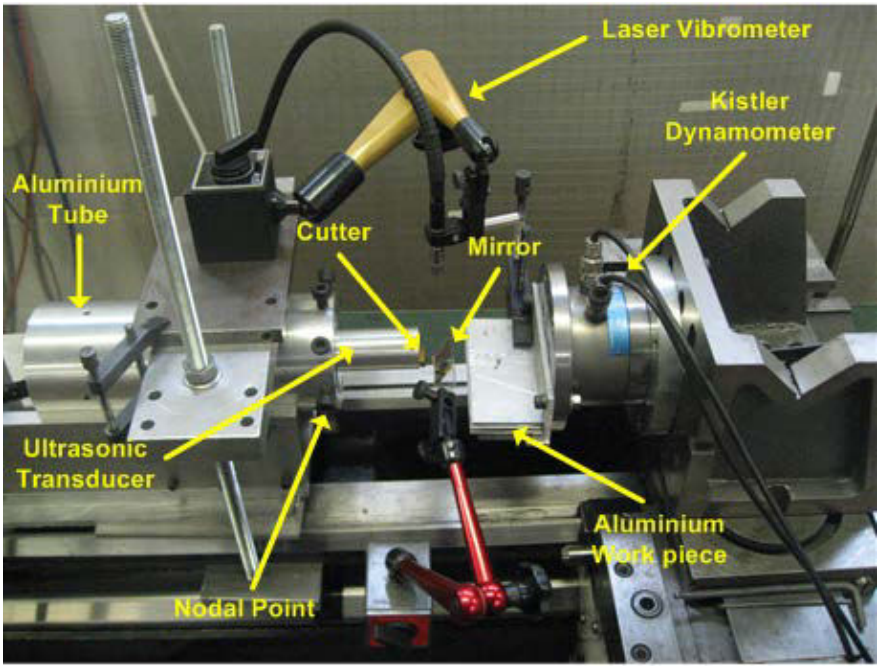

Figure 4.13 : Experimental setup of vibro-impact

As discussed previously that an applied load can significantly change the amplitude-frequency characteristic and generate a strong nonlinearity as well as create an instability in

the ultrasonic vibrating system which is undesirable for the autoresonant control. This emphasises the great importance of simulating the effect of an applied load during machining process (vibro-impact) in Matlab-Simulink in order to evaluate the model accuracy.

Experimental setup of vibro-impact is shown in Figure 4.13. It can be seen instead of performing the vibro-impact experiment on the Ultrasonically Assisted Drilling (UAD), Ultrasonically Assisted Broaching (UAB) was applied. During Ultrasonically Assisted Broaching (UAB), more space was available for a cutter to make grooves as the work piece feeds towards the ultrasonic transducer. In addition, it was more convenient for the laser vibrometer to record the vibration signals. Furthermore, a Kistler dynamometer (manufactured in Winterthur Switzerland, type 9271a, SN 40817) could be used to identify the ultrasonic vibration occurrence when a cutter was engaged into the work piece. With an activation of ultrasonic vibration, a sudden drop in charge amplifier's (KIAG SWISS Type:5001) output was expected to prove the advent of ultrasonic vibration. In contrast, if the Ultrasonically Assisted Drilling (UAD) was chosen, a laser vibrometer could not be properly used since the rotational motion of ultrasonic transducer was undesired for a laser beam to capture signals from the reflection film. Alternatively, even if ultrasonic transducer was put at the saddle side to enable the use of the laser vibrometer, work piece needed to be placed into the three jaw chuck to rotate. As a result, ultrasonic vibration was unable to be identified as a Kistler dynamometer was not used. In addition, a drill bit's dynamic motion was more complicated than a cutter. The purpose of the vibro-impact is to create a simple load model for numerical simulation.

In Figure 4.13, ultrasonic transducer was fixed at the nodal point (the 1^{st} and 2^{nd} step concentrator connection point) by an aluminium tube which was held tightly to the lathe. Work piece material was aluminium alloy with grade number 1050 and hardness $45HV$. The aluminium sheets were stacked up against the vertical plane of the Kistler dynamometer. Therefore, the Kitsler dynamometer could react quickly as soon as cutting process began. Moreover, in order to provide the laser vibrometer with more space for recordings, a mirror has been manually adjusted to reflect the laser beam onto the surface of the reflection film that was attached on the tip of a cutter. In order to illustrate the experimental setup shown in Figure 4.13 in details, Figure 4.14 has been drawn.

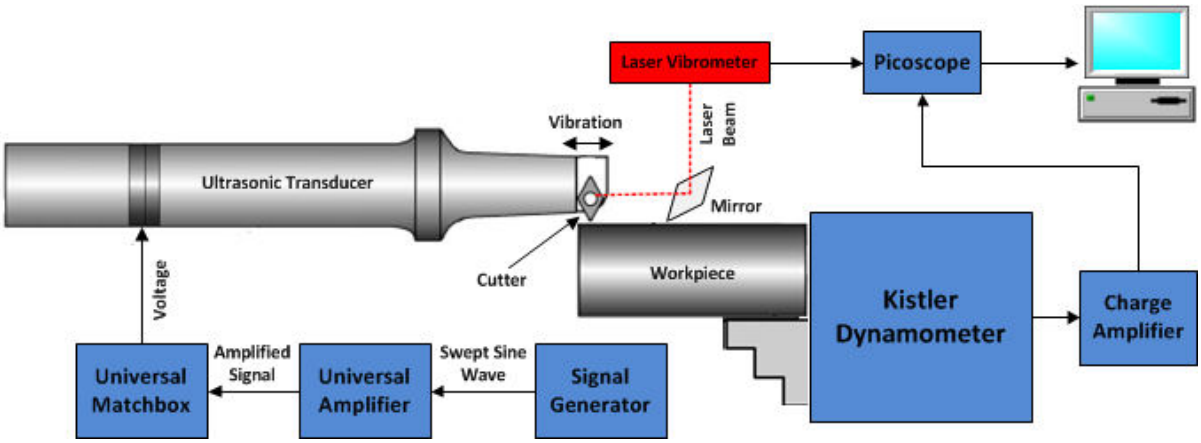

Figure 4.14 : Detailed experimental setup of vibro-impact

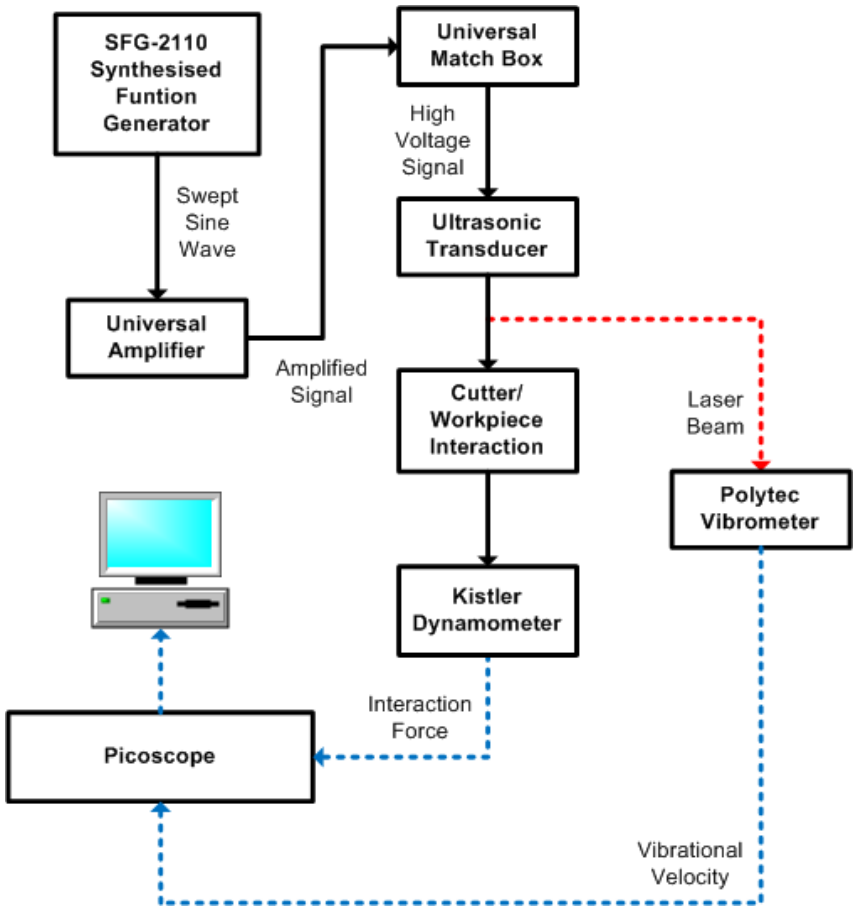

Figure 4.15 : Schematic diagram of instrumentation of vibro-impact experiment

The schematic diagram of the vibro-impact process and the components connections have been illustrated in Figure 4.15. Initially, a SFG-2110 Synthesised Function Generator produced a swept sine wave to a universal amplifier to intensify the actuation signal. The amplifier's output was further supplied to a universal matchbox (transformer) to adjust the high impedance and low voltage signal to low impedance and high voltage signal to excite

the ultrasonic transducer. A Polytec Vibrometer (Manufactured in Polytec Germany, OFV 512 & OFV 3001) was used to collect ultrasonic vibration samples during vibro-impact. In the meanwhile, a Kistler dynamometer was employed to record the axial feed force. Recorded signals were stored in a PicoScope (PicoScope 4424 with bandwidth $20MHz$, details in [82]) which was further interfaced with a computer to perform data processing.

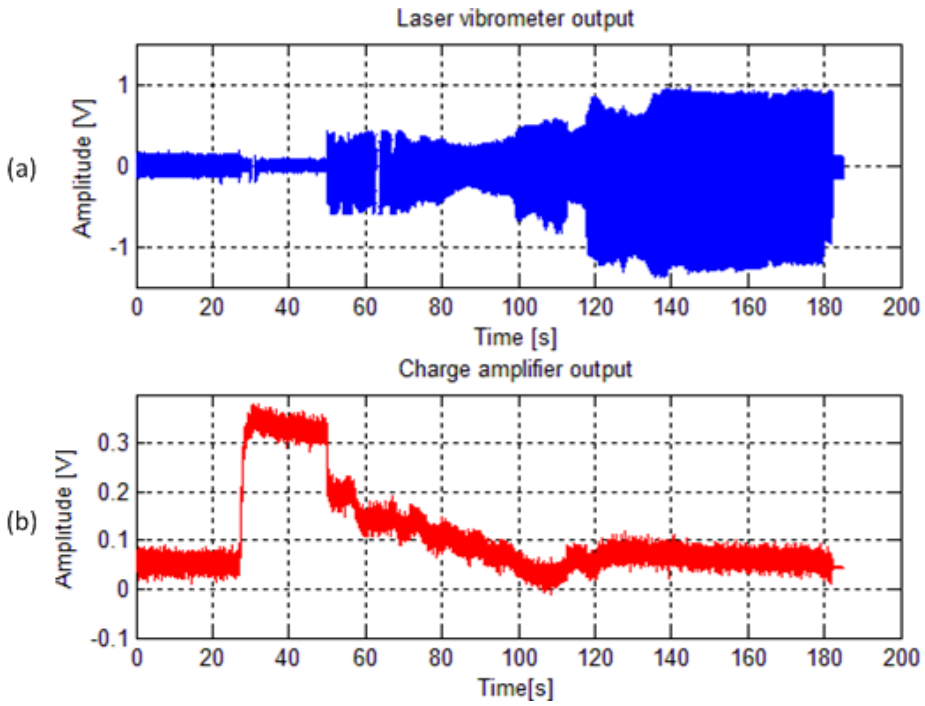

Figure 4.16 : Characteristics of ultrasonic transducer during Ultrasonically Assisted Broaching (UAB): (a) laser vibrometer's output, (b) charge amplifier's output

During vibro-impact, a slow rotational speed 40rev/min with a slow feed rate 0.03mm/rev was selected. Experimental results are shown in Figure 4.16. In the beginning, the ultrasonic vibration was deactivated and the work piece was fed to the ultrasonic transducer. It can be seen that the ultrasonic vibration was nearly zero. At 25sec, the initial contact between the cutter and the work piece happened which resulted in a sudden increase in the charge amplifier's (charge amplifier is an amplifier connected to the Kistler dynamometer transducer which is used to amplifier the tiny current generated by the quartz in the dynamometer, the charge amplifier's output is proportional to the measured thrust force, calibration of the Kistler dynamometer has been done which can be found in Chapter Seven) output and this Conventional Broaching (CB) process lasted for 25secs. At 50sec, the ultrasonic vibration was switched on. As a result, a drop in the charge amplifier's output and increases in the laser vibrometer's output have been witnessed. Since an applied load altered the frequency-

amplitude characteristic of the ultrasonic transducer, it was sensible to adjust the activation frequency to bring the ultrasonic vibrating system to a newly established resonance regime. This process happened from 50sec to 120sec. It can be clearly observed, the ultrasonic vibration gradually climbed to a higher level. At 120sec, the ultrasonic vibration arrived at a new resonant regime. It can be seen that the charge amplifier's output dropped considerably compared with the Conventional Broaching (CB) process.

Laser vibrometer's steady state level was around $2.2V$ peak-to-peak shown in (a) in Figure 4.16. Another notable point was the signal seemed asymmetric around zero which was caused by the applied load. A new resonant frequency was explored as $19.43KHz$ eventually. Taking the sensitivity of the laser vibrometer 1000mm/s/V into account, the zero-to-peak ultrasonic vibration can be hence calculated:

$$\mathrm{A}_2 = \frac{1.1}{\omega} = \frac{1.1}{2\times\pi\times19430} \approx 9\mu m \tag{4.79}$$

As mentioned in [15], an axial load of the cutting tool is described with a help of a nonlinear dynamic characteristics related to the tool's displacement x and speed $\dot{x}$, which is a generally ill-defined function of cutting end vibration x. Under stationary conditions of machining, the load can be transformed with a help of harmonic linearization as follows [5,6]:

$$F = Kx + C\dot{x} + P \tag{4.80}$$

P is the permanent component of the technological load under ultrasonic vibration (vibro-induced force). K and C are coefficients characterising the equivalent elastic and dissipative components of the applied load. Vibro-induced force P acts as an average and permanent static load on the feed drive during machining applications and it is equalised by the drive equipment. As a result, only dynamic force is taken into account [15].

Theoretically, the interaction force between a cutter and a work piece can be described by the dynamic characteristic of the working process, which relates the force F acting on the work piece to the tool's displacement x and speed $\dot{x}$ [8]. In the simplest form, this characteristic comprises of a linear force dependence on the tool displacement or speed:

$$F_e = Kx$$
$$F_d = C\dot{x} \tag{4.81}$$

The 1st dependence F_e in equation (4.81) describes a linear elastic load which appears during the continuous deformation of an elastic specimen with stiffness K. In this instance, deformation takes place in the elastic zone of the material's stress-strain characteristic. The 2nd dependence F_d describes a linear dissipative load which has a coefficient of resistance C that arises when the vibration occurs in a viscous fluid [36]. The complete characteristic is well-known as a Kelvin-Voigt model [43]:

$$F = Kx + C\dot{x} \tag{4.82}$$

Equation (4.82) describes a linear elastic-dissipative load which will be encountered during the deformation of elastic-viscous materials in experiment.

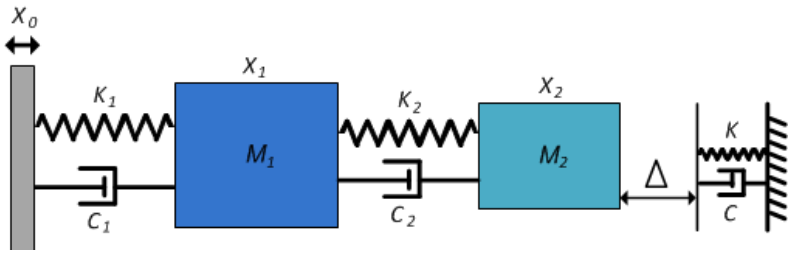

Figure 4.17 : Ultrasonic transducer interaction with an external load

Figure 4.17 illustrates an ultrasonic transducer model interaction with an external load of Kelvin-Voigt model. The load is modelled parallel of a linear elastic spring and a viscous damper as followed the structure of Kelvin-Voigt model. Δ represents the initial interference between the ultrasonic transducer and the applied load. Negative Δ indicates an initial interference while positive Δ means an initial gap. This model can describe the dynamic loading of the ultrasonic transducer during machining processing [12]. Due to the introduction of Δ, interaction force shown in equation (4.82) can be further revised as:

$$F = \begin{cases} Kx + C\dot{x}, & x > 0,\ Kx + C\dot{x} > 0 \\ 0, & x > 0,\ Kx + C\dot{x} \leq 0 \\ 0, & x < 0 \end{cases} \tag{4.83}$$

$x = x_2 - \Delta$ denotes relative displacement between the ultrasonic transducer and the applied load, K represents the contact stiffness and C is the damping coefficient, x_2 is the absolute displacement at the end of the 2nd step concentrator.

Equation (4.83) characterises the entire vibro-impact interaction force between the ultrasonic transducer and the limiter (applied load). Initially, assuming there is a gap between the ultrasonic transducer and the limiter, i.e. $\Delta > 0$, the ultrasonic transducer starts its oscillation towards the limiter. After a distance Δ, the ultrasonic transducer has its initial contact with the limiter which produces the interaction force expression of 1st term in equation (4.83). After the relative displacement x arrives at its maximal, the ultrasonic transducer is rebounded by the limiter. Intuitively, the ultrasonic transducer will not be separated from the limiter until it reaches $x = 0$. However, there is a particular case the expression of $Kx + C\dot{x} \leq 0$ holds up. Physically, it means the ultrasonic transducer is detached from the limiter due to the property of the viscous damper while the relative displacement x is still positive. In other words, the limiter is not able to follow the dynamic motion of the ultrasonic transducer before the relative displacement reaches 0, which gives rise to the 2nd term in equation (4.83). This has been proved in simulation. Eventually, when the relative displacement x becomes negative, the ultrasonic transducer is temporarily separated from the limiter before the entire process starts again which produces the 3rd term in equation (4.83).

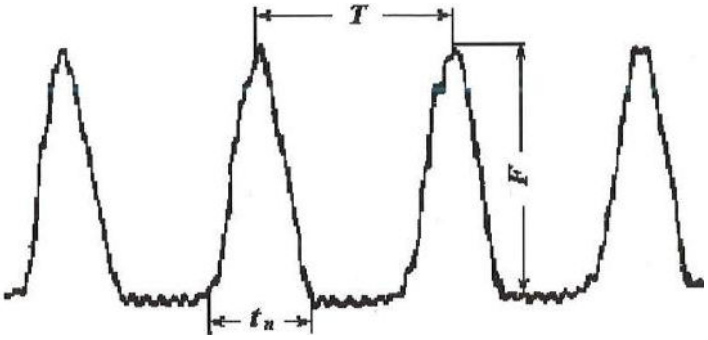

Figure 4.18 : Oscilloscope reading of interaction force between tool and work piece
Reproduced From [9]

Additionally, it should be noted that the limiter is a non-mechanical element since it consists of no mass. However, it joins as a part of the mechanical system of the ultrasonic transducer during contact. However, if the ultrasonic transducer is separated from the limiter, it is automatically removed from the mechanical system. In order to calculate the parameters of

the applied load, oscilloscope readings indicate force interaction between tool and work piece obtained experimentally is shown in Figure 4.18 [9]. Figure 4.18 shows the interaction force has an impulsive character which is caused by the vibro-impact nature. Interaction force acts during the time interval t_n with a maximum force amplitude F. During interval $T - t_n$, the tool is temporarily separated from the work piece but still vibrating, interaction force becomes 0. In addition, it is observed the relation between t_n and T is $T \approx 2t_n$.

In Kelvin-Voigt model, both the initial interference Δ and the contact stiffness K can impose influence on interaction force F shown in equation (4.83) which has been implemented in Matlab-Simulink. The value of the initial interference Δ can be chosen arbitrarily small, depending on the work piece material and machining conditions [68]. The value of the contact stiffness K and the damping coefficient C can be adjusted to match the ultrasonic vibration amplitude at the end of the 2nd step concentrator obtained in Ultrasonically Assisted Broaching (UAB) vibro-impact experiment.

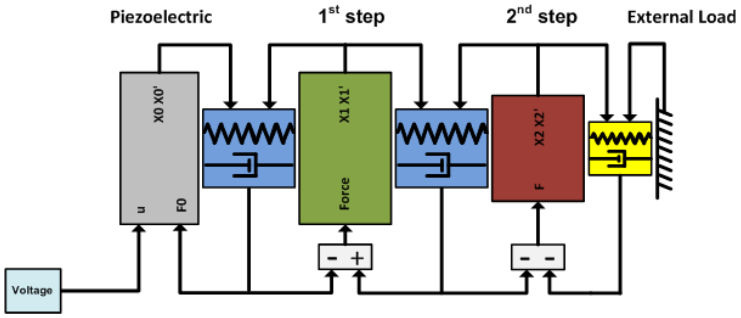

Figure 4.19 : Matlab-Simulink model of ultrasonic transducer with applied load

Due to the introduction of the applied load to the ultrasonic transducer, a revision on Matlab-Simulink model is shown in Figure 4.19. Yellow block represents the applied load in a form of the Kelvin-Voigt model. The supplied voltage magnitude remains $200V$. As a result, by tuning parameters K, C and Δ in Matlab-Simulink model, following values can be obtained:

$$\begin{aligned} \Delta &= -2 \times 10^{-7}\ m \\ K &= 1 \times 10^{8}\ N/m \\ C &= 26\ Ns/m \end{aligned} \tag{4.84}$$

Simulation results of the ultrasonic transducer in association with the applied load are illustrated in Figure 4.20. (a) shows the steady state ultrasonic vibration magnitude of the 2nd

step concentrator with the applied load, red dashed line represents the initial interference between the 2nd step concentrator and the applied load, i.e. Δ in equation (4.84). (b) illustrates the interaction force F shown in equation (4.83). From (a) it can be observed that the ultrasonic vibration amplitude is about $9\mu m$ zero-to-peak which complies with experiment results shown in equation (4.79). Another notable point is ultrasonic transducer is vibrating asymmetrically around zero line, which coincides with the experimental results shown in Figure 4.16 (a). In contrast, asymmetry response is not observed in Figure 4.12 when ultrasonic transducer is working in idle condition (no applied load).

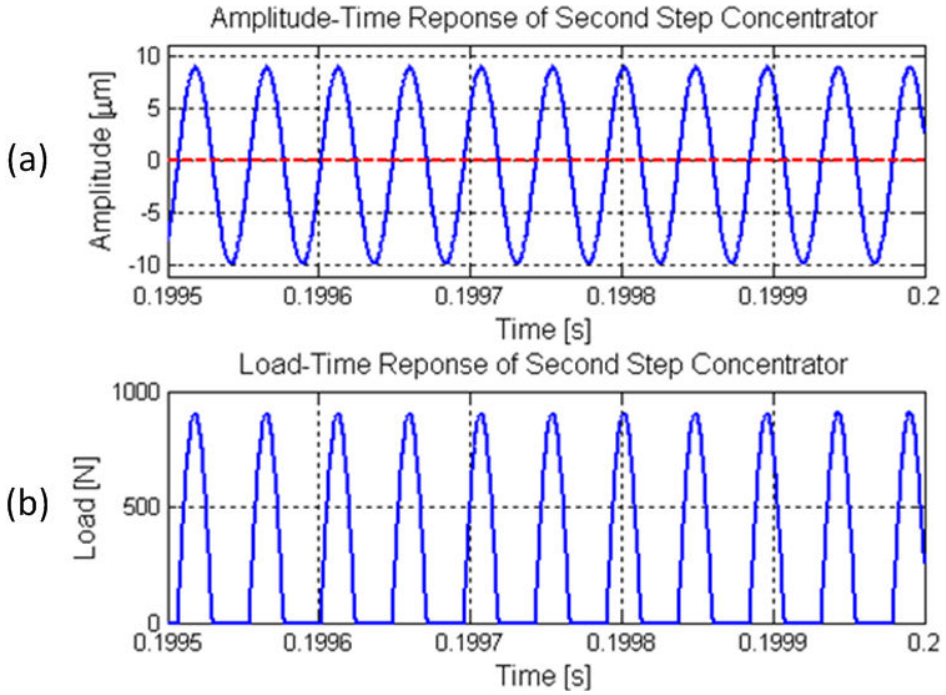

Figure 4.20 : Steady state ultrasonic vibration and interaction force of the loaded ultrasonic vibrating system: (a) ultrasonic vibration, (b) interaction force

Figure 4.20 (b) depicts the interaction force F shown in equation (4.83) during vibro-impact, the peak force is around $900N$. This interaction force characteristic presents a high similarity with the curve shown in Figure 4.18, which proves the validity and feasibility of the use of the Kelvin-Voigt model. The resonant frequency of the loaded ultrasonic vibrating system shown in Figure 4.17 is calculated in equation (4.85). Ultrasonic vibrating system activated with this frequency produces no overshoot in the transient response.

$$f_r \approx 21.176KHz \tag{4.85}$$

Therefore, the modelling of an ultrasonic transducer and an applied load in Matlab-Simulink has been accomplished. Accuracy of the model has been confirmed experimentally which lays the foundation for an autoresonant control system design.

4.5 Summary

This chapter mainly focuses on the creation of a 2-DOF model which most efficiently and effectively resembles the electromechanical ultrasonic transducer used in the experiments. Eigenvalue-eigenvector method is used to identify the natural frequency, stiffness, damping coefficients and masses of the 2-DOF model, and results are accurate which have been validated by experimental measurements.

In addition, a vibro-impact experiment on Ultrasonically Assisted Broaching (UAB) has been performed to derive a reliable and accurate applied load model. Kelvin-Voigt model which contains an elastic spring and a viscous damper connected parallel has been selected as the form of the applied load; its parameters are calculated based on the agreement between the experimental measurements and the computer simulation. In next chapter, the autoresonant control system model will be introduced and described elaborately.

Chapter Five Control System Model

As introduced before in Figure 1.6 that an applied load can change the amplitude-frequency characteristic of a vibrating system severely and cause nonlinearity and instability. In order to tackle the instability problems associated with fixed frequency control or even adjusted frequency control, autoresonant control systems have been developed [10]. Amplitude-phase characteristics of ultrasonic vibrating systems show flat resonant peaks and their curves are single-valued, therefore an autoresonant control system requires no precise maintenance of phase shift in the feedback loop to maintain the systems near resonance [17].

Autoresonant control is a self-sustaining excitation of a vibration mode at the natural frequency of a mechanical system, which maintains the resonant condition of oscillations automatically by means of positive feedback based on the transformation (phase shift) and amplification of the signal from a sensor [67]. In this chapter, an emphasis is laid on the establishment of an autoresonant control system model, which consists of elaborate descriptions of the autoresonant control algorithm and theoretical analysis of mechanical feedback, current feedback and power feedback. In addition, comparisons between theoretical analysis and experimental measurements are involved.

5.1 Autoresonant Control Algorithm

The aim of the autoresonant control is to maintain the nonlinear oscillation mode of an electromechanical transducer (ultrasonic vibration amplitude at the end of the 2^{nd} step concentrator numerically and ultrasonic vibration magnitude at the tip of a drill bit experimentally) at a desired level (resonant regime) during machining (vibro-impact). This is based on the fact that during resonance, the phase lag between the vibrations of the working element (a drill bit) and the excitation force (driving voltage) is a constant [67].

Theoretically, an autoresonant control system generates a control signal by means of shifting the phase of a sensor signal and changing the amplitude through an amplifier and a universal matchbox (transformer). The produced powerful signal is then supplied to the piezoelectric transducer to generate an exciting force which energises the ultrasonic vibration system and forms the loop. According to a sensor selection, a control system can use different signals in the feedback loop. A control system based on mechanical feedback measures the ultrasonic

vibration signal at the end of 2nd step concentrator and applies it to a phase shifter and a universal amplifier etc. In the case of electrical feedback, two sensors can be adopted namely a current sensor and a power sensor. Once a current sensor is employed, it works as a feedback signal which is handled by a phase shifter and an amplifier etc to drive the ultrasonic transducer. However, in the case of power feedback, power signal is used to determine the actual control effort needed while current signal is transformed and amplified to form the positive feedback.

By changing the phase shift in the autoresonant loop allows the precise control of the vibrating state and by changing the amplification factor is able to control the vibration level [16]. In a better interpretation, a phase shifter acts as a minor precise tuning element in the autoresonant loop while adjusting the amplification gain of an amplifier allows keeping the ultrasonic vibration at a desired level.

During the actual ultrasonic drilling process with the presence of an applied load, the level of ultrasonic vibration will be change in a time varying condition. In order to evaluate the level of change in oscillations, Root Mean Square (RMS) for three feedback sensors is traced. With evaluation of the RMS of different sensors, elaboration of new control values according to a specific algorithm is performed and set up [16]. Basically, the control algorithm include initial testing of the oscillating system, i.e. calculation of the optimal phase shift which produces the maximal amplitude of vibrations at the initial state, amplitude control (adjusting the amplification gain of an amplifier only), phase control (control of a phase shifter only) and combined control (control of both elements). Amplitude control, phase control and combined control will be introduced literally. Regarding the calculation of the optimal phase shift, it will be carried out and analysed respectively with different filters applications for mechanical feedback, current feedback and power feedback together with the autoresonant control simulation results in Chapter Six.

5.1.1 Phase Control Algorithm

Phase control is designed to establish a phase shift value during vibro-impact in order to provide the optimal phase shift in the system and maintain the ultrasonic vibration at the resonant state. The phase control algorithm is demonstrated and explained in Figure 5.1. As introduced in [16], by changing the phase shift of a sensor signal in the autoresonant loop

allows an efficient control of the vibrating state. In other words, since an applied load can alter the resonant frequency of the ultrasonic vibrating system which inevitably changes the amplitude-phase characteristic, the optimal phase shift has to be adjusted accordingly to ensure the resonance is always maintained. As known, amplitude-phase characteristic of an ultrasonic vibrating system under loading is gently sloping near resonance in contrast to the nonlinear sharp peak of frequency-amplitude characteristic; a small variation in amplitude-phase characteristic will not lead to a significant drop in the level of the ultrasonic vibration.

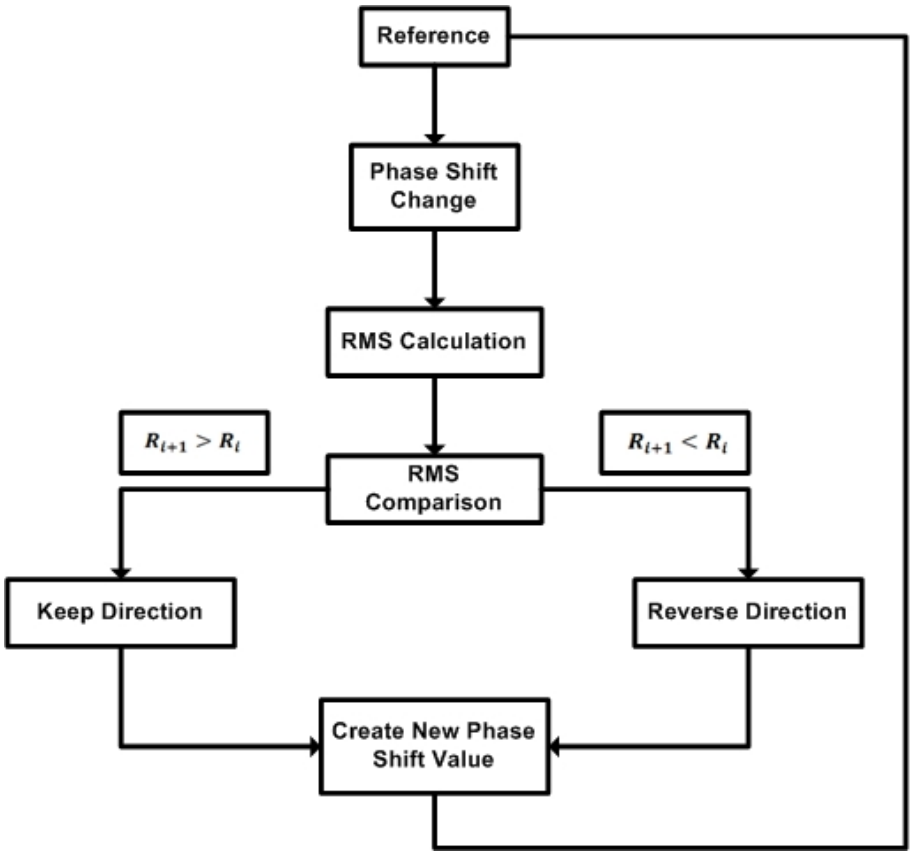

Figure 5.1 : Schematic diagram of the phase control algorithm

Reproduced and Revised From [68]

Hence, the following phase control algorithm can be proposed. The phase shift is changed by 0.01 phase control units (1 phase control unit equals 2π) initially and the changes in RMS of the feedback signal are recorded. If the monitored RMS of the 'current' control cycle with change in the phase shift is greater than the one in the previous control cycle, the direction of change remains for the next control cycle. Otherwise the direction is reversed. In this way the resonant regime is always kept. Taking mechanical feedback control as an example, the feedback signal is the ultrasonic vibration at the end of the 2^{nd} step ultrasonic transducer

which is measured by a laser vibrometer or an inductive sensor. Initially phase shift has been increased based on the optimal phase shift value and RMS is calculated and denoted as R_{i+1}, and if R_{i+1} is larger than the RMS value calculated before the phase shift is increased which is denoted as R_i, the phase shift will be increased again in the next control cycle. Otherwise the phase shift is decreased. However, a particular case when R_{i+1} equals R_i should be considered. Such situation was never encountered during numerical simulation because the RMS of the sensor's signal always changes in time to reach to the desired value R_d.

5.1.2 Amplitude Control Algorithm

The amplitude control algorithm provides an automatic control in an autoresonant loop by adjusting the amplification gain which is further applied to the manipulated sensor signal after the phase shifter in order to keep the RMS of the reference signal at a constant level during the ultrasonic machining process [16]. Obviously, during ultrasonic machining process an applied load can drastically affect the level of the ultrasonic vibration and an essential drop in oscillation is expected as the applied load increases. In order to compensate for the change in the level of oscillations, an amplitude value based on the following algorithm is created:

$$A_{i+1} = A_i \frac{R_d}{R_{i+1}} \tag{5.1}$$

Where R_d represents the desired RMS of the feedback sensor signal, A_i is the control voltage amplitude in the 'current' control cycle; R_{i+1} is RMS of the sensor signal obtained in the next control cycle after the amplitude control algorithm is established, A_{i+1} is the elaborated control voltage amplitude to be set up. It should be noted that the newly developed amplitude control algorithm has been improved from the one formulated in [16]. Amplitude control algorithm shown in equation (5.1) employs the RMS of the sensor signal in the next control cycle R_{i+1} instead of using R_i in the 'current' control cycle. The improved algorithm computes the newly elaborated control voltage amplitude A_{i+1} based on the RMS in the same control cycle R_{i+1} which can ensure the calculation accuracy of A_{i+1}. In contrast, amplitude control algorithm described in [16] predicts elaborate control voltage amplitude $A_{i+1}$with the RMS in the previous control cycle R_i which can deteriorate the precise calculation. According to equation (5.1), the change in newly elaborated control voltage amplitude A_{i+1}

depends on the behaviour of the RMS of the sensor signal obtained in the next control cycle R_{i+1}. If R_{i+1} is greater than R_d, then the control voltage A_{i+1} will decline and vice versa. Therefore, by adjusting the control voltage amplitude automatically can change the supplied voltage to the ultrasonic transducer thus keep ultrasonic vibration at a desired level.

According to the technical brochure of Morgan Electronics [83], the acoustic power handling capacity of a radiating transducer is limited by several factors, including dynamic mechanical strength of the ceramic, reduction in efficiency due to dielectric losses and mechanical losses, depolarisation of the ceramic due to electric field and temperature rise, instability resulting from the positive feedback between dielectric losses and internal heating etc. These factors might reduce the efficiency of the ultrasonic transducer, distort the waveform of the ultrasonic vibration as well as shift the resonant frequency. Practically, it has been experimentally proven that the ultrasonic transducer remains its linearity only within a range. Any supplied voltage value exceeds this range will lead to a waveform distortion and occurrence of nonlinearity which is inappropriate for the ultrasonic transducer's operation. The supplied voltage to the piezoelectric transducer causing the linear dependence of the amplitude of oscillation has been examined experimentally and results are shown in Figure 5.2.

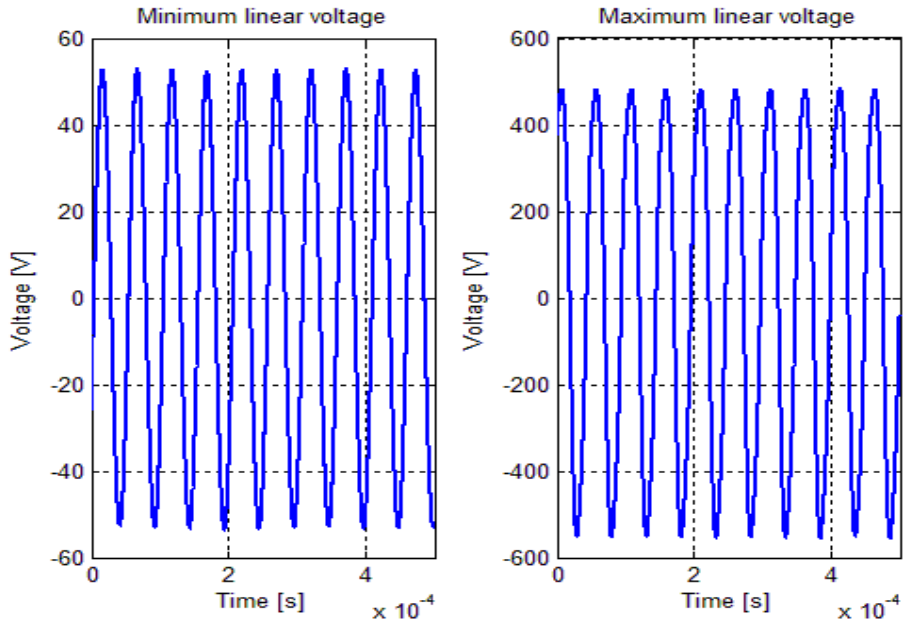

Figure 5.2 : Supplied voltage linear zone dependence of vibration amplitude identification: (a) minimum voltage, (b) maximum voltage

It can be observed that the minimum voltage is $50V$ zero-to-peak in (a) and the maximum voltage is around $500V$ zero-to-peak in (b). During experiments, the resonant regime has been manually achieved by tuning the excitation frequency from a SFG-2110 Synthesized Function Generator. After this, the amplification knob is adjusted accordingly to explore the linear response of the ultrasonic vibration. Meanwhile, an electronic differential probe GE8115 is used to measure the supplied voltage. The linear interval of the supplied voltage which generates the linear ultrasonic vibrations is $50V \sim 500V$ zero-to-peak. Therefore, each set of the calculated control voltage amplitude in the autoresonant control system will be checked to see whether it lies within the linear interval. For those exceed the upper limit, $500V$ will be used. Likewise, for those are less than the minimum, $50V$ will be used.

5.1.3 Amplitude-Phase Combined Control Algorithm

The combined amplitude-phase control algorithm enables the possibility of simultaneous control of the phase shift and the control voltage amplitude. As introduced in section 5.1.1, phase control is to maintain the resonant regime against the change in the feedback sensor's level during machining. Due to the fact that the amplitude-phase characteristic of an ultrasonic transducer is flat near the resonant peak during machining, a slight change in phase shift will not significantly affect the level of the ultrasonic vibration. Once there is a significant drop in the level of oscillation because of essential applied load, amplitude control needs to take part in to compensate the changes in the level of vibration and stabilise it.

In order to execute the switch between phase control and amplitude control, a new term R_c is introduced which represents the critical RMS of a feedback sensor signal. If the difference between R_d and the RMS in the 'current' control cycle R_i is less than R_c, then the sequence flows through phase control algorithm and a new phase shift will be calculated and used for next control cycle, in the meanwhile, control voltage amplitude remains as the previous cycle. On the other hand, when R_i exceeds R_d by more than R_c then the amplitude control algorithm will be executed, i.e. a new control voltage amplitude is established according to equation (5.1). However, phase shift remains unchanged. The combined amplitude-phase control algorithm is illustrated in Figure 5.3.

The amplitude-phase combined control algorithm is a comprehensive control which aims at keeping the ultrasonic vibration at a desired level during machining. Its basic principle has

been described, regarding the details of how phase shift is executed and control voltage is changed, these will be introduced later. In the next section, a created Matlab-Simulink model is introduced which consists of all elements and functions in the autoresonant control loop.

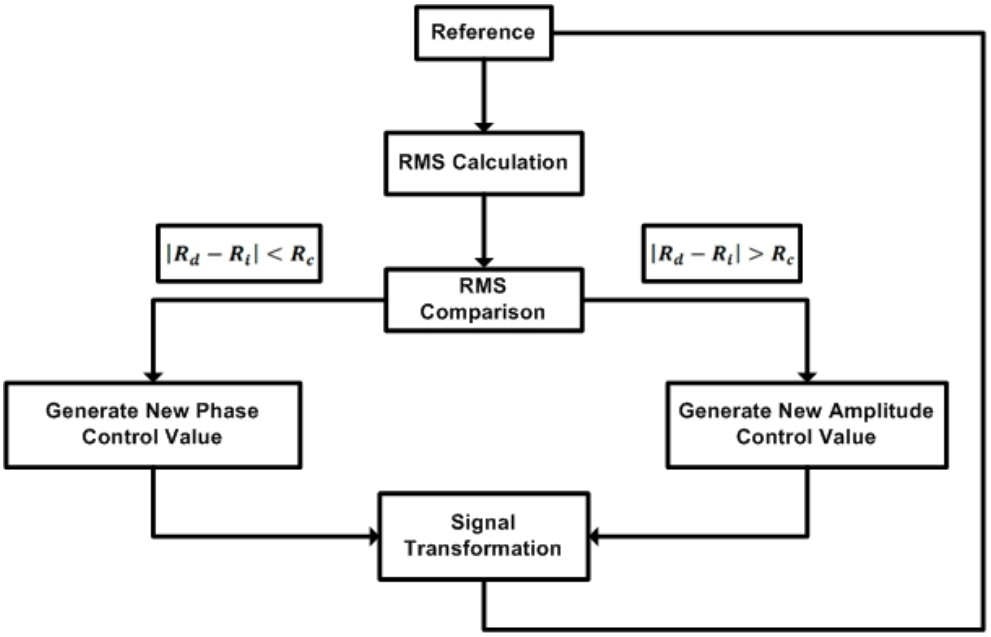

Figure 5.3 : Schematic diagram of amplitude-phase combined control algorithm

Reproduced and Revised From [68]

5.2 Autoresonant Control Model in Matlab-Simulink

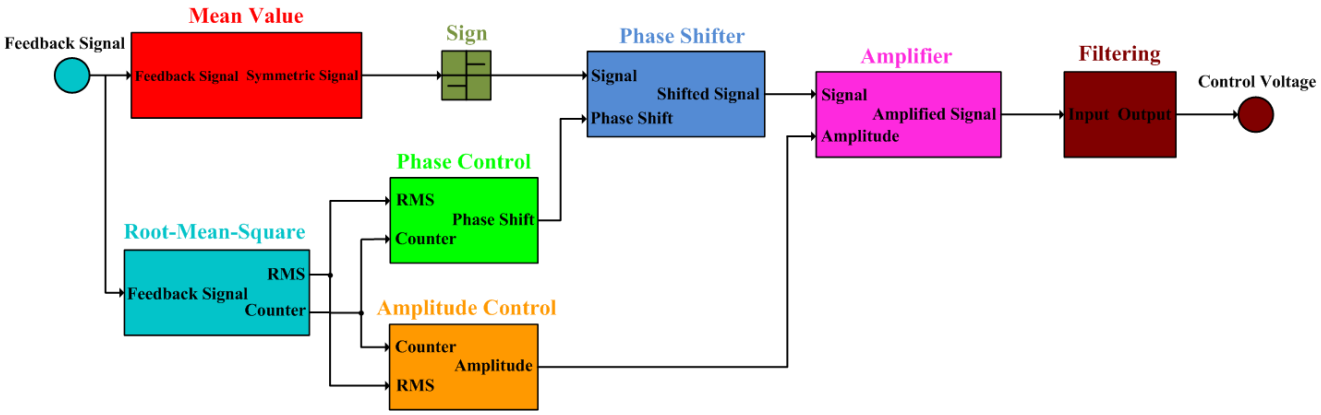

Figure 5.4 : Autoresonant control system structure in Matlab-Simulink

Reproduced and Revised from [68]

The autoresonant control algorithm including phase control, amplitude control and combined amplitude-phase control is illustrated in Figure 5.4. There are 8 function blocks in this autoresonant control diagram and each of them will be introduced in details.

- **Root-Mean-Square**

Root-Mean-Square block is designed to collect the sensor samples and calculate the RMS for each control cycle (will be defined by the author in the computer simulation). Input to the block is the sensor signals and output from the block is the RMS and counter values (integer number of oscillation periods which constitutes one control cycle). Depending on the feedback type, a sensor signal could be the ultrasonic vibration at the end of the 2nd step of an ultrasonic transducer, a current or a power of a piezoelectric transducer. In order to compute the RMS, following equation has been established:

$$RMS = \sqrt{\frac{1}{T}\int_0^T s(t)^2 dt} \tag{5.2}$$

In equation (5.2), RMS is the calculated Root-Mean-Square value of the 'current' control cycle, T is the period of a control cycle which normally equals several hundreds of oscillation periods. Selection of T will be introduced later. $s(t)$ represents a sensor signal. Design of this block can be found in Appendix III. Another notable point is that the RMS remains constant within one control cycle and will not change until the beginning of next one.

- **Phase Control**

Phase control block is designed to adjust the phase shift according to the change in the RMS of a sensor signal. As described in section 5.1.1 that phase control aims at keeping the ultrasonic vibrations at theresonant state during Ultrasonic Machining (USM) process. In this block, RMS of each control cycle is calculated based on the collected sensor samples. The calculated RMS is compared with the RMS in previous cycle. If the RMS in the 'current' control cycle has increased from the previous one, then the phase shift will be added by 0.01 phase control unit. Otherwise a 0.01 phase control unit will be subtracted.

Inputs to the phase control block are the RMS values and counter values calculated by the Root-Mean-Square block. Counter values are recorded as a number of oscillation periods used to form one control cycle. Output from this block is the actual phase shift value determined by the phase control algorithm which will be further processed by the phase shifter block. The detailed structure of this block is shown in Appendix III.

- **Amplitude Control**

Amplitude control block is designed to control the autoresonant loop automatically with the help of adjustment of an amplification gain in order to provide extra power to the ultrasonic transducer to maintain the ultrasonic vibration at a desired level during an applied load. The amplitude control block is designed to ensure the stability caused by the positive feedback.

The elaborated amplitude control value is calculated in equation (5.1). There are two inputs to this block which are identical to those to the phase control block. Output from this block is the calculated amplitude values which will be supplied into the amplifier block. Consequently, function of the combined amplitude-phase control algorithm can be easily implemented in association with phase control and amplitude control. The structure of the amplitude control block is demonstrated in Appendix III.

- **Mean Value**

Mean value block is designed to calculate the mean values of a sensor signal which is well-known as bias and then subtract it from the original sensor signals. For instance, the ultrasonic vibration at the end of the 2nd step of an ultrasonic transducer is asymmetric around zero with an applied load which has been proven numerically and experimentally. However, this procedure is negligible for current feedback and power feedback because electric signals are symmetric. Input to this block is a sensor signal and output from this block is a symmetric signal. An equation used to calculate the mean value of a sensor signal is shown below:

$$\overline{s(t)} = \frac{1}{T}\int_0^T s(t)dt \tag{5.3}$$

Where $s(t)$ represents a sensor signal, T is one oscillation period and $\overline{s(t)}$ are the mean values of the sensor signals. Technically, the mean values remain constant within one oscillation period. The structure of the mean value block can be found in Appendix III.

- **Sign**

This block is designed to transform a sinusoidal wave into a square wave with a unity gain. Basically, for a symmetric sinusoidal signal centred around zero, this block convers its half

positive wave into a positive straight unity line and transforms its half negative wave into a negative straight unity line. Therefore, a set of square wave is generated with an exactly same frequency as the original sensor signal. The converted square wave is prepared for the phase shifter.

- **Phase Shifter**

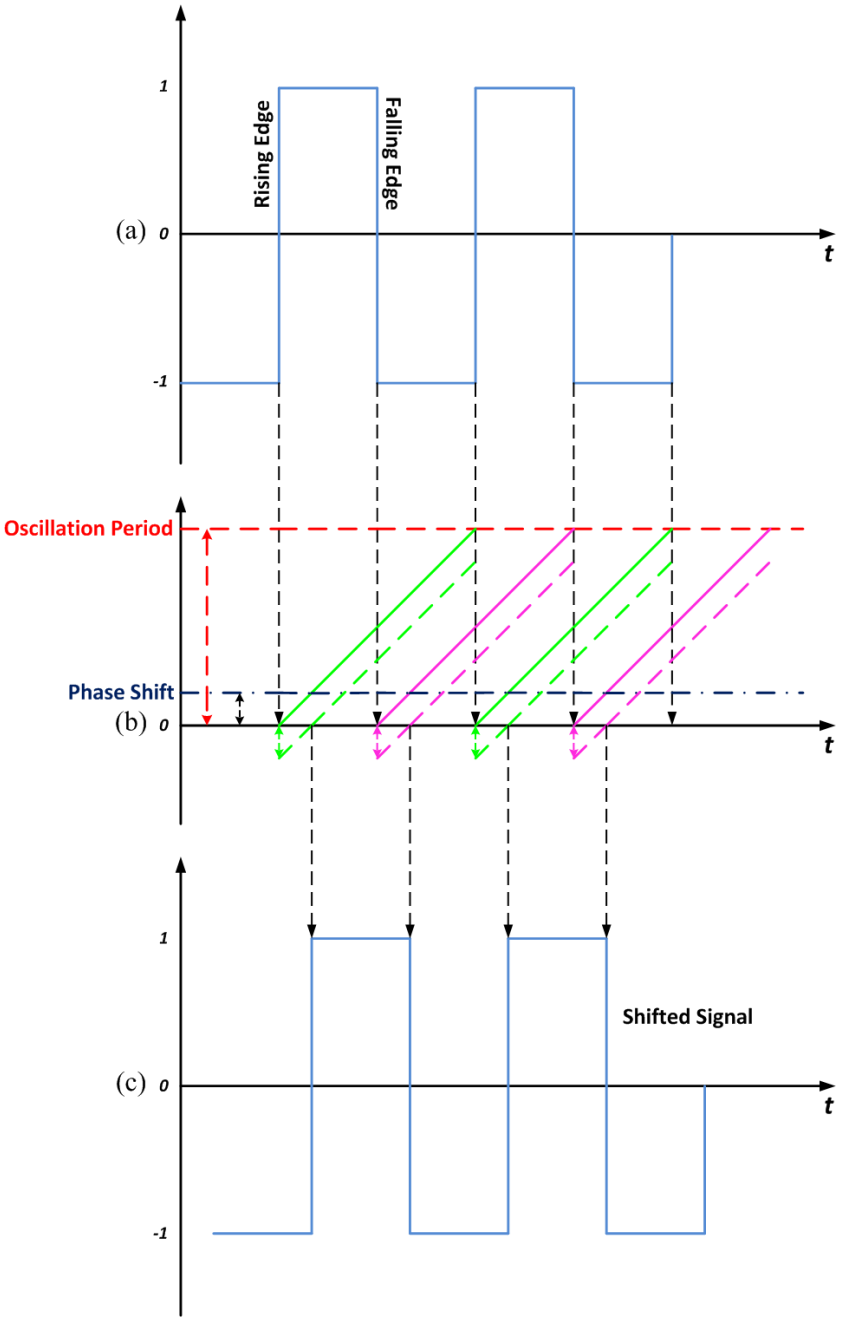

Figure 5.5 : Principle of a phase shifter: (a) original square wave, (b) phase shift, (c) shifted square wave

Reproduced and Revised from [68]

The phase shifter block is designed to shift the phase of the square wave signal according to the phase shift value calculated from phase control block. It should be noted that this block is only applicable to a square wave signal. The underlying principle of the phase shifter block is shown in Figure 5.5.

The square wave signal with unity gains is the source of the phase shifter block which is shown in (a) in Figure 5.5. Clearly, the original square wave signal consists of one rising edge and one falling edge within one oscillation period. In order to shift the square wave and generate a new one, the phase shift value calculated from the phase control block has been used. In (b), the phase shift value has been multiplied by one oscillation period which is expressed as a part of one oscillation period. Red dashed line represents one oscillation period and dark blue dash dot line stands for the phase shift as a part of one oscillation period. Once a rising edge is detected, the phase shifter performs an integration of a unity constant and produces an inclined green solid line. The same procedure has been applied to a falling edge which generates an inclined pink solid line. After each rising edge and falling edge has been integrated, the phase shift is subtracted from the integration respectively. Resultant inclined lines are shown in dash lines in green for rising edge and pink for falling edge. These newly produced inclined lines meet zero at shifted points which establish a new square wave with corresponding rising edges and falling edges shown (c). In this way, phase shifting process is executed. The newly generated square wave can be further processed by an amplifier. Theoretically, the phase shifter is able to handle a phase shift in an interval $[0,2\pi]$. Design of the phase shifter block in Matlab-Simulink can be referred to Appendix III.

- **Amplifier**

This block is designed to amplify the shifted square wave by multiplying a control voltage calculated from the amplitude control block.

- **Filtering**

This block is designed to smooth the amplified square wave signal. Basically, this is done to get rid of the high frequency components (noises) which might damage the piezoelectric transducer. Practically, depending on the type of the control feedback, different filters should

be used. For instance, a low-pass filter is suitable for mechanical feedback. In contrast, current feedback employs a band-pass Butterworth filter.

5.3 Control Strategies of Mechanical Feedback and Electrical Feedback

As introduced in section 1.1 that there are mainly two types of control strategies depending on sensor selections, which are either mechanical feedback with mechanical sensors or electrical feedback with electrical sensors.

- Mechanical Feedback
  Mechanical feedback employs a mechanical sensor to measure the displacement/velocity/acceleration of an ultrasonic transducer during vibro-impact

- Electrical Feedback Sensor
  Electrical feedback uses an electrical sensor to consider the electrical parameters as feedback signals, which are either a current or a power of a piezoelectric transducer

In the case of mechanical feedback control, a mechanical sensor is chosen to measure the mechanical vibration. The vibration signals could be displacement, velocity or acceleration. Generally, mechanical sensors include a laser vibrometer, an accelerometer, an ultrasonic microphone and an inductive (magnetic) sensor. A laser vibrometer and an inductive sensor will be used in the autoresonant control in Ultrasonically Assisted Drilling (UAD). The advantages of a mechanical sensor are it detects the ultrasonic vibration directly from the cutting zone which guarantees the accuracy and reliability for autoresonant control design. Despite such advantages, however, mechanical feedback sensors are difficult to be appropriately mounted under ultrasonic machining conditions. Moreover, cost of mechanical feedback sensors is relatively high.

For electrical feedback control aspect of view, an electrical sensor is selected to record the electrical characteristics of an ultrasonic transducer during operation. Briefly, a current sensor and a power sensor are available in experiments. Being different from mechanical feedback sensors, electrical feedback sensors are cheaper and their possibility of remote operation is preferable and suitable for industrial applications. Nevertheless, such sensors can only reflect the ultrasonic vibration in an indirect way. In spite of this, electrical feedback sensors are

easier to be fixed on an ultrasonic transducer compared with mechanical feedback sensors. Therefore, electrical sensors will also be employed in experiments.

As introduced before, an autoresonant control design relies on the amplitude-phase characteristics of an ultrasonic transducer with an applied load, even though such characteristics are time varying under machining conditions. The excitation force of an ultrasonic transducer is produced through piezoelectric effect. However, for mechanical feedback and electrical feedback, observation variables are different depending on the locations on an ultrasonic transducer. Consequently, amplitude-frequency-phase characteristics of these two types of control strategies are expected to show differently. For the ultrasonic transducer model displayed in Figure 4.9, the excitation force produced by the piezoelectric transducer is directly applied to the 1st step concentrator, whereas, depending on the type of feedback control strategies, observation points for optimal phase shift are:

- For mechanical feedback, an inductive sensor or a laser vibrometer measures the ultrasonic vibration signal at the end of the 2nd step of an ultrasonic transducer which indicates the observation variable is the absolute displacement of the 2nd step x_2.

- For electrical feedback, a current sensor measures the current of an piezoelectric transducer. According to equation (4.63) and equation (4.73), current is computed as the derivative of the electrical charge, which is related to both the excitation force F_0 and the input voltage u. The excitation force F_0 can be expressed as a function of the displacement of the piezoring x_0 and the displacement of the 1st step concentrator x_1. In addition, the input voltage u can be transformed as a function of the excitation force F_0 and the piezoring displacement x_0. Therefore, the observation point for electrical feedback is the absolute displacement of the 1st step x_1.

In order to obtain the amplitude-phase-frequency characteristics for both observation variables x_1 and x_2, two methods can be used. The 1st method relies on the frequency response of the linearization of the ultrasonic transducer model shown in Figure 4.9. The linear relationship between the input and output of the ultrasonic transducer can be expressed as a transfer function. In comparison, the 2nd method is to employ the ultrasonic transducer differential equations shown from (4.71) to (4.73). A further transformation of these differential equations will be executed to acquire the amplitude-phase-frequency

characteristics for both observation points. Features of the amplitude-phase characteristics for both observations points and their implications will be analysed. In addition, comparisons and discussions of the results for these two methods will also be involved. After the analysis of the amplitude-phase-frequency characteristics for both feedback types, amplitude-frequency characteristics of mechanical feedback signal, i.e. the displacement of 2nd step x_2 and electrical feedback signal i.e. the current and power of the piezoelectric transducer will be calculated respectively. Similarly, there are 2 methods to perform the calculations. One of them is to numerically analyse and utilize the dynamic different equations of the ultrasonic transducer from (4.71) to (4.73). Another approach is to simulate the ultrasonic transducer Matlab-Simulink model shown in Figure 4.10 within an interested frequency range. Results of these 2 methods will be compared and further analysed. In the end, the experimental measurements will be brought in to compare with the simulation results.

5.3.1 Amplitude-Phase-Frequency Characteristics Calculation Using Linearization of Ultrasonic Transducer Model

Theoretically, for a Linear-Time-Invariant (LTI) system with a transfer function $G(s)$, its output with a sine wave indicates the input is also a sine wave, but with a different amplitude and phase. Assuming that the input to the system is $u(t)$ and the output is $y(t)$, then the output response at a particular frequency $\omega = 2\pi f$ is given by the gain and the phase of the frequency response $G(j\omega)$ at that frequency ω. For a system shown in Figure 5.6, assuming the input and output after the initial transients are:

$$\begin{aligned} u(t) &= Usin(\omega t) \\ y(t) &= Ysin(\omega t + \varphi) \end{aligned} \tag{5.4}$$

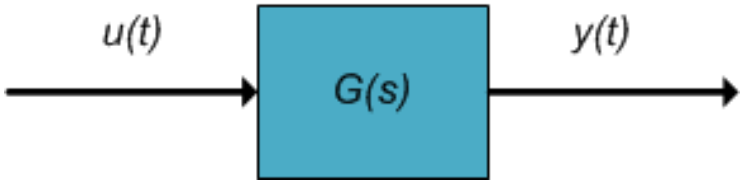

Figure 5.6 : A Linear-Time-Invariant (LTI) system

The gain and the phase at a particular frequency ω are then given by:

$$|G(j\omega)| = \frac{Y}{U}$$
$$\angle G(j\omega) = \varphi \tag{5.5}$$

By choosing a range of interested frequencies ω and computing the corresponding gain and phase values, the full amplitude-phase-frequency response of the Linear-Time-Invariant (LTI) system can be obtained. In the simulation of the ultrasonic transducer model shown in Figure 4.9, the input is the supplied voltage u which is shown in equation (4.74) and the outputs are the ultrasonic vibration x_1 and x_2 which are 2 interested points of observations. Since the transfer function describes the input to the output relation of the 2nd step ultrasonic transducer vibration x_2 is displayed in equation (4.76), a transfer function can be similarly derived for the 1st step ultrasonic vibration x_1. This is done with the linearization on the dynamic equation shown in (4.71) and (4.72) on the model shown in Figure 4.9 on the ultrasonic transducer model's equilibrium point. The input to the linearized model is the supplied voltage u and the output from the linearized model is the 1st step displacement x_1. These 2 transfer functions are shown in equation (5.6) and equation (5.7). Therefore, according to equation (5.5), the output response and the phase shift can be easily calculated for different frequency ω for both transfer functions (observation points).

$$G_1 = \frac{X_1(s)}{U(s)} = \frac{1.49s^2+108.1s+1.693\times10^{10}}{s^4+131.2s^3+2.028\times10^{10}s^2+6.551\times10^{11}s+4.979\times10^{19}} \tag{5.6}$$

$$G_2 = \frac{X_2(s)}{U(s)} = \frac{108.1s+1.693\times10^{10}}{s^4+131.2s^3+2.028\times10^{10}s^2+6.551\times10^{11}s+4.979\times10^{19}} \tag{5.7}$$

As shown in equation (5.6) and equation (5.7), s represents the Laplace operator, G_1 and G_2 describe the relation between the input to the ultrasonic transducer which is the supplied voltage and the outputs which are the ultrasonic vibration of the 1st step and the 2nd step. $U(s)$, $X_1(s)$ and $X_2(s)$ are the Laplace transformation of $u(t)$, $x_1(t)$ and $x_2(t)$. Therefore, the amplitude-phase-frequency characteristics for both observation points can be easily calculated with the help of equation (5.5) over an interested frequency range. Taking into account the natural frequencies shown in equation (4.78) of the unloaded ultrasonic transducer model shown in Figure 4.9, the interested frequency range is selected to be $f \in [5KHz \sim 25KHz]$. In Figure 5.7, the 3-D amplitude-frequency-phase characteristics and their corresponding projections are displayed. It should be noted that the blue solid curves

represent the characteristics when the ultrasonic vibration of the 2nd step x_2 is the observation point; the red dashed curve lines show the characteristic when the ultrasonic vibration of the 1st step x_1 is the observation point. It should be noted that, the phase values for both curves are all positive. Practically it means the output (the ultrasonic vibration of the 1st step x_1 and the 2nd step x_2) of the ultrasonic transducer lags the input supplied voltage u.

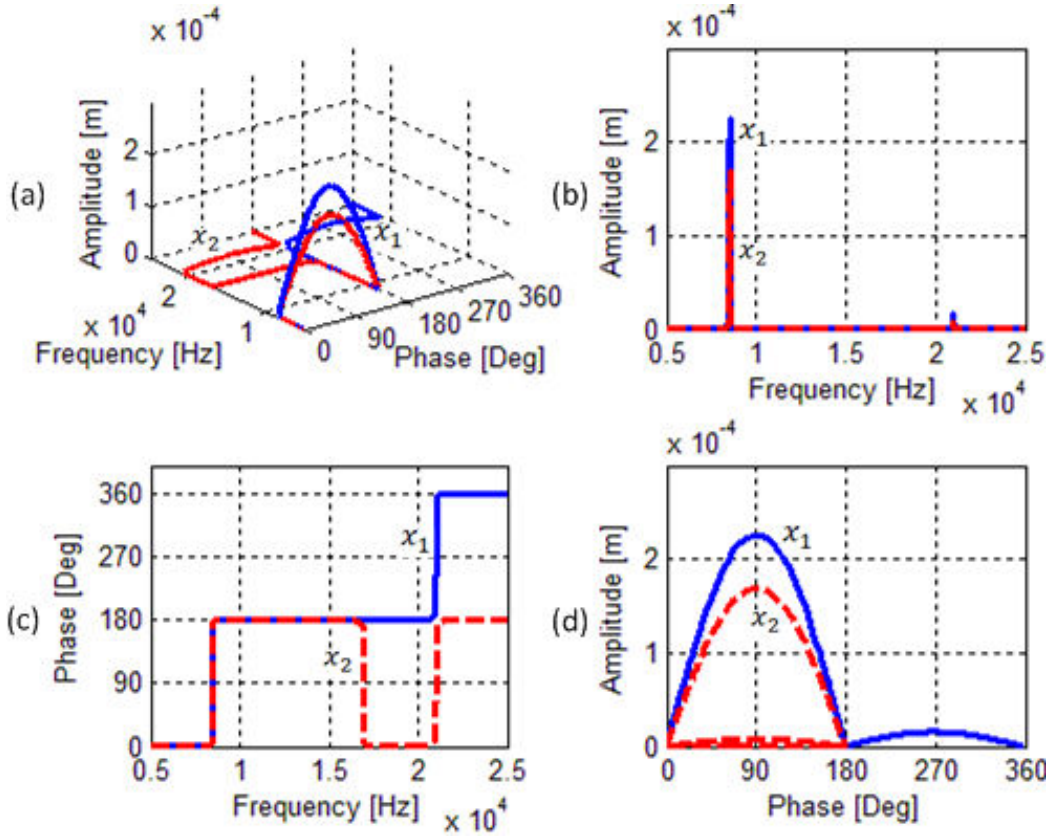

Figure 5.7 : Amplitude-Phase-Frequency characteristics for two observation points x_1 and x_2 of the linearization method: (a) 3-D amplitude-phase-frequency, (b) amplitude-frequency, (c) phase-frequency, (d) amplitude-phase

In order to verify the accuracy of the calculated amplitude-phase-frequency characteristics for both observation points, another method can be adopted in the next section which is based on the transformation of the dynamic differential equations of the ultrasonic transducer.

5.3.2 Amplitude-Phase-Frequency Characteristics Calculation Using Dynamic Differential Equations of Ultrasonic Transducer Model

Since the input to the ultrasonic transducer model is the supplied voltage u, it is sensible to combine the piezoelectric transducer model described in section 4.2 with the 2-DOF concentrator model shown in Figure 4.7. Recalling the piezoelectric transducer equations:

$$\begin{aligned} x_0 &= \frac{1}{k_{01}} F_0 + k_{02} u \\ F_0 &= C_1(\dot{x}_1 - \dot{x}_0) + K_1(x_1 - x_0) \end{aligned} \tag{5.8}$$

Where u is supplied voltage, x_0 is the small displacement of a piezoring, q is the electrical charge stored in a piezoring and F_0 is the interaction force (actuation force) between a piezoring and the 1st step concentrator. k_{01}, k_{02} are the known parameters which are $k_{01} = \frac{1}{3.84\times10^{-11}}$ and $k_{02} = 3.4 \times 10^{-10}$. x_1 is the displacement in the middle of the 1st step concentrator, K_1 and C_1 are concentrator stiffness and damping coefficient of the 1st step.

Observing the expression of x_0 in equation (5.8), it implies that the piezoelectric transducer (piezoring) has two components. One of them is the scaled supplied voltage $k_{02}u$, another component is $\frac{1}{k_{01}} F_0$. It can be considered that k_{01} is the contact stiffness of one piezoelectric ring which interacts with the 1st step concentrator at force F_0. However, the interaction force F_0 is related to both stiffness and damping coefficient of the 1st step concentrator, which means theoretically the stiffness k_{01} and K_1 are not connected simply in series. As a result, k_{01} is connected to the 1st spring-damper set directly without any mass in the middle which is shown in (b) in Figure 5.9. However, this is not a reasonable linkage between dynamic components because a mass is indispensable in a dynamic system.

As known to all, a dynamic system without a mass attached is not a purely mechanical system. On the other hand, however, as can be seen in Figure 5.8 that the contributions to interaction force F_0 from damper C_1 and spring K_1 are significantly different. Contribution from damper C_1 (red curve) can be neglected compared to contribution from K_1 (blue curve). Therefore, the approximation can be made that the interaction force F_0 is only generated by the spring K_1. Consequently, the stiffness k_{01} can be considered to connect in series with the stiffness K_1 and these two springs are arranged in parallel with the damper C_1 which is demonstrated in (c) in Figure 5.9 with the supplied voltage u acting as the input signal.

The dynamic partial differential equations (4.71) and (4.72) of the ultrasonic transducer hence can be further modified into:

$$\begin{aligned} M_1\ddot{x}_1+C_1(\dot{x}_1-k_{02}\dot{u})+k_s(x_1-k_{02}u)+C_2(\dot{x}_1-\dot{x}_2)+K_2(x_1-x_2)=0 \\ M_2\ddot{x}_2-C_2(\dot{x}_1-\dot{x}_2)-K_2(x_1-x_2)=0 \end{aligned} \tag{5.9}$$

Where in equation (5.9), k_s is the effective contact stiffness of 2 springs connected in series. Supplied voltage u acts as the input to the ultrasonic transducer which can be assumed as the following form:

$$k_s = \frac{k_{01}K_1}{k_{01}+K_1} \tag{5.10}$$

$$u = Ue^{j\omega t} \tag{5.11}$$

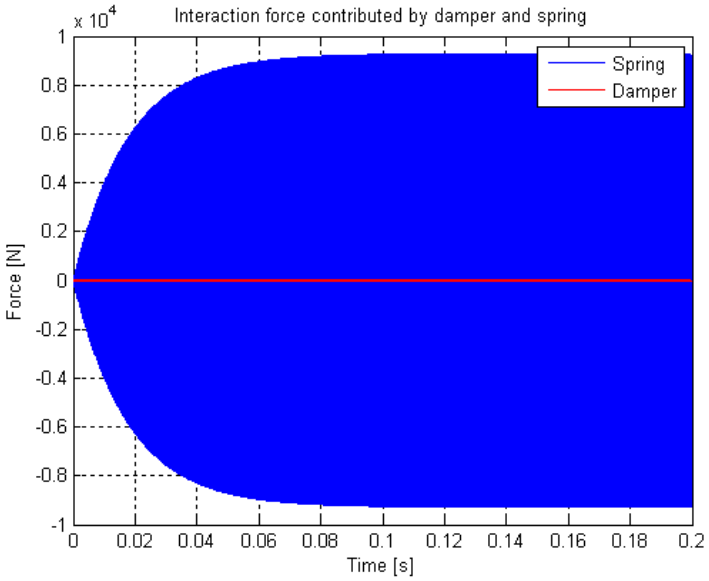

Figure 5.8 : Actuation force contribution from the stiffness and damping coefficient

Substitute equation (5.11) into equation (5.9) produces:

$$\begin{aligned} M_1\ddot{x}_1+(C_1+C_2)\dot{x}_1+(k_s+K_2)x_1-C_2\dot{x}_2-K_2x_2=k_sk_{02}Ue^{j\omega t}+C_1k_{02}Uj\omega e^{j\omega t} \\ M_2\ddot{x}_2-C_2\dot{x}_1+C_2\dot{x}_2-K_2x_1+K_2x_2=0 \end{aligned} \tag{5.12}$$

Rearranging the above equations into matrix form gives:

$$M\ddot{X}+C\dot{X}+KX=Fe^{j\omega t} \tag{5.13}$$

Where $X = \begin{bmatrix} x_1 \\ x_2 \end{bmatrix}$ is the displacement vector of the ultrasonic transducer, $M = \begin{bmatrix} M_1 & 0 \\ 0 & M_2 \end{bmatrix}$ is the mass matrix, $C = \begin{bmatrix} C_1 + C_2 & -C_2 \\ -C_2 & C_2 \end{bmatrix}$ is the damping matrix, $K = \begin{bmatrix} k_s + K_2 & -K_2 \\ -K_2 & K_2 \end{bmatrix}$ is the stiffness matrix and $F = \begin{bmatrix} k_s k_{02} U + C_1 k_{02} U j\omega \\ 0 \end{bmatrix}$ is the actuation force vector. After the transient response, the ultrasonic vibrations will gradually arrive at the steady states with the following forms:

$$\begin{aligned} x_1 &= X_1 e^{j\omega t - \varphi_1} = \overline{X}_1 e^{j\omega t} \\ x_2 &= X_2 e^{j\omega t - \varphi_2} = \overline{X}_2 e^{j\omega t} \end{aligned} \tag{5.14}$$

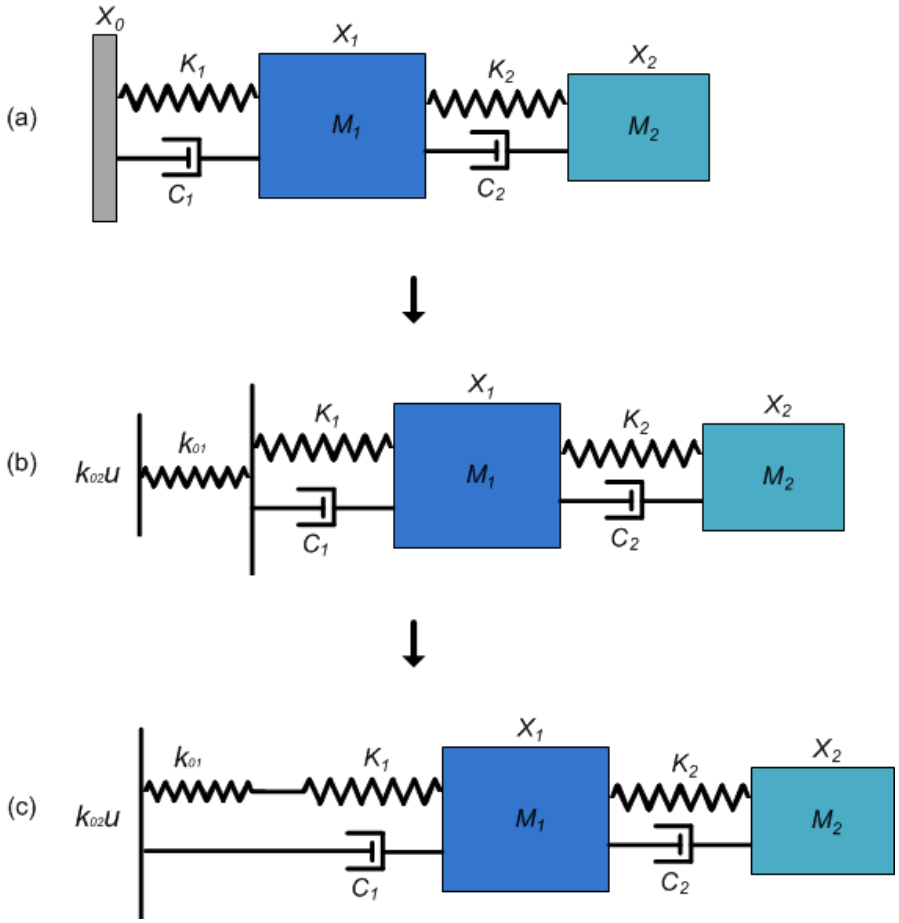

Figure 5.9 : Ultrasonic transducer model transformation: (a) original ultrasonic transducer, (b) ultrasonic transducer with input supplied voltage (non-mechanical), (c) ultrasonic transducer with input supplied voltage (mechanical)

Where X_1 and X_2 are the ultrasonic vibration amplitudes of the 1st step and 2nd step concentrator, φ_1 and φ_2 are the phase shifts with respect to the actuation force (supplied

voltage), $\overline{X}_1$ and $\overline{X}_2$ are the complex vibration amplitudes of the 1st step and 2nd step concentrator which take into account phase shifts. By replacing the expressions of x_1 and x_2 into equation (5.13), the relation between the system vibrations X and the actuation force (supplied voltage) F can be obtained:

$$(-\omega^2 M + j\omega C + K)\bar{X} = F \tag{5.15}$$

$\bar{X} = \begin{bmatrix} \overline{X}_1 \\ \overline{X}_2 \end{bmatrix}$ is the complex vibration amplitude vector. Dynamic stiffness is equal to the ratio between a force which acts on the measurement point and the complex displacement amplitude [8]. Therefore, the dynamic stiffness matrix of the ultrasonic transducer becomes:

$$W(j\omega) = [-\omega^2 M + j\omega C + K] \tag{5.16}$$

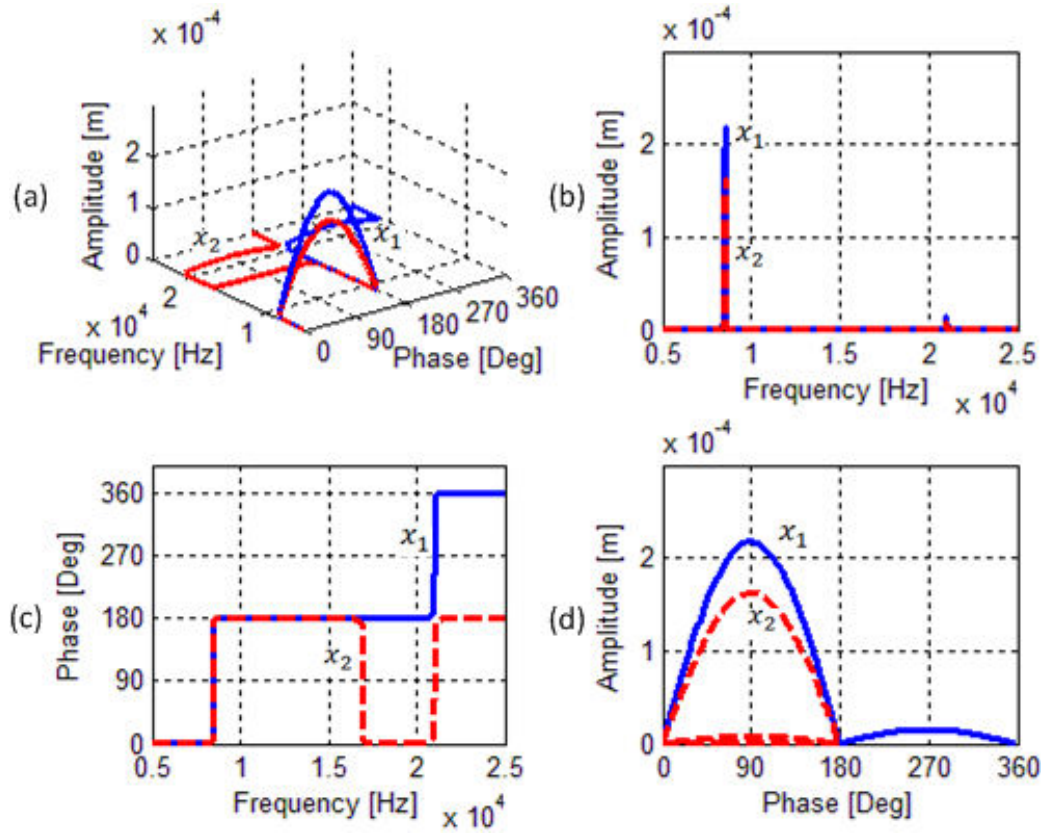

Figure 5.10 : Amplitude-Phase-Frequency characteristics for two observation points x_1 and x_2 of dynamic differential method: (a) 3-D amplitude-phase-frequency, (b) amplitude-frequency, (c) phase-frequency, (d) amplitude-phase

Therefore, the complex vibration amplitude X_1, X_2 and the corresponding phase shift φ_1, φ_2 can be calculated with the same interested frequency range $f \in [5KHz{\sim}25KHz]$. The amplitude-phase-frequency characteristics of the ultrasonic transducer for both observation variables are shown in Figure 5.10. Similarly, the blue solid curves show the observation point of the ultrasonic vibration of the 2nd step concentrator x_2 and red dashed curves illustrate the observation point of the ultrasonic vibration of the 1st step concentrator x_1. In addition, it can be observed clearly that Figure 5.7 and Figure 5.10 have a close agreement in shape, resonant frequency and magnitude. Therefore, both methods are applicable and feasible for amplitude-phase-frequency characteristics calculation of the ultrasonic transducer.

5.3.3 Amplitude-Phase Characteristic Analysis for both Observation Points

Since the autoresonant control strategy relies on the amplitude-phase characteristic, amplitude-phase characteristics for both feedback types (observation points) are enlarged for successive analysis which is shown in Figure 5.11. Blue curve represents the characteristic when the 2nd step ultrasonic vibration x_2 is selected to be observed and red dashed curve stands for the observation point of the 1st step ultrasonic vibration x_1. Several features can be concluded from this picture.

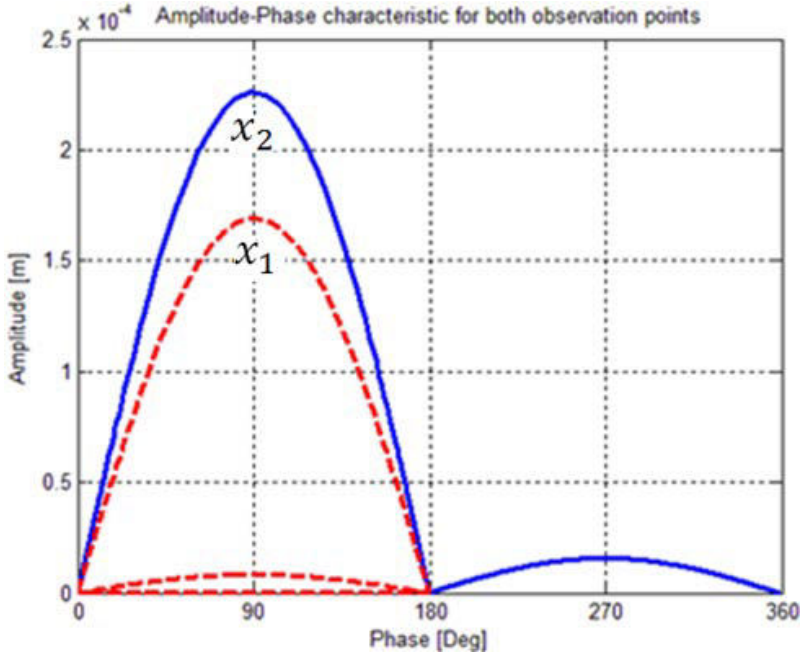

Figure 5.11 : Amplitude-phase characteristic for both observation points x_1 and x_2

- Both curves present a gently sloping bell shape near the resonant peak. In comparison, the amplitude-frequency characteristic shown in (b) in either Figure 5.7 or Figure 5.10 exhibits an extremely sharp peak near the resonant frequencies which strongly suggests the possibility and feasibility of the employment of phase control.

- At phase shift $\frac{\pi}{2}$, one of the vibration magnitudes of the 1st step concentrator and the vibration amplitude of the 2nd step concentrator demonstrates a several hundred micrometres value which seems unreasonably large. This was not observed during experiments with resonant frequency around $8.5KHz$. This is due to the limitation of simplification of the ultrasonic transducer into a 2-DOF model. In other words, a simplified 2-DOF model is only valid within a certain range in terms of resonant frequency and vibration amplitude. The performance of a 2-DOF model is not guaranteed for those frequencies out of the range.

- The blue curve which represents the characteristic of the ultrasonic vibration x_2 at the end of the 2nd step concentrator displays a single-valued property. In other words, one phase shift corresponds to fixed amplitude. In contrast, the red-dashed curve that stands for the characteristic of the ultrasonic vibration in the middle of the 1st step concentrator x_1 exhibits certain ambiguity which indicates one phase shift reflects three different vibration amplitudes.

In Figure 5.11, it is clear that one phase shift generates 3 oscillation regimes with different vibration amplitudes when the 1st step concentrator's ultrasonic vibration x_1 is selected to be the observation point. These 3 oscillation regimes are excited respectively with 3 different frequencies shown in (b) in Figure 5.7 and Figure 5.10. The first 2 regimes are the products of the 1st and 2nd oscillation modes and the 3rd regime with the lowest amplitude is known as an 'anti-resonant' regime. Nonetheless, despite the first 2 resonant regimes can be seen clearly, the 'anti-resonant' regime seems less obvious. Therefore, the display of amplitude of (b) in Figure 5.7 and Figure 5.10 has been further revised into logarithm when the 1st step concentrator's ultrasonic vibration x_1 is involved both in excitation and observation.

Figure 5.12 shows the amplitude-frequency characteristic when the 1st step concentrator's ultrasonic vibration x_1 is selected to be the excitation signal and the observation point. Clearly, 2 resonant regimes with resonant frequencies $8.5KHz$ and $21.0KHz$ corresponds to

the first 2 vibration regimes shown in Figure 5.11. The 3rd vibration regime displays a distinct property of an 'anti-resonant' regime which arrives at the valley peak and this 'anti-resonant regime' is the one shown in Figure 5.11 with the lowest magnitude. According to numerical calculation, the 'anti-resonant' vibration regime has a anti-resonant frequency $17.0KHz$.

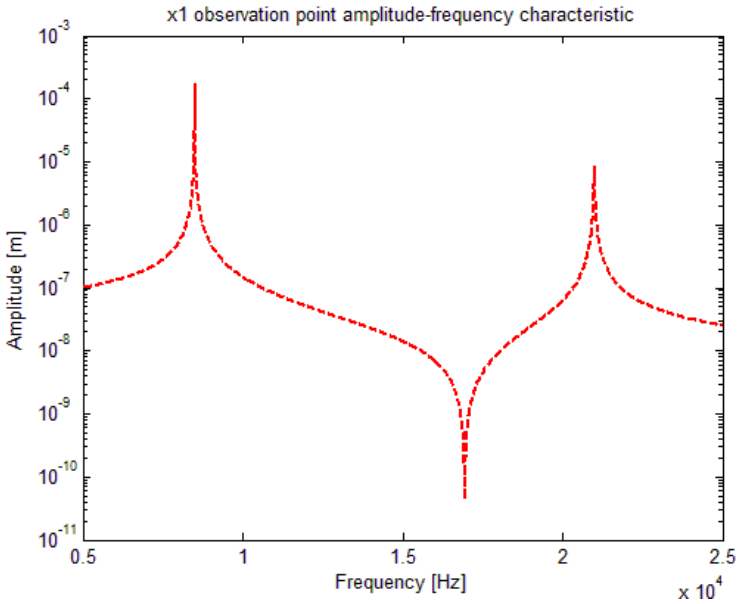

Figure 5.12 : Amplitude-frequency characteristic of 1st step as excitation and observation

In the following sections, stability analysis for these 3 vibration regimes will be executed in computer simulation. Generally speaking, the procedure for the stability investigation is that the ultrasonic transducer is initially excited with 3 vibration regimes' resonant frequencies. After the ultrasonic vibration arrives at a steady state level, the loop is closed and the ultrasonic vibration of the 1st step concentrator x_1 is employed as the feedback signal. Meanwhile, changes in the ultrasonic vibration for both the 1st step x_1 and the 2nd step x_2 are monitored. Theoretically, a continuation of the ultrasonic vibration is expected after the loop is closed which confirms a stability of the corresponding vibration regime. In comparison, a sudden change (disappearance or essential increase) in the ultrasonic vibration signal concludes instability.

5.3.3.1 Stability Analysis of 1st Resonant Regime

As calculated before, the 1st resonant regime has a resonant frequency $8.5KHz$. Therefore, the ultrasonic transducer model is initially excited with this frequency. When the ultrasonic vibration arrives at its steady-state, the loop is closed with the ultrasonic vibration of 1st step

x_1 acting as the feedback signal and the phase shift is tuned to be near $\frac{\pi}{2}$ as indicated in Figure 5.11. Simultaneously, the ultrasonic vibrations of both steps of the ultrasonic transducer are recorded accordingly.

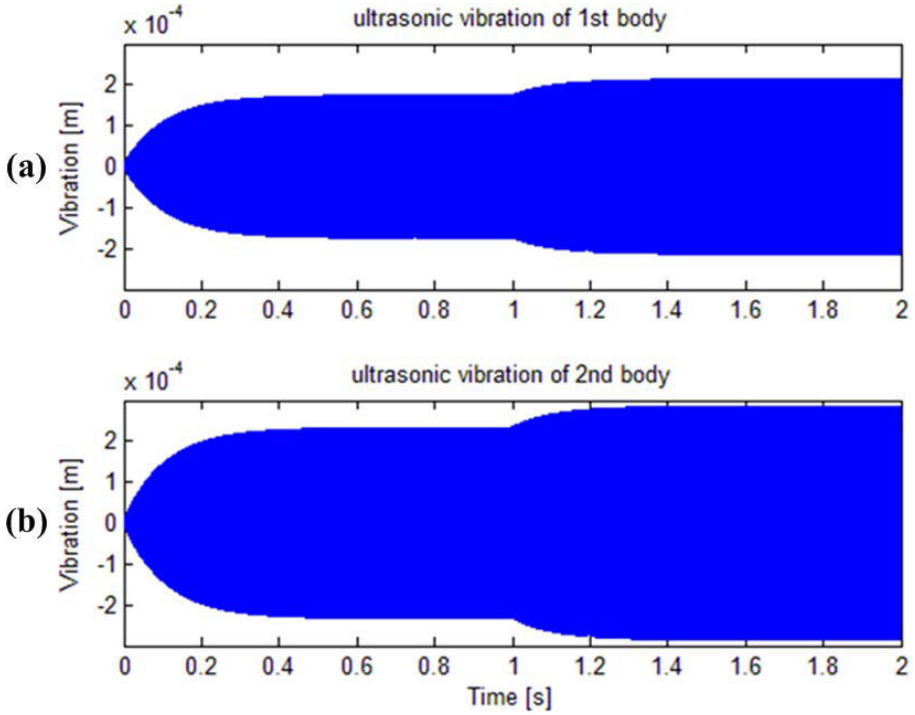

Figure 5.13 : Stability analysis of 1st resonant regime with observation point x_1 : (a) amplitude response of 1st step, (b) amplitude response of 2nd step

In Figure 5.13, ultrasonic vibrations of the 1st step and 2nd step ultrasonic transducer are displayed. As can be seen, the ultrasonic vibrations for both steps are gradually boosted up and reach their steady states at 0.4sec. The steady state vibration amplitudes for both steps are equivalent to the 1st peak values shown in Figure 5.11 (blue solid curve and red dashed curve). After the ultrasonic transducer oscillates for a reasonably long time, the loop is closed at 1.0sec. Clearly, both steps continue to oscillate as before even though the level of oscillations is increased by certain amount which is likely caused by the filter within the loop. The filter is used to rectify an amplified and phase-shifted square wave to create a quasi-sinusoidal signal with reasonable magnitude which is then supplied into the ultrasonic transducer. Filter design will be described elaborately in Chapter Six. Consequently, since the self-sustaining process has not lead to a sudden change to the ultrasonic vibration for both steps, it can be concluded that the 1st resonant regime is stable.

5.3.3.2 Stability Analysis of 2nd Resonant Regime

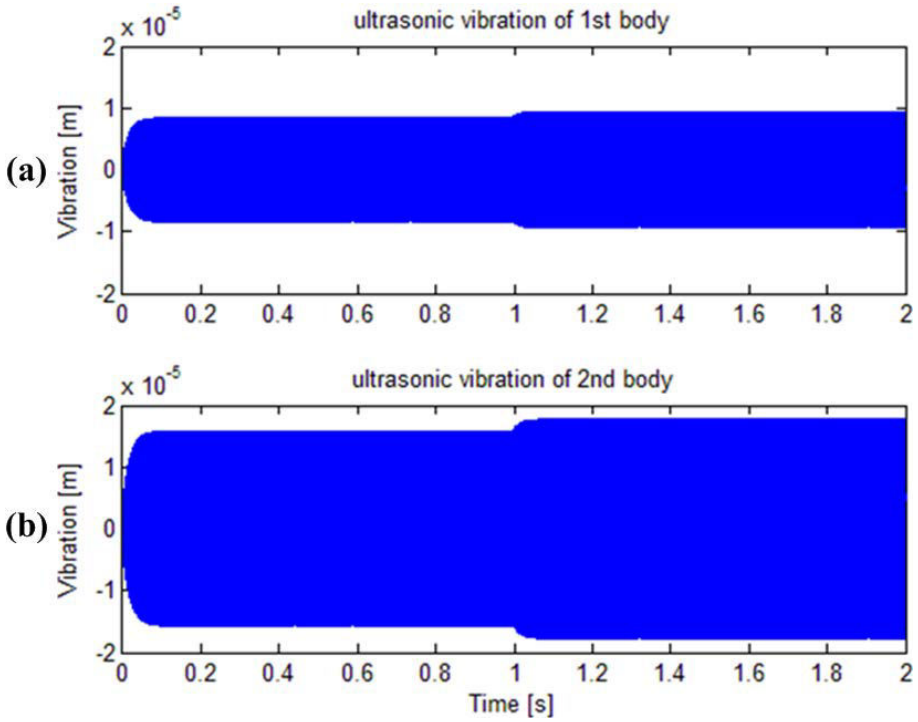

Figure 5.14 : Stability analysis of 2nd resonant regime with observation point x_1: (a) amplitude response of 1st step, (b) amplitude response of 2nd step

The 2nd regime oscillates at a resonant frequency $21.0KHz$ which is shown in Figure 5.12. Consequently, the supplied voltage u uses this frequency to initially boost up the ultrasonic transducer. The operation procedure is exactly the same as the description in section 5.3.3.1. In Figure 5.14, the 1st step and 2nd step ultrasonic vibrations are illustrated. Clearly, both steps ultrasonic vibrations quickly climb to their corresponding steady states which take less than 0.1secs. The steady state oscillation amplitudes have equal values as the amplitudes shown in Figure 5.11. After this, the ultrasonic transducer keeps vibrating before the loop is closed which takes place at 1.0sec. Both steps continue to vibrate as usual in spite of a slight increase in the amplitude, which again, is caused by the filtering process. As a result, the 2nd resonant regime is also a stable vibration regime because the closed loop system produces no essential change to the ultrasonic vibration amplitudes for both steps.

5.3.3.3 Stability Analysis of Anti-Resonant Regime

The 'anti-resonant' frequency shown in Figure 5.12 is approximately $17.0KHz$. Hence, the ultrasonic transducer is activated with this frequency initially. Procedure remains same. In

Figure 5.15, results are shown. In the beginning, the ultrasonic transducer is actuated and the ultrasonic vibrations seem small which corresponds to the 'anti-resonance' values for both steps. At 1.0sec, the loop is closed and the 1st step ultrasonic vibration acts as the feedback signal. It can be observed that the ultrasonic vibrations suddenly soar into huge values for both steps. The closed loop ultrasonic vibration steady state values equal the steady state values of the 1st resonant regime. In other words, the feedback system 'jumps' from the 'anti-resonant' regime to the 1st resonant regime. Therefore, as a 'jump' phenomenon takes place in the closed loop system, the 'anti-resonant' regime is instable.

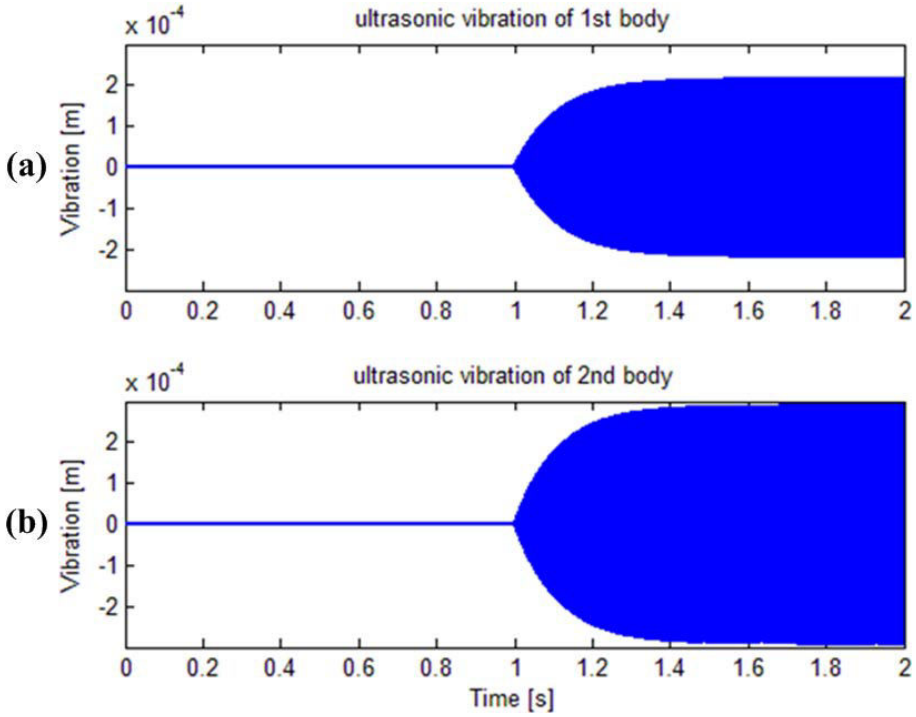

Figure 5.15 : Stability analysis of 'anti-resonant' regime with observation point x_1: (a) amplitude response of 1st step, (b) amplitude response of 2nd step

5.3.3.4 Conclusion of Stability Analysis

According to stability analysis of the 1st resonant regime, 2nd resonant regime and the 'anti-resonant' regime, it can be concluded that both resonant regimes can be maintained under phase control. In contrast, the 'anti-resonant' regime exhibits a 'jump' to the 1st resonant regime in the closed loop which indicates the 'anti-resonant' regime is unstable and physically cannot be attained under phase control.

Even though both resonant regimes are stable and can be controlled under phase control, one phase shift corresponds to 2 different vibration amplitudes when the 1st step ultrasonic vibration x_1 participates in both excitation and observation. This non-single valued property will cause 'confusion' to the closed loop system under phase control when the current is selected as the feedback signal. Therefore, a filtration process is strongly recommended for the electrical feedback in order to pick up the desired vibration regime whilst filter out the others. According to the computer simulation, this filtration process brings tremendous problems to the control design as a filter can shift the phase of the amplified square wave. This additional phase shift introduced by a filter is uncontrollable and unchangeable with autoresonant control. Filter selection and electrical feedback will be investigated and examined closely with mechanical feedback later.

5.3.4 Amplitude-Frequency Characteristics Investigation for Ultrasonic Vibration, Current and Power

It has been introduced in section 5.3 that mechanical feedback and electrical feedback employ different sensor signals. Mechanical feedback uses a mechanical sensor to measure the ultrasonic vibration. In contrast, electrical feedback employs electrical signals to form the feedback loop which can be either a current or a power of a piezoelectric transducer. In order to examine the effect on the control system design for these 2 feedback types, amplitude-frequency characteristics of the ultrasonic vibration, current and power have been numerically and experimentally obtained. Basically, there are 2 methods to calculate the amplitude-frequency characteristics numerically. One method relies on the dynamic differential equations described in section 5.3.2. Dynamic equations for current and power can be subsequently deducted according to the current expression in equation (4.63). Another way is to simulate the ultrasonic transducer model in Matlab-Simulink within an interested frequency range then record the ultrasonic vibration, current and power respectively. Apart from the numerical computation, an experiment has been performed to record 3 signals. In the end, comparison and analysis of the amplitude-frequency characteristics for mechanical feedback and electrical feedback will be involved.

5.3.4.1 Amplitude-Frequency Characteristics Calculation Using Dynamic Differential Equations of Ultrasonic Transducer

As shown in Figure 5.8 that the interaction force F_0 contribution from the elastic spring K_1 is essential compared to the contribution from the viscous damper C_1. Therefore, the interaction force F_0 displayed in equation (5.8) can be modified:

$$\begin{aligned} x_0 &= \frac{1}{k_{01}} F_0 + k_{02} u \\ F_0 &\approx K_1 (x_1 - x_0) \end{aligned} \tag{5.17}$$

Recalling the electrical charge q in equation (4.63) of the piezoelectric transducer, by taking the derivative to the charge with respect to time obtains the current which has the following form:

$$\begin{aligned} q &= k_{03} F_0 + k_{04} u \\ i &= \dot{q} = k_{03} \dot{F}_0 + k_{04} \dot{u} \end{aligned} \tag{5.18}$$

Where $k_{03} = 3.4 \times 10^{-10}$ and $k_{04} = 2.1 \times 10^{-9}$ are the coefficients shown in equation (4.63), q is the electrical charge, u is the supplied voltage and i is the current flows through the piezoelectric transducer. After rearrangement of equation (5.17), expression of the interaction force F_0 in terms of x_1 and u can be obtained as:

$$F_0 = \frac{k_{01} K_1 x_1 - k_{01} k_{02} K_1 u}{k_{01} + K_1} \tag{5.19}$$

Substituting the expression of F_0 shown in equation (5.19) into equation (5.18) produces the current:

$$i = \frac{k_{01} k_{03} K_1 \dot{x}_1 + (k_{01} k_{04} + k_{04} K_1 - k_{01} k_{02} k_{03} K_1) \dot{u}}{k_{01} + K_1} \tag{5.20}$$

Thus, the current expression is derived. It is presumed that after the ultrasonic transducer passes its transient response and reaches the steady state, the current also arrives at its steady state which has following form:

$$i = I e^{j\omega t - \varphi_i} = \bar{I} e^{j\omega t} \tag{5.21}$$

I is the current amplitude and φ_i is the phase shift between the current i and the supplied voltage u, $\bar{I}$ is the complex amplitude of the current i which takes the phase shift φ_i into account. Moreover, the steady state ultrasonic vibration of the 1st step concentrator and the supplied voltage u has been assumed in section 5.3.2. Therefore after substitution of equation (5.21) into equation (5.20) allows:

$$\bar{I} = \frac{j\omega}{k_{01}+K_1}[k_{01}k_{03}K_1\bar{X}_1 + (k_{01}k_{04} + k_{04}K_1 - k_{01}k_{02}k_{03}K_1)U] \tag{5.22}$$

Hence, the amplitude-frequency characteristics for the current can be calculated within the interested frequency range. In the case of power, it is assumed to be a sinusoidal signal at steady state, and then it can be calculated in the following format:

$$P = \frac{1}{T}\int_0^T uidt \tag{5.23}$$

P is the average power of the ultrasonic transducer, u is the supplied voltage and i is the current, T is the calculated period of oscillations. Assume the supplied voltage u and the current i with following form:

$$\begin{aligned} u &= Ue^{j\omega t} \\ i &= Ie^{j\omega t-\varphi_i} \end{aligned} \tag{5.24}$$

Substituting equation (5.24) into equation (5.23) gives the expression of the average power :

$$P = \frac{1}{2}UIcos(\varphi_i) = \frac{1}{2}UI\Re e\left[e^{j\varphi_i}\right] = \frac{1}{2}\Re e(ui) \tag{5.25}$$

Where $\Re e$ represents the real part of a complex number. Since the expressions of the voltage u and current i have been introduced in equation (5.24), the average power can then be calculated successively by taking the real part of the product of the supplied voltage u and the current i.

In Figure 5.16, the amplitude-frequency characteristics of the ultrasonic vibration at the end of the 2nd step concentrator, current and average power are shown respectively. 3 curves are obtained within an interested range of $f \in [20.5KHz \sim 21.5KHz]$ which centres around the ultrasonic vibration resonant frequency $21.0KHz$. It can be observed clearly that the resonant

peak of the ultrasonic vibration (a) has an accurate coincidence with the peak in average power (b) as well as with current (c) even if the current seems to have a slight reflection after the minimal value. As described before, an autoresonant control system always targets at the resonant regime. Since three signals coincide at the same resonant frequency, the supplied voltage u used to drive the ultrasonic transducer in the feedback loop in Matlab-Simulink model for mechanical feedback, current feedback and power feedback is supposed to have a similar value. This can be verified in Chapter Six. In next section, the characteristics results acquired from computer simulation will be demonstrated.

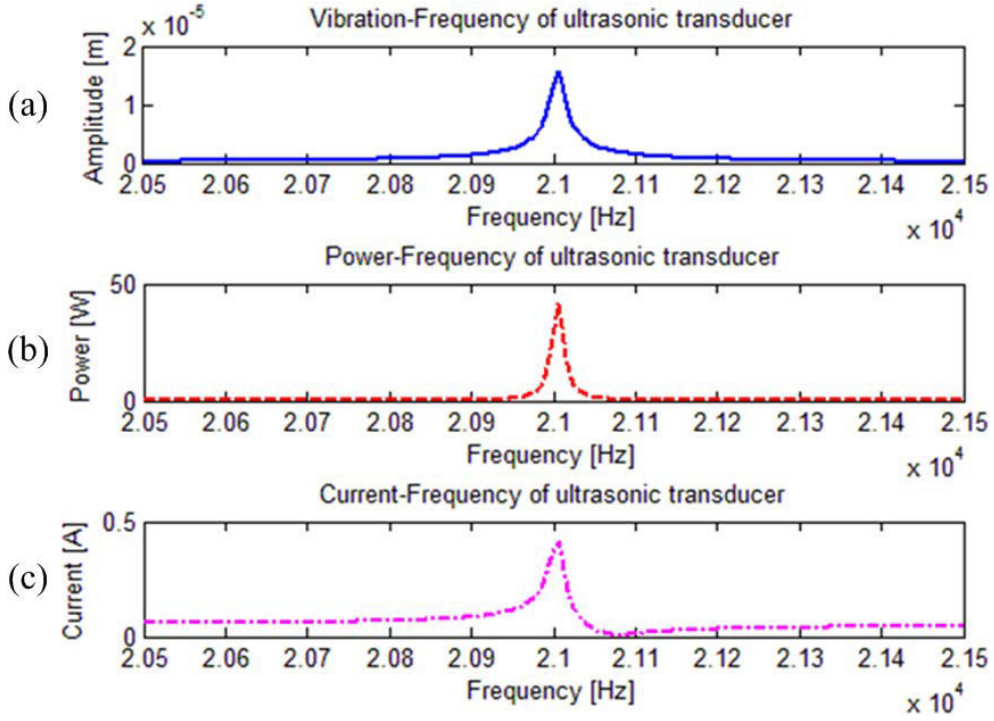

Figure 5.16 : Amplitude-Frequency characteristics of three signals using dynamic equation method: (a) ultrasonic vibration of 2nd step concentrator, (b) power, (c) current

5.3.4.2 Amplitude-Frequency Characteristics Calculation Using Computer Simulation of Ultrasonic Transducer

Another approach used to calculate the amplitude-frequency characteristics for the ultrasonic vibration of the 2nd step x_2, current and power is to use computer simulation of an ultrasonic transducer model. During simulation process, an interested frequency interval is $f \in [20.5KHz \sim 21.5KHz]$. The ultrasonic vibration at the end of the 2nd step concentrator, current and power of the piezoelectric transducer are recorded literally.

Figure 5.17 demonstrates the amplitude-frequency characteristics of the ultrasonic vibration of the 2nd step, average power and current of the piezoelectric transducer. As can be seen, the ultrasonic vibration meets at a same resonant frequency with the current and the power which indicates a similar supplied voltage u in feedback loop. In conclusion, both approaches used to calculate amplitude-frequency characteristics of mechanical feedback signal and electrical feedback signals are accurate and effective. In order to verify the preciseness of the amplitude-frequency characteristics obtained for numerical model, an experiment on an electromechanical ultrasonic transducer has been carried.

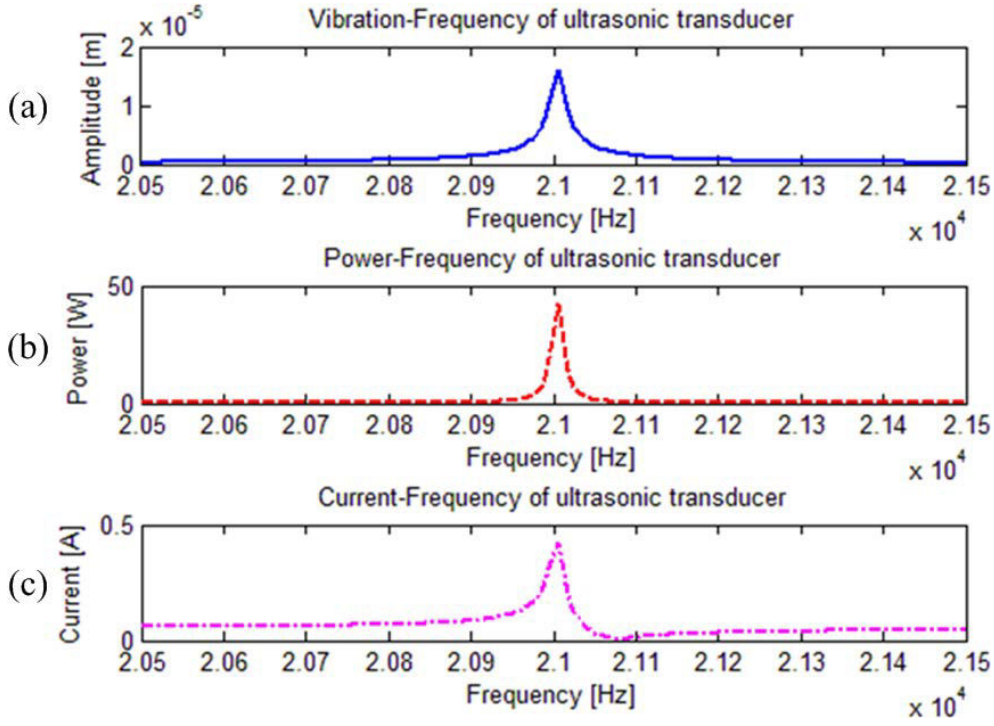

Figure 5.17 : Amplitude-Frequency characteristics of three signals using computer simulation method: (a) ultrasonic vibration of 2nd step concentrator, (b) power, (c) current

5.3.4.3 Amplitude-Frequency Characteristics of Experiment

In order to acquire the characteristics of an electromechanical ultrasonic transducer (without a drill bit attached), an experiment has been performed and the schematic diagram of the experimental setup is shown Figure 5.18. To start with the experiment, a swept sine wave is generated from a SFG-2110 Synthesized Function Generator with reasonable amplitude. Before the swept sine wave is supplied into a universal amplifier, the resonant frequency f_r of the ultrasonic vibration is manually explored by slowly changing the excitation frequency. Therefore, an interested frequency range can be defined which centres around f_r. The swept

sine wave is fed to a universal amplifier to amplify the driving signal at a primary stage. After this, the amplified signal is supplied into a universal matchbox (transformer) to adjust the high impedance of the universal amplifier to the low impedance of the ultrasonic transducer (structure and explanation of the universal matchbox will be introduced in Appendix I). As a result, a high voltage is generated by the universal matchbox (transformer) which is used to drive the ultrasonic transducer. A GE8115 Differential Probe is employed to collect the supplied voltage signals, the measurement range of the differential probe is $-1500V \sim 1500V$. Furthermore, a LEM HEME Ltd PR 30 Current probe is connected in order to acquire samples of the current flows through the piezorings. In addition, a power sensor has been manufactured to calculate the product of the voltage u and the current i in real time. After the instantaneous power has been collected, the average power of the ultrasonic transducer can be computed using the following equation:

$$P = \frac{1}{T}\int_0^T uidt \tag{5.30}$$

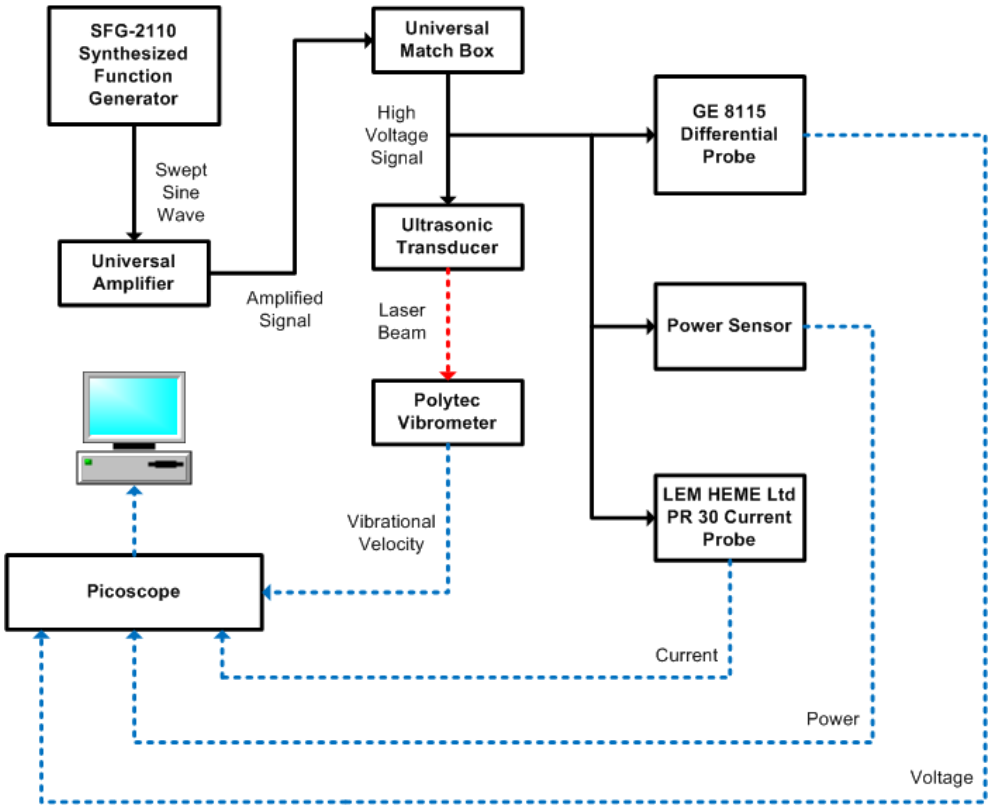

Figure 5.18 : Experimental schematic diagram to acquire amplitude-frequency characteristics of ultrasonic vibration, current, power and voltage

P represents the average power, T is one oscillation period, u and i are the voltage and the current. Apart from the electrical signals, the actual mechanical vibration at the end of the 2nd step concentrator x_2 is measured by a Polytec Vibrometer. This is realized by shining a laser beam to the vertical surface of a flatly attached reflection film at the end of the 2nd step concentrator. Eventually, both mechanical signal and electrical signals are stored in a PicoScope which is further connected to a computer for data processing. The increment of the excitation frequency has been chosen as $0.01KHz$ in order to allow sufficient frequency points to be captured. This high resolution is important especially for those characteristics near resonance.

Results obtained from experiment are showed in Figure 5.19. As can be seen, the ultrasonic vibration's resonance (a) coincides with the resonance of the average power (b) and the current (c). Besides, the shape of 3 signals conforms to the numerical curves which enhance the numerical results. The distinction between the numerical calculation and the experiment is the shift in the resonant frequency. Nonetheless, a simple 2-DOF ultrasonic transducer model exhibits a high validity and similarity to the electromechanical ultrasonic transducer in spite of such resonant frequency shift.

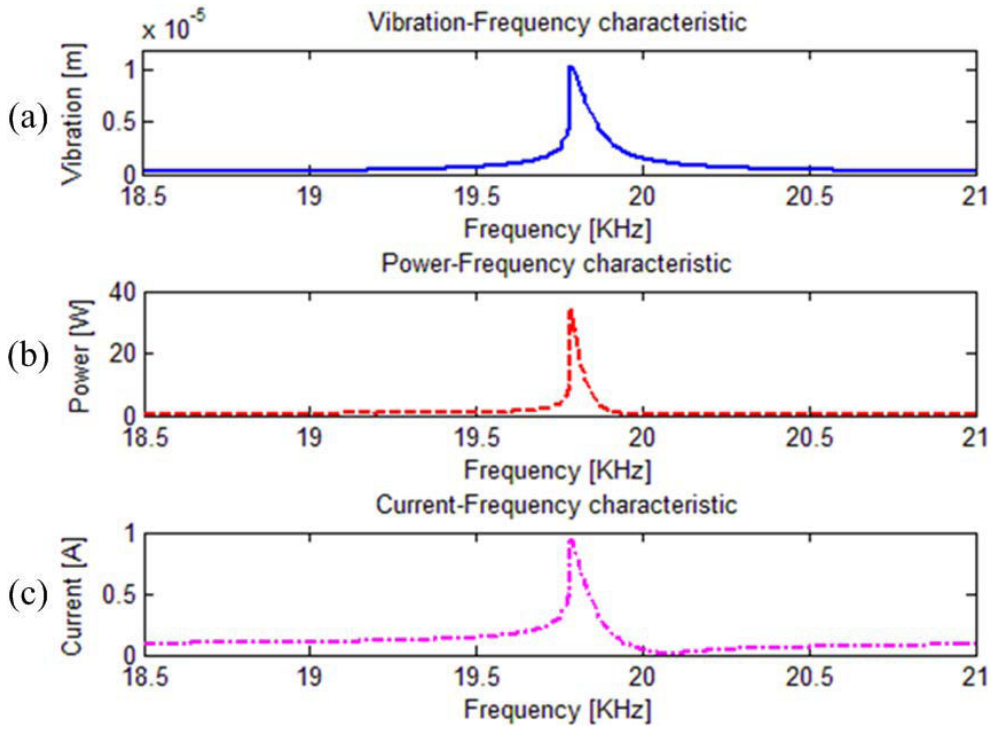

Figure 5.19 : Amplitude-Frequency characteristics obtained experimentally: (a) ultrasonic vibration of 2nd step concentrator, (b) power, (c) current

The supplied voltage u is recorded simultaneously which is shown in Figure 5.20. Clearly, the resonant frequency of the voltage signal also coincides with other 3 signals. However, the shape of the voltage shows a more drastic change over the resonant frequency compared with the current. The maximum voltage is nearly $300V$ where the minimum voltage is around $20V$. At the frequency range beyond resonance, voltage remains around $100V$.

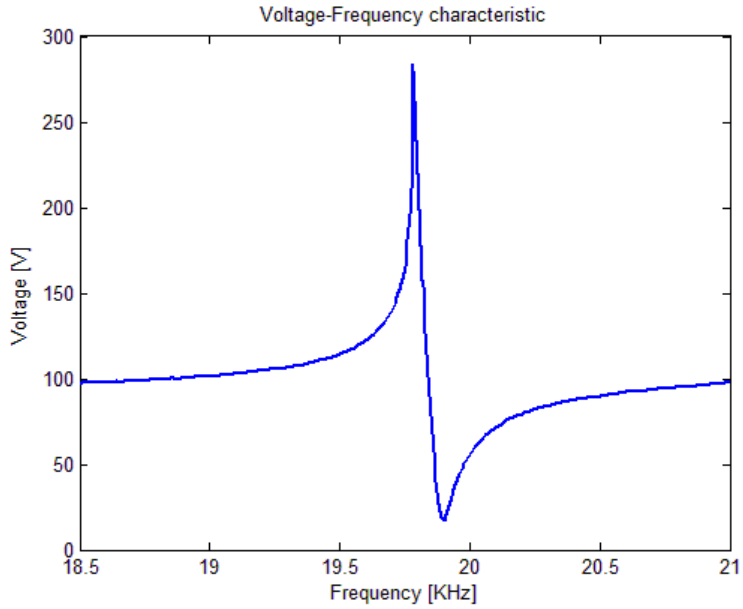

Figure 5.20 : Amplitude-Frequency characteristic of the supplied voltage

As a matter of fact, the supplied voltage u depends on several factors. One of them is the air gap distance between two ferrite cores in the universal matchbox. It has been experimentally found by adjusting the position of one ferrite is able to change the voltage level and signals wave forms significantly. The ultrasonic vibration amplitude can be optimized (maximized) by adjusting the position of the ferrite core. Investigation and optimization of the universal matchbox can be found in Appendix I. The supplied voltage u has been selected as $200V$ in the numerical simulation which is a normal working voltage of the ultrasonic transducer at resonance.

5.4 Summary

In this chapter, the algorithms of phase control, amplitude control and phase-amplitude combined control have been introduced. A Matlab-Simulink model describes these algorithms is illustrated and each function block is explained and analysed in details.

In order to better understand the autoresonant control system, the characteristics for both mechanical feedback and electrical feedback systems are obtained with a number of reliable and feasible methods. Results of these methods show a high similarity with each other which confirmed the validity and accuracy of the 2-DOF model. Due to the fact that the key principle of the autoresonant control is to control the phase between the input and output of the ultrasonic transducer, the amplitude-phase characteristics for mechanical feedback observation point x_2 and electrical observation point x_1 are depicted. The conclusion implies that the amplitude-phase characteristic of the mechanical feedback observation point x_2 displays a bell-shape feature with a one-to-one mapping between the phase shift value and the amplitude value. This suggests that a simple low pass filter is able to rectify the square wave to act as the supplied voltage. In contrast, the amplitude-phase characteristic for the electrical feedback observation point x_1 exhibits an ambiguity property. In other words, the non-single value feature indicates that one phase shift reflects 3 different oscillation regimes. These regimes' stabilities have been investigated numerically which recommends a proper filtration process in order to pick up the desired oscillation regime.

In addition, the amplitude-frequency characteristics for mechanical feedback vibration x_2 and electrical feedback signals (current i and average power P) are computed in numerical simulation with several methodologies. These characteristics have been recorded in experiment too in order to validate the numerical results. As mechanical feedback signal reflects the ultrasonic vibration x_2 in a direct way whilst electrical feedback only reflect it in an indirect way, this theoretical investigation and experimental analysis comparison seems necessary for the impact these two feedback types may impose on the autoresonant control system design.

Chapter Six Control Evaluation in Numerical Simulation

This chapter is dedicated to the numerical simulation of the control evaluation for several feedback control strategies. Before mechanical feedback and electrical feedback are tested, frequency controlled ultrasonic vibration will be explored.

Mechanical feedback employs a mechanical sensor to measure the actual ultrasonic vibration at the end of the 2nd step concentrator x_2 and apply it as a feedback signal. Since mechanical feedback directly reflects the ultrasonic vibration, it is supposed to present a better control than electrical feedback. In contrast, electrical feedback uses electrical characteristics of a piezoelectric transducer which can be either a current or a power as a feedback signal. Due to the fact that electrical signals reflect the ultrasonic vibration in an indirect way, this type of feedback control is assumed to present a more inferior result than mechanical feedback. Basically, the effectiveness of electrical feedback control relies on the dynamic coupling (formula) between electrical parameters and mechanical vibration.

An autoresonant control system is designed to keep the ultrasonic vibration at the end of 2nd step x_2 at a desired level during vibro-impact process. In numerical simulation,the applied load will be changed and the RMS of the sensor signals will be monitored for each control cycle. Generally speaking, as can be seen in Figure 4.17, there are several parameters in Kelvin-Voigt model affecting the applied load (feed force). One of them is the contact stiffness K which is an essential contributor to the loading; the other one is the viscous damper C which an insignificant contributor to the applied load. In addition, change in initial interference Δ is also a subject of interest for control evaluation. Therefore, two types of tests are evaluated: change in contact stiffness K and change in initial interference Δ between the ultrasonic transducer and the applied load.

The range of the change for the increase in contact stiffness is $K \in [1 \times 10^8 N/m \sim 7 \times 10^8 N/m]$ with an increment $1 \times 10^8 N/m$. The interval of the change in initial interference is $\Delta \in [-2 \times 10^{-7} m \sim -1 \times 10^{-5} m]$ with an increment $-2 \times 10^{-6} m$. Changes for both contact stiffness K and initial interference Δ are applied to mechanical feedback, current feedback and power feedback respectively. It should be noted that in numerical simulation,

the ultrasonic transducer is not attached with a drill bit. In other words, tool effect is not explored and control evaluation is purely carried out on the ultrasonic transducer.

6.1 Frequency Control

In order to evaluate and compare all the control strategies, the loaded ultrasonic vibrating system controlled with a fixed resonant frequency will be examined first. The procedure for the frequency controlled ultrasonic vibrating system is: the ultrasonic transducer described in Figure 4.17 with the parameters shown in equation (4.84) has been initially excited by a supplied voltage u with a resonant frequency shown in equation (4.85). The ultrasonic vibration at the end of the 2nd step concentrator x_2 is monitored. Once the steady state vibration is reached, the contact stiffness K or the initial interference Δ is increased and the changes in the ultrasonic vibration of the 2nd step x_2 are recorded.

6.1.1 Change in Contact Stiffness

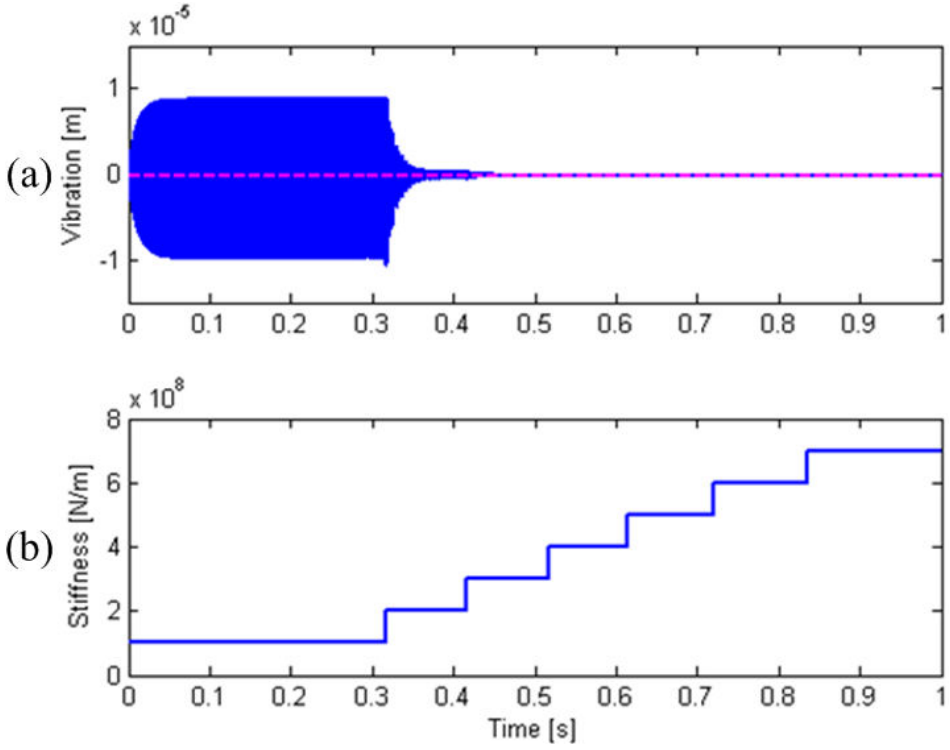

Figure 6.1 : Frequency controlled ultrasonic vibration during changing contact stiffness K : (a) ultrasonic vibration at the end of 2nd step concentrator, (b) change in contact stiffness K

Results of the frequency controlled ultrasonic vibration during changing the contact stiffness K are shown in Figure 6.1. (a) shows the 2nd step ultrasonic vibration x_2 during the change in

the contact stiffness K (b). Pink dashed line in (a) stands for the initial interference $\Delta = -2 \times 10^{-7} m$. As can be seen, initially, the ultrasonic vibration gradually climbs to its steady state $9\mu m$ zero-to-peak. After this, it maintains at a steady state for a while. During this period, parameters of the applied load conform to the values in equation (4.84). At 0.3sec, due to a sudden increase in the contact stiffness K from $1 \times 10^8 N/m$ to $2 \times 10^8 N/m$, the 2nd step ultrasonic vibration x_2 drops to a low level. As the contact stiffness K ascends continually to $7 \times 10^8 N/m$, the ultrasonic vibration x_2 completely vanishes in the end.

In conclusion, the 2nd step ultrasonic vibration x_2 seems to react sensitively to the change in the contact stiffness K. Therefore, the ultrasonic vibration cannot be properly maintained through a fixed frequency excitation while increasing the contact stiffness K.

6.1.2 Change in Initial Interference

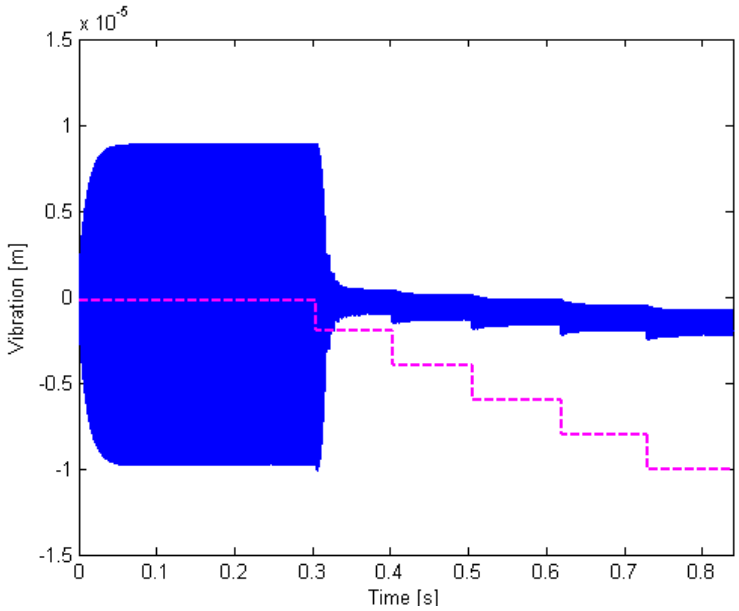

Figure 6.2 : Frequency controlled 2nd step ultrasonic vibration during changing initial interference Δ

Results of the frequency controlled 2nd step ultrasonic vibration x_2 during changing initial interference Δ are displayed in Figure 6.2. Blue curves represent the 2nd step ultrasonic vibration x_2 and pink dashed stepped line stands for the change in initial interference Δ. Obviously, the 2nd step ultrasonic vibration x_2 is boosted up to a steady state value $9\mu m$ zero-to-peak initially and then the initial interference Δ is changed from $-2 \times 10^{-7} m$ to $-2 \times$

$10^{-6}m$ which leads to an essential decrease in the ultrasonic vibration magnitude at the end of 2nd step concentrator x_2. As the initial interference Δ keeps on increasing, the 2nd step ultrasonic vibration level x_2 remains low. Another important notice is that the ultrasonic vibration tends to shift downwards which is likely caused by the increase in the initial engagement Δ of the ultrasonic transducer into the applied load. Consequently, a fixed frequency excitation on the ultrasonic transducer is not able to maintain the 2nd step ultrasonic vibration against the change in the initial interference Δ.

6.1.3 Conclusion

According to the simulation of a frequency controlled ultrasonic vibration, both change in the contact stiffness K and in the initial interference Δ have a significant impact on the ultrasonic vibration at the end of 2nd step concentrator x_2. As parameters change, the 2nd step ultrasonic vibration x_2 drops significantly. Hence, a robust control is strongly suggested to maintain the 2nd step ultrasonic vibration x_2 therefore autoresonance control has been developed.

6.2 Mechanical Feedback Control

Mechanical feedback uses the actual ultrasonic vibration at the end of 2nd step concentrator x_2 as feedback signal and aims at maintaining the ultrasonic vibration of 2nd step x_2 at a desired level against the change in the contact stiffness K or the initial interference Δ of the applied load. Before mechanical feedback control is evaluated, a filter complementation on the control system will be carried out.

6.2.1 Low-Pass Filter with a High Cut-Off Frequency

As introduced in Chapter Five that the filtering block in autoresonant control feedback system plays a role in rectification (smoothing) of the amplified square wave in order to generate a quasi-sine wave which eliminates the high frequency components. This quasi-sine wave can be further supplied to the ultrasonic transducer to excite it and thus form the feedback loop. Moreover, the filtering process can essentially eliminate a possible damage to the piezorings due to high frequency noises. In other words, a properly designed filter is required to cut off the high frequency components.

According to the amplitude-phase characteristic of observation point x_2 shown in Figure 5.11, the curve is smooth and gently sloping near resonance. More importantly, the characteristic of x_2 is single-valued (one phase corresponds to one vibration magnitude) which suggests a low-pass filter to the mechanical feedback in order to effectively get rid of the high frequency noises. As is known to all, due to the frequency dependence property, a filter involvement will inevitably introduce additional amplitude changes and phase shifts to the original square wave (the square wave which has been operated by the phase shifter block and the amplitude control block) which cannot be properly controlled by autoresonance. Therefore, a properly designed filter is significant in feedback. After a careful consideration, a first-order low-pass filter has been selected; a low-pass filter is a filter that passes low frequency signals but attenuates (reduces the magnitude of) signals with frequencies higher than the cut-off frequency. The transfer function of a first-order low-pass filter chosen for the mechanical feedback system is obtained:

$$G(s) = \frac{1}{0.000002s+1} \tag{6.1}$$

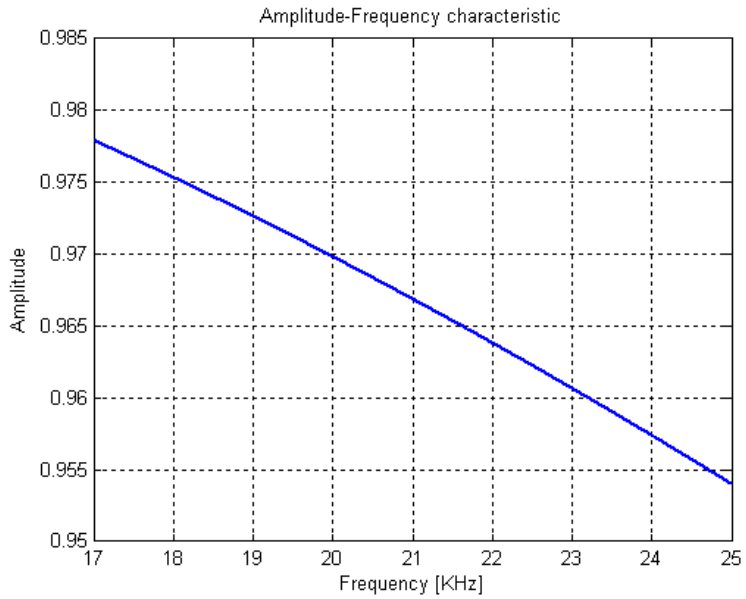

Figure 6.3 : Amplitude-frequency characteristic of the low-pass filter

s is the Laplace operator. Time constant in this transfer function is $\tau = 0.000002$ therefore the cut-off frequency in the amplitude-frequency characteristic of the transfer function shown in equation (6.1) is $\omega = \frac{1}{\tau} = 500000 rad/s$ which equals $80 KHz$. Amplitude-frequency and phase-frequency characteristics are illustrated in Figure 6.3 and Figure 6.4.

An interested frequency range to evaluate the low-pass filter has been selected $f \in [17KHz{\sim}25KHz]$ which centres on the ultrasonic transducer natural frequency shown in equation (4.85). As can be seen in Figure 6.3, amplitude of the low-pass filter is kept roughly at a constant level over a $8KHz$ frequency range. To be exact, the gain that the feedback loop is likely to benefit is around 0.965 which corresponds the resonant frequency (4.85) of the ultrasonic vibrating system shown in Figure 4.17. As the contact stiffness K or the initial interference Δ increases, the resonant frequency of the ultrasonic vibrating system will shift. However, maximal change in the resonant frequency is no more than $1KHz$ (calculated numerically) which according to Figure 6.3, the gain value of the low-pass filter hardly changes. This is desirable for the autoresonant control design because the amplitude change in the 2nd step ultrasonic vibration x_2 caused by the low-pass filter can be neglected.

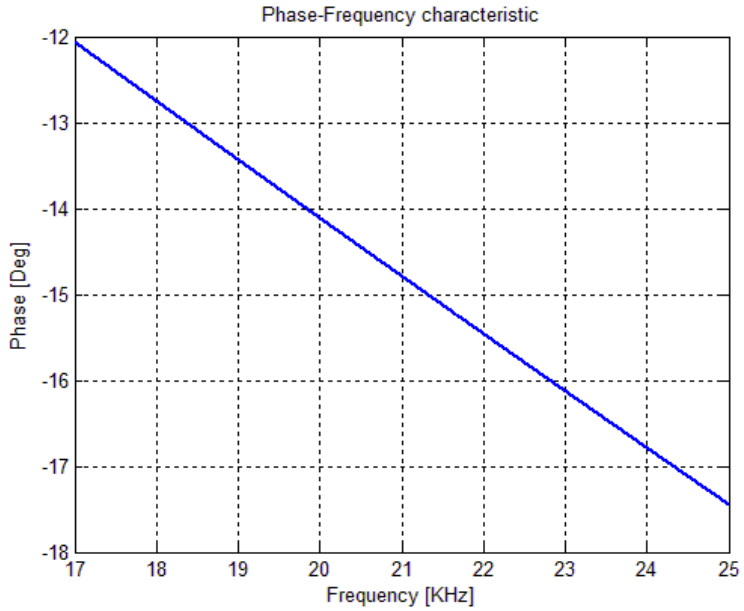

Figure 6.4 : Phase-frequency characteristic of the low-pass filter

Phase-frequency characteristic of the low-pass filter (6.1) is displayed in Figure 6.4. This characteristic is obtained in the same frequency range $f \in [17KHz{\sim}25KHz]$. It can be observed that the phase shift introduced by the low-pass filter is insignificant. Phase change due to the low-pass filter over the interested frequency range produce has a value $-12{\sim}-17$ degrees. Since change in the contact stiffness K or the initial interference Δ will shift the resonant frequency of the loaded ultrasonic transducer by no more than $1KHz$, phase shift introduced by the low-pass filter has a static value around -15 degrees. This value will not

essentially affect autoresonant control system because this is only a minor phase shift caused by the low-pass filter.

Effectiveness of the low-pass filter smoothing the amplified square wave into a quasi-sin wave has been examined and results are shown in Figure 6.5. Observing the input square wave and the output quasi-sin wave, several conclusions can be drawn.

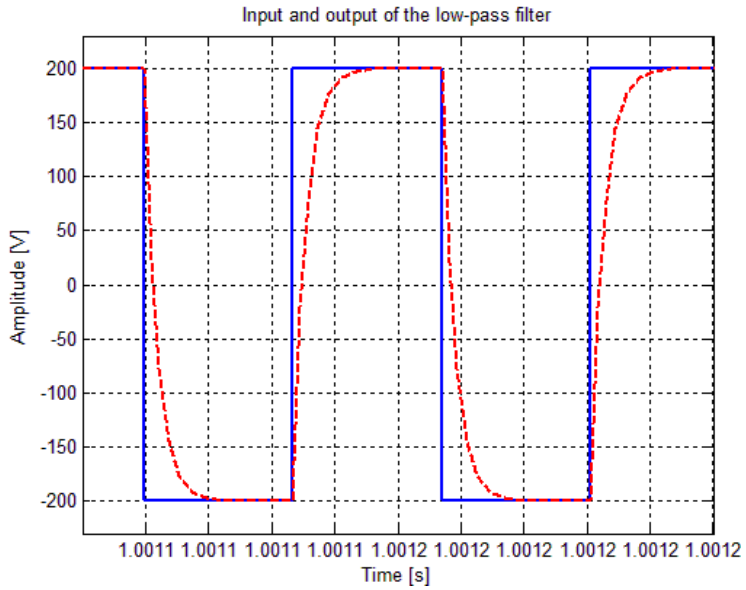

Figure 6.5 : Input and output of the low-pass filter: blue solid square wave – input to the low-pass filter, red dashed curve – output from the low-pass filter

- The input signal and the output signal have a similar magnitude

- Output from the low-pass filter shows a minor phase shift and it will not drastically affect the autoresonant control system

- Although the output signal is not a purely sine wave, it is still a workable actuation signal in the feedback. On the other hand, the low-pass filter is able to reduce the high frequency components which might cause serious damages to the piezorings.

Consequently, the selected low-pass filter has been applied to the mechanical feedback control. In next section, amplitude-phase characteristic of the mechanical feedback system will be presented before the control evaluation is examined because the autoresonant control algorithm is based on phase control.

6.2.2 Amplitude-Phase Characteristic of Mechanical Feedback

Before mechanical feedback control is investigated, amplitude-phase characteristic of the loaded ultrasonic transducer shown in Figure 4.17 should be obtained. To identify which phase shift generates the optimal (maximal) vibration magnitude at the end of 2nd step concentrator x_2, the phase has been slowly changed from a starting point and the peak values of the ultrasonic vibration of 2nd step concentrator x_2 have been tracked literally. Amplitude-phase characteristic of the mechanical feedback is shown in Figure 6.6.

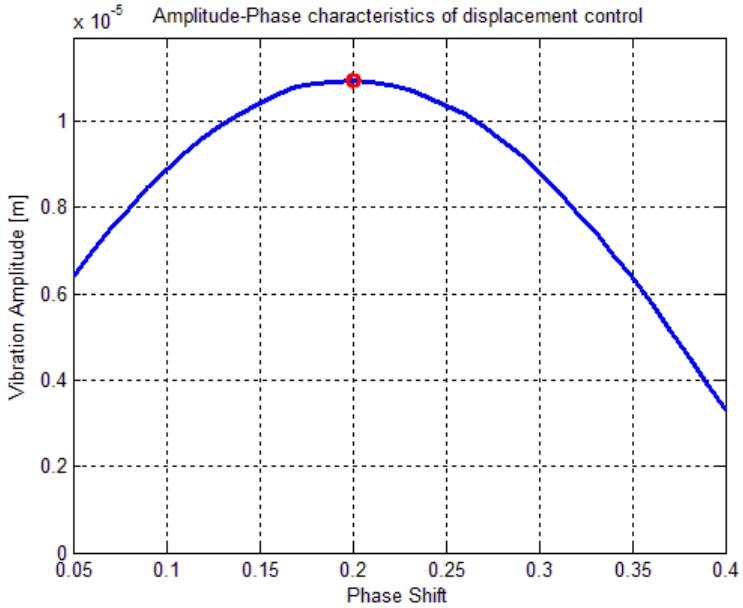

Figure 6.6 : Amplitude-phase characteristic of the loaded ultrasonic transducer with mechanical feedback control

It can be seen clearly, the curve is smooth and gently sloping near the peak which maps 0.2 phase control unit with a nearly $11\mu m$ zero-to-peak amplitude x_2. It should be noted that 1 phase control unit equals 2π. Therefore the phase shift which gives the maximal ultrasonic vibration magnitude is:

$$0.2 * 2\pi = 0.4\pi \tag{6.2}$$

Equation (6.2) indicates that by setting up a 0.4π phase shift between the 2nd step ultrasonic vibration x_2 and the supplied voltage u to the ultrasonic transducer, the feedback is able to tune itself at the most efficient state. Generally speaking, amplitude-phase characteristic curve is reasonably flat around the resonance; hence amplitude will not change significantly

with a minor phase shift around the optimal value. In following sections, control evaluation against the change in the contact stiffness K and the initial interference Δ will be evaluated.

6.2.3 Change in Contact Stiffness

Mechanical feedback control aims at maintaining the ultrasonic vibration at the end of 2nd step concentrator x_2 at a constant level against the change in the applied load. The feedback signal is the actual ultrasonic vibration of 2nd step concentrator x_2. Mechanical feedback employs x_2 as an actuating signal and computes the RMS of x_2 for each control cycle in order to perform phase control and amplitude control according to the described amplitude-phase control algorithm in section 5.1. Results are shown in Figure 6.7 during change in the contact stiffness K in the applied load.

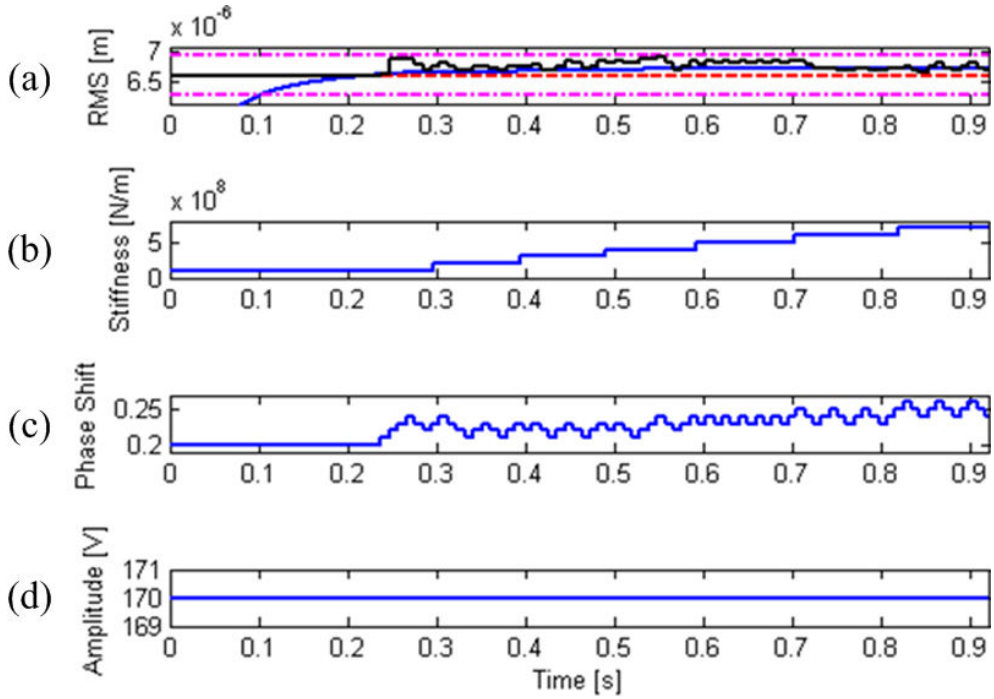

Figure 6.7 : Mechanical feedback during change in contact stiffness K: (a) RMS of the feedback signal, (b) change in contact stiffness, (c) phase control, (d) amplitude control

Figure 6.7 (a) illustrates the RMS of the feedback signal x_2 (black curve); pink dash-dotted line illustrates the boundaries of the phase control zone, in this case, $R_c = 5\%R_d$. Red dotted line represents the desired value of the ultrasonic vibration at the end of 2nd step x_2 in the loaded ultrasonic transducer which has a notation R_d. Since the displacement of 2nd step x_2 in the loaded ultrasonic transducer has a value $9\mu m$ zero-to-peak, the desired RMS of x_2 is

chosen to be $R_d \approx 6.6\mu m$. Blue curve stands for the RMS of x_2 calculated in infinite time which has an equation:

$$RMS = \sqrt{\frac{1}{\infty}\int_0^{\infty} s(t)^2 dt} \tag{6.3}$$

In equation (6.3), RMS indicates the RMS value calculated in infinite time, $s(t)$ is the sensor signal. Figure 6.7 (b) depicts the change in contact stiffness K. Again, the range is $K \in [1 \times 10^8 N/m \sim 7 \times 10^8 N/m]$ with an increment $1 \times 10^8 N/m$. (c) shows phase control and (d) demonstrates amplitude control.

Operation procedure for the mechanical feedback control is: the closed loop of the mechanical feedback with the ultrasonic vibration of 2nd step x_2 acting as the feedback signal and the actuating signal. However, the 2nd step ultrasonic vibration amplitude x_2 shown in Figure 6.6 presents a nearly $11\mu m$ zero-to-peak amplitude with an optimal phase shift 0.4π. This mismatches the desired $9\mu m$ zero-to-peak which seems to be caused by the low-pass filter. Therefore, the amplitude of the square wave has been adjusted to $170V$ zero-to-peak which is further applied to the low-pass filter in order to generate a quasi-sin wave to drive the ultrasonic transducer. Optimal phase shift 0.4π is set up initially in the closed loop. The newly established $170V$ driving voltage produces a $9\mu m$ zero-to-peak vibration magnitude at the end of 2nd step in the closed loop. The RMS of the displacement at the end of 2nd step x_2 has been calculated for each control cycle. After the RMS signal stabilises, the combined amplitude-phase algorithm will be applied. In this case, the stabilisation time for the RMS has been explored as 5000 oscillation periods which equals around 0.25secs illustrated in Figure 6.7. The actual control cycle mentioned in equation (5.2) is chosen to be 200 oscillation periods which equals around 0.01secs illustrated in Figure 6.7 (a) and (c). Control algorithm is not executed until the steady state of the RMS is reached.

As can be seen clearly in Figure 6.7 that during the change in contact stiffness K, the RMS of 2nd step vibration x_2 for each control cycle does not leave phase control zone which gives rise to no amplitude control participation shown in (d). This can be explained that the amplitude-phase characteristic of the 2nd step ultrasonic vibration x_2 is reasonably flat around resonance. In other words, the ultrasonic vibration of 2nd step x_2 can be controlled steadily by the phase

control algorithm which is demonstrated in (c). Obviously, change in the phase is about 0.06 phase control units starting from the optimal value 0.2 phase control units. Resonant frequency of the loaded ultrasonic transducer with parameters in equation (4.84) is around $21.176KHz$ which is calculated in equation (4.85). As the contact stiffness K changes, the resonant frequency gradually shifts to $21.906KHz$ when $K = 7 \times 10^8 N/m$. In order to fully understand the control effectiveness, the 2nd step ultrasonic vibration x_2 and the applied load during change in the contact stiffness K are shown in Figure 6.8.

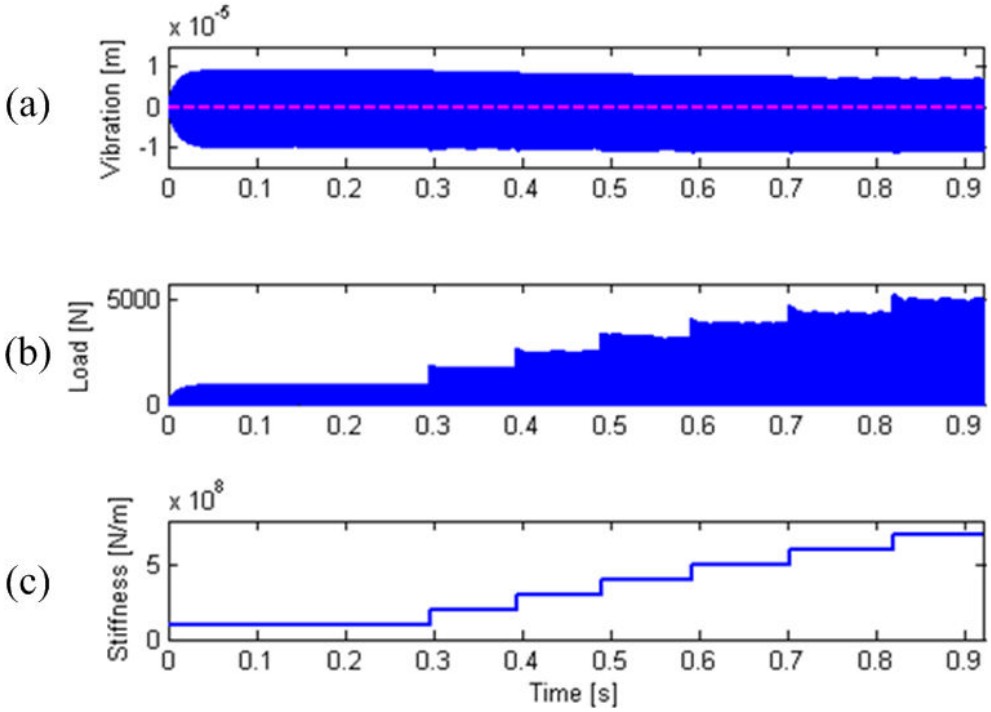

Figure 6.8 : Mechanical feedback controlled 2nd step ultrasonic vibration during change in contact stiffness K: (a) controlled ultrasonic vibration, (b) change in applied load, (c) change in contact stiffness

Figure 6.8 (a) depicts ultrasonic vibration at the end of 2nd step concentrator x_2 while changing the contact stiffness K of the applied load (c). The vibration signal seems stable despite essential increase in the contact stiffness K. Another observation is the ultrasonic vibration x_2 tends to shift downwards as the increase in K; this is caused by the increase in the applied load. (b) illustrates the applied load as the increase in the contact stiffness K. Loading climbs up gradually from less than $1000N$ initially to nearly $5000N$ eventually. Essential increase in the contact stiffness K imitates a promotion in the material (work piece) elasticity. In spite of this, the mechanical feedback control is still capable of handling such a

drastic change and keeping the 2nd step ultrasonic vibration x_2 at a constant level. This promising result implies the importance of a direct employment of the ultrasonic vibration as a feedback signal and enhances the reliability and feasibility of the mechanical feedback application.

Figure 6.9 is the enlarged picture of (a) in Figure 6.7. As can be seen, the black curve (RMS of x_2 for each control cycle) stays within the phase control zone (pink dash-dotted line) which is kept closely to the desired RMS of the 2nd step ultrasonic vibration x_2 (shown in red-dashed straight line). The maximum deviation of mechanical feedback in RMS of x_2 monitoring from its desired $R_d = 6.6\mu m$ is around $0.3\mu m$ which equals $4\%R_d$.

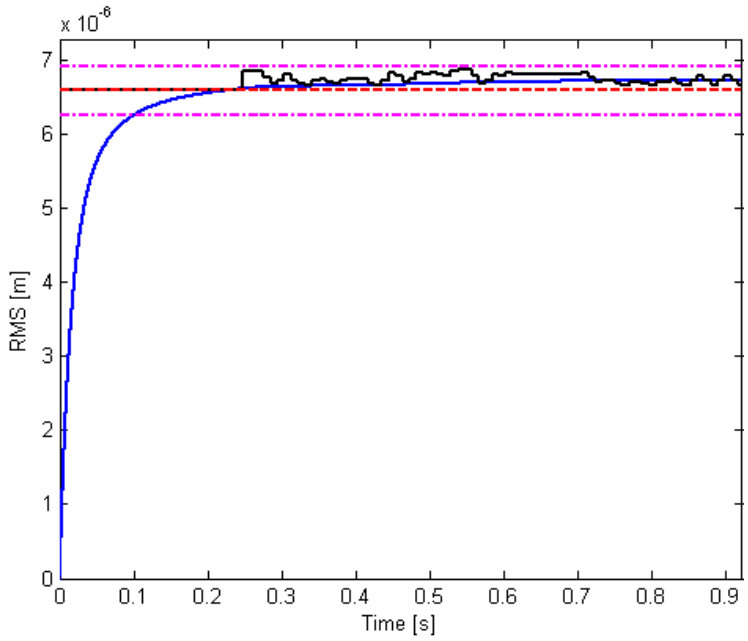

Figure 6.9 : RMS of the 2nd step ultrasonic vibration during change in contact stiffness K

6.2.4 Change in Initial Interference

Another parameter can also be changed to examine the efficiency of the mechanical feedback is the initial interference Δ. It has been described that the change in $\Delta \in [-2 \times 10^{-7}m \sim -1 \times 10^{-5}m]$ with an increment $-2 \times 10^{-6}m$. Change in the initial interference Δ will inevitably shift the resonant frequency of the loaded ultrasonic transducer which according to numerical calculation, resonant frequency shifts from $21.176KHz$ to $21.188KHz$. Results of the mechanical feedback control during the change in initial interference Δ are shown in Figure 6.10.

Similarly, in Figure 6.10 (a) black curve is the RMS of x_2 for each control cycle, blue curve stands for the RMS of the 2nd step ultrasonic vibration x_2 calculated in infinite time, pink dash-dotted lines define the upper and lower boundaries of the phase control zone which is chosen to be $R_c = 5\%R_d$, red dashed line is the desired RMS of the 2nd step ultrasonic vibration x_2 that equals $R_d = 6.6\mu m$.

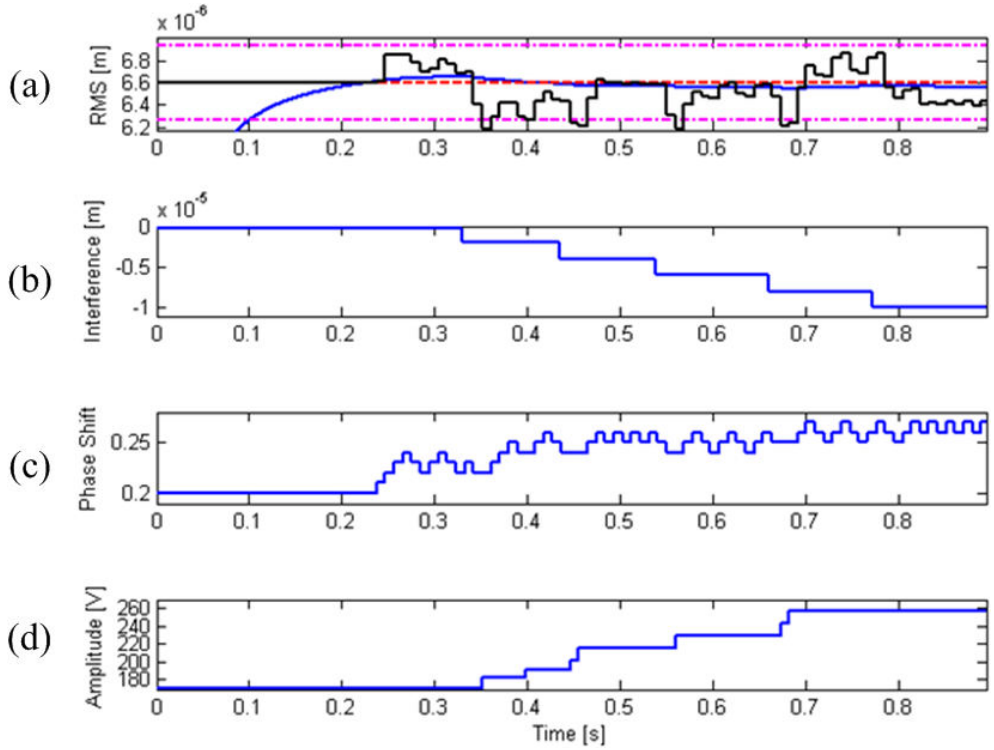

Figure 6.10 : Mechanical feedback during change in initial interference Δ: (a) RMS of the feedback signal, (b) change in initial interference Δ, (c) phase control, (d) amplitude control

As can be seen, RMS of x_2 (black curve) drops out of phase control zone a number of times, which means by purely adjusting the phase is not able to keep the 2nd step ultrasonic vibration x_2 as a constant. Therefore, amplitude control has to be involved to inject more power into the ultrasonic transducer in order to compensate the drop in the 2nd step ultrasonic vibration x_2 due to the change in the machining conditions (change in initial interference Δ). Amplitude control has been showed in (d). Amplitude of the square wave has been increased from initial $170V$ to nearly $260V$ when the initial interference changes from $-2 \times 10^{-7}m$ to $-1 \times 10^{-5}m$ illustrated in (b). Phase control in this case increases from 0.2 phase control units to 0.27 phase control units. For the change in the initial interference Δ, algorithm of the

combined amplitude-phase algorithm has been employed to maintain the 2nd step ultrasonic vibration x_2.

Figure 6.11 illustrates the mechanical feedback controlled ultrasonic vibration of 2nd step concentrator x_2 and applied load during the change in the initial interference Δ. As can be seen in (a) that the 2nd step ultrasonic vibration x_2 can be generally kept at a constant level during change in the initial interference Δ (pink dashed line). Similar to the case of change in the contact stiffness K, controlled ultrasonic vibration presents a shifting downwards characteristic because of the change in the initial interference Δ. Physically it means an increase engagement of a tool into the target work piece. Applied load increases from initial $1000N$ to more than $1500N$ in the end which is essentially smaller than the applied load increase in the case of change in the contact stiffness K.

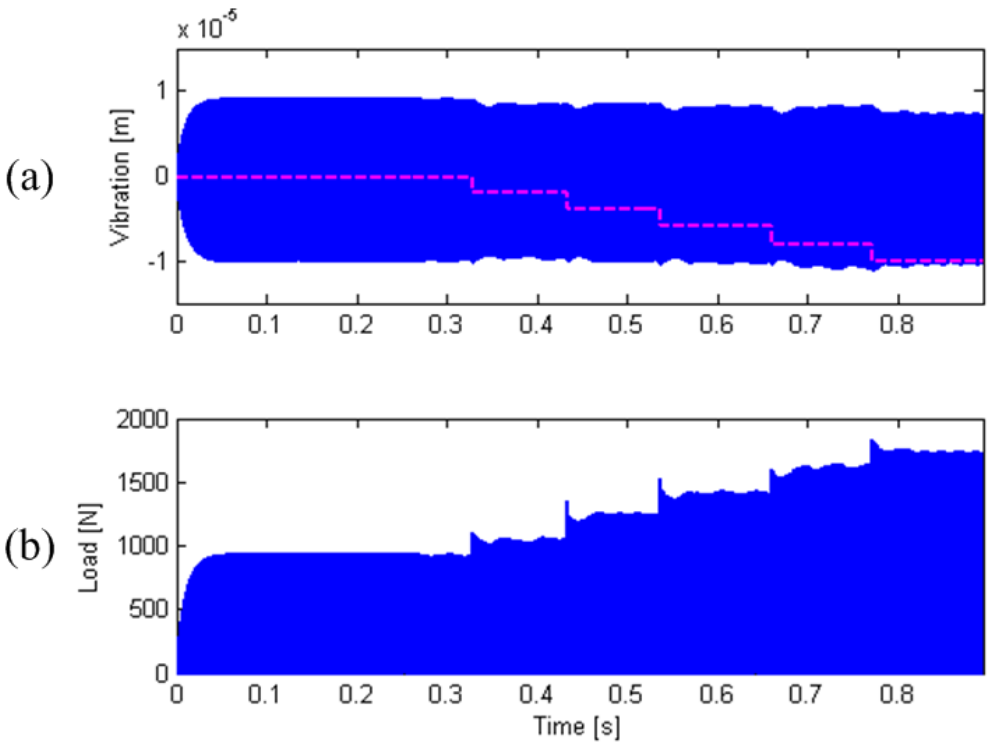

Figure 6.11 : Mechanical feedback controlled 2nd step ultrasonic vibration during change in initial interference Δ: (a) controlled ultrasonic vibration, (b) change in applied load

Figure 6.12 is the enlarged picture of (a) in Figure 6.10. As can be seen, the RMS of x_2 drops out of phase control zone a number of times which suggests an amplitude control participation. As a result, an extra power supply provided by the amplitude control automatically restores the RMS of 2nd step ultrasonic vibration x_2 to the desired level R_d. The

maximal deflection of RMS of x_2 from its desired R_d against change in the initial interference Δ is about $0.4\mu m$ that equals $6\%R_d$. Results presented above prove autoresonant control is able to cope with the change in the initial interference Δ with a combined amplitude-phase control algorithm.

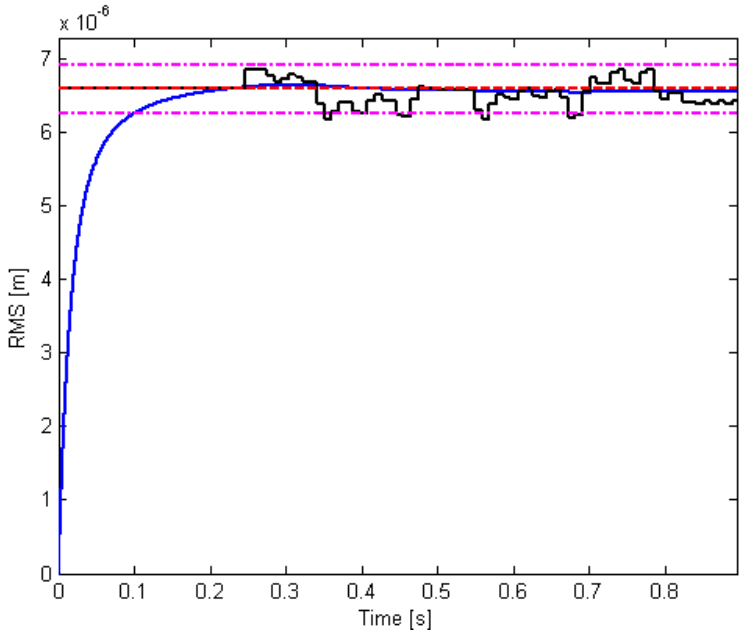

Figure 6.12 : RMS of the 2nd step ultrasonic vibration during change in initial interference Δ

6.2.5 Conclusion

In conclusion, mechanical feedback control is capable of maintaining the ultrasonic vibration of the 2nd step concentrator x_2 at a constant level. In the case of change in the contact stiffness K, phase control algorithm suffices to keep the 2nd step ultrasonic vibration x_2 at a desired level. Maximal deflection of the RMS of the ultrasonic vibration x_2 is $0.3\mu m$ which equals $4\%R_d$. In contrast, change in the initial interference Δ in the applied load model requires a combined amplitude-phase control algorithm for the loaded ultrasonic transducer to acquire more power to keep the ultrasonic vibration of 2nd step x_2 at a constant. Deviation of RMS of x_2 in change in the initial interference Δ is $0.4\mu m$ equals $6\%R_d$.

In next section, electrical feedback control will be evaluated. Basically, electrical feedback control consists of two strategies which are current feedback control and power feedback control. Filter design is introduced before the control efficiency is evaluated. The influence of different bandwidth of filters selection on the autoresonant control will be investigated.

Electrical feedback will also be tested on the change in the contact stiffness $K \in [1 \times 10^8 N/m \sim 7 \times 10^8 N/m]$ with an increment $1 \times 10^8 N/m$ and the change in the initial interference $\Delta \in [-2 \times 10^{-7} m \sim -1 \times 10^{-5} m]$ with an increment $-2 \times 10^{-6} m$.

6.3 Current Feedback Control

In this section, current feedback control will be examined during the change in the contact stiffness K and the change in the initial interference Δ. Before the autoresonant control on the current feedback is examined, filters design will be carried out. As analysed in Figure 5.11 in section 5.3.3 that the amplitude-phase characteristic displays an ambiguity property when the 1st step concentrator vibration x_1 is chosen to be the observation point. Therefore, it is strongly suggested a filtration process participation into the feedback. In other words, in the amplitude-phase characteristic, one phase shift reflects several vibration magnitudes which will inevitably bring 'confusion' to feedback when the current i is selected to be the feedback signal. Hence, a band-pass filter is recommended to pick up the wanted vibration regimes. In addition, in order to check the filter bandwidth effect on the autoresonant control, several bandwidths will be applied to rectify the amplified square wave signal in the current feedback.

Current feedback control uses the current i as both a feedback signal and an actuation signal. The target of the current feedback control is to maintain the 2nd step ultrasonic vibration x_2 through stabilising current during the change in the applied load. Current feedback control is an indirect control method compared with mechanical feedback control, so the control is expected to be not efficient as mechanical feedback control.

Recalling the expressions of the current of the piezoelectric transducer shown in equation (5.18) has the following form:

$$i = \dot{q} = k_{03}\dot{F}_0 + k_{04}\dot{u} \tag{6.4}$$

Where $k_{03} = 3.4 \times 10^{-10}$ and $k_{04} = 2.1 \times 10^{-9}$ are coefficients shown in equation (4.63), q is the charge, u is the supplied voltage and F_0 is the interaction force between a piezoring and the 1st step concentrator. The expression of x_0 and F_0 are shown in the following:

$$x_0 = \frac{1}{k_{01}} F_0 + k_{02} u \tag{6.5}$$

$$F_0 = C_1(\dot{x}_1 - \dot{x}_0) + K_1(x_1 - x_0) \tag{6.6}$$

Where k_{01} and k_{02} are parameters shown in equation (4.63) and K_1 and C_1 are parameters shown in equation (4.59) and (4.75).

6.3.1 Band-Pass Filter Design

As described in Figure 5.11 that the amplitude-phase characteristic is ambiguous when the 1st step ultrasonic vibration x_1 is the observation point which suggests a band-pass filter participation to filter out the desired oscillation regime. After several types of band-pass filter investigations, a 2nd order Butterworth filter has been eventually employed. A Butterworth filter is a type of signal processing filter designed to have as flat a frequency response as possible in the pass-band which also refers to as a maximally flat magnitude filter. Ideally, a filter should not only completely reject the unwanted frequencies but should also have an uniform sensitivity for the wanted frequencies.

The frequency response of a Butterworth filter is maximally flat (i.e. has no ripples) in the pass-band and rolls off towards zero in the stop-band. Figure 5.11 shows 3 possible oscillation regimes when the 1st step concentrator ultrasonic vibration x_1 is selected to be the observation point. Each of the 3 oscillation regimes reflects a different amplitude-frequency characteristic. Consequently, by choosing a proper bandwidth for a Butterworth filter allows the desired oscillation regime to be kept while the other 2 are rejected. Due to the fact that during change in the contact stiffness K of the applied load, the resonant frequency shifts from $21.176KHz$ to $21.906KHz$, the bandwidth of a Butterworth filter has been selected to centre around $21.54KHz$ consequently. 3 bandwidths of the Butterworth filters have been chosen which are $19.54KHz{\sim}23.54KHz$ corresponds to a $4KHz$ bandwidth, $17.54KHz{\sim}25.54KHz$ corresponds to a $8KHz$ bandwidth and $15.54KHz{\sim}27.54KHz$ corresponds to a $12KHz$ bandwidth. These 3 filters bandwidths centre on $21.54KHz$. The frequency range used to calculate the characteristics of the Butterworth filters is selected $f \in [12KHz{\sim}30Khz]$. The transfer functions for the $4KHz$, $8KHz$, and $12KHz$ Butterworth filters are:

$$G_{4KHz} = \frac{6.317\times10^{8}s^{2}}{s^{4}+3.554\times10^{4}s^{3}+3.695\times10^{10}s^{2}+6.454\times10^{14}s+3.297\times10^{20}} \quad (6.7)$$

$$G_{8KHz} = \frac{2.527\times10^{9}s^{2}-2.739\times10^{-10}s-398.8}{s^{4}+7.109\times10^{4}s^{3}+3.79\times10^{10}s^{2}+1.257\times10^{15}s+3.128\times10^{20}} \quad (6.8)$$

$$G_{12KHz} = \frac{5.685\times10^{9}s^{2}-3.082\times10^{-10}s-566.3}{s^{4}+1.066\times10^{5}s^{3}+3.948\times10^{10}s^{2}+1.802\times10^{15}s+2.855\times10^{20}} \quad (6.9)$$

Figure 6.13 demonstrates the amplitude-frequency characteristics for 3 bandwidths Butterworth filters. Blue solid curve represents a $4KHz$ bandwidth Butterworth filter, red dashed curve stands for a $8KHz$ bandwidth Butterworth filter and green dash-dotted curve shows a $12KHz$ bandwidth Butterworth filter. As can be seen clearly, 3 Butterworth filters have a flat magnitude response within their own pass-band. In contrast, for those frequencies beyond the pass-band, magnitude response falls quickly to a low level. Theoretically, a wider bandwidth in a Butterworth filter is advised to participate in the feedback since it provides a wider range of flat magnitude response. This provides the loaded ultrasonic transducer with more freedom to adapt itself in order to deal with the change in the applied load.

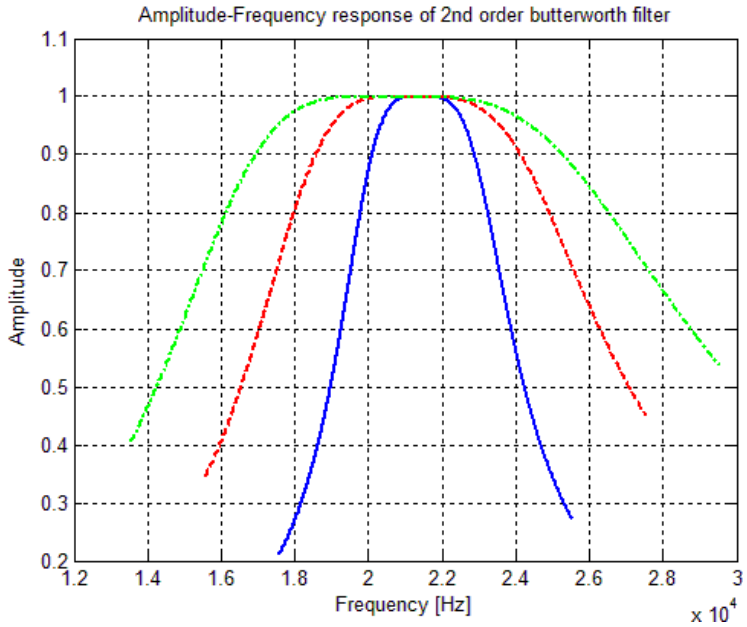

Figure 6.13 : Amplitude-frequency characteristic of 3 bandwidths Butterworth filters: blue solid curve – $4KHz$ bandwidth, red dashed curve - $8KHz$ bandwidth, green dash-dotted curve - $12KHz$ bandwidth

Phase-frequency characteristics of 3 bandwidths Butterworth filters are shown in Figure 6.14. Blue solid curve means a $4KHz$ bandwidth Butterworth filter, red dashed curve stands for a $8KHz$ bandwidth Butterworth filter and green dash-dotted curve shows a $12KHz$ bandwidth Butterworth filter. Clearly, a narrower band Butterworth filter presents a more drastic change in phase compared with a wider one. The phase shift introduced by the filter is uncontrollable by the phase control algorithm. As can be seen, the phase shift for a $4KHz$ Butterworth filter equals $140\sim-140$ degrees, the phase shift for a $8KHz$ and a $12KHz$ Butterworth filter have a similar phase shift within their corresponding pass-band. However, the slopes of the $8KHz$ and the $12KHz$ Butterworth filters are much gentler in comparison with the slope of the $4KHz$ Butterworth filter. Generally, the change in phase caused by the filter needs to be small around the operation frequency. A conclusion hence can be pre-drawn that a $8KHz$ and a $12KHz$ Butterworth filters are supposed to be more efficient than a $4KHz$ Butterworth filter.

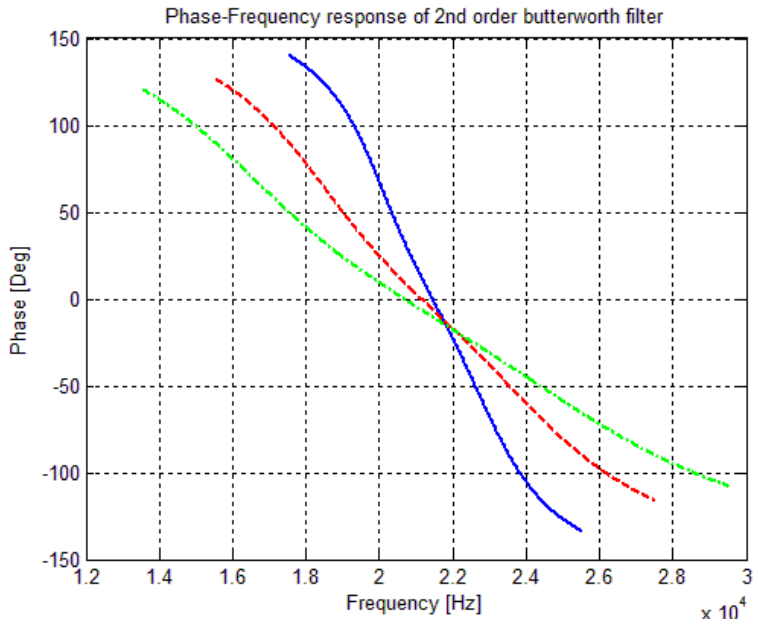

Figure 6.14 : Phase-frequency characteristic of 3 bandwidths Butterworth filters: blue solid curve – $4KHz$ bandwidth, red dashed curve - $8KHz$ bandwidth, green dash-dotted curve - $12KHz$ bandwidth

Smoothed square waves by 3 bandwidths Butterworth filters have been shown in Figure 6.15. Blue square wave represents the amplified input signal into the 2^{nd} order Butterworth filters, red curve is the output from a $4KHz$ bandwidth Butterworth filter, green dashed curve stands for the output from a $8KHz$ bandwidth Butterworth filter and pink dash-dotted curve indicates the output from a $12KHz$ bandwidth Butterworth filter. As can be seen, the square

wave has been smoothed by 3 Butterworth filters at a frequency $21.176KHz$ which is the resonant frequency of the loaded ultrasonic transducer with parameters shown in equation (4.85). Phase shifts of the generated sinusoidal waves reflect the $21.176KHz$ corresponded phase values in Figure 6.14 for 3 Butterworth filters. Another notable point in Figure 6.15 is that each of the filtered sinusoidal wave signals has enlarged amplitudes than the amplitude of the square wave. However, according to Figure 6.13, the gain of the Butterworth filters within the pass-band is unity. This seems controversial. However, the amplification is because a Butterworth filter only takes the 1st harmonic frequency corresponded component which is always larger than the amplitude of the square wave. The 2nd, 3rd and higher order of harmonic frequency components have been effectively removed by the Butterworth filters.

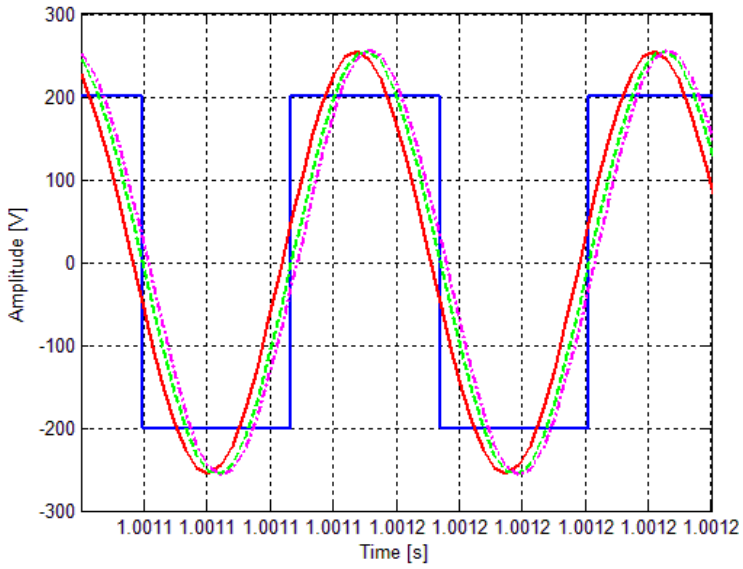

Figure 6.15 : Input and output of the 2nd order Butterworth filters: blue square wave – input to the filters, red curve – output from a $4KHz$ filter, green dashed curve – output from a $8KHz$ filter, pink dash-dotted curve – output from a $12KHz$ filter

6.3.2 Amplitude-Phase Characteristics of Current and 2nd step Ultrasonic Vibration

Equation (6.4) shows the current calculation which will be used to form the current feedback. The current i is related to both the interaction force F_0 between a piezoring and the 1st step concentrator and the supplied voltage u. Current i has been used as both the feedback signal and the actuation signal.

This section is dedicated to the investigation of autoresonance control of the current feedback with 3 bandwidths Butterworth filters applications. Results are compared and analysed. Control evaluation is carried out on the change in the contact stiffness K and the change in the initial interference Δ of the applied load model described in Figure 4.17. Before the control is evaluated, the amplitude-phase characteristics of the current feedback for both the current i and the 2nd step ultrasonic vibration x_2 for 3 Butterworth filters need to be obtained.

Since the current feedback relies on the amplitude-phase characteristic of the current i flows through the piezoelectric transducer as it acts as both the feedback signal and the actuation signal, it is sensible to obtain the amplitude-phase characteristic of the current i initially. Meanwhile, it is worth to draw the amplitude-phase characteristic of the 2nd step ultrasonic vibration x_2.

Operation procedure of this process is that the loop is closed in the beginning and the phase shift is slowly changed with an increment 0.01 phase control unit between the current i and the supplied voltage u. Both current i and the 2nd step ultrasonic vibration x_2 is recorded accordingly. It should be noted that there are 3 Butterworth filters with $4KH$,$8KHz$ and $12KHz$ bandwidths respectively. These filters will be applied to the current feedback literally. Therefore, 3 amplitude-phase characteristics for the current i and 3 characteristics for the 2nd step ultrasonic vibration x_2 are obtained.

6.3.2.1 Amplitude-Phase Characteristics of a $4KHz$ Butterworth Filter

Figure 6.16 illustrates the current amplitude-phase characteristic of the loaded ultrasonic transducer with a $4KHz$ bandwidth Butterworth filter application. As can be seen, when the phase shift between the current i and the supplied voltage u is 0.08 phase control units which equals 0.16π, the optimal regime for current feedback is reached with a peak value $0.323A$ zero-to-peak. Physically, it indicates by setting up a 0.16π phase shift in the feedback loop allows the current to tune itself at the most efficient state.

Figure 6.17 demonstrates the amplitude-phase characteristic of the 2nd step ultrasonic vibration x_2 with a $4KHz$ bandwidth Butterworth filter application. It can be observed that a 0.05 phase shift equivalently 0.1π ensures the 2nd step ultrasonic vibration x_2 to have a

resonant regime with an amplitude $11.93\mu m$ zero-to-peak. Due to the Butterworth filter effect, a 0.08 phase shift corresponded ultrasonic vibration amplitude also has a mismatch with desired amplitude $9\mu m$ zero-to-peak. Therefore, the supplied voltage u has been tuned in order to match the 2^{nd} step ultrasonic vibration amplitude $9\mu m$ zero-to-peak at resonance. As a result, optimal phase shift with an application of a $4KHz$ bandwidth Butterworth filter in the current feedback control is tuned to be 0.16π.

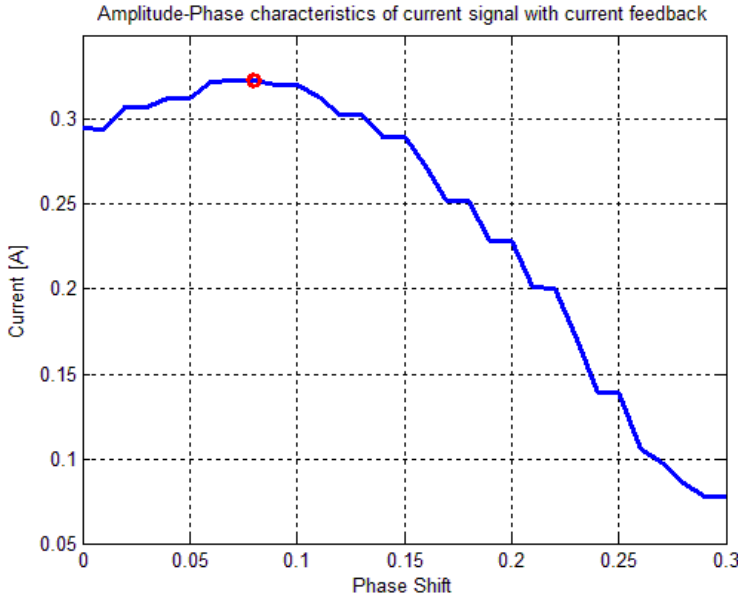

Figure 6.16 : Current amplitude-phase characteristic of the loaded ultrasonic transducer

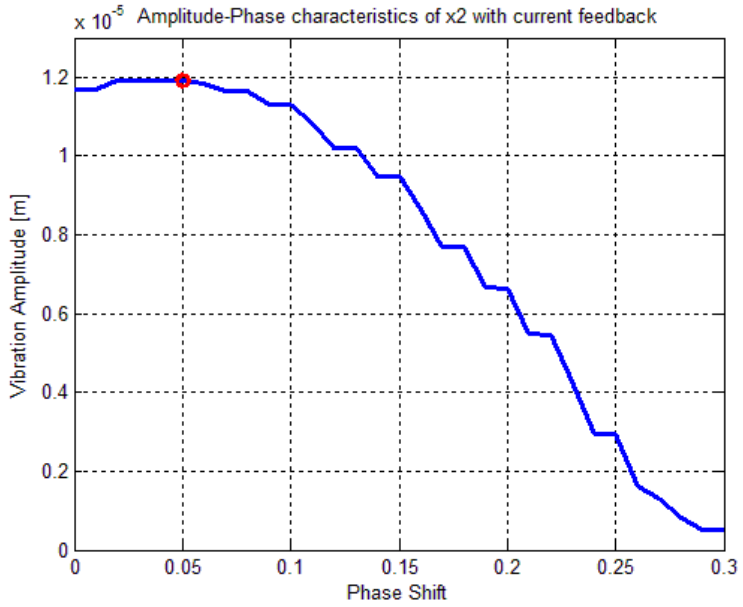

Figure 6.17 : 2^{nd} step ultrasonic vibration amplitude-phase characteristic of the loaded ultrasonic transducer

6.3.2.2 Amplitude-Phase Characteristics of a 8KHz Butterworth Filter

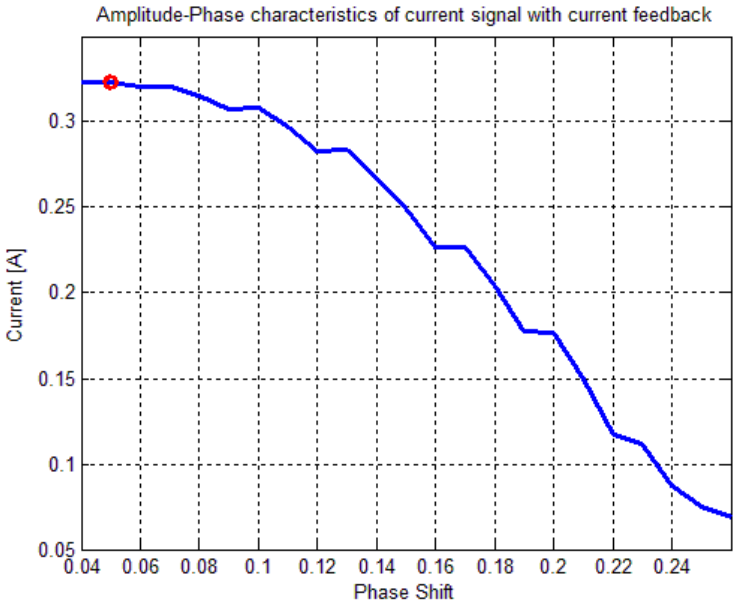

Figure 6.18 : Current amplitude-phase characteristic of the loaded ultrasonic transducer

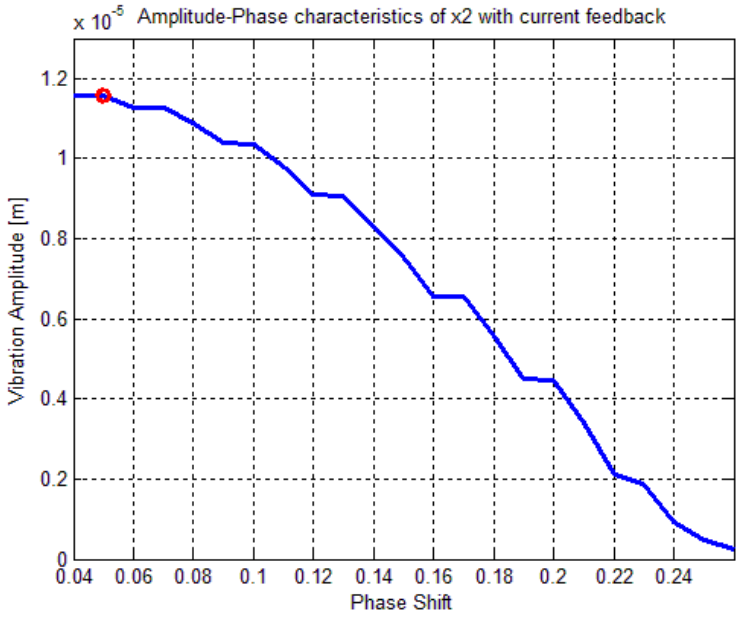

Figure 6.19 : 2nd step ultrasonic vibration amplitude-phase characteristic of the loaded ultrasonic transducer

Figure 6.18 presents the current amplitude-phase characteristic of the loaded ultrasonic transducer with a 8KHz bandwidth Butterworth filter application. The 8KHz Butterworth filter enables the current feedback to reach its resonant state at a phase shift 0.05 phase

control units which equals 0.1π. In other words, the current i has a maximal amplitude $0.323A$ zero-to-peak with a phase shift 0.1π.

Figure 6.19 depicts the 2nd step ultrasonic vibration x_2 amplitude-phase characteristic with a $8KHz$ bandwidth Butterworth filter application. Clearly, a phase shift 0.05 phase control unit (0.1π) permits the 2nd step ultrasonic vibration x_2 to reach its resonant state with an amplitude $11.59\mu m$ zero-to-peak. Therefore, for a $8KHz$ bandwidth Butterworth filter application, phase shift has been tuned as 0.1π to guarantee the ultrasonic transducer to reach the current resonant regime. Again, due to the Butterworth filter effect, the supplied voltage u will be adjusted to conform to the ultrasonic vibration amplitude at the end of the 2nd step of the loaded ultrasonic transducer to be $9\mu m$ zero-to-peak at the resonant state.

6.3.2.3 Amplitude-Phase Characteristics of a $12KHz$ Butterworth Filter

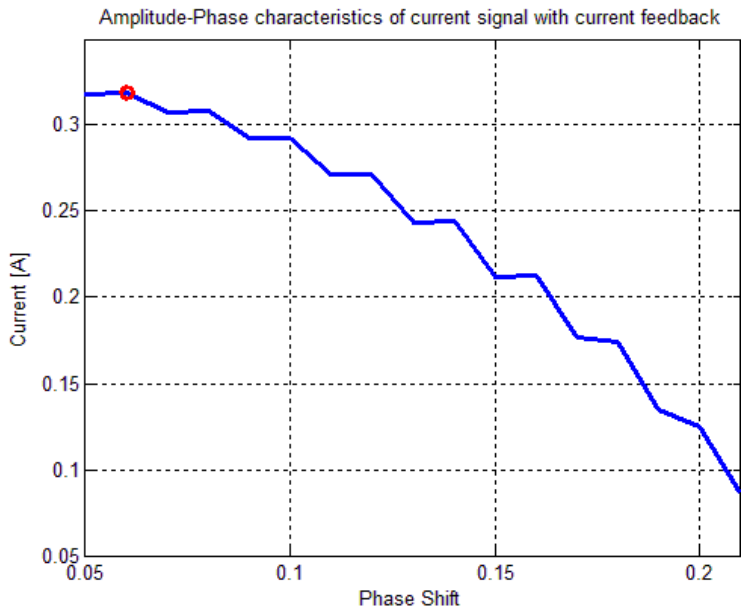

Figure 6.20 : Current amplitude-phase characteristic of the loaded ultrasonic transducer

The amplitude-phase characteristics of the current i and the 2nd step ultrasonic vibration x_2 with a $12KHz$ bandwidth Butterworth filter application are illustrated in Figure 6.20 and Figure 6.21. In Figure 6.20, it indicates that the current i arrives at its resonant state with a phase shift 0.06 phase control units (0.12π) and amplitude of current is $0.319A$ zero-to-peak. Figure 6.21 implies that a shift of 0.05 phase control units (0.1π) permits the 2nd step ultrasonic vibration x_2 to reach its resonant state with an amplitude $11\mu m$ zero-to-peak. The

supplied voltage u has to be adjusted in order to match the desired 2nd step ultrasonic vibration amplitude $9\mu m$ zero-to-peak.

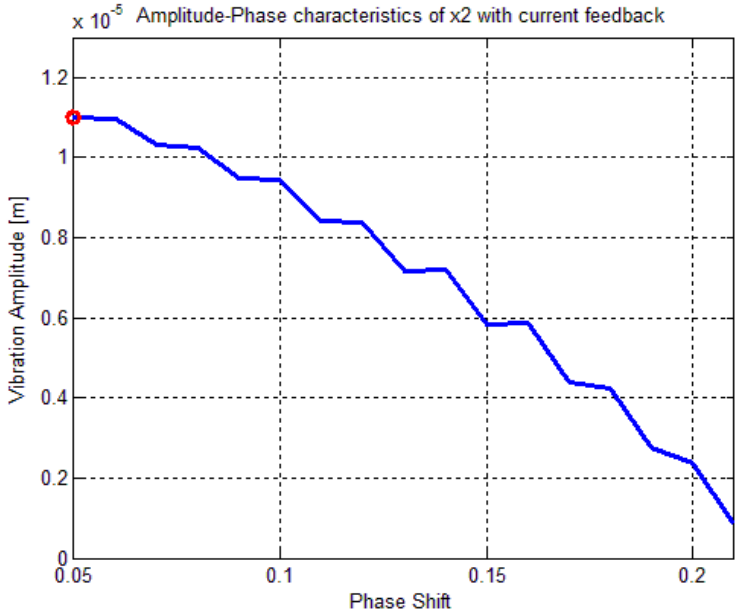

Figure 6.21 : 2nd step ultrasonic vibration amplitude-phase characteristic of the loaded ultrasonic transducer

As a result, the optimal phase shift value for the current feedback control system for 3 bandwidths Butterworth filters are obtained respectively. Simultaneously, current feedback controlled 2nd step ultrasonic vibration optimal phase shift values are also calculated. These optimal phase shift values are shown in Table 6.1. As can be seen, the peak response of the 2nd step ultrasonic vibration x_2 with current feedback control seems to be achieved with a fixed phase shift 0.1π despite the change in the bandwidth in Butterworth filters. Another notable point is that only the $8KHz$ bandwidth Butterworth filter generates a coincidence phase shift between the current i and the 2nd step ultrasonic vibration x_2.

Table 6.1 : Optimal phase shift values of the current and the 2nd step ultrasonic vibration for 3 bandwidths Butterworth filters

Bandwidth / Optimal Ph.Shift	$4KHz$	$8KHz$	$12KHz$
Current	0.16π	0.1π	0.12π
2nd step ultrasonic vibration	0.1π	0.1π	0.1π

In next section, these optimal phase shifts will be applied to the current feedback control on the loaded ultrasonic transducer model in Matlab-Simulink. Before the current feedback is evaluated, amplitude of the square wave of the supplied voltage u should be computed in order to match the 2nd step ultrasonic vibration amplitude $9\mu m$ zero-to-peak for 3 bandwidths Butterworth filters. The adjusted voltage amplitudes are shown in Table 6.2.

Table 6.2 : Square wave voltage amplitude for three bandwidths Butterworth filters

Bandwidth	$4KHz$	$8KHz$	$12KHz$
Voltage amplitude (V)	170	170	183

6.3.3 Change in Contact Stiffness

6.3.3.1 A 4KHz Butterworth Filter

For a $4KHz$ bandwidth Butterworth filter application in the current feedback, the supplied voltage amplitude of the square wave is around $170V$ zero-to-peak shown in Table 6.2. Therefore, the corresponding current amplitude can be calculated by applying the phase shift 0.16π shown in Table 6.1 to the feedback loop. The desired RMS of current i hence is $0.18A$ which produces the RMS of the 2nd step ultrasonic vibration x_2 $6.6\mu m$. The current feedback control results are shown in Figure 6.22.

(a) represents the RMS of the current for each control cycle (200 oscillation periods, same as the mechanical feedback) shown in black line. Blue curve is the current RMS calculated in infinite time. Red dashed straight line represents the desired RMS of the current which is $R_d = 0.18A$ and pink dash-dotted lines are the boundaries of the phase control zone. In this case, $R_c = 10\%R_d$. (b) demonstrates the increase in the contact stiffness K in the applied load and the range is $K \in [1 \times 10^8 N/m \sim 7 \times 10^8 N/m]$. (c) indicates the phase control during the change in the contact stiffness K and it conforms to the phase control algorithm. (d) is amplitude control which follows the amplitude control algorithm. As can be seen, RMS of the feedback signal (current) does not leave the phase control zone (pink dash-dotted line). Therefore, no change is witnessed in the amplitude control and it is kept as a constant $170V$. For phase control, the value generally decreases from 0.08 phase control units to almost 0.01 phase control unit despite some fluctuations during the change in the contact stiffness K. This is caused by the additional phase shift introduced by a $4KHz$ Butterworth filter as can be observed in phase-frequency characteristic in Figure 6.14. The resonant frequency of the

loaded ultrasonic transducer shifts from $21.176KHz$ to $21.906KHz$ due to the change in the contact stiffness K which inevitably gives rise to a considerable phase shift in the Butterworth filter. A narrow bandwidth Butterworth filter exhibits a relatively drastic phase shift compared to a wider bandwidth Butterworth filter.

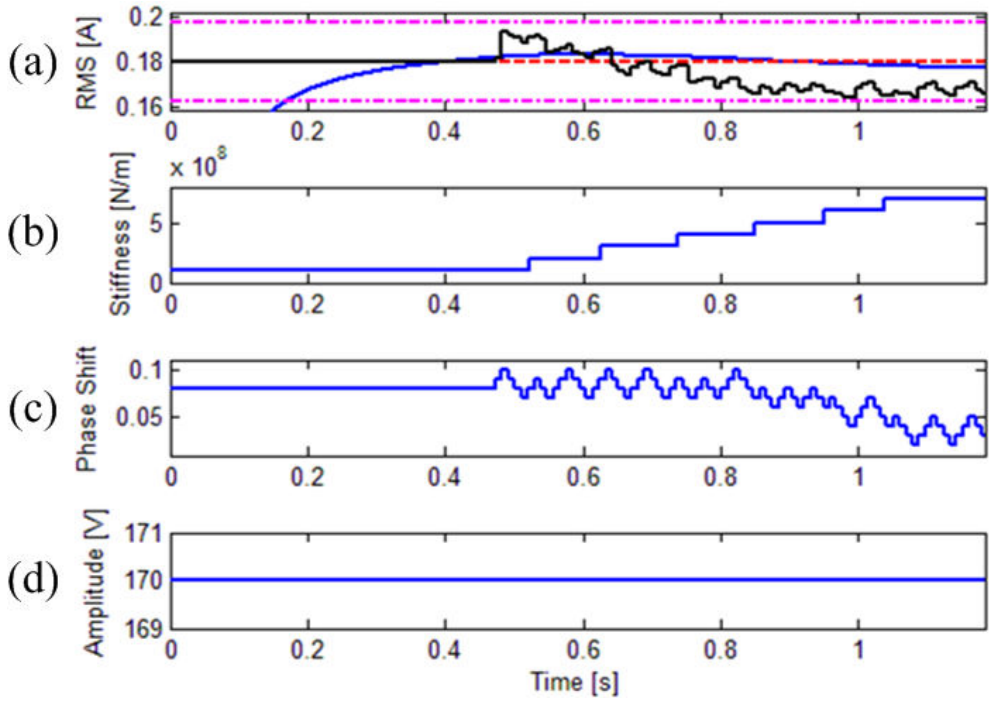

Figure 6.22 : Current feedback during changing contact stiffness: (a) RMS of feedback signal (current), (b) change in contact stiffness, (c) phase control, (d) amplitude control

Figure 6.23 shows the controlled current during the change in the contact stiffness K. As can be seen in (a), current remains stable during the change in K (b) despite some moderate drops and ripples. However, the target of the current feedback is to maintain the ultrasonic vibration of 2nd step concentrator x_2 as a constant by keeping the current signal stable. Hence, it is advisable to evaluate the control of 2nd step ultrasonic vibration x_2.

Figure 6.24 demonstrates the current feedback controlled ultrasonic vibration of 2nd step concentrator x_2 with a $4KHz$ bandwidth Butterworth filter application. As can be seen in (a), the 2nd step ultrasonic vibration x_2 is kept at a stable level during the change in the contact stiffness K (c). Applied load (b) increases essentially from $1000N$ to nearly $5000N$. Red dashed line in (a) represents the initial interference $\Delta = -2 \times 10^{-7}m$. Generally speaking, the 2nd step ultrasonic vibration x_2 tends to shift downwards which has been observed also in the

mechanical feedback control. This is caused by a significant increase in the contact stiffness K. A difficult-to-engage into the material due to the elasticity increase produces certain asymmetry in the 2nd step ultrasonic vibration x_2.

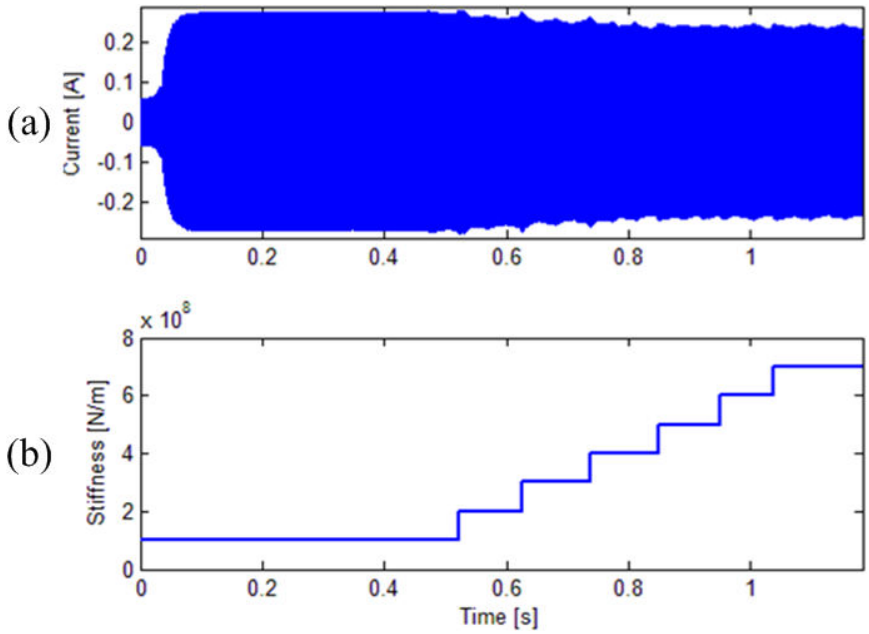

Figure 6.23 : Current feedback controlled current during changing contact stiffness K: (a) controlled current, (b) change in contact stiffness

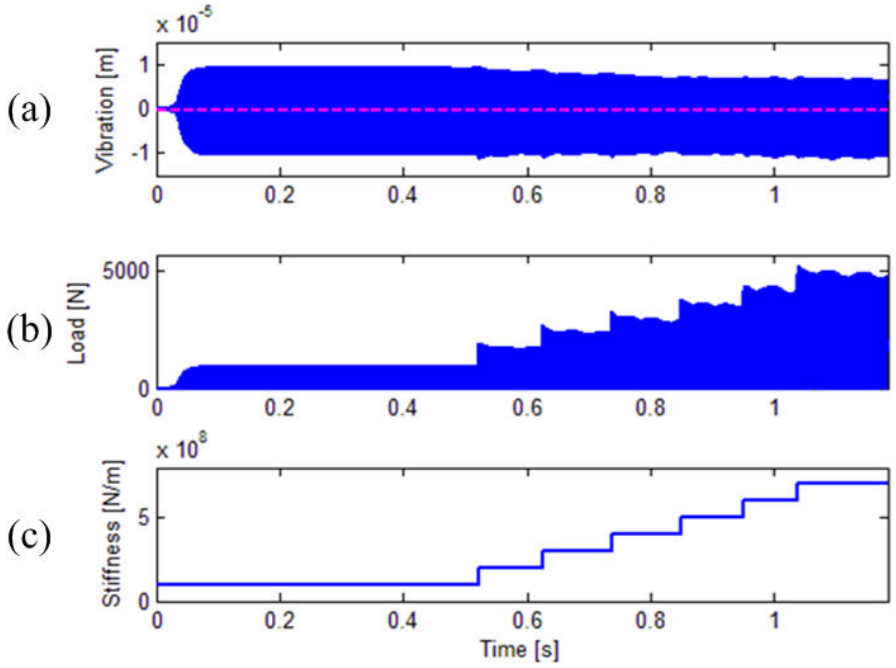

Figure 6.24 : Current feedback controlled 2nd step ultrasonic vibration during change in contact stiffness K: (a) controlled ultrasonic vibration, (b) change in applied load, (c) change in contact stiffness

Figure 6.25 depicts the RMS of the current i and the 2nd step ultrasonic vibration x_2 respectively. (a) is the enlarged image of (a) in Figure 6.22. As can be seen, only phase control algorithm is applied during the change in the contact stiffness K due to the fact that the RMS of feedback signal (current) does not leave the phase control zone. (b) demonstrates the RMS of the 2nd step ultrasonic vibration x_2 for each control cycle (black curve). The maximal deviation of the RMS of the 2nd step ultrasonic vibration x_2 from the desired level $R_d = 6.6\mu m$ is around $0.7\mu m$ which equals $11\%R_d$. To this point, current feedback with an application of a $4KHz$ bandwidth Butterworth filter during the change in the contact stiffness K seems inferior than the mechanical feedback control which only has a RMS $0.3\mu m$ ($4\%R_d$) deflection. In next section, a $8KHz$ bandwidth Butterworth filter application on the current feedback during the change in the contact stiffness K will be carried out.

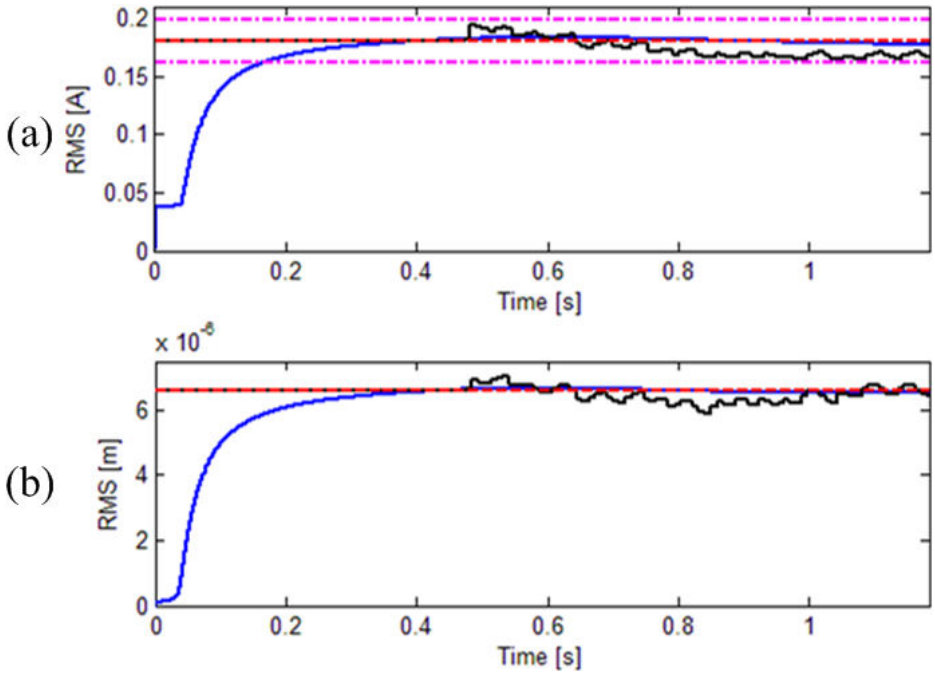

Figure 6.25 : (a) RMS of current, (b) RMS of 2nd step ultrasonic vibration

6.3.3.2 A 8KHz Butterworth Filter

For a $8KHz$ bandwidth Butterworth filter application in the current feedback, the supplied voltage amplitude is also$170V$ zero-to-peak shown in Table 6.2. The desired RMS of the current is $0.18A$ which generates RMS of the 2nd step ultrasonic vibration $6.6\mu m$. In Figure 6.26, (a) represents the RMS of the current i for each control cycle (200 oscillation periods, same as the mechanical feedback) shown in black line. Blue curve is the current RMS

calculated in infinite time. Red dashed straight line represents the desired RMS of the current i which is $R_d = 0.18A$ and pink dash-dotted boundaries are the phase control zone. In this case, $R_c = 10\%R_d$. (b) demonstrates the increase in the contact stiffness K in the applied load and the range is $K \in [1 \times 10^8 N/m \sim 7 \times 10^8 N/m]$. (c) is the phase control during the change in the contact stiffness K and it conforms to the phase control algorithm. (d) is the amplitude control which follows the amplitude control algorithm. As can be seen, RMS of the feedback signal (current) does not leave the phase control zone (pink dash-dotted line) which leads to no changes in the amplitude control. For phase control, the value generally decreases from 0.05 phase control units to 0.03 phase control unit. Compared with a $4KHz$ Butterworth filter application, a $8KHz$ filter effect on the phase shift seems much alleviated because of an increased bandwidth.

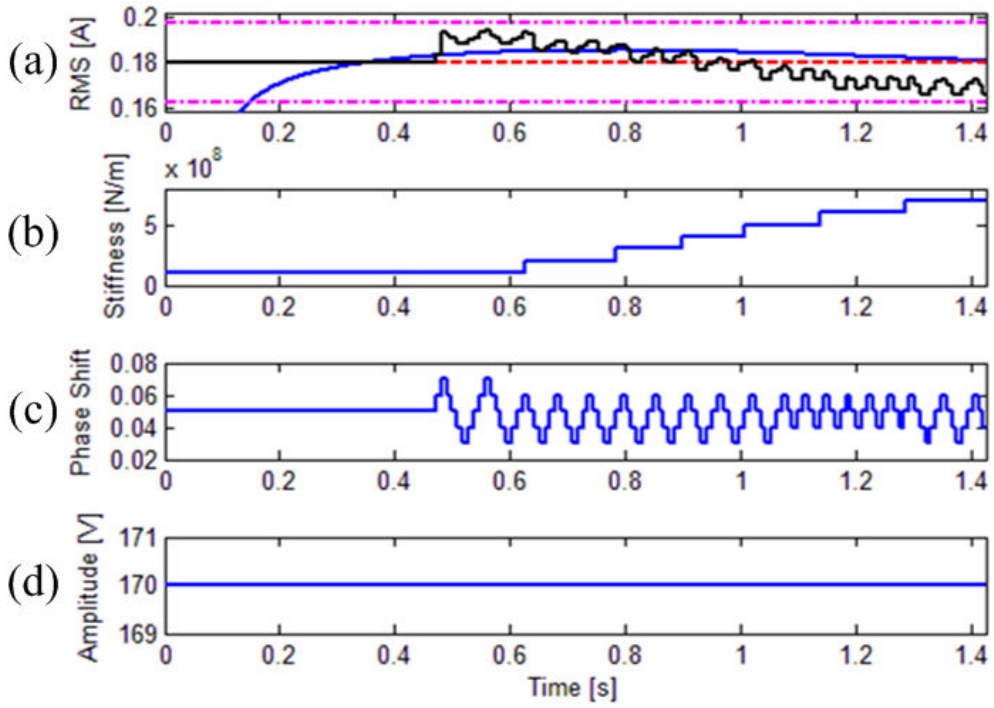

Figure 6.26 : Current feedback during change in contact stiffness K: (a) RMS of the feedback signal (current), (b) change in contact stiffness, (c) phase control, (d) amplitude control

Figure 6.27 shows the controlled current during the change in the contact stiffness K. As can be seen in (a) that the current remains stable during the change in the contact stiffness (b). This is similar to a $4KHz$ bandwidth Butterworth filter application. Nonetheless, the aim of the current feedback is to keep the 2nd step ultrasonic vibration x_2 at a constant level by

maintaining current i steady. Consequently, it is important to examine the control of the 2nd step ultrasonic vibration x_2.

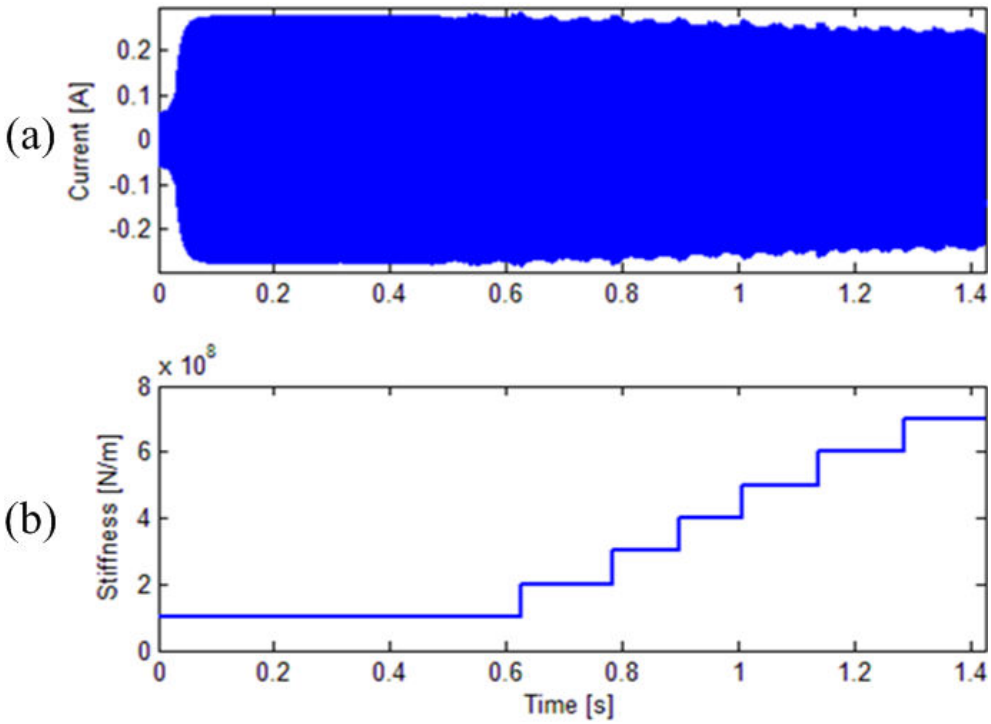

Figure 6.27 : Current feedback controlled current during change in contact stiffness K: (a) controlled current, (b) change in contact stiffness

Figure 6.28 shows the current feedback controlled ultrasonic vibration of 2nd step concentrator x_2 with a $8KHz$ bandwidth Butterworth filter application. As can be seen in (a), being similar to the $4KHz$ filter application case, the 2nd step ultrasonic vibration x_2 is kept at a stable level during the change in the contact stiffness K (c). Applied load (b) increases considerably from $1000N$ to nearly $5000N$. Red dashed line represents the initial interference $\Delta = -2 \times 10^{-7} m$. Again, the 2nd step ultrasonic vibration x_2 tends to shift downwards which is caused by a significant increase in the contact stiffness K.

Figure 6.29 depicts the RMS of the current i and the 2nd step ultrasonic vibration x_2. (a) is the enlarged picture of (a) in Figure 6.26. (b) demonstrates the RMS of the 2nd step ultrasonic vibration x_2 for each control cycle (black curve). According to the simulation results, maximal deflection in RMS of the 2nd step ultrasonic vibration x_2 from the desired value $R_d = 6.6\mu m$ is around $0.5\mu m$ that equals $8\% R_d$. To this point, the current feedback with application of a $8KHz$ bandwidth Butterworth filter during the change in the contact stiffness

K seems slightly worse than the mechanical feedback which only has a RMS $0.3\mu m$ ($4\%R_d$) deviation. However, the application of a $8KHz$ bandwidth Butterworth filter in current feedback still demonstrates certain improvement from a $4KHz$ bandwidth Butterworth filter which has a $0.7\mu m$ that equals $11\%R_d$. In next section, a $12KHz$ bandwidth Butterworth filter application during the change in contact stiffness K will be examined.

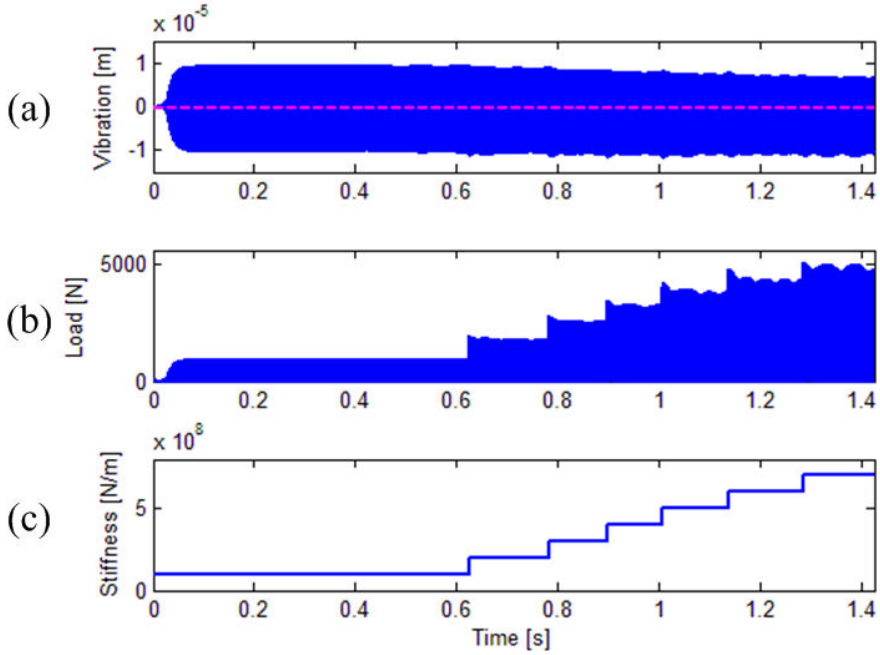

Figure 6.28 : Current feedback controlled 2nd step ultrasonic vibration during change in contact stiffness K: (a) controlled ultrasonic vibration, (b) change in applied load, (c) change in contact stiffness

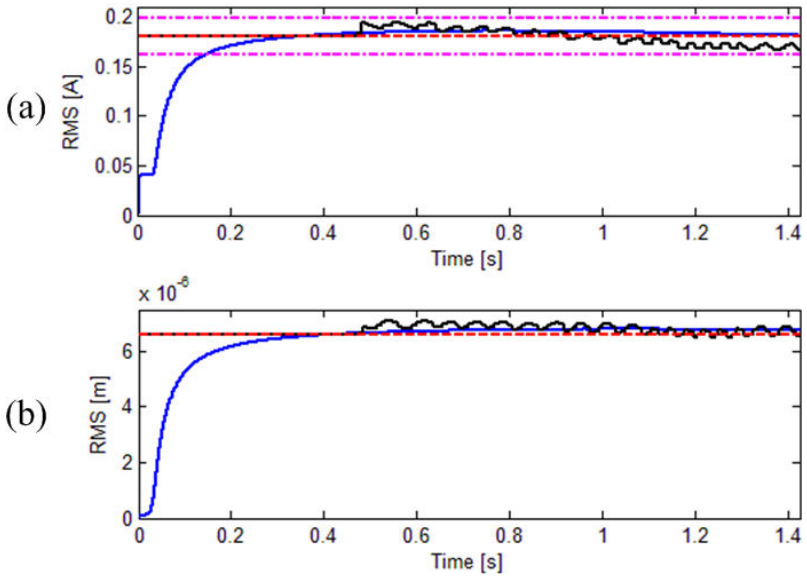

Figure 6.29 : (a) RMS of current, (b) RMS of 2nd step ultrasonic vibration

6.3.3.3 A $12KHz$ Butterworth Filter

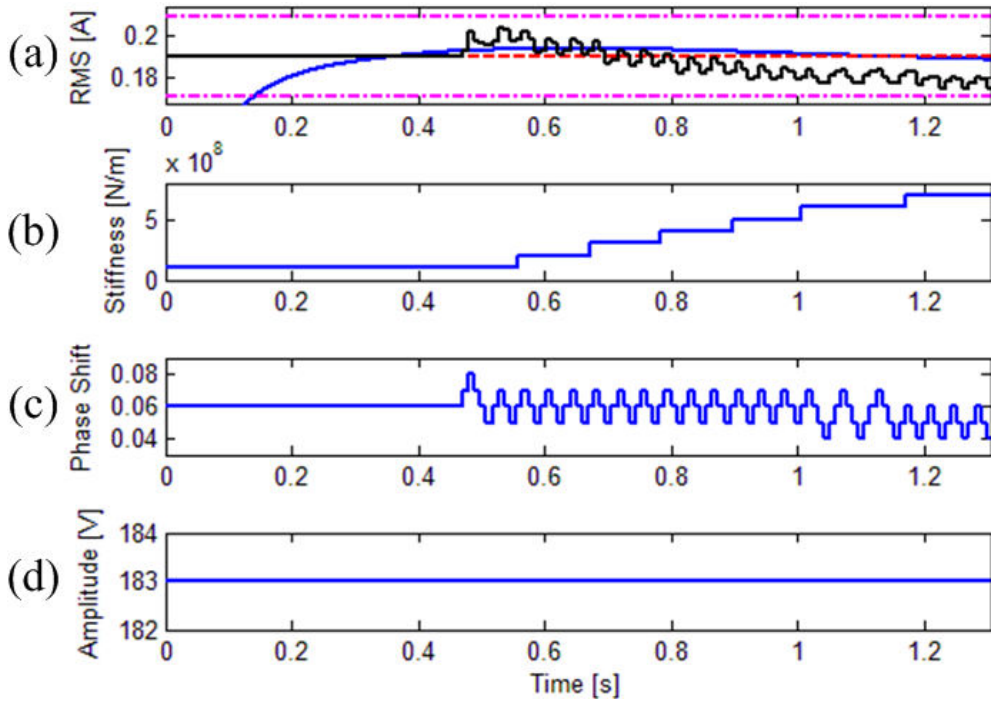

Figure 6.30 : Current feedback during change in contact stiffness K: (a) RMS of the feedback signal (current), (b) change in contact stiffness, (c) phase control, (d) amplitude control

For a $12KHz$ bandwidth Butterworth filter application in the current feedback, the supplied voltage amplitude of the square wave is $183V$ zero-to-peak shown in Table 6.2 and the desired RMS of current is adjusted to be $0.19A$. In Figure 6.30, (a) represents the RMS of the current for each control cycle (200 oscillation periods, same as the mechanical feedback) shown in black line. Blue curve is the current RMS calculated in infinite time. Red dashed straight line represents the desired RMS of current which is $R_d = 0.19A$ and pink dash-dotted boundaries are the phase control zone. In this case, $R_c = 10\%R_d$. (b) demonstrates the increase in the contact stiffness K and the range is $K \in [1 \times 10^8 N/m \sim 7 \times 10^8 N/m]$. (c) is the phase control during the change in the contact stiffness K and it conforms to the phase control algorithm. (d) is the amplitude control which follows the amplitude control algorithm. As can be seen, RMS of the feedback signal (current) does not leave the phase control zone (pink dash-dotted line). Therefore, there is no change in the amplitude control and it is kept as a constant $183V$. For the phase control, the value moderately decreases from 0.06 phase control units to 0.04 phase control unit. Compared with the $4KHz$ Butterworth filter case, the $12KHz$ Butterworth filter effect on the phase shift has a similar response to the $8KHz$ Butterworth filter.

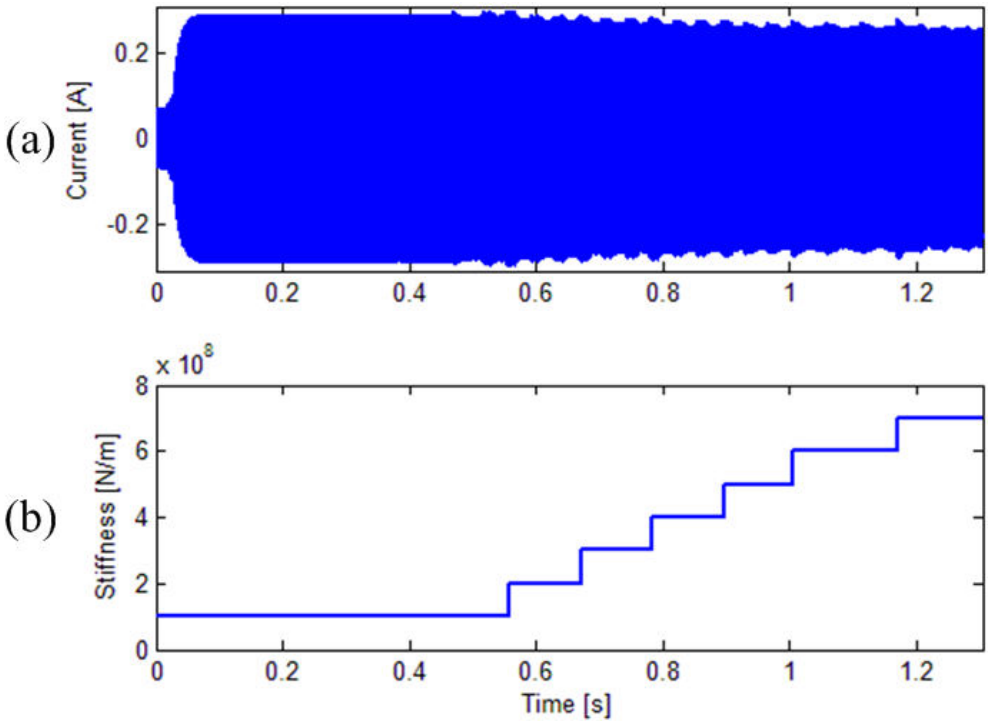

Figure 6.31 : Current feedback controlled current during change in contact stiffness K: (a) controlled current, (b) change in contact stiffness

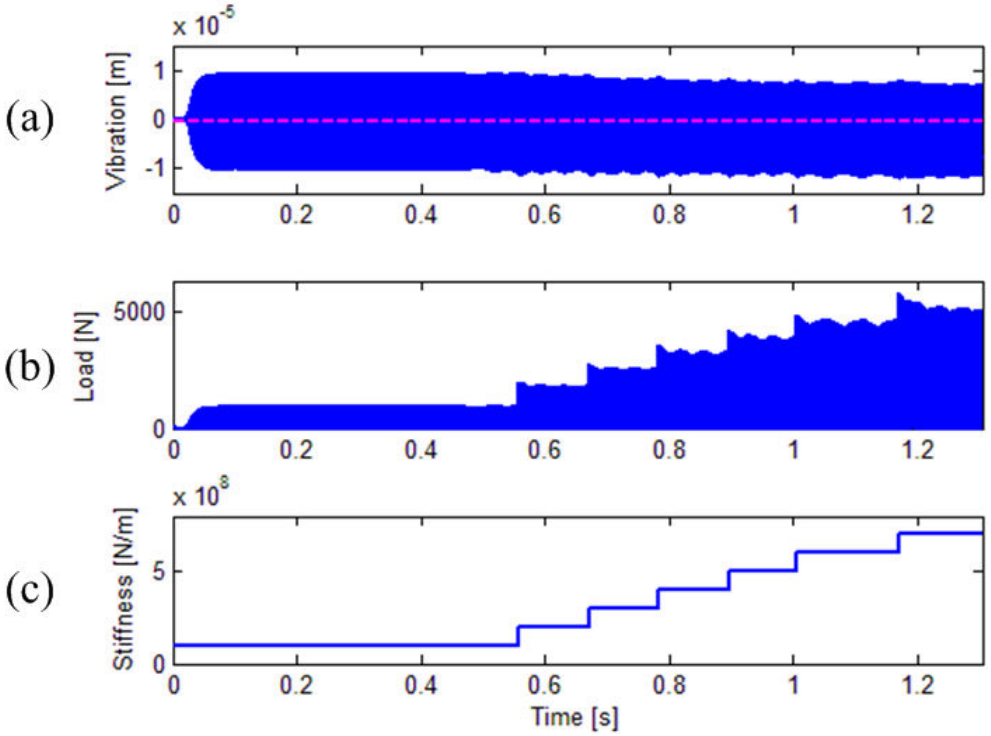

Figure 6.32 : Current feedback controlled 2nd step ultrasonic vibration during change in contact stiffness K: (a) controlled ultrasonic vibration, (b) change in applied load, (c) change in contact stiffness

Figure 6.31 shows the controlled current during the change in the contact stiffness K. As can be seen in (a), current remains stable during the change in the contact stiffness K (b). The response is similar to both the $4KHz$ bandwidth Butterworth filter and the $8KHz$ bandwidth Butterworth filter. Nonetheless, the aim of the current feedback is to keep the 2nd step ultrasonic vibration x_2 as a constant level by maintaining the current i. Consequently, it is important to examine the control of the 2nd step ultrasonic vibration x_2.

Figure 6.32 shows the current feedback controlled ultrasonic vibration of 2nd step concentrator x_2 with a $12KHz$ bandwidth Butterworth filter application. As can be seen in (a), being similar to the $4KHz$ and the $8KHz$ bandwidths Butterworth filters cases, the 2nd step ultrasonic vibration x_2 is kept at a stable level during the change in the contact stiffness K (c). Applied load (b) increases essentially from $1000N$ to nearly $5000N$. Red dashed line represents the initial interference $\Delta = -2 \times 10^{-7} m$. The ultrasonic vibration x_2 tends to shift downwards as expected which is also observed in the mechanical feedback as well as the current feedback control for the $4KHz$ and the $8KHz$ bandwidths Butterworth filters cases. This is caused by a significant increase in the contact stiffness K which makes a cutting tool more difficult to penetrate into the work piece.

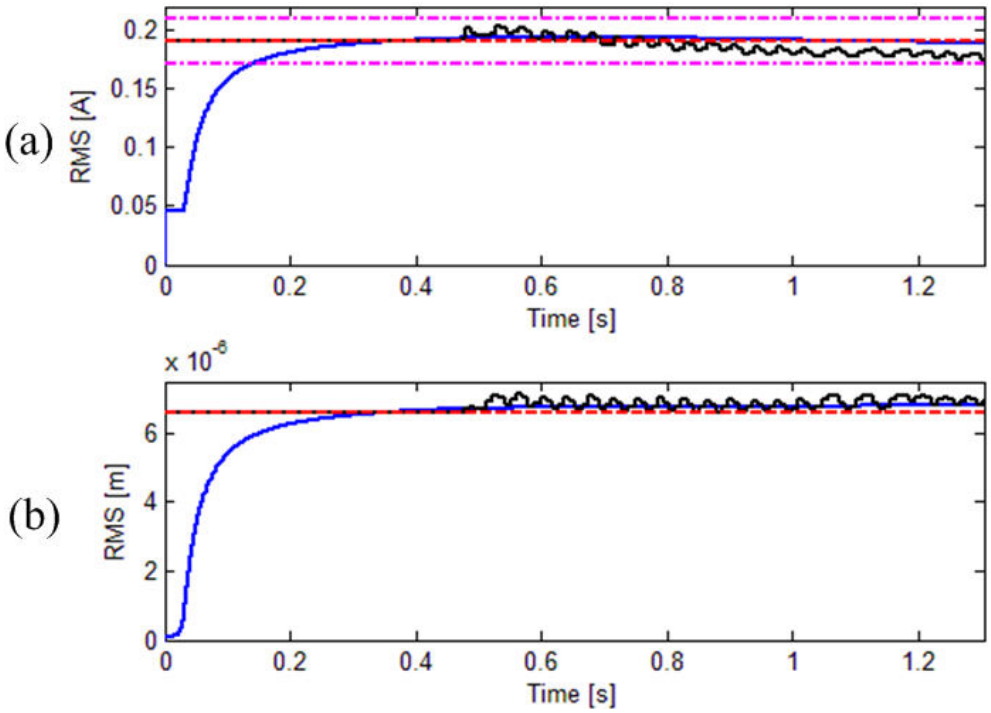

Figure 6.33 : (a) RMS of current, (b) RMS of 2nd step ultrasonic vibration

Figure 6.33 depicts the RMS of the current i and the 2nd step ultrasonic vibration x_2. (a) is the enlarged picture of (a) in Figure 6.30. As can be seen, phase control is able to keep the current i as a constant during the change in the contact stiffness K. (b) demonstrates the RMS of the 2nd step ultrasonic vibration x_2 for each control cycle (black curve). Maximal deflection of the RMS of the 2nd step ultrasonic vibration x_2 from the desired value $R_d = 6.6\mu m$ is around $0.5\mu m$ which equals $8\%R_d$. To this point, a $12KHz$ bandwidth Butterworth filter application in the current feedback control during the change in the contact stiffness K seems worse than the mechanical feedback which only has a RMS $0.3\mu m$ ($4\%R_d$) deviation. However, the performance of a $12KHz$ bandwidth Butterworth filter application is still better than the $4KHz$ bandwidth Butterworth filter application which has a deviation $0.7\mu m$ ($11\%R_d$) and is similar to the $8KHz$ bandwidth Butterworth filter application which has a deflection $0.5\mu m$ ($8\%R_d$). In next section, current feedback control during the change in the initial interference Δ for 3 bandwidths Butterworth filters will be examined and compared.

6.3.4 Change in Initial Interference

6.3.4.1 A $4KHz$ Butterworth Filter

For a $4KHz$ bandwidth Butterworth filter application in the current feedback, the supplied voltage amplitude is around $170V$ zero-to-peak, the desired RMS of current hence is $0.18A$ and the optimal phase shift is 0.16π initially which is same as the case of the $4KHz$ Butterworth filter during the change in the contact stiffness K. In Figure 6.34, (a) represents the RMS of the current for each control cycle (200 oscillation periods, same as the mechanical feedback) shown in black line. Blue curve is the current RMS calculated in infinite time. Red dashed straight line represents the desired RMS of the current which is $R_d = 0.18A$ and pink dash-dotted boundaries are the phase control zone. In this case, $R_c = 10\%R_d$. (b) demonstrates the increase in the initial interference Δ in the applied load and the range is $\Delta \in [-2 \times 10^{-7}m \sim -1 \times 10^{-5}m]$. (c) is the phase control during the change in the initial interference Δ and it conforms to the phase control algorithm. (d) is the amplitude control and it conforms to the amplitude control algorithm. As can be seen, RMS of the feedback signal (current) leaves phase control zone (pink dash-dotted line) several times which causes increase in the amplitude control to nearly $220V$ eventually. For phase control, the value generally decreases from 0.08 phase control units to almost 0.04 phase control unit which seems less drastic compared with the change in the contact stiffness K.

This is because the increase in the initial interference Δ shifts the resonant frequency of the loaded ultrasonic transducer only from $21.176KHz$ to $21.188KHz$.

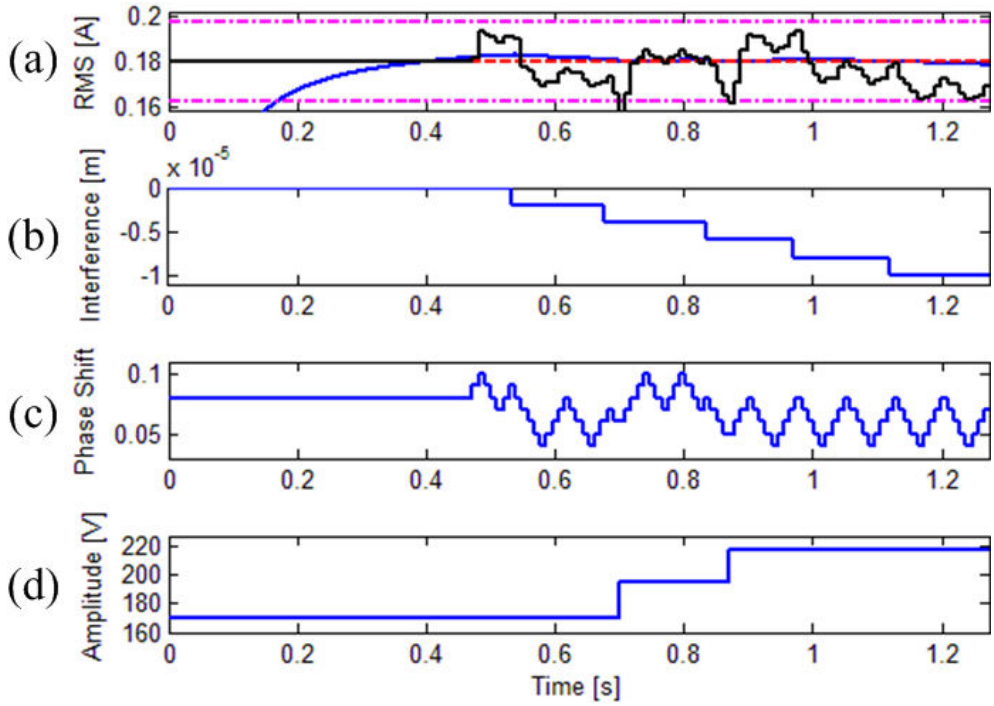

Figure 6.34 : Current feedback during change in initial interference Δ: (a) RMS of feedback signal (current), (b) change in initial interference, (c) phase control, (d) amplitude control

Figure 6.35 shows the controlled current during the change in the initial interference Δ. As can be seen in (a), current remains stable during the change in the initial interference Δ (b) even though some increases have been detected because of extra supplied voltage. However, the target of the current feedback is to maintain the ultrasonic vibration of 2nd step concentrator x_2 at a constant level by keeping current i stable. Therefore, it is important to evaluate the control of 2nd step ultrasonic vibration x_2.

Figure 6.36 demonstrates the current feedback controlled 2nd step ultrasonic vibration x_2 with a $4KHz$ bandwidth Butterworth filter application. As can be seen in (a), the 2nd step ultrasonic vibration x_2 is kept at a stable level during the change in the initial interference Δ shown in pink dashed line. Applied load (b) increases from $1000N$ to nearly $1500N$. Generally speaking, the 2nd step ultrasonic vibration x_2 fluctuates around the desired level with the help of the amplitude control.

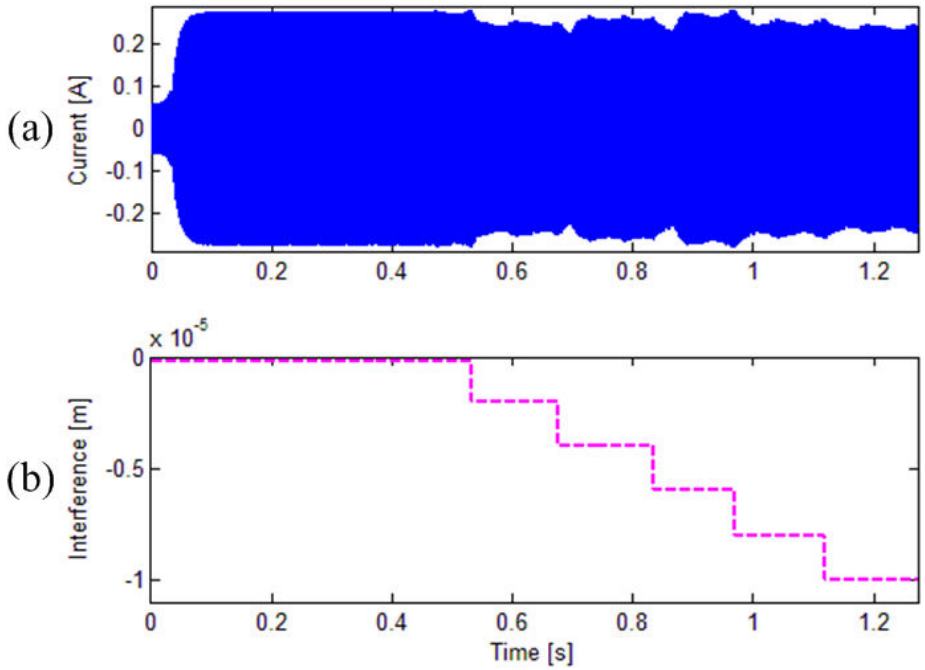

Figure 6.35 : Current feedback controlled current during change in initial interference Δ: (a) controlled current, (b) change in initial interference

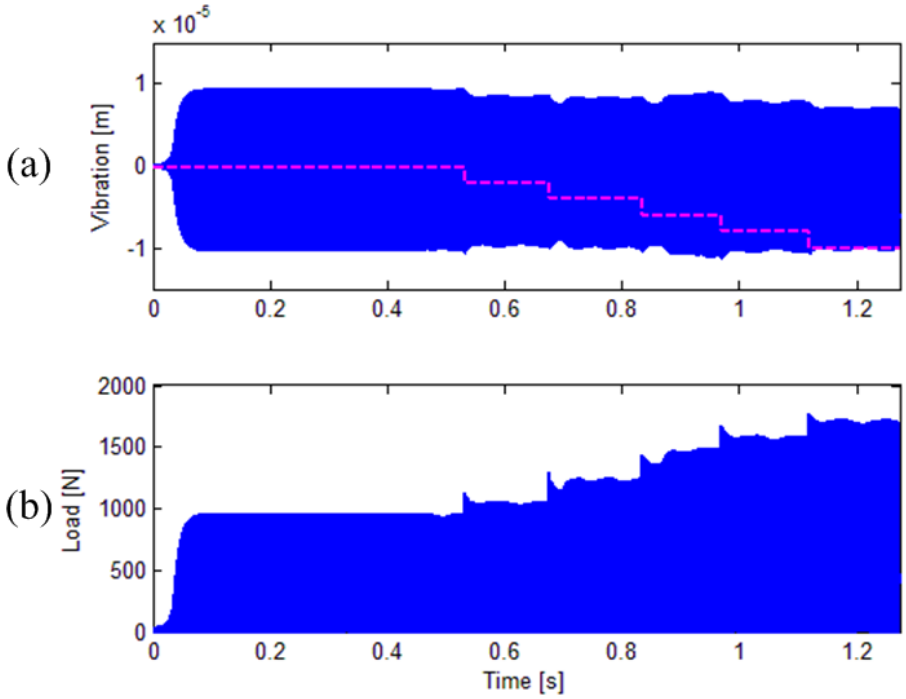

Figure 6.36 : Current feedback controlled 2nd step ultrasonic vibration during change in initial interference Δ: (a) controlled ultrasonic vibration, (b) change in nonlinear loading

Figure 6.37 depicts the RMS of the current and the ultrasonic vibration of 2nd step concentrator. (a) is the enlarged picture of (a) in Figure 6.34. Amplitude-phase combined

control algorithm has been applied during the current feedback control as a result of the RMS dropping out of the phase control zone. (b) demonstrates the RMS of the ultrasonic vibration of 2nd step concentrator x_2 for each control cycle (black curve). Maximal deflection of the RMS of the 2nd step ultrasonic vibration x_2 from the desired value $R_d = 6.6\mu m$ is around $0.8\mu m$ which equals $12\%R_d$. To this point, the current feedback with an application of a $4KHz$ bandwidth Butterworth filter during the change in the initial interference Δ seems worse than the mechanical feedback which only has a RMS $0.4\mu m$ ($6\%R_d$) deflection. In next section, a $8KHz$ bandwidth Butterworth filter application on the current feedback control during the change in the initial interference Δ will be carried out.

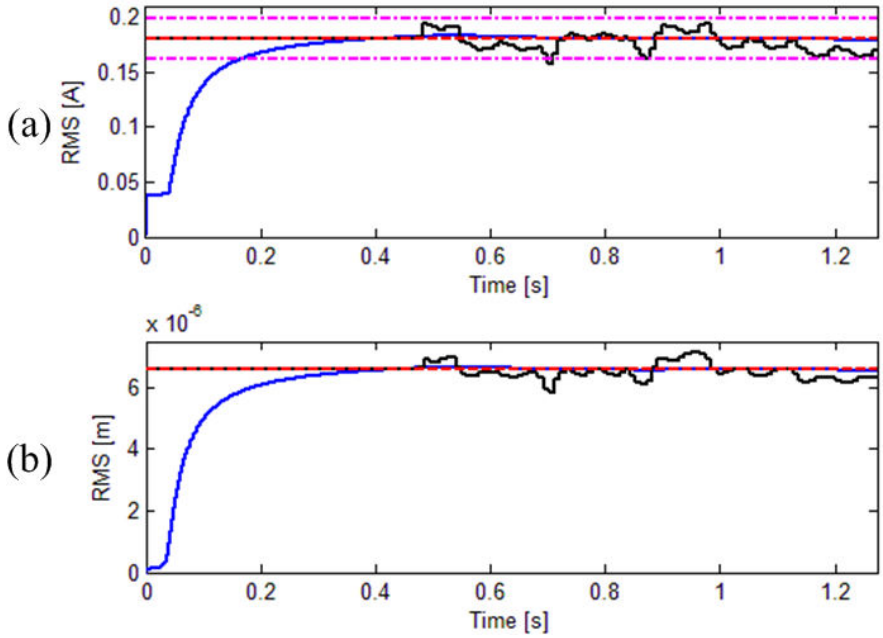

Figure 6.37 : (a) RMS of current, (b) RMS of 2nd step ultrasonic vibration

6.3.4.2 A $8KHz$ Butterworth Filter

For a $8KHz$ bandwidth Butterworth filter application on the current feedback control, the supplied voltage amplitude is $170V$ zero-to-peak, optimal phase shift is 0.1π and the desired RMS of the current hence is $0.18A$ which generates the RMS of the 2nd step ultrasonic vibration $6.6\mu m$. The conditions are same as the $8KHz$ Butterworth filter application during the change in the contact stiffness K. In Figure 6.38, (a) represents the RMS of the current for each control cycle (200 oscillation periods, same as the mechanical feedback) shown in black line. Blue curve is the current RMS calculated in infinite time. Red dashed straight line represents the desired RMS of the current which is $R_d = 0.18A$ and pink dash-dotted

boundaries are the phase control zone. In this case, $R_c = 10\%R_d$. (b) demonstrates the increase in the initial interference Δ in the applied load and the range is $\Delta \in [-2 \times 10^{-7}m \sim -1 \times 10^{-5}m]$. (c) is the phase control during the change in the initial interference Δ and it conforms to the phase control algorithm. (d) is the amplitude control which follows the amplitude control algorithm. As can be seen, RMS of the feedback signal (current) leaves the phase control zone (pink dash-dotted line) several times; therefore, the supplied voltage amplitude has been increased to nearly $220V$ eventually. For phase control, the value generally maintains the 0.05 phase control units despite some fluctuations.

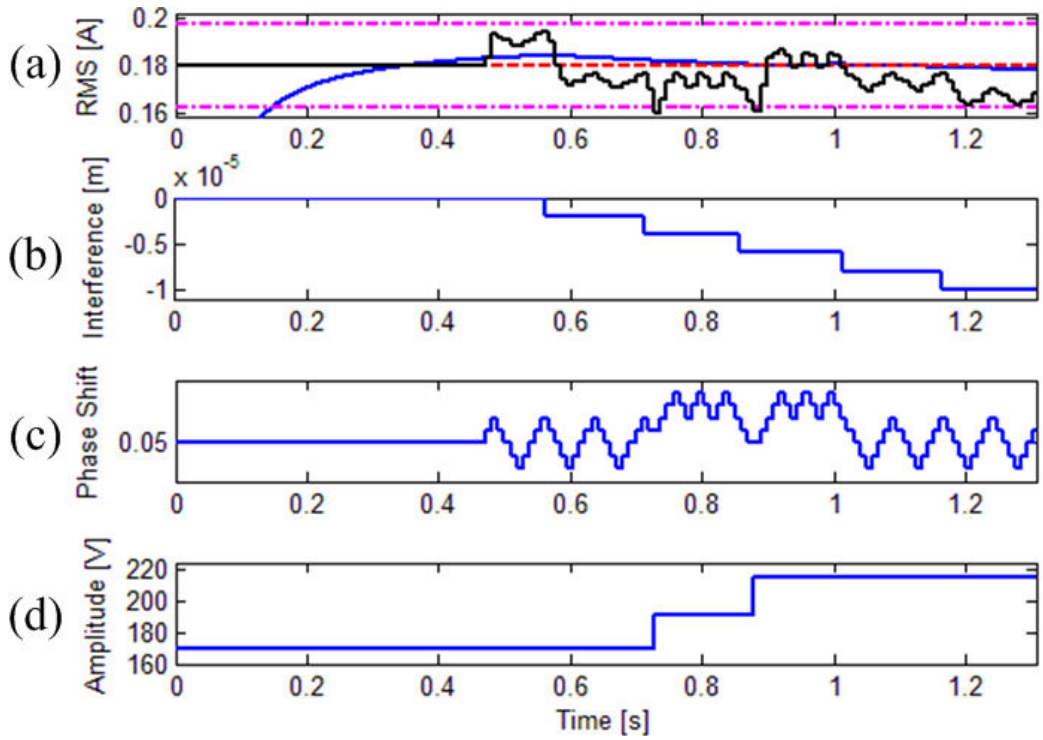

Figure 6.38 : Current feedback during change in initial interference Δ: (a) RMS of feedback signal (current), (b) change in initial interference, (c) phase control, (d) amplitude control

Figure 6.39 shows the controlled current during the change in the initial interference Δ. As can be seen in (a), the current remains stable during the change in Δ despite some fluctuations which is caused by the increase in the supplied voltage. However, the target of current feedback is to maintain the 2nd step ultrasonic vibration x_2 at a constant by keeping the current i stable. As a result, it is important to evaluate the control of 2nd step ultrasonic vibration x_2.

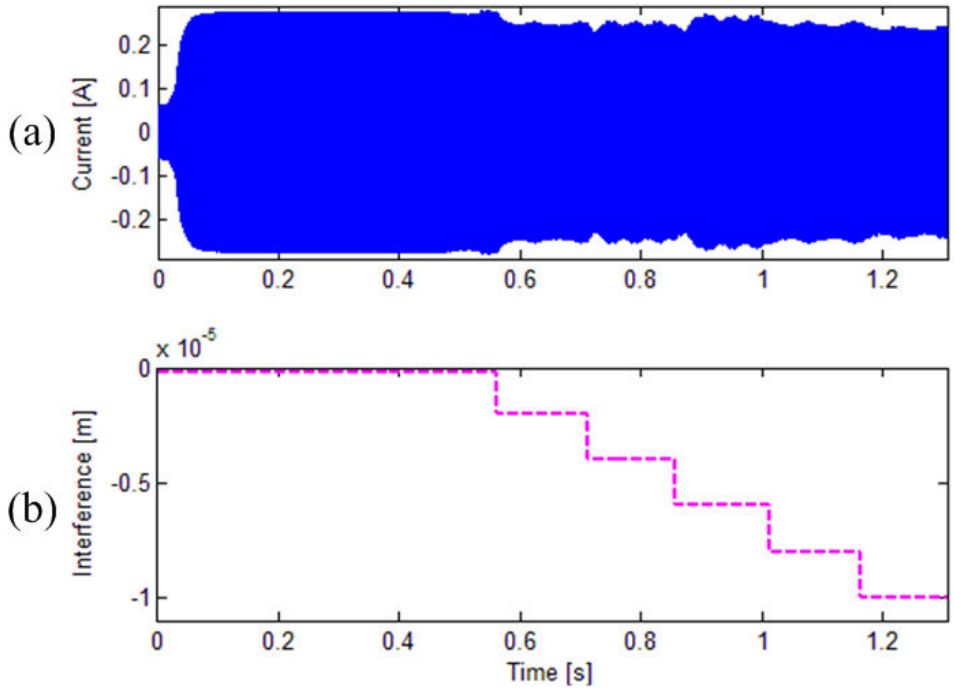

Figure 6.39 : Current feedback controlled current during change in the initial interference Δ: (a) controlled current, (b) change in initial interference

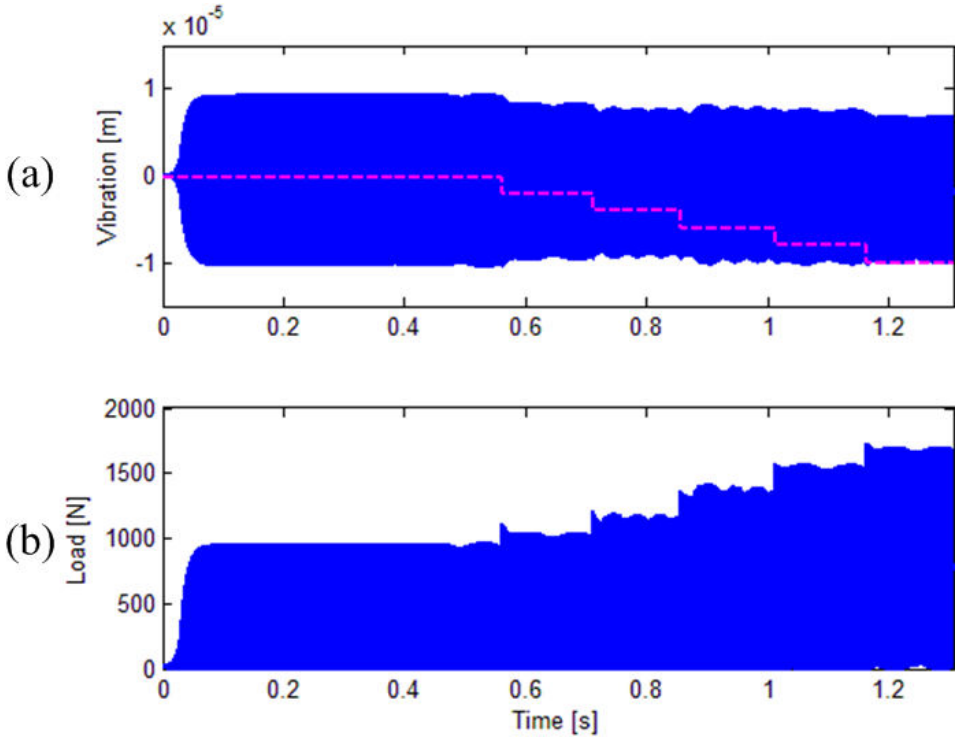

Figure 6.40 : Current feedback controlled ultrasonic vibration of 2nd step concentrator during changing initial interference : (a) controlled ultrasonic vibration of 2nd step, (b) change in nonlinear loading

Figure 6.40 demonstrates the controlled ultrasonic vibration of 2nd step concentrator x_2 with the current feedback associated with a $8KHz$ bandwidth Butterworth filter. As can be seen in (a), the 2nd step ultrasonic vibration x_2 is kept at a stable level during the change in the initial interference (pink dashed line). Applied load (b) increases slightly from $1000N$ to over $1500N$. Generally, the 2nd step ultrasonic vibration x_2 tends to shift downwards which is also observed in the mechanical feedback. However, the control seems not as perfect as mechanical feedback but behaves similarly to the $4KHz$ bandwidth Butterworth filter case.

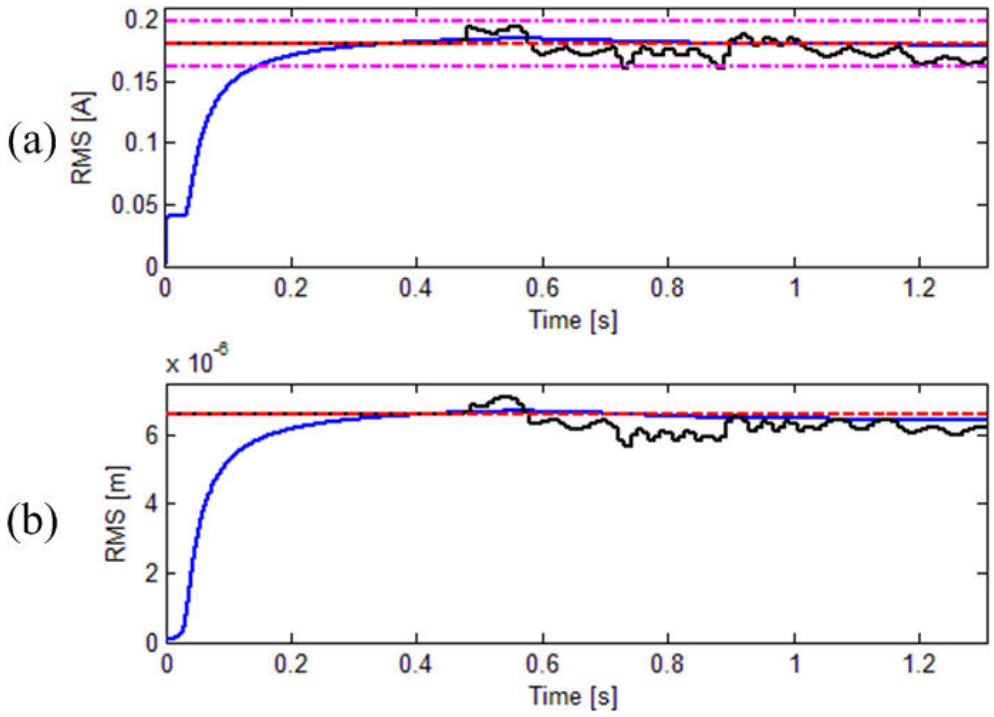

Figure 6.41 : (a) RMS of current, (b) RMS of 2nd step ultrasonic vibration

Figure 6.41 depicts the RMS of the current and the ultrasonic vibration of 2nd step concentrator. (a) is the enlarged image of (a) in Figure 6.38. In this case, amplitude-phase combined control algorithm is applied during the change in the initial interference Δ. (b) demonstrates the RMS of the ultrasonic vibration of 2nd step concentrator x_2 for each control cycle (black curve). Maximal deviation in RMS of the 2nd step ultrasonic vibration x_2 from the desired level $R_d = 6.6\mu m$ is around $0.9\mu m$ which equals $14\%R_d$. To this point, current feedback with an application of a $8KHz$ bandwidth Butterworth filter during the change in the initial interference Δ seems worse than the mechanical feedback which only has a RMS $0.4\mu m$ ($6\%R_d$) deviation. However, the performance is similar to the $4KHz$ bandwidth Butterworth filter application which has $0.8\mu m$ ($12\%R_d$) deflection. In next section, a

$12KHz$ bandwidth Butterworth filter application on the current feedback control during the change in the initial interference Δ will be carried out.

6.3.4.3 A $12KHz$ Butterworth Filter

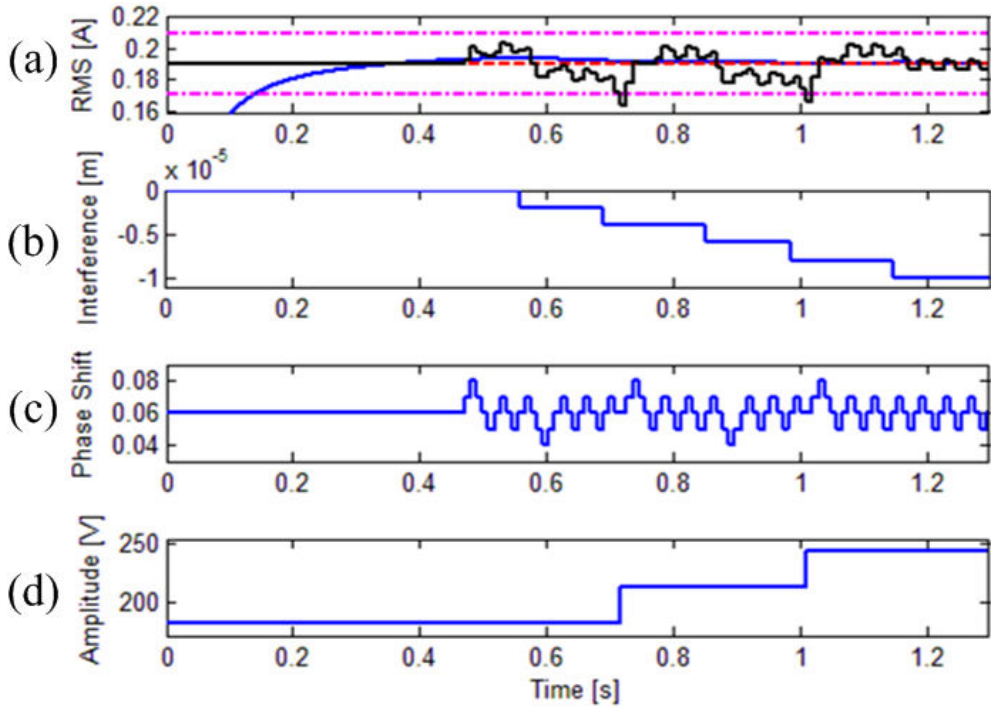

Figure 6.42 : Current feedback during change in initial interference Δ: (a) RMS of feedback signal (current), (b) change in initial interference, (c) phase control, (d) amplitude control

For a $12KHz$ bandwidth Butterworth filter application on the current feedback control, the supplied voltage is around $183V$ zero-to-peak, optimal phase shift is 0.12π and the desired RMS of the current is $0.19A$ which produces the RMS of the ultrasonic vibration at the end of 2nd step x_2 $6.6\mu m$. The situation is exactly identical to the $12KHz$ bandwidth Butterworth filter application during the change in the contact stiffness K. In Figure 6.42, (a) represents the RMS of the current i for each control cycle (200 oscillation periods, same as the mechanical feedback) shown in black line. Blue curve is the current RMS calculated in infinite time. Red dashed straight line represents the desired RMS of the current which is $R_d = 0.19A$ and pink dash-dotted boundaries are the phase control zone. In this case, $R_c = 10\%R_d$. (b) demonstrates the increase in the initial interference Δ in the applied load. Similarly, the range is $\Delta \in [-2 \times 10^{-7}m \sim -1 \times 10^{-5}m]$. (c) is the phase control during the change in the initial interference Δ and it conforms to the phase control algorithm. (d) is the amplitude control and it follows the amplitude control theory. As can be seen, RMS of the

feedback signal (current) leaves the phase control zone (pink dash-dotted line) several times. Therefore, the amplitude control has been excited to nearly $250V$ eventually. For phase control, the value generally maintains 0.06 phase control units.

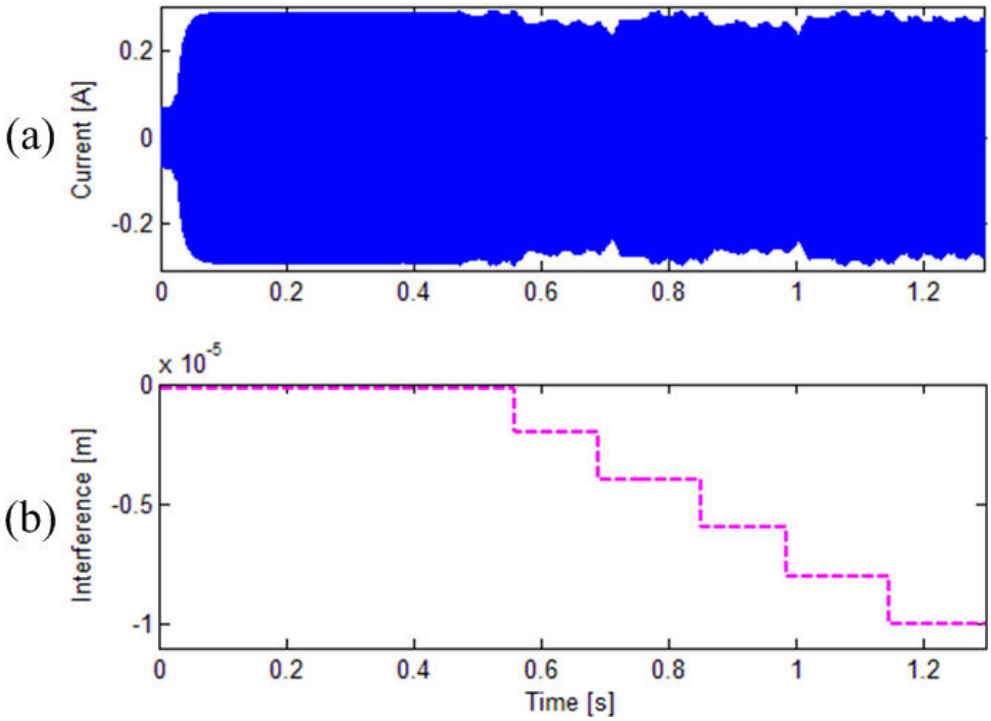

Figure 6.43 : Current feedback controlled current during change in the initial interference Δ: (a) controlled current, (b) change in initial interference

Figure 6.43 shows the controlled current during the change in the initial interference Δ. As can be seen in (a), current remains stable during the change in the initial interference (b) in spite of some ups and downs which is caused by the additional supplied power. However, the target of the current feedback is to maintain the 2nd step ultrasonic vibration x_2 at a constant by keeping current i stable. As a result, it is important to evaluate the control of the 2nd step ultrasonic vibration x_2.

Figure 6.44 demonstrates the current feedback controlled 2nd step ultrasonic vibration x_2 combined with a $12KHz$ bandwidth Butterworth filter. As can be seen in (a), the 2nd step ultrasonic vibration x_2 is kept at a stable level during the change in the initial interference Δ. Applied load (b) increases slightly from $1000N$ to $1500N$. Generally speaking, the 2nd step ultrasonic vibration x_2 tends to shift downwards which is also observed in the mechanical

feedback. However, the control seems not as perfect as the mechanical feedback but similar to the $4KHz$ and $8KHz$ bandwidths Butterworth filters applications.

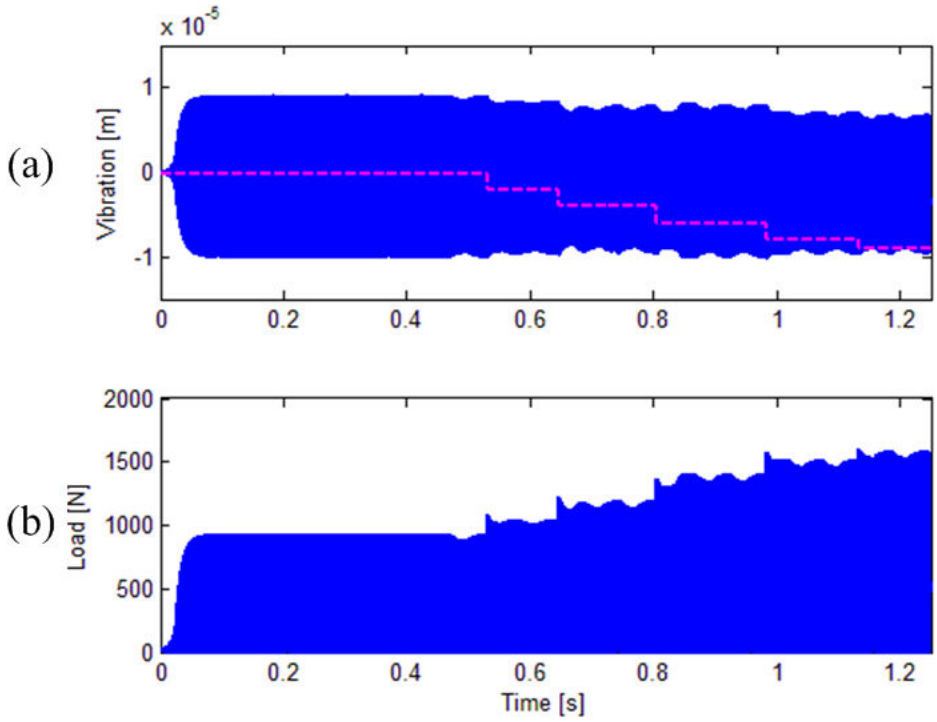

Figure 6.44 : Current feedback controlled 2nd step ultrasonic vibration during change in initial interference Δ: (a) controlled ultrasonic vibration, (b) change in nonlinear loading

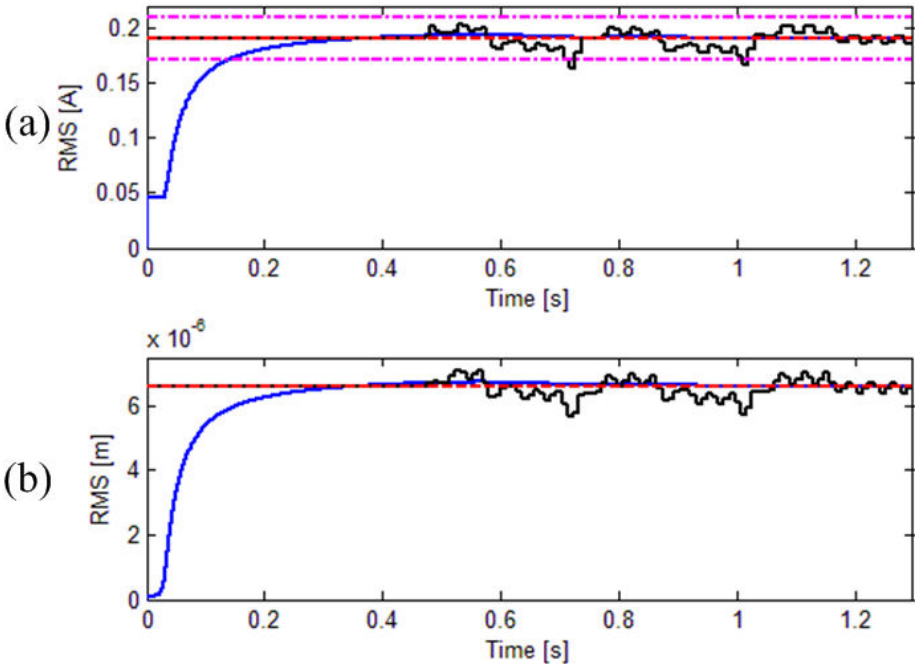

Figure 6.45 : (a) RMS of current, (b) RMS of 2nd step ultrasonic vibration

Figure 6.45 depicts the RMS of the current i and the ultrasonic vibration of 2nd step concentrator x_2. (a) represents the enlarged picture of (a) in Figure 6.42. The combined phase-amplitude control algorithm has been applied in this case. (b) demonstrates the RMS of the ultrasonic vibration of 2nd step concentrator x_2 for each control cycle (black curve). The maximal deviation of the RMS from the desired value $R_d = 6.6\mu m$ is around $1\mu m$ which equals $15\%R_d$. To this point, the current feedback with application of a $12KHz$ bandwidth Butterworth filter during the change in the initial interference Δ seems worse than the mechanical feedback control which only has a RMS $0.4\mu m$ ($6\%R_d$) deviation. However, the performance has a comparable similarity to the $4KHz$ and the $8KHz$ bandwidths Butterworth filters applications which have $0.8\mu m$ ($12\%R_d$) and $0.9\mu m$ ($14\%R_d$) deflections respectively.

6.3.5 Conclusion

In the above sections, the current feedback with 3 bandwidths Butterworth filters has been thoroughly investigated. The current feedback control for each situation presents various performances. The reason for this difference is due to the current feedback is an indirect control strategy of 2nd step ultrasonic vibration x_2. Therefore, the effectiveness of controlling the 2nd step ultrasonic vibration x_2 completely relies on the dynamic coupling between the current i and the ultrasonic vibration of 2nd step concentrator x_2 and how accurately that the current can reflect the mechanical vibration.

3 bandwidth Butterworth filters exhibit a comparable control on the ultrasonic vibration of 2nd step concentrator x_2 during the change in the contact stiffness K although the $8KHz$ and the $12KHz$ bandwidths Butterworth filters seem to keep the 2nd step ultrasonic vibration x_2 closer to the desired level. A similar performance has been observed in the control during the change in the initial interference Δ even if the control of a $4KHz$ Butterworth filter application is slightly better than the $8KHz$ and $12KHz$ Butterworth filters. In order to visually witness and compare the control with different bandwidths Butterworth filters application, maximal deflection calculated from the desired level of the 2nd step ultrasonic vibration x_2 for each bandwidth Butterworth filter application has been shown in Table 6.3.

It should be noted that the phase control zone (critical RMS denoted as R_c) and desired current RMS value R_d for each bandwidth Butterworth filter application is different. The

principle is to allow the change in the contact stiffness K to be coped only with the phase control algorithm in order to compare with each other without the help of the amplitude control. However, once the phase control zone is determined for one bandwidth Butterworth filter application, it is kept during the change in the initial interference Δ. Due to different bandwidths Butterworth filters effect, the control voltage amplitudes are tuned to match the desired amplitude of ultrasonic vibration of 2nd step concentrator $9\mu m$ zero-to-peak which corresponds to a RMS $R_d = 6.6\mu m$.

Table 6.3 : Deviation from the desired RMS level of the 2nd step ultrasonic vibration for three bandwidths Butterworth filters

Bandwidth / Deflection	$4KHz$	$8KHz$	$12KHz$
Change in contact stiffness	$0.7\mu m$ (11%)	$0.5\mu m$ (8%)	$0.5\mu m$ (8%)
Change in initial interference	$0.8\mu m$ (12%)	$0.9\mu m$ (14%)	$1.0\mu m$ (15%)

As can be seen clearly in Table 6.3, the $8KHz$ bandwidth Butterworth filter produces a comparably lower level of deviation from the desired RMS of the 2nd step ultrasonic vibration x_2 even though the deflection of the $8KHz$ filter is slightly larger than that of the $4KHz$ during change in the initial interference Δ. Therefore, the $8KHz$ Butterworth filter has been selected to perform the power feedback control. In next section, power feedback control during the change in the contact stiffness K and during the change in the initial interference Δ will be carried out. The amplitude-phase characteristics of the average power P and the 2nd step ultrasonic vibration x_2 will be obtained before the control is evaluated.

6.4 Power Feedback Control

As introduced before, power feedback control employs the average power P as the feedback signal but still uses the current i to actuate the positive feedback loop (detailed block diagram please refer to Figure 7.2 and Figure 7.3). The purpose of the power feedback control is to keep the 2nd step ultrasonic vibration x_2 as a constant level and this is achieved by maintaining the average power P of the loaded ultrasonic transducer. In order to operate the power feedback at the most efficient state, the phase shift which produces the maximal average power P for the loaded ultrasonic transducer has to be obtained. The characteristic

curve is achieved by slowly changing the phase shift in the feedback and tracking the peak value of the average power P. The increment for the phase shift is 0.01 phase control unit.

6.4.1 Amplitude-Phase Characteristic of Power and 2nd step Ultrasonic Vibration

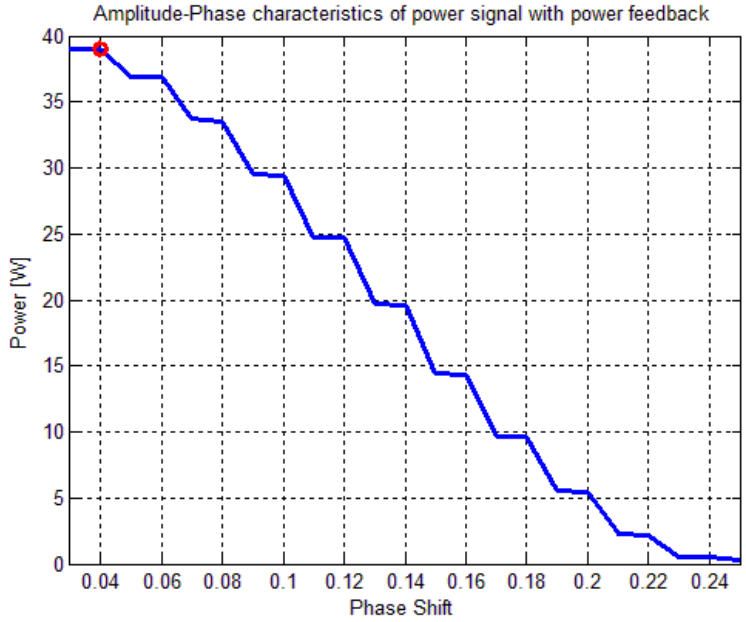

Figure 6.46 : Power amplitude-phase characteristic of the loaded ultrasonic transducer

As investigated in the current feedback in section 6.3.3.2 and section 6.3.4.2, a $8KHz$ bandwidth Butterworth filter generates the overall best control during the change in the contact stiffness K and in the initial interference Δ. Consequently, power feedback is established based on this bandwidth Butterworth filter.

Power feedback uses the average power P as the feedback signal to define the actual phase shift and the supplied voltage needed for the current to perform the positive feedback based on the combined amplitude-phase algorithm. A quasi sine wave is generated by a $8KHz$ bandwidth Butterworth filter. Amplitude-phase characteristic of the average power P is showed in Figure 6.46.

As can be seen, the average power P arrives at its most efficient state with a phase shift 0.04 phase control units. The peak average power P value is around $39.05W$. In other words, a 0.04 phase control unit will be applied to the power feedback in order to operate the loaded

ultrasonic transducer at the most efficient state. Meanwhile, it is also important to depict the amplitude-phase characteristic of the 2nd step ultrasonic vibration x_2. Results are shown in Figure 6.47.

Similarly, a phase shift 0.04 phase control units enables the ultrasonic vibration of 2nd step x_2 to reach its resonant state with an oscillation amplitude $11.78\mu m$ zero-to-peak. As a result, the amplitude for the square wave has to be tuned in order to match the desired vibration amplitude of 2nd step $9\mu m$ zero-to-peak. Amplitude of square wave is calculated as $170V$.

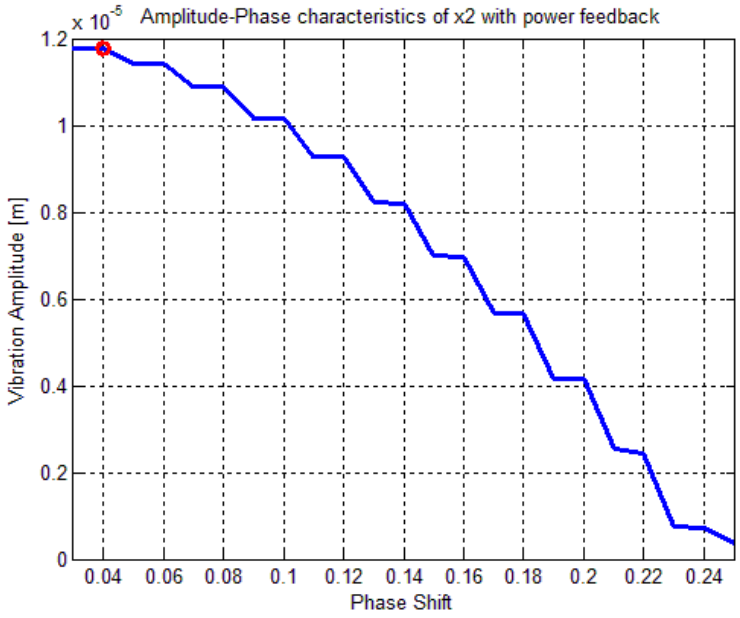

Figure 6.47 : Amplitude-phase characteristic of loaded ultrasonic transducer vibration

6.4.2 Change in Contact Stiffness

Change in contact stiffness for the applied load has a range $K \in [1 \times 10^8 N/m \sim 7 \times 10^8 N/m]$ which shifts the loaded ultrasonic transducer resonant frequency from $21.176KHz$ to $21.906KHz$. The desired RMS value of the average power P is $R_d = 27.5W$. The power feedback control during the change in the contact stiffness K is illustrated in Figure 6.48.

As can be seen in Figure 6.48, (a) demonstrates the RMS of the average power P which acts as the feedback signal. Black curve represents the power RMS calculated for each control cycle (200 oscillation periods, same as the mechanical feedback and current feedback) while the blue curve stands for the RMS of the average power P calculated in infinite time. Pink

dash-dotted boundary defines the phase control zone. In this case $R_c = 35\%R_d$ to make sure only the phase control algorithm is applied during the change in the contact stiffness K. Red-dashed straight line is the desire RMS of the average power P. As the increase in the contact stiffness K (b), RMS of the average power P does not leave the phase control zone even if it tends to decline drastically. Therefore, only phase control algorithm has been applied (c). Phase control generally fluctuates around its optimal value 0.04 phase control units. (d) shows the amplitude control.

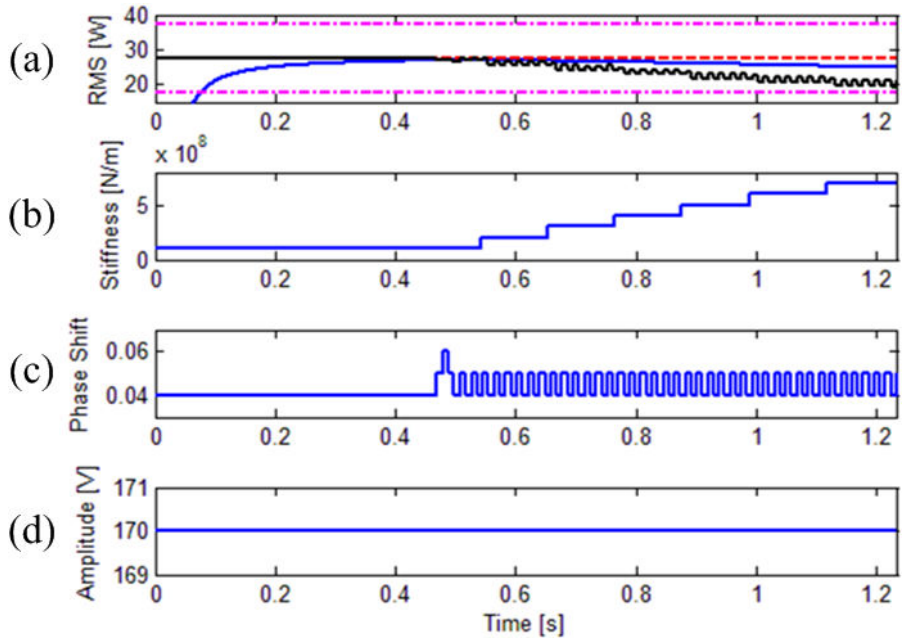

Figure 6.48 : Power feedback during change in contact stiffness K: (a) RMS of feedback signal (average power), (b) change in contact stiffness, (c) phase control, (d) amplitude control

Figure 6.49 shows the controlled average power during the change in the contact stiffness K. As can be seen in (a), RMS of the average power decreases from $27.5W$ to around $20W$. Physically, it means that a considerable amount of power has consumed to deal with the increase in the elasticity in the material (changed vibro-impact regime). (b) indicates the increase in the contact stiffness K.

Figure 6.50 illustrates the power feedback controlled 2nd step ultrasonic vibration x_2 during the change in the contact stiffness K. In (a), the 2nd step ultrasonic vibration x_2 generally can be kept at a constant level as the increase in the contact stiffness K (c). The 2nd step ultrasonic

vibration x_2 tends to shift downwards which has been observed in the mechanical feedback and the current feedback. This is caused by the essential increase in the contact stiffness K which changes the elasticity property of the applied load. Such change makes the cutting tool more difficult to penetrate into the work piece. Red dashed straight line represents the initial interference $\Delta = -2 \times 10^{-7} m$. Significant increase in the contact stiffness K leads to the 2nd step ultrasonic vibration x_2 asymmetric around the red dashed line. The applied load has gradually risen from $1000N$ to $5000N$.

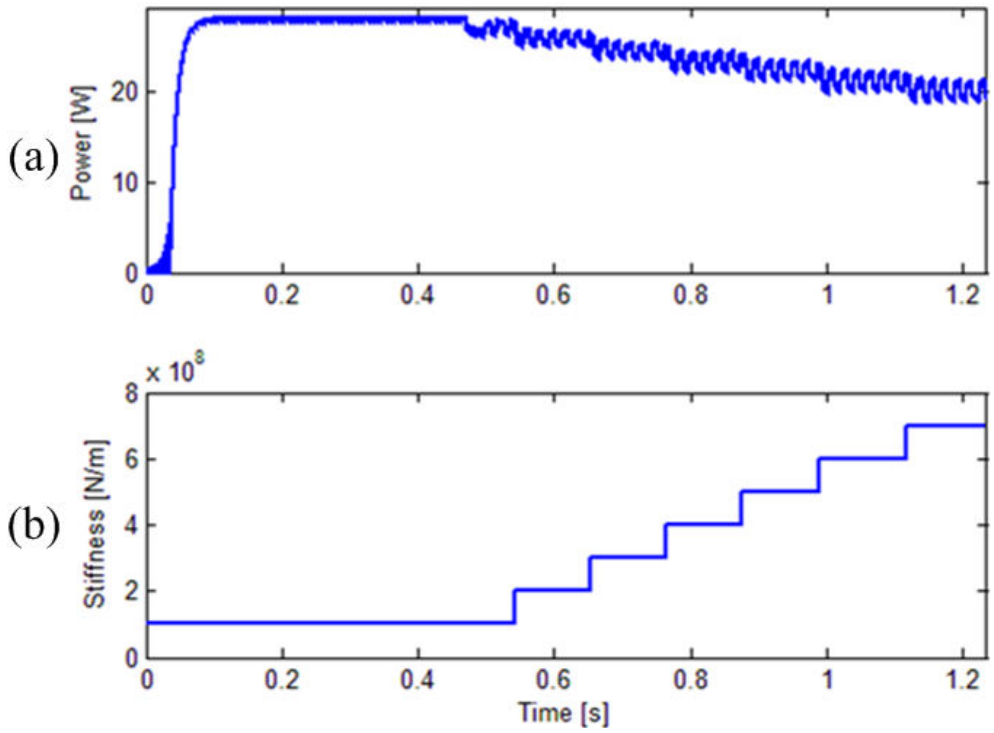

Figure 6.49 : Power feedback controlled average power during change in contact stiffness K: (a) controlled power, (b) change in contact stiffness

Figure 6.51 shows the RMS of the average power P and RMS of the 2nd step ultrasonic vibration x_2. As can be observed in (a), RMS of the average power P for each control cycle never leaves the phase control zone. However, it has a significant drop from its desired level. In (b), the RMS of the ultrasonic vibration at the end of 2nd step concentrator x_2 for each control cycle seems closely adhered to the desired level (red dashed straight line). Maximal deviation of the RMS of the 2nd step ultrasonic vibration x_2 from its desired level is around $0.4\mu m$ which equals $6\%R_d$. This performance is slightly worse than the mechanical feedback deviation $0.3\mu m$ ($4\%R_d$) however is better than the current feedback with a $8KHz$ bandwidth Butterworth filter deviation $0.5\mu m$ ($8\%R_d$).

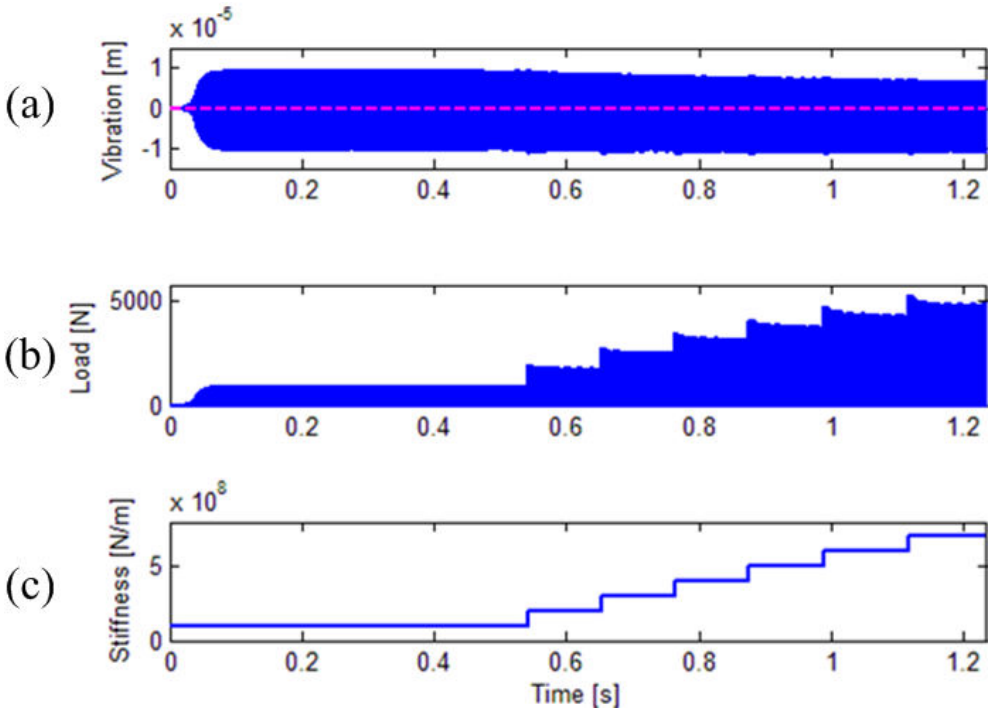

Figure 6.50 : Power feedback controlled 2nd step ultrasonic vibration during change in contact stiffness K: (a) controlled ultrasonic vibration, (b) change in applied loading, (c) change in contact stiffness

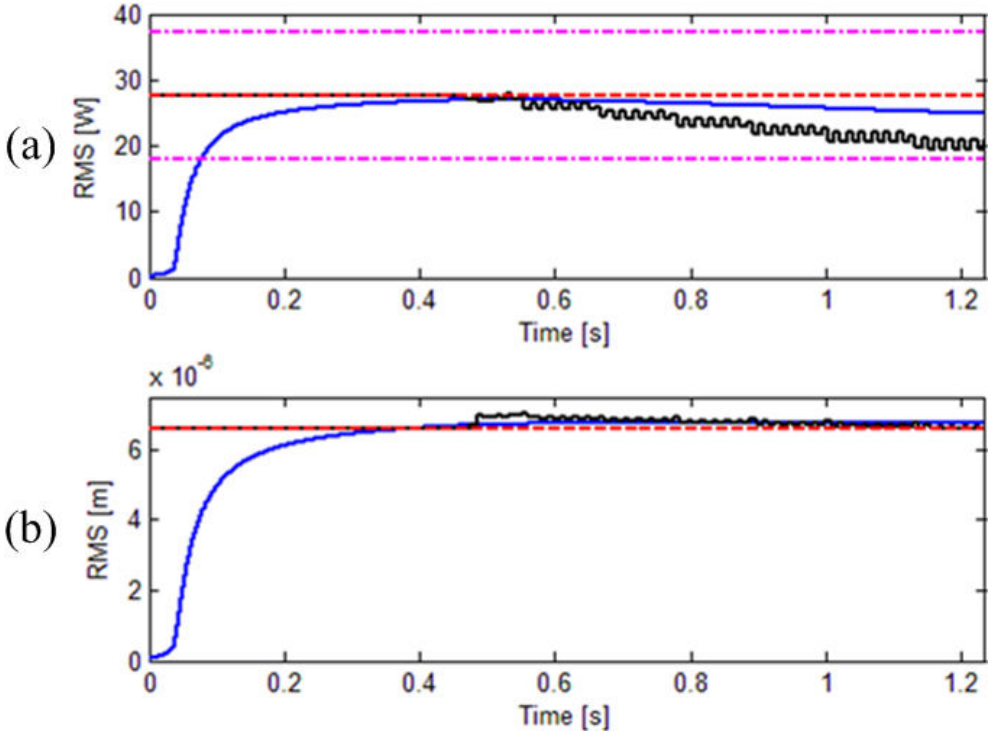

Figure 6.51 : (a) RMS of average power, (b) RMS of 2nd step ultrasonic vibration

6.4.3 Change in Initial Interference

The change in the initial interference is $\Delta \in [-2 \times 10^{-7}m \sim -1 \times 10^{-5}m]$ which gives rise to the resonant frequency of the loaded ultrasonic transducer shifts from $21.176KHz$ to $21.188KHz$. The desired RMS level of the average power P remains $R_d = 27.5W$. In this case, the phase control zone is selected to be $R_c = 10\%R_d$ which matches the condition of the current feedback in order to involve the amplitude-phase combined control algorithm during the change in the initial interference Δ.

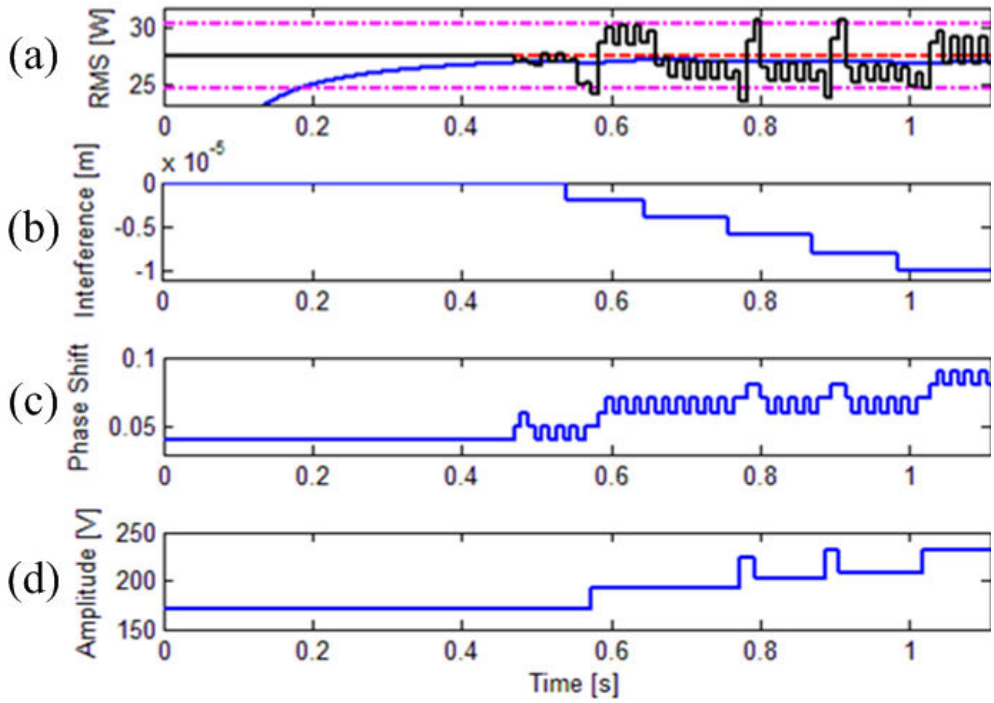

Figure 6.52 : Power feedback during changing initial interference: (a) RMS of feedback signal (average power), (b) change in initial interference, (c) phase control, (d) amplitude control

Clearly, in Figure 6.52 (a), RMS of the average power P for each control cycle (200 oscillation periods black line) exceeds the phase control zone (pink dash-dotted line) several times which results in the change in the amplitude control (d) from $170V$ to nearly $240V$ with ups and downs. Phase control increases from 0.04 phase control units to nearly 0.08 phase control units in order to tune itself at the most efficient resonant state. (b) demonstrates the change in the initial interference Δ.

Figure 6.53 shows the RMS monitoring of the average power and the 2nd step ultrasonic vibration x_2. In (a), the RMS of the average power P is maintained at the desired level with fluctuations which are caused by the sudden changes in the supplied voltage u. (b) shows the change in the initial interference Δ.

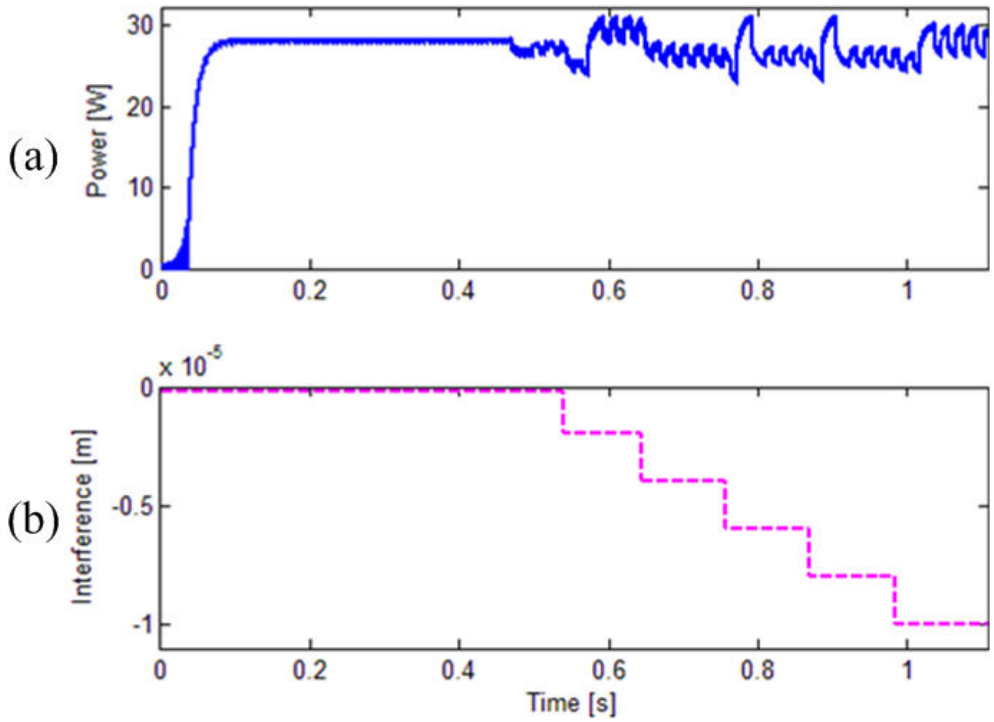

Figure 6.53 : Power feedback controlled average power during changing initial interference: (a) controlled power, (b) change in initial interference

Figure 6.54 depicts the power feedback controlled 2nd step ultrasonic vibration x_2. In (a), it shows that the 2nd step ultrasonic vibration x_2 declines to a moderately lower level during the change in the initial interference Δ shown in pink dashed line. (b) demonstrates the interaction force increases gradually from $1000N$ to nearly $1500N$.

Figure 6.55 illustrates the RMS of the average power P and the 2nd step ultrasonic vibration x_2 for each control cycle. In (a), it shows the RMS of the average power P drops out of the phase control zone several times which suggests an amplitude-phase combined control algorithm. In (b), the RMS of the 2nd step ultrasonic vibration x_2 has been drawn. As can be seen, the maximal deflection from the desired level of RMS of the 2nd step ultrasonic vibration x_2 is $0.9\mu m$ which equals $14\%R_d$. This performance has a similarity to the current feedback with a $8KHz$ bandwidth Butterworth filter application $9\mu m$ $(14\%R_d)$ deflection.

However, compared with the mechanical feedback during the change in the initial interference Δ with a deviation $0.4\mu m$ $(6\%R_d)$, the power feedback control has a worse performance.

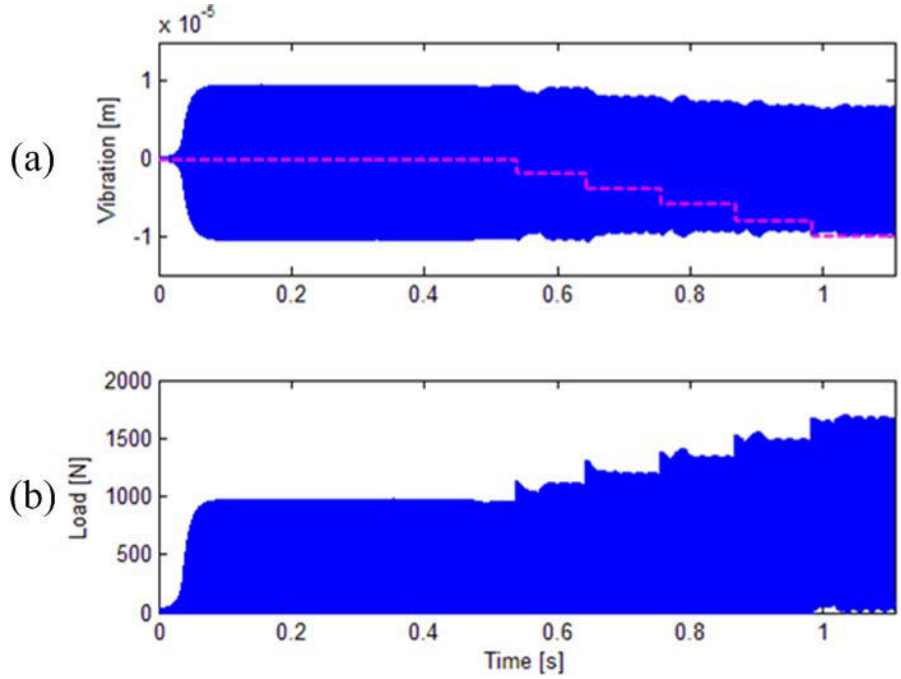

Figure 6.54 : Power feedback controlled 2nd step ultrasonic vibration during change in initial interference Δ: (a) controlled ultrasonic vibration, (b) change in nonlinear loading

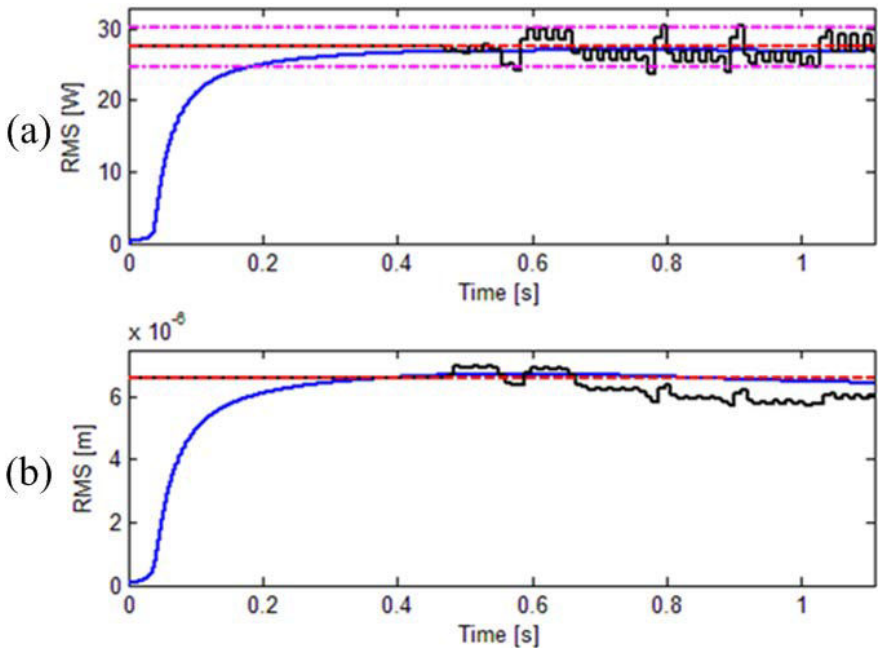

Figure 6.55 : (a) RMS of power, (b) RMS of 2nd step ultrasonic vibration

6.5 Summary

In this chapter, the mechanical feedback control, current feedback control and power feedback control are obtained together with the fixed frequency control. Comparison and analysis emphasise the importance of the employment of the autoresonant control. 3 bandwidths Butterworth filters have been employed in the current feedback to explore the filter effect on the control during the change in the contact stiffness K and during the change in the initial interference Δ. In conclusion, a $8KHz$ bandwidth Butterworth filter has been selected as it produces a more superior control on the 2nd step ultrasonic vibration x_2.

In order to compare the mechanical feedback control, current feedback control and power feedback control, the maximal deflections from the desired level of RMS of the 2nd step ultrasonic vibration $R_d = 6.6\mu m$ have been calculated and shown in Table 6.4. As can be observed, mechanical feedback shows the overall best control of the 2nd step ultrasonic vibration x_2 during the change in the contact stiffness K and in the initial interference Δ. Current feedback and power feedback presents a similar performance. Generally speaking, 3 feedback control strategies share a similar performance during the change in the contact stiffness K. In terms of the change in the initial interference Δ, mechanical feedback shows a high superiority than current feedback and power feedback.

Table 6.4 : Deviation from the desired level of RMS of the 2nd step ultrasonic vibration for 3 feedback controls

Feedback / Deflection	Mechanical	Current	Power
Change in contact stiffness	$0.3\mu m$ (4%)	$0.5\mu m$ (8%)	$0.4\mu m$ (6%)
Change in initial interference	$0.4\mu m$ (6%)	$0.9\mu m$ (14%)	$0.9\mu m$ (14%)

Chapter Seven Experimental Results

In order to verify the simulation results with different control strategies and explore the drill bits effect on the control efficiency, experiment results are presented. Literally, the following control strategies will be investigated: fixed frequency control, mechanical feedback control, current feedback control and power feedback control. A prototype autoresonant control system has been manufactured and tested with the technical support of Dr. Alan Meadows. Experiments were carried out on a Harrison M300 lathe. A number of aluminium alloy specimens have been used and eventually the aluminium alloy plates with grade number 5083 are selected. These work pieces have hardness 77HV with thickness 15mm. Two sizes of drill bits 3mm and 6mm in diameter are used. A fixed rotational speed of the spindle in combination with various feed rates has been employed in order to examine the robustness and the limitations of the listed control strategies. Characteristics of the ultrasonic transducers have been recorded. In addition, holes surface roughness has been evaluated.

7.1 Q Factor of 2-Step Ultrasonic Transducer with a 3mm Drill Bit

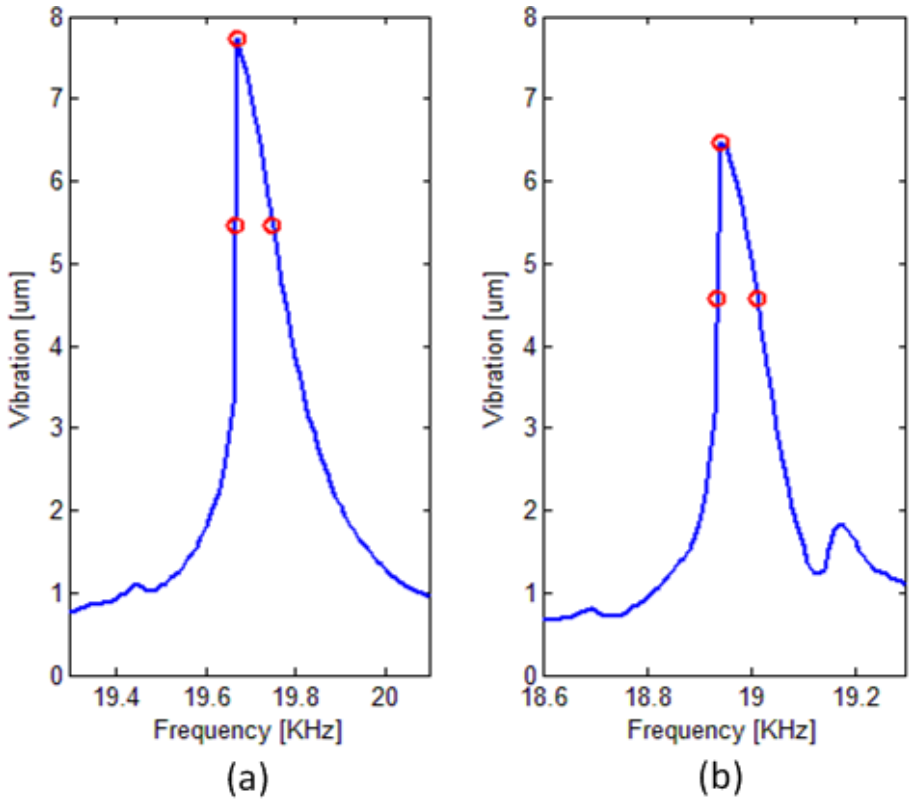

Figure 7.1 : Q factor of the 2-step ultrasonic transducer: (a) no tool, (b) a 3mm drill bit

Before autoresonant control is applied to a 2-step ultrasonic transducer to evaluate the control effectiveness, it is advisable to calculate the Q factor of the ultrasonic vibrating system without and with a 3mm drill bit attached so as to study the difficulties that might be encountered during machining. Figure 7.1 illustrates the Q factor calculations in two conditions: (a) a 2-step ultrasonic transducer without any tool attached, (b) attached with a 3mm standard twist drill bit. A 3mm drill bit was properly clamped to ensure no loose screws effect. During data acquisition, the ultrasonic vibrations at the end of 2nd step x_2 have been measured with a laser vibrometer (Manufactured by Polytec, OFV 512 + OFV3001) together with the excitation frequencies. A proper range sweep of frequencies was established which centred on the resonant frequency for each condition. As can be observed in Figure 7.1, according to the definition of Q factor, the resonant frequency and half power ($\sqrt{2}/2$ maximum magnitude) corresponding frequencies are marked in red circles. The ratio between the resonant frequency and the bandwidth (Q factor) has been calculated and shown in Table 7.1.

Table 7.1 shows the resonant frequencies and bandwidths as well as the calculated Q factor values for the ultrasonic vibrating system without and with an attachment of a 3mm drill bit. The resonant frequency shifts to a lower value when there was a 3mm drill bit attached which conforms to the findings in [16]. In addition, a 3mm drill bit with mass 28 grams attached to the 2-step ultrasonic transducer results in a 17% decrease in the 2nd step ultrasonic vibration x_2. This suggests a waveform change of the ultrasonic vibrating system with an attachment of a small 3mm drill bit. The Q factor of the ultrasonic vibrating system increases by a small amount with a 3mm drill bit attachment and values conform to the value of properly tuned ultrasonic transducer, as stated in [68], which is normally in the range 200-250 for the same sweep rate. In following sections, the experimental setup of the autoresonant control will be introduced and each component will be described elaborately.

Table 7.1 : Q factor of a 2-step ultrasonic transducer with and without a 3mm drill bit

Tool Attachment	Resonant Frequency (KHz)	Bandwidth (KHz)	Quality Factor
None	19.67	0.0842	233
A 3mm drill bit	18.94	0.0773	245

7.2 Experimental Devices

Figure 7.2 demonstrates the autoresonant control schematic diagram of the Ultrasonically Assisted Drilling (UAD) process. There are mainly 3 parts: sensor contour (1), autoresonant control contour (2) and data recording contour (3). In the following, each component will be introduced.

7.2.1 Autoresonant Control System

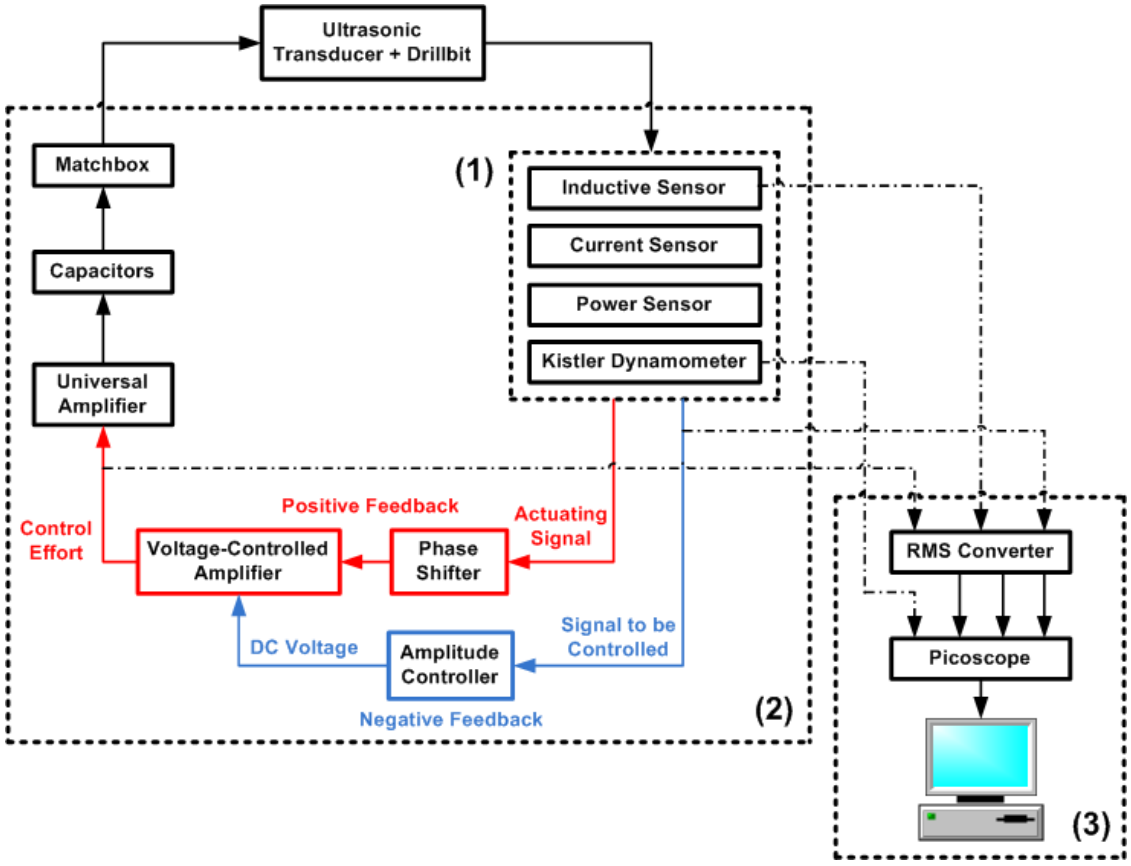

Figure 7.2 : Autoresonant control schematic diagram

Autoresonant control schematic diagram is illustrated in Figure 7.2. In order to explain the negative feedback loop and positive feedback loop in details, an autoresonant control block diagram has been drawn and shown in Figure 7.3. The working principles of positive feedback and negative feedback loop will be explained elaborately in the following sections.

An autoresonant control system consists of several performance sensors, a phase shifter, an amplitude controller, a voltage-controlled amplifier, a universal amplifier, a capacitors box and a universal matchbox. Now each of these components will be considered.

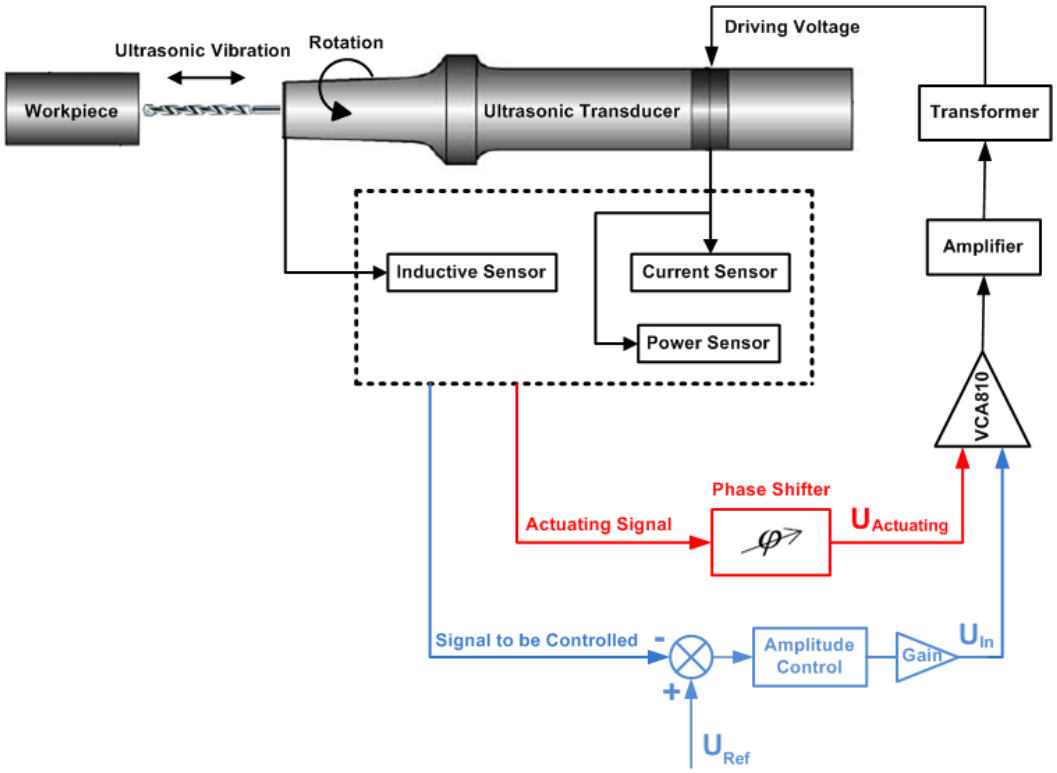

Figure 7.3 : Autoresonant control block diagram: for mechanical feedback, both actuating signal and signal to be controlled is the ultrasonic vibration; for current feedback, both actuating signal and signal to be controlled is the current; for power feedback, actuation signal is the current and signal to be controlled is the power

- **Performance Sensors (Box 1)**

There are 4 sensors used in the autoresonant control experiments, namely an inductive sensor, a current sensor, a power sensor and a Kistler dynamometer. Depending on the control strategy, different sensor signals are employed to form different feedback loops. Mechanical feedback uses the ultrasonic vibration of the 2-step transducer x_2 during Ultrasonically Assisted Drilling (UAD) process and considers it as both the 'actuating signal' and the 'signal to be controlled' (shown in Figure 7.2 and Figure 7.3). These 2 signals are to define the optimal phase shift and automatically adjust the supplied voltage u to the piezoelectric transducer. Both current feedback and power feedback employ the current signal as the 'actuating signal' in the positive feedback. However, power feedback adopts power as the 'signal to be controlled' to perform the negative feedback where current feedback still uses the current sensor's output to participate in the negative feedback. A Kistler dynamometer is used to measure the axial feed force during ultrasonic assisted drilling process.

Inductive Sensor

The structure of the inductive sensor designed and employed in the experiments can be found in Figure 7.4. Basically, it comprises a magnet which is bonded concentrically to a wooden frame with the same dimension that is wrapped around with coils. The centric hole diameter of the inductive sensor is slightly larger than the diameter of the 2nd step concentrator to allow reasonable clearances during measurements.

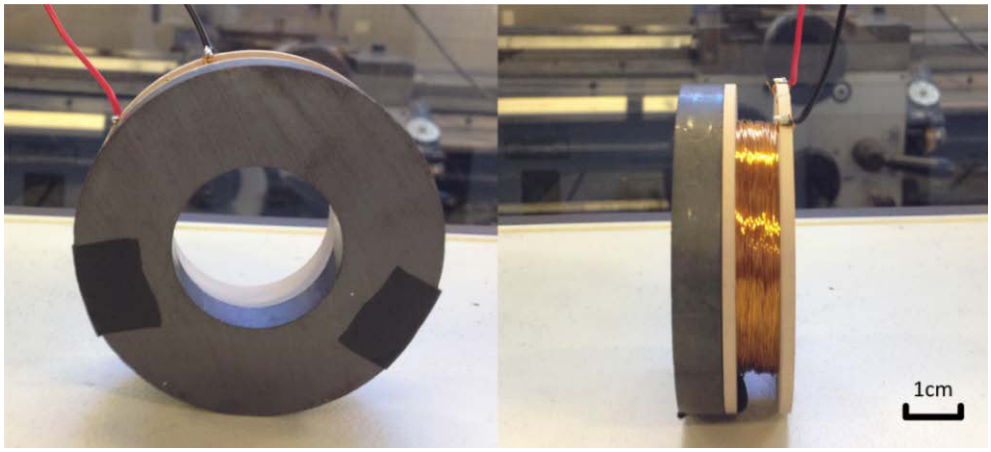

Figure 7.4 : Inductive sensor

When the ultrasonic vibrating system is activated, the grub screws (used to grip the drill bit) and the drill bit (high speed steel, cobalt material) vibrate longitudinally in the hole of the inductive sensor hence change the flux flowing through the magnet. As a result, the intense vibration generates a strong signal in the coil due to the presence of the magnetic field. In Figure 7.4, the red wire is the live terminal while black wire stands for earth. The value of the inductive sensor's inductance was measured by an 'Atlas LCR' meter as $13.24mH$.

In order to examine the reliability and accuracy of the inductive sensor, a calibration experiment has been performed. The experimental setup is shown in Figure 7.5. The inductive sensor was clamped firmly and located at the end of the 2nd step of the ultrasonic transducer. To compare with the signals captured by the inductive sensor, the laser vibrometer (Manufactured by Polytec, OFV512 + OFV 3001) was used as standard equipment. The procedure of the calibration is that the ultrasonic transducer was excited with a frequency generator (GW INSTEK SFG-2110 Synthesized Function Generator) and a range of frequency points near the resonance together with the ultrasonic vibration at the end of the 2nd step have been recorded for both sensors. Results are shown in Figure 7.6.

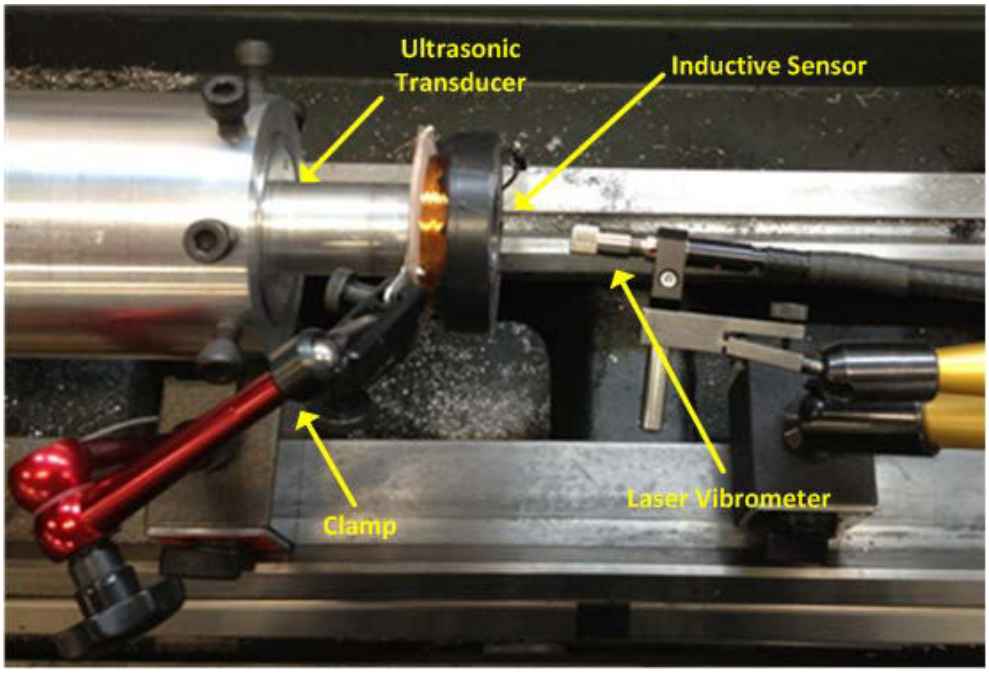

Figure 7.5 : Experimental setup for inductive sensor calibration

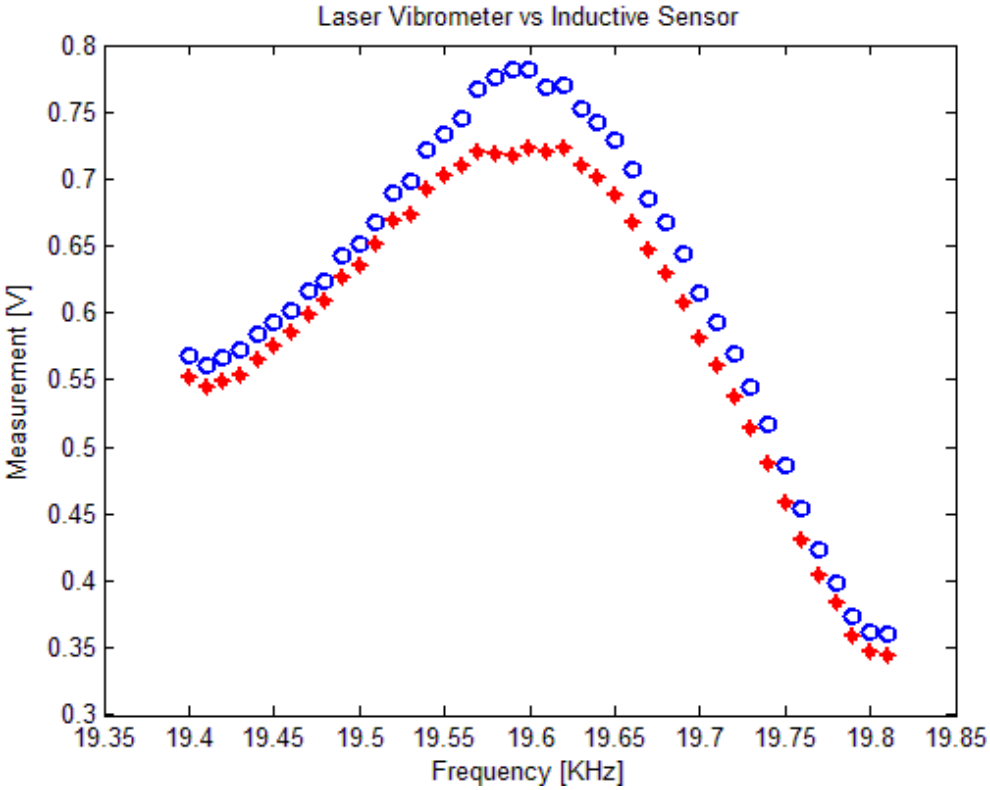

Figure 7.6 : Inductive sensor calibration

As can be seen, the blue circles curve represents the signal output of the laser vibrometer while the red stars curve shows the signal output of the inductive sensor. As can be seen, both curves exhibit a consistent trajectory except certain discrepancies near the resonance.

Therefore, such a high similarity suggests that the inductive sensor is a reliable device which can be a replacement of the laser vibrometer. The practical use of this inductive sensor has several advantages compared with laser vibrometer: First of all, its manufacturing cost is significantly lower than the laser vibrometer. In addition, for particular industrial application such as Ultrasonically Assisted Drilling (UAD), a laser vibrometer cannot be used due to the fact that the optical measurement requires a perfectly flat reflection surface which should be non-rotating in order to capture steady signals. Such requirement cannot be met when an ultrasonic transducer rotates. Alternatively, an inductive sensor can be simply placed around the ultrasonic transducer to capture signals from the magnetic field without any physical contact with the target objects. The inductive sensor signals are only related to the strength of the magnetic field created irrespective the geometries of the objects. Consequently, the development and calibration of such proximity sensor is prominent and useful.

Current Sensor

A Hall Effect current sensor (manufactured by LEM, Switzerland) [16] has been used in the experiments to measure the current signal flowing through the piezoelectric transducer. The current sensor is placed between the output of the universal matchbox (transformer) and the input to the ultrasonic transducer.

Power Sensor

A power sensor was manufactured for the Ultrasonically Assisted Drilling (UAD) experiments. The circuit diagram of the power sensor is illustrated in Figure 7.7. As can be seen, $'U'$ represents the supplied voltage signal measured by the differential probe. A $0.22\mu F$ capacitor has been placed afterwards in order to smooth the signal. A quad operational amplifier (LM348N, details in [79]) is employed with a negative feedback tuneable gain potential meter $50K\Omega$. It should be noted that the operational amplifier performs an inverting amplification. Theoretically, the positive terminal of an operational amplifier is connected directly to the earth potential during the inverting amplification. In Figure 7.8, however, 2 $1K\Omega$ resistors are added both for negative terminal and positive terminal to balance each other. A similar connection can be observed in the case of the current signal where the current amplification set uses a fixed $100K\Omega$ resistor as a gain.

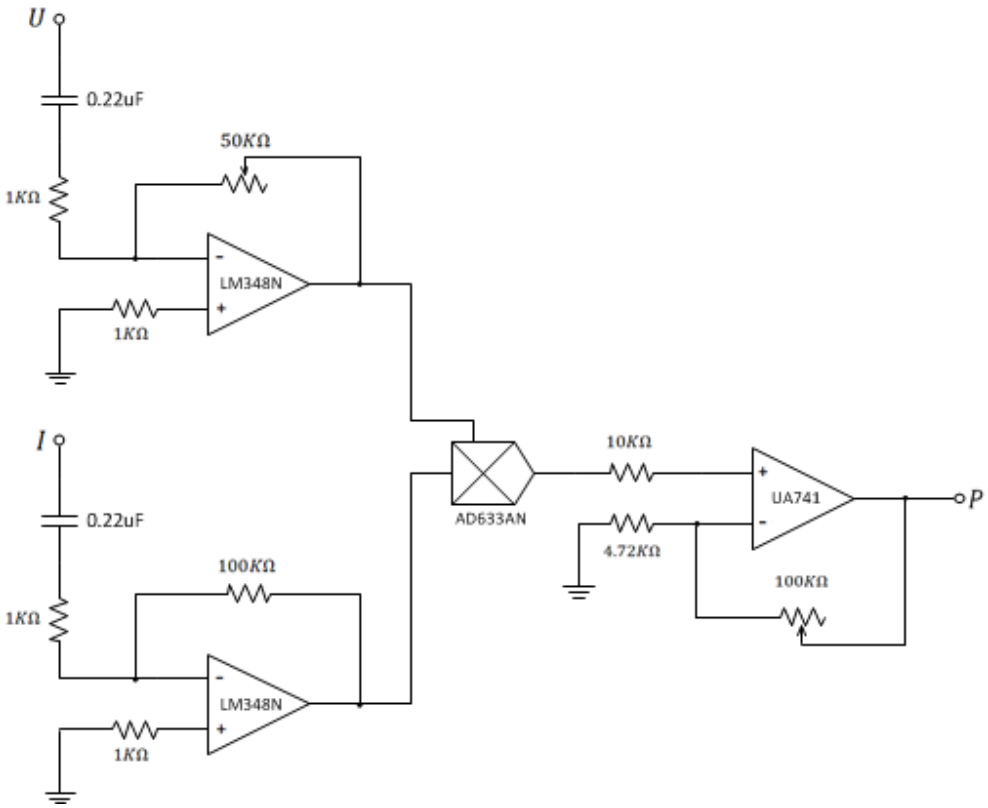

Figure 7.7 : Power sensor circuit diagram

After the voltage signal and the current signal are captured at a primary stage, they are supplied into a four-quadrant multiplication integrated circuit (AD633AN, details in [80]) to calculate the product. Once the product is obtained, the signal is supplied to the positive terminal of a secondary stage operational amplifier (UA741CN, details in [85]) through a $10K\Omega$ resistor. The negative terminal is connected to earth through a $4.72K\Omega$ resistance and the negative feedback is an adjustable $100K\Omega$ resistor. The UA741CN performs a non-inverting amplification as the amplifier's output signal is supposed to be a true scaled reflection of the instantaneous power. It should be addressed that 2 potential meters ($50K\Omega$ and $100K\Omega$) can be adjusted independently to obtain a desired level of the instantaneous power before machining. The rest of the selected resistor values are for the protection of the signals overloading.

Kistler Dynamometer

Figure 7.8 shows the structure of a two-component piezoelectric Kistler dynamometer (manufactured in Winterthur Switzerland, type 9271a, SN 40817). The dynamometer is able to measure simultaneously a force parallel to the transducer axis and a moment in the plane

normal to the line of application of the force. The electrical charges generated by the platform are strictly proportional to the applied loads to be measured; the charge amplifiers convert the dynamometer's outputs into analogue DC voltage signals to be recorded by a PicoScope and a computer. 2 signal ports are shown in Figure 7.8 and the resonant frequency of the dynamometer is about $4KHz$ in axial direction in practice for both ports. However, the charge amplifiers (KIAG SWISS Type:5001) used to amplify the low current signal generated by the inbuilt quartz in the dynamometer has a bandwidth $f_c = 100Hz$ which is too slow to follow the ultrasonic frequency during vibro-impact. Therefore, signal outputs of the charge amplifiers are calculated in average. During Ultrasonically Assisted Drilling (UAD), only axial force is recorded to identify steady thrust feeding force.

Figure 7.8 : Kistler dynamometer

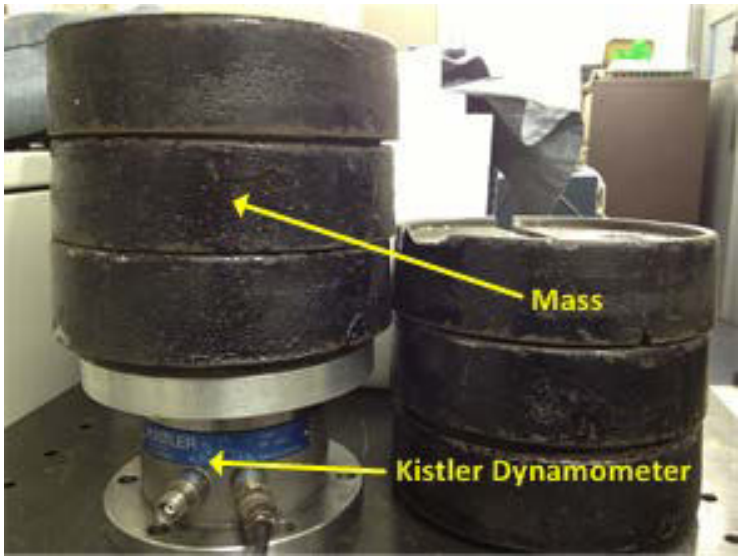

Figure 7.9 : Kistler dynamometer calibration experimental setup

Figure 7.9 illustrates the Kistler dynamometer's calibration experimental setup. There are 6 mass blocks and each of them weighs $5KG$. The Kistler dynamometer was placed on the ground with the axial force channel connected to a PicoScope for data recording. During calibration, each mass has been stacked up to the top of the Kistler dynamometer literally after the stabilization of the charge amplifier's output. Signals correspond to $[5KG, 10KG, 15KG, 20KG, 25KG, 30KG]$ have been recorded subsequently.

Figure 7.10 demonstrates the Kistler dynamometer calibration with 4 amplification gains $[100, 200, 500, 1000]$ which are tunable on the charge amplifier's channel. As can be observed, the charge amplifier's outputs present a clear linearity regardless of varying the gains or the weights. The amplification gain 100 has been used to record the axial feed force during drilling. The sensitivity of the gain 100 can be calculated according to the blue circles as $33N/V$.

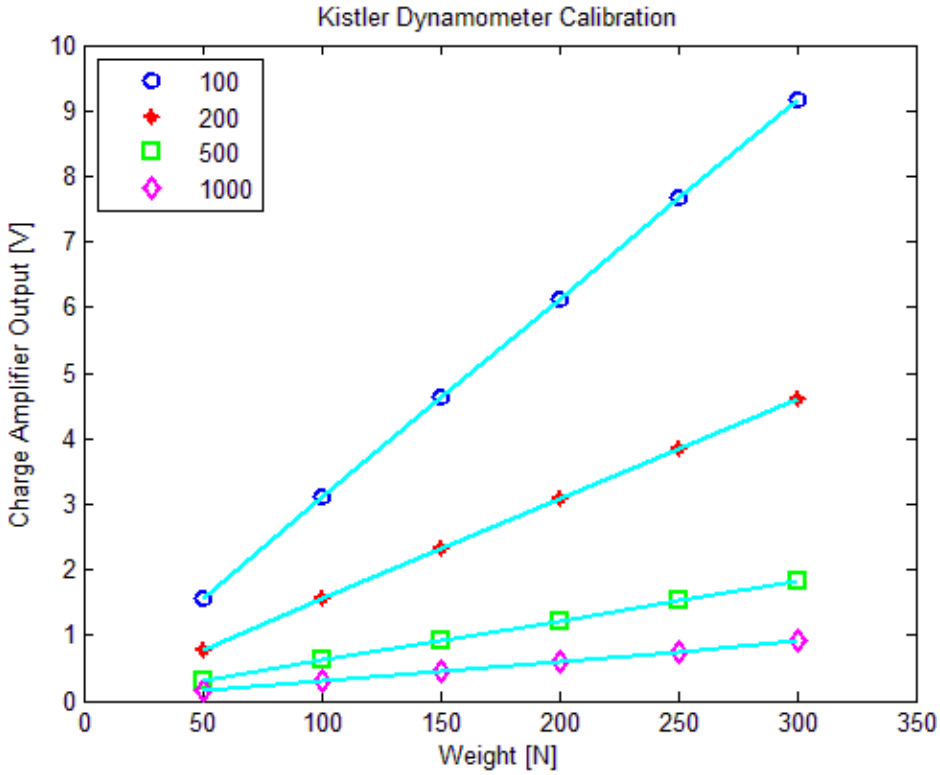

Figure 7.10 : Kistler dynamometer calibration

- **Universal Amplifier**

A 200W MOSFET (Metal-Oxide-Semiconductor Field-Effect Transistors) universal amplifier (Model No MF200 manufactured and supplied from B.K. Electronics) [71] shown

in Figure 7.11 was placed after the voltage-controlled amplifier. For both the frequency controlled ultrasonic vibrating system and the autoresonant control feedback, the universal amplifier is an indispensable element to amplify the signal at a primary stage. The gain of the universal amplifier has been experimentally found as 65 and its signal linear operational zone is $\pm 70V$. Any output exceeds this interval will be truncated and thus affect the signal waveform. However, reasonable overload in the universal amplifier has been observed during experiments.

Figure 7.11 : 200W MOSFET amplifier

- **Capacitors**

Between the universal amplifier and the universal matchbox (transformer), an additional box that consists of two capacitors of $16\mu F$ connected in parallel has been placed. Generally speaking, the transformer in the universal matchbox desires to work with pure AC signals because DC signals might produce a constant current flow which generates an electrical field thus influence the ultrasonic vibrating system. Moreover, DC signals can also produce heat. Therefore, the capacitor box is employed to eliminate DC signals in the transformer. More importantly, it can purify the universal amplifier's output signal.

- **Universal Matchbox**

A matchbox is used to adjust a low voltage and high current signal of the universal amplifier to a high voltage and low current signal to the ultrasonic transducer. This process is achieved by a transformer consisting of an input coil set and an output coil set inside the matchbox shown in Figure 7.12. The detailed connections of input and output of the universal matchbox can be found in Appendix I. The model number of the matchbox used in this project is EVB-

2 supplied by FFR Ultrasonics [68]. It should be noted that an additional component marked as 'compensating coil' wound around a vertical ferrite core has been designed with a value of $100\mu H$ in order to shunt the ultrasonic transducer's capacitance. In a better interpretation, the 2-step ultrasonic transducer acts as a capacitor with a value $8.16nF$ measuredby an 'Atlas LCR' meter. To achieve maximum energy propagation, the compensating coil is used to form an LC circuit with the ultrasonic transducer.

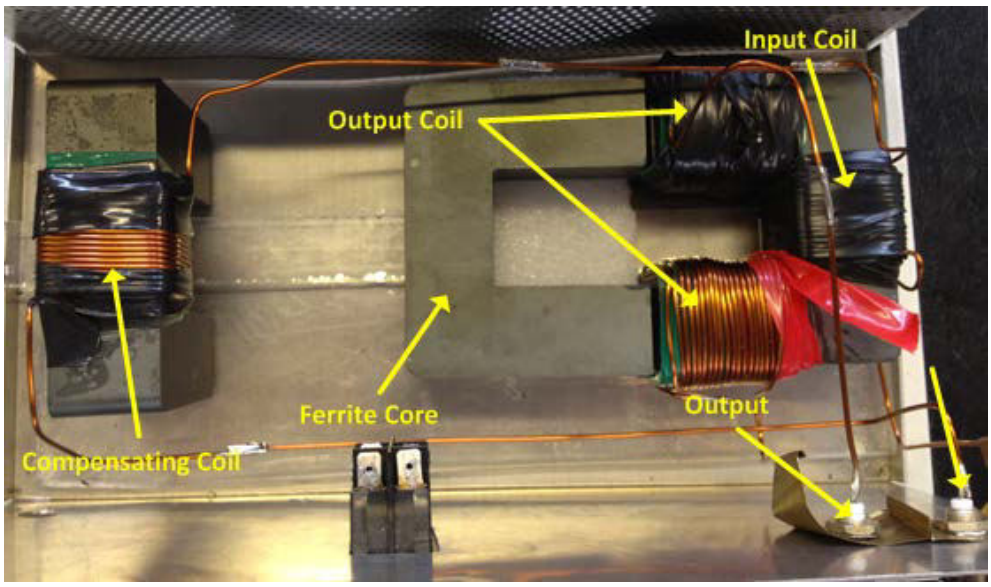

Figure 7.12 : Universal matchbox components

A piece of 'U' shape ferrite core has been placed in the matchbox to generate a magnetic field shown in Figure 7.12. The other ferrite core is wound with input and output coils. Measurements of the inductance of the input port and output port indicate a considerable change when shifting the position the core. When the cores are closely attached, the input inductance is $357\mu H$ and the output inductance is $17.25mH$. However, an input inductance $85\mu H$ and output inductance $1.96mH$ has been recorded when a gap occurs between the cores and the transformer set as a result of the flux change in the magnetic field. This phenomenal change in the inductance for both ports affected the voltage level significantly during experiments. As a result, the ultrasonic vibration level of the ultrasonic transducer was influenced drastically too. Consequently, the position of the core seems essential to determine the ultrasonic vibration and therefore needs to be appropriately and precisely calibrated. The detailed analysis and optimization of the matchbox ferrite cores are introduced in Appendix I.

- **Phase Shifter**

The phase shifter is designed to provide a full circle (360°) phase shift within the resonant frequency range $15KHz \sim 25KHz$ of the ultrasonic transducer using both manual and remote control [16]. As can be seen in Figure 7.13, the knob can be adjusted in order to bring the ultrasonic vibrating system to the resonance. There is a switch that allows the gain settings to be either 1 or 10 to inject more power into the universal matchbox (transformer). As observed during experiments, however, a gain setting 10 will normally cause output signal overloading. The gain of the phase shifter is frequency dependent, therefore the phase shifter has been put before the voltage-controlled amplifier (shown in Figure 7.2 and Figure 7.3) to limit the signal level [16]. At the back face of the phase shifter, another port is available to perform the automatic phase shift controlled by a DC signal. In this project, however, the phase shifter is operated manually. In other words, once the knob is adjusted to bring the ultrasonic vibrating system to a desired resonant regime, it remains unchanged during machining.

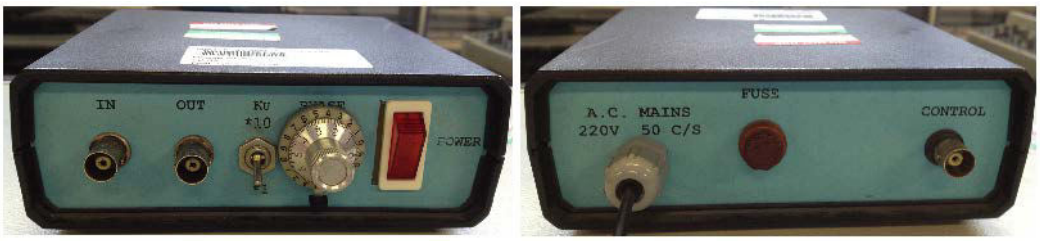

Figure 7.13 : Phase shifter

As explained before that the phase-amplitude characteristic of the ultrasonic vibrating system presents a bell shape which implies little effect imposed on the phase controlled ultrasonic vibrating system even though the resonant frequency will be shifted when the machining condition changes. An essential drop of the ultrasonic vibration level due to the harsh machining process can be tackled by an amplitude controller in combination with a voltage-controlled amplifier. Observations on the frequency shift of the ultrasonic transducers when the vibro-impact happens during experiments show a less than $0.2KHz$ value. This slight resonant frequency shift indicates little change in the phase-amplitude characteristics.

- **Amplitude Controller**

An amplitude controller is employed to generate a DC control voltage signal for the voltage-controlled amplifier. Compared with the phase shifter, the amplitude controller plays a role in supplying more power against the change in the 'signal to be controlled' measured by a performance sensor. The amplitude controller circuits are shown in Figure 7.14. 'Signal to be controlled' can be the 2nd step ultrasonic vibration x_2, the current i or the power P. The detailed working principle of the amplitude controller circuit is described below.

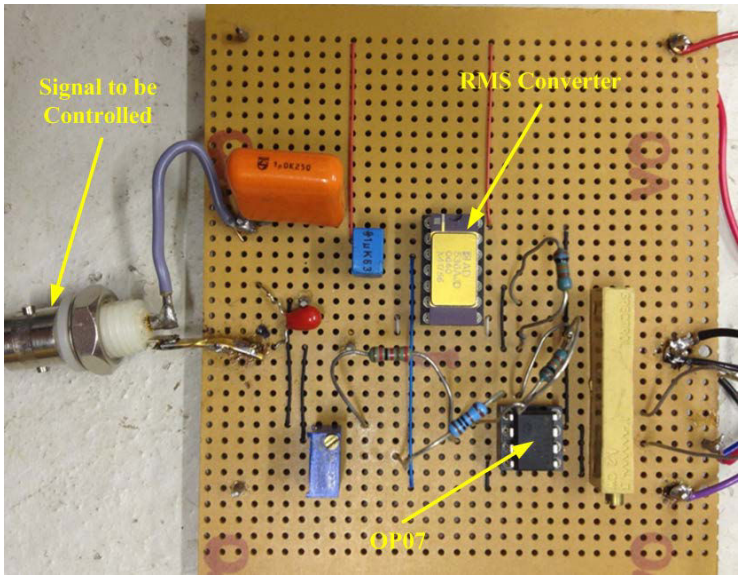

Figure 7.14 : Amplitude controller

Figure 7.15 illustrates the amplitude controller circuits' components. In the beginning, the True RMS-to-DC converter (AD536ADJ details in [72]) collects the performance sensors' samples marked as 'U_{Sensor}' which is the 2nd step ultrasonic vibration, the current or the instantaneous power depending on the feedback type. After this, a $12K\Omega$ resistor is placed in case of signal overload. The true RMS value of the sensor signal is further compared with a DC voltage determined by a potential meter $50K\Omega$ which is placed between a $12V$ power supply and the earth potential. During operation, the potential meter $50K\Omega$ is adjusted to ensure a similar signal level between the negative terminal and the positive terminal. The difference is further amplified by an OP07 (details in [73]) offset amplifier. A $50K\Omega$ potential meter has been connected in the negative feedback loop of the OP07 amplifier which is adjustable to determine the negative feedback loop gain. Subsequently, a DC voltage is generated marked as 'U_{DC}'. Theoretically, during vibro-impact process the sensor signal

will drop due to energy loss on the tip of a drill bit. This drop will give rise to a decrease at the positive terminal of the offset amplifier OP07. Hence, a negative difference value will be produced which is amplified by the adjustable potential meter $50K\Omega$ in order to bring the $'U_{DC}'$ to the operational zone for the voltage-controlled amplifier further on (the voltage-controlled amplifier will be introduced next).

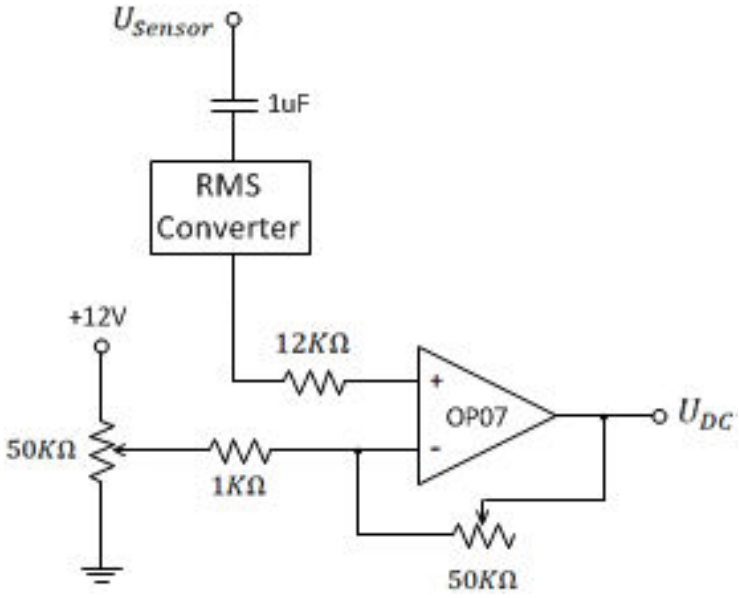

Figure 7.15 : Amplitude controller circuits diagram

- **Voltage-Controlled Amplifier**

In order to implement the negative feedback loop, a voltage-controlled amplifier (VCA810 details in [74]) has been placed after the phase shifter. The structure of the voltage-controlled amplifier circuit is shown in Figure 7.16 and the detailed connection of the components is illustrated in Figure 7.17.

As can be seen, the input to the voltage-controlled amplifier is an AC actuating signal which is the output of the phase shifter. Depending on the feedback type, the actuating signal could be the 2nd step ultrasonic vibration measured by the inductive sensor during mechanical feedback control, the current flowing through the piezoelectric transducer measured by the current sensor during current feedback control and during power feedback control. A $10K\Omega$ potential meter (normally not used or tuned to be $0K\Omega$) has been put after the actuating signal in case of signal overloading. The control input to the voltage-controlled amplifier is the DC voltage signal generated by the amplitude controller marked as 'U_{DC}'.

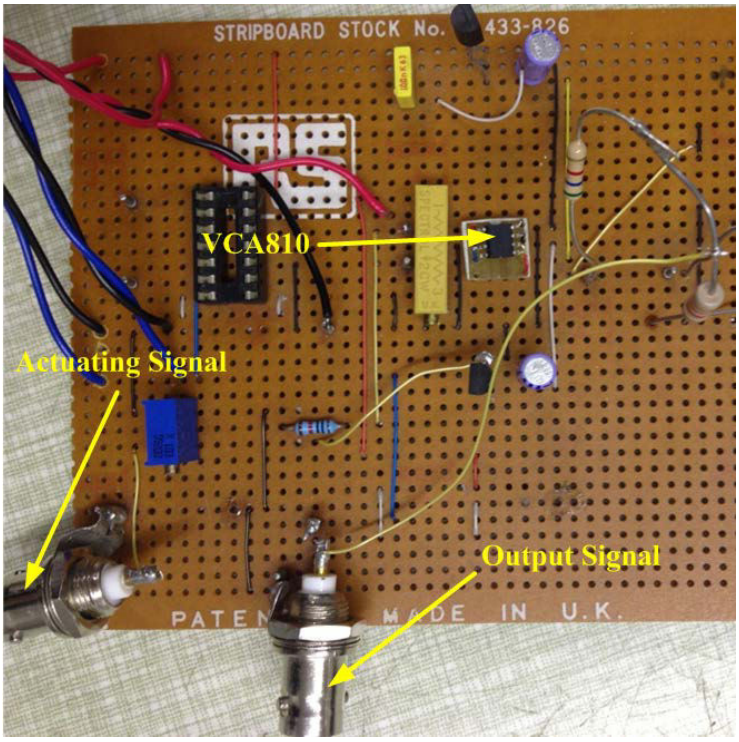

Figure 7.16 : Voltage-controlled amplifier

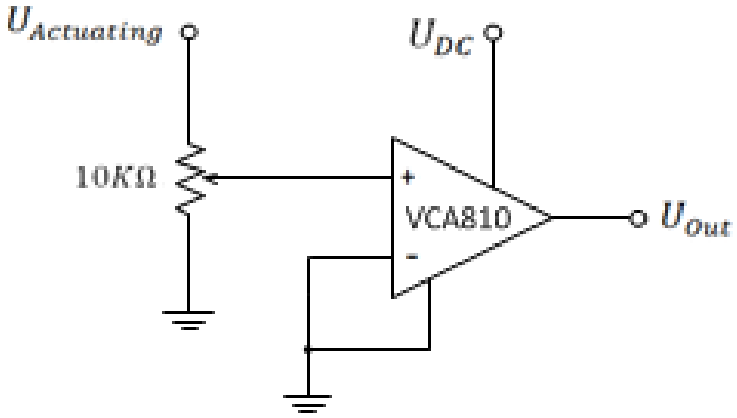

Figure 7.17 : Voltage-controlled amplifier circuit diagram

The main improvement of the autoresonant control on Ultrasonically Assisted Drilling (UAD) in comparison with the previous autoresonant control on Ultrasonically Assisted Turning (UAT) is the replacement of the limiter with a DC-coupled, wideband, continuously variable, voltage-controlled gain amplifier VCA810. The application of the VCA810 not only gets rid of the use of either a low-pass filter or a Butterworth filter to recreate a sine wave supplied voltage signal base on a square wave produced by the limiter, but also reduces the strong nonlinearity caused by the limiter. Basically, the operational range of the VCA810 is between $-40dB \sim 40dB$ with a control voltage varying from $0V$ to $-2V$ (U_{DC}). Within this

range, VCA810 is able to attenuate or amplify a sine wave without breaching its original waveform.

Being different from the autoresonant control principle described in section 5.1 (numerical simulations), the experiments employ the phase shifter, the amplitude controller and the voltage-controlled amplifier simultaneously and process them in real time. It should be re-emphasized that the phase shifter is an essential element in positive feedback loop for autoresonant control and the amplitude controller acts in the negative feedback loop which is an element for additional power injection during harsh machining conditions.

7.2.2 Data Recording Units (Box 3)

There are 3 components used to record and process the data of the autoresonant controlled ultrasonic vibrating system which are the True RMS-to-DC converters (AD536ADJ details in [72]), a 4-channel PicoScope and a computer. Each of them will be introduced below.

In Figure 7.18 the True RMS-to-DC converter circuit is shown. The input to the circuit is the AC signal to be observed. The RMS converter collects samples and calculates the DC level RMS value which is transferred to the output port. In order to understand the detailed connections in the circuit board, the electrical diagram is drawn and presented in Figure 7.19.

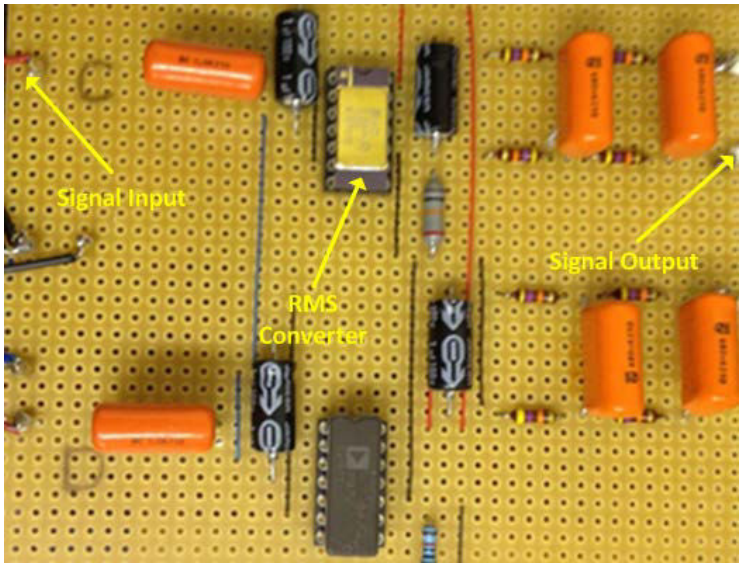

Figure 7.18 : True RMS Converter circuit

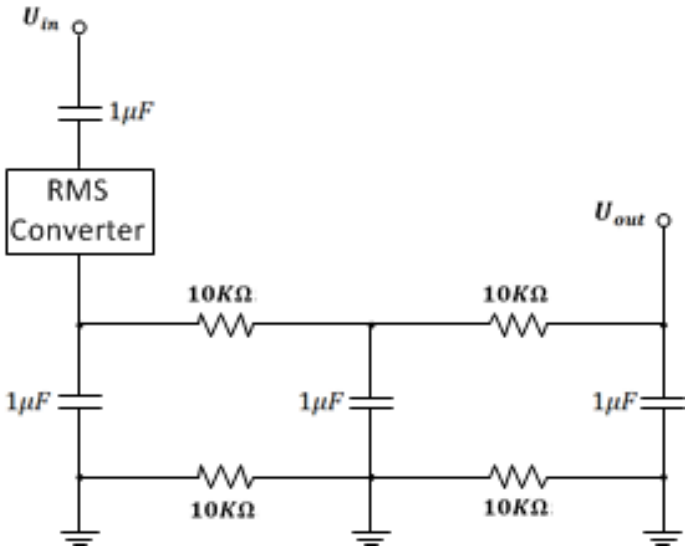

Figure 7.19 : True RMS Converter circuit diagram

The input 'U_{in}'to the RMS converter is the AC signal to be observed. In this project, several sensor signals are monitored simultaneously depending on the feedback type which might be the inductive sensor's output (the 2nd step ultrasonic vibration x_2), the 'signal to be controlled' (the signal used to determine the required amount of effort for the ultrasonic vibrating system) and the voltage-controlled amplifier's output (the universal amplifier's input, actual original driving signal of the ultrasonic transducer) as shown in Figure 7.2 and Figure 7.3. A $1\mu F$ capacitor has been put after the input AC signals to smooth them and eliminate the DC components. In order to filter the unwanted high frequency noises, 2 RC circuits (resistance $10K\Omega$ and capacitance $1\mu F$) [76] have been employed before the pure DC RMS signal 'U_{out}' is recorded. It should be noted that a same set of RC filters are connected to earth potential. The reason for this is the rotational motion of the ultrasonic transducer and the high power voltage inverter used to drive the lathe had a great impact on the signal recording during experiments. Such effect results in a non-zero value in the earth potential. This is likely caused by the high frequency components and therefore low pass filters are used to ensure a zero signal level in the earth potential. There are 4 sets of RMS converters available in the experiments.

In order to record the RMS signals produced by the True RMS-to-DC converters, a 4-channel PicoScope (PicoScope 4424 with a bandwidth $20MHz$, details in [82]) was used. The PicoScope is connected to a TOSHIBA laptop to process the RMS signals for further

analysis. The PicoScope allows maximum 4 signals to be monitored and recorded simultaneously during experiments.

7.3 Autoresonant Control Analysis for Different Strategies and Drill Bits

In this section, fixed frequency control, mechanical feedback, current feedback and power feedback on 2 sizes of drill bits with a fixed rotational speed of the spindle in combination with several feed rates are examined. The listed control strategies are applied on 2 sizes of drill bits which are 3mm and 6mm in diameter. As explained in [15], only in drilling small holes with diameters smaller than 3mm a drill bit can be treated as a small lamp mass attached to the ultrasonic transducer. In contrast, with an increase in diameters of holes a successful application of the Ultrasonically Assisted Drilling (UAD) needs acoustical matching of the drill bit as a continuous system with a transducer. Therefore, a drill bit greater than 3mm in diameter with a reasonable length, complicated geometry and dynamics should be treated as an additional step of waveguide (concentrator).

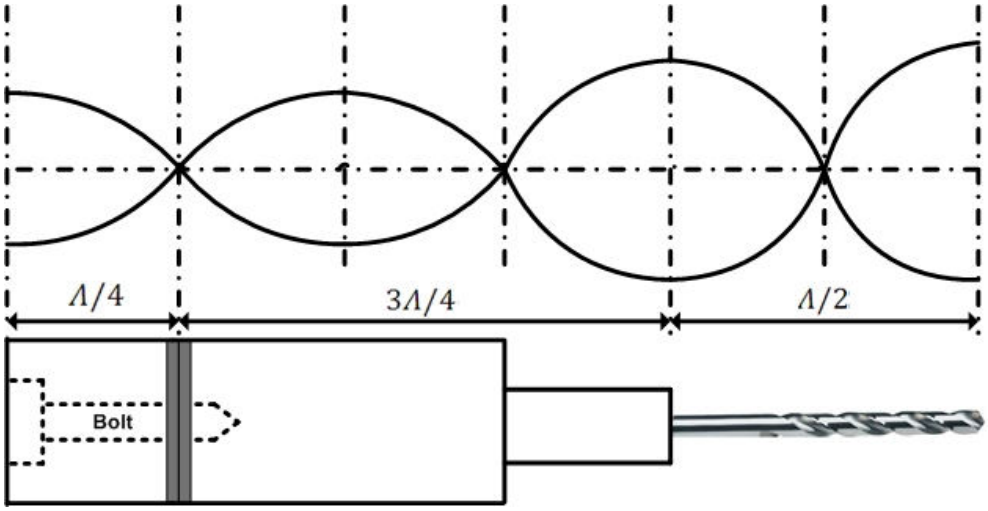

Figure 7.20 : Properly adjusted ultrasonic vibrating system waveform

Figure 7.20 illustrates an ideal situation of a possible waveform of a properly tuned 2-step ultrasonic transducer with a drill bit during resonance. It has been experimentally proved that at the end of 2nd step concentrator the ultrasonic vibration achieves a maximal without a drill bit attached. However, a drill bit attachment requires a proper acoustic matching with the ultrasonic transducer in order to ensure the additional step (drill bit) as a continuation of the original vibrating system. Due to the material and geometry difference, such waveform

shown in Figure 7.20 is difficult to be achieved which has been confirmed experimentally. On the other hand, however, the 2nd step ultrasonic vibration is physically in relation with the ultrasonic vibration magnitude on the tip of a drill bit. Therefore, owing to the unavailable information of the ultrasonic vibration on the tip of a drill bit during machining, the ultrasonic vibration at the end of the 2nd step concentrator x_2 has been selected as the observation point for the ultrasonic vibration.

7.3.1 A 3mm Diameter Standard Drill Bit

During the Ultrasonically Assisted Drilling (UAD) process, a 3mm diameter HSS-Co 8% tin coated heavy duty jobber drill bit was used. Point angle of the 3mm drill bit is $135°$ and helix angle is $28°$. The overall length is 61mm and flute length is 33mm with weight 28 grams. 4 grub screws were used to clamp a 3mm drill bit at the end of the 2nd step concentrator x_2 uniformly and tightly from 4 directions. The entire ultrasonic vibrating system was properly centred with the help of a centring gauge. Such a 3mm drill bit needs no proper tuning since it can be treated as a small mass. The rotational speed of the spindle for the application of the 3mm drill bit was fixed as 40rev/min. 3 feed rates 0.03mm/rev, 0.06mm/rev and 0.09mm/rev were applied. Experimental setup of a 3mm drill bit application during the autoresonant control is shown in Figure 1.1.

7.3.1.1 Frequency Control

In frequency control, a SFG-2110 synthesized function generator was used to generate an actuating sinusoidal signal with a resonant frequency and proper amplitude which is supplied to the universal amplifier and the universal matchbox (transformer) to drive the ultrasonic vibrating system. During the Ultrasonically Assisted Drilling (UAD), RMS of the 2nd step ultrasonic vibration x_2 was measured by an inductive sensor because the information of the ultrasonic vibration is unavailable on the tip of a 3mm drill bit. Meanwhile, the RMS of the control effort which is the actual original driving signal of the universal amplifier is recorded. As introduced before that the linear operational interval of universal amplifier is $\pm 70V$ with a gain 65 which corresponds to a RMS $0.76V$, any amplitude greater than this will be truncated. However, certain reasonable overloading is necessary for high feed rate. Results of the frequency control are illustrated in Figure 7.21.

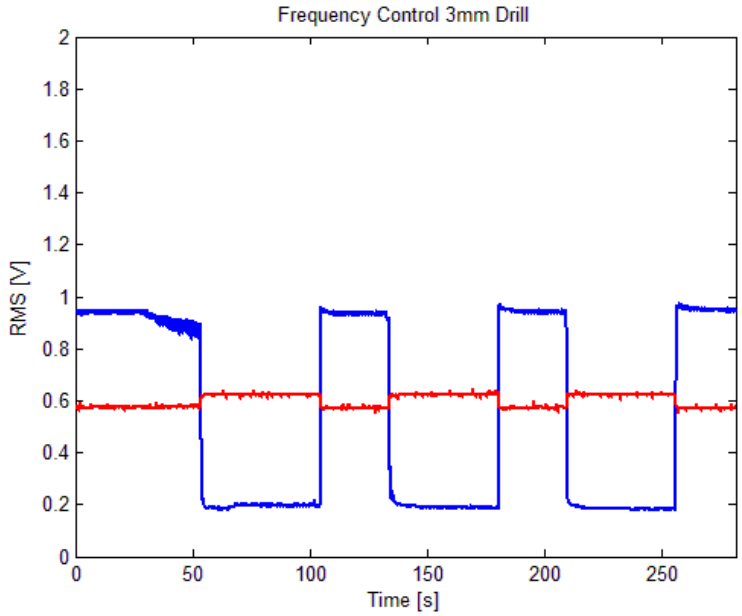

Figure 7.21 : Frequency controlled 2nd step ultrasonic vibration and control effort

As can be seen, a RMS $0.6V$ and $18.76KHz$ actuating signal (red curve, also the control effort) produced a RMS $0.95V$ of an ultrasonic vibration signal at the end of the 2nd step concentrator (blue curve) in idle condition (no applied load). According to the inductive sensor calibration shown in Figure 7.6, the frequency driven ultrasonic transducer has a nearly $6.5\mu m$ vibration amplitude zero-to-peak at the end of the 2nd step concentrator with the attachment of a 3mm drill bit.

In the beginning, the ultrasonic vibration was activated and the ultrasonic transducer ran up to 30sec without contact with the work piece. Since then, the initial contact started with a feed rate 0.03mm/rev and a rotation 40rev/min rotation. The frequency control was able to deal with the vibro-impact process to 50sec before the tip of the 3mm drill bit was completely engaged into the aluminium work piece. After that RMS of the 2nd step ultrasonic vibration dropped to an insignificant level $0.2V$ and thus led to a failure of control. The drill bit and aluminium work piece were separated at 105sec and then the 2nd step ultrasonic vibration x_2 retrieved itself. 2 other higher feed rates 0.06mm/rev and 0.09mm/rev have been applied which happened at 135sec and 210sec, both feed rates caused the RMS of the 2nd step ultrasonic vibration signal x_2 decreased to a similar low level as the case of 0.03mm/rev and therefore control failed. For 3 feed rates, control effort hardly changed. Due to the fact that the 2nd step ultrasonic vibration x_2 dropped significantly during the contact with the

aluminium work piece, the ultrasonic vibrating system lost its benefits hence no obvious feed force reduction was observed.

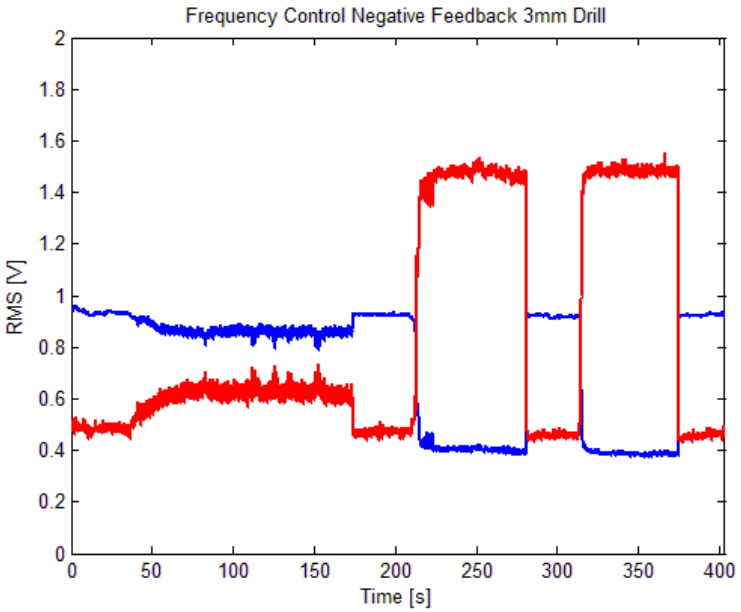

Figure 7.22 : Frequency control in association with amplitude control 2nd step ultrasonic vibration and control effort

In order to explore whether the 2nd step ultrasonic vibration can be maintained with the help of the amplitude control system, negative feedback loop shown in Figure 7.2 and Figure 7.3 has been connected to the frequency controlled ultrasonic vibrating system. During this process, the function generator's output signal with a pre-defined frequency acts as the 'actuating signal' and the inductive sensor's output (the RMS of the 2nd step ultrasonic vibration) is the 'signal to be controlled'. The phase shifter was removed from the loop and the output of the voltage-controlled amplifier is supplied to the universal amplifier to drive the ultrasonic vibrating system. Results are shown in Figure 7.22.

As can be seen in Figure 7.22, the initial contact between the 3mm drill bit and the work piece took place at 40sec with a rotation 40rev/min and a feed rate 0.03mm/rev. RMS of the 2nd step ultrasonic vibration x_2 dropped moderately and the RMS of the control effort increased against the drop in the 2nd step ultrasonic vibration x_2. This process implies a fast and accurate working principle of the negative feedback control loop which is to compensate the decrease in the RMS of the 2nd step ultrasonic vibration signal. The drill bit and the work piece were separated at 175sec. Feed rates 0.06mm/rev and 0.09mm/rev were applied at

210sec and 315sec. As a result, RMS of the 2nd step ultrasonic vibration decreased to $0.4V$ and RMS of the control effort increased considerably to $1.5V$ for both feed rates which completely exceeded the linear operational region of the universal amplifier. Drilling depths for three feed rates were 2.7mm, 2.8mm and 3.6mm.

In comparison with the frequency control, the ultrasonic vibrating system with the help of the amplitude control system was able to deal with a low feed rate 0.03mm/rev. However, for high feed rates 0.06mm/rev and 0.09mm/rev, the 2nd step ultrasonic vibration x_2 decreased considerably even if the amplitude control system generated enormous voltage for the ultrasonic transducer to compensate for the change in the sensor signal. The remarkable drop in the inductive sensor's signal for high feed rate can be attributed to the high Q factor of the ultrasonic vibrating system attached with a 3mm drill bit. A high feed rate driven ultrasonic vibrating system had a larger resonant frequency shift in the frequency-amplitude characteristic which consequently caused the ultrasonic vibration magnitude x_2 decreased to a low level. Nonetheless, the stable RMS of the 2nd step ultrasonic vibration with the help of amplitude control system for 0.06mm/rev and 0.09mm/rev feed rates showed a $0.4V$ value as a result of tremendously increased voltage supply. However, since the RMS of the control efforts completely exceeded the linear operational zone of the universal amplifier for high feed rates, RMS of the 2nd step ultrasonic vibration would not increase over $0.4V$. In contrast, as shown in Figure 7.21, high feed rates resulted in a $0.2V$ stable RMS of the 2nd step ultrasonic vibration without the amplitude control participation.

In order to verify the existence of the ultrasonic vibration on the tip of the 3mm drill bit during drilling, feed force measurement has been recorded by the Kistler dynamometer. Results are shown in Figure 7.23. The initial contact between the 3mm drill bit and the work piece happened at 30sec. Due to the participation of the amplitude control, Ultrasonically Assisted Drilling (UAD) lasted for 65secs with a spindle rotation 40 rev/min and a feed rate 0.03mm/rev. Thrust force during this process is less than $5N$. At 95sec, both the frequency generator and the control system were switched off and the ultrasonic vibration disappeared. The steady feed force turned into nearly $25N$ as a result of the Conventional Drilling (CD) domination. The control system was turned on after the separation of the drill bit and the work piece and higher feed rates 0.06mm/rev and 0.09mm/rev were applied at 185sec and 340sec. After the Kistler dynamometer's output signal became stable, the control system was

turned off. As a result, the thrust drilling force immediately climbed up to a higher level. The steady feed force of the Ultrasonically Assisted Drilling (UAD) for 0.06mm/rev was $40N$ and for 0.09mm/rev was $75N$. In contrast, $50N$ amd $105N$ feed forces were detected for both feed rates when the Conventional Drilling (CD) took place.

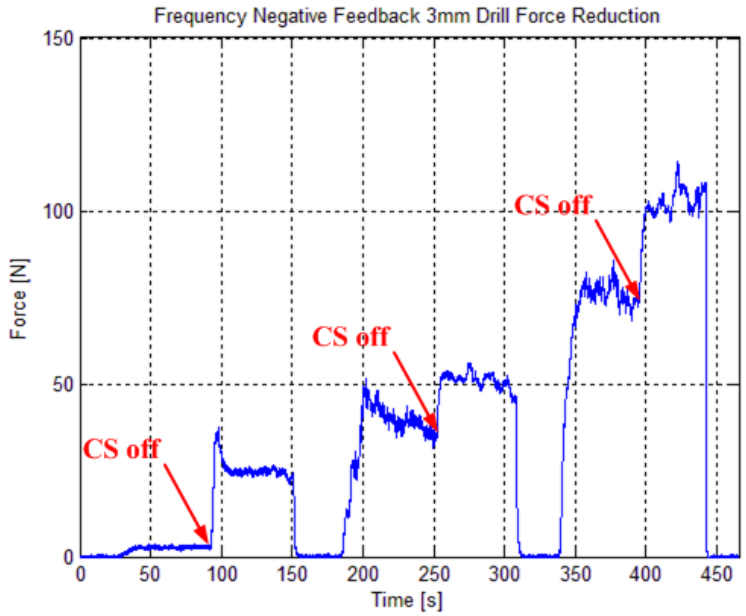

Figure 7.23 : Frequency control with amplitude control feed force versus Conventional Drilling (CD)

According to the feed force recording shown in Figure 7.23, results appeared to correspond to the 2nd step ultrasonic vibration x_2 information shown in Figure 7.22. For the feed rate 0.03mm/rev, the amplitude control system was able to maintain the 2nd step ultrasonic vibration x_2 at a desired level (even though a moderate drop was witnessed) which gave rise to a considerable force reduction compared with the Conventional Drilling (CD). For feed rates 0.06mm/rev and 0.09mm/rev, the amplitude control system produces tremendous voltage for the universal amplifier to compensate for the change in RMS of the 2nd step ultrasonic vibration x_2 despite it dropped to $0.4V$. As a result, certain reasonable force reductions were obtained in comparison with the Conventional Drilling (CD). Moreover, RMS level of the 2nd step ultrasonic vibration x_2 seems to be corresponding to the force reduction which is a direct reflection of the ultrasonic vibration information on the tip of the 3mm drill bit. Therefore, the assumption that the 2nd step ultrasonic vibration x_2 is proportional to the 3mm drill bit tip ultrasonic vibration holds up. Therefore, the 2nd step ultrasonic vibration x_2 can be chosen as an observation point.

7.3.1.2 Mechanical Feedback

Mechanical feedback employs the actual ultrasonic vibration of the 2nd step x_2 measured by an inductive sensor as both the 'actuating signal' and the 'signal to be controlled' as indicated in Figure 7.2 and Figure 7.3. The aim of this strategy is to maintain the ultrasonic vibration on the tip of the 3mm drill bit at a constant during drilling. This is done through keeping the 2nd step ultrasonic vibration x_2 stable based on the assumption that it is in proportion with the ultrasonic vibration on the tip of the 3mm drill bit. Since the mechanical feedback measures and controls the mechanical vibration directly, it is supposed to have the overall best results. The operational procedure of mechanical feedback control is that the phase shifter was manually adjusted in order to bring the RMS of the 2nd step ultrasonic vibration x_2 to the resonance. After this the potential meter '$50K\Omega$' shown in Figure 7.15 connected between the negative port of offset amplifier OP07 and output 'U_{DC}' was tuned to the maximum in order to allow the negative feedback to have the maximum gain. Then the potential meter marked as '$50K\Omega$' connected between the $12V$ and the earth was tuned until both the outputs of the voltage-controlled amplifier (control effort) and the inductive sensor's output presented a reasonable peak value. During drilling, the phase shifter and each element in the negative feedback were fixed. Results of the mechanical feedback are shown in Figure 7.24.

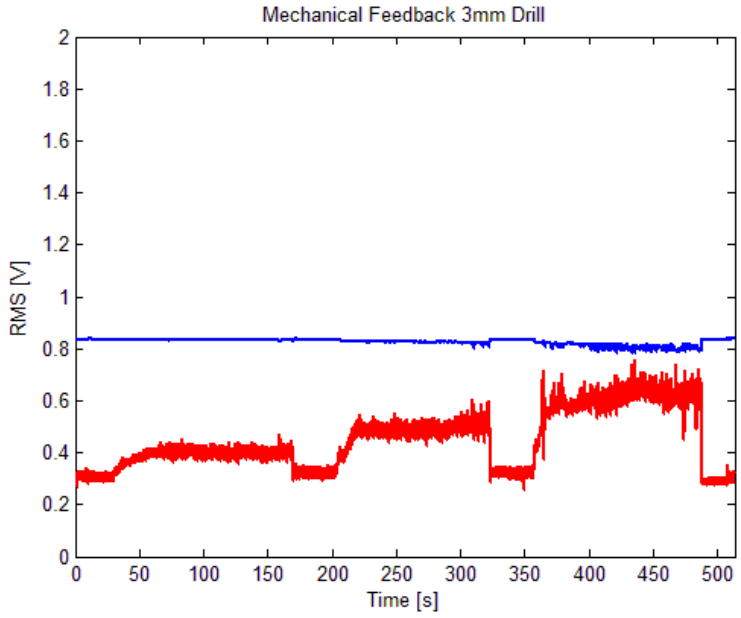

Figure 7.24 : Mechanical feedback controlled 2nd step ultrasonic vibration and control effort

The red curve represents the RMS of the control effort and the blue line is the RMS of the 2nd step ultrasonic vibration x_2. An ultrasonic vibration level $0.85V$ was obtained with a RMS of

the control effort $0.3V$. As can be seen, the initial contact between the drill bit and the work piece happened at 30sec with a 0.03mm/rev feed rate and a 40rev/min rotation. As the drill bit was engaged deeper into the material, the ultrasonic vibrating system required more power to deal with the energy loss on the 3mm drill bit tip. RMS of the control effort increased from $0.3V$ to more than $0.4V$. Meanwhile, RMS of the 2nd step ultrasonic vibration x_2 was maintained at a constant level. At 170sec, the drill bit and the work piece were separated with a recovery of both RMS in the 2nd step ultrasonic vibration x_2 and RMS in the control effort. At 205sec, a higher feed rate 0.06mm/rev was applied. The Ultrasonically Assisted Drilling (UAD) process lasted for 120secs with the control effort increased from $0.3V$ to more than $0.5V$ which is twice as high as of the previous feed rate. RMS of the 2nd step ultrasonic vibration slightly decreased as the drill bit penetrated deeper into the work piece but still can be kept at a desired level. The drill bit was removed from the work piece at 325sec. 0.09mm/rev feed rate was applied at 360sec. For this feed rate, the 2nd step ultrasonic vibration x_2 could still be maintained even if a more obvious drop was witnessed when the drill bit was deeply engaged. RMS of the control effort increased from $0.3V$ to nearly $0.7V$. For all 3 feed rates, the control effort climbed up gradually against the change in the inductive sensor signals and as the feed rate increased, the control effort showed a proportional trend as the change in the RMS of the 2nd step ultrasonic vibration x_2 which seemed to drop proportionally. It should be emphasized that the resonant frequency has been monitored; the maximal change in the resonant frequency was no more than $0.2KHz$ which hardly altered the phase in the phase-amplitude characteristic of the ultrasonic vibrating system. Drilling depths for three feed rates were 2.8mm, 4.8mm and 7.8mm.

In order to examine the existence of the ultrasonic vibration on the tip of the 3mm drill bit, feed force was monitored during drilling and results are shown in Figure 7.25. The initial contact with a 0.03mm/rev feed rate and a 40rev/min rotation happened at 15sec with the mechanical feedback control and the Ultrasonically Assisted Drilling (UAD) process lasted for 65secs until the feed force stabilised. The thrust force level during this period was low. At 80sec, the mechanical feedback control system was switched off which resulted in a sudden increase in the thrust force to $25N$. This process showed the transition from the Ultrasonically Assisted Drilling (UAD) to the Conventional Drilling (CD). The drill bit and the work piece were separated at 135sec and the control system was turned on. A higher feed rate 0.06mm/rev was applied at 170sec and feed force increased to $6N$. This Ultrasonically

Assisted Drilling (UAD) process lasted until 225sec with a switch-off of the mechanical feedback control system. As a result, Conventional Drilling (CD) took place which produced a nearly $60N$ force. Feed rate 0.09mm/rev was executed at 330sec with a sudden increase in the feed force which confirmed the drill bit tip penetration process into the material. The thrust force gradually arrived at its stable regime with an approximately $12N$ value. The mechanical feedback system was turned off at 400sec which resulted in a considerable increase in the thrust force to more than $110N$. Such tremendous force reductions from the Conventional Drilling (CD) to the Ultrasonically Assisted Drilling (UAD) for 3 feed rates proved a strong ultrasonic vibration at the tip of the 3mm drill bit. In contrast to the frequency control with help of the amplitude control shown in Figure 7.22 and Figure 7.23, mechanical feedback control was able to handle a feed rate up to 0.09mm/rev.

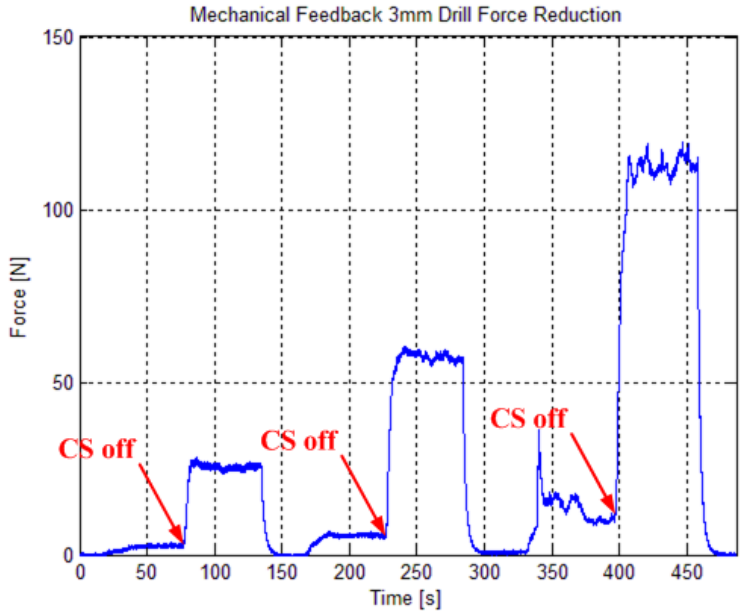

Figure 7.25 : Mechanical feedback feed force reduction versus Conventional Drilling (CD)

7.3.1.3 Current Feedback

Current feedback uses a current probe which is placed between the universal matchbox (transformer) and the ultrasonic transducer to measure the current i flowing through the piezoelectric transducer and consider it as both the 'actuating signal' and the 'signal to be controlled' in the feedback loop. This strategy aims at maintaining the 2nd step ultrasonic vibration x_2 that is proportional to the ultrasonic vibration on the tip of the 3mm drill bit at a constant level during drilling. This is done through stabilising the current signal i. Since current feedback controls the 2nd step ultrasonic vibration x_2 in an indirect way, the

effectiveness of the control entirely relies on the dynamic coupling between the current i and the mechanical vibration x_2 characteristics. The experimental procedure is the phase shifter was adjusted to reach the current resonance and then the potential meter shown in Figure 7.15 marked as '$50K\Omega$' was tuned to the maximum to allow the maximum gain in the negative feedback loop and the other '$50K\Omega$' potential meter was adjusted until both the output of the voltage-controlled amplifier (control effort) and the output of the current probe reached resonance. It should be addressed that no band-pass filters or Butterworth filters were employed to tackle the ambiguity characteristic of the current signal during drilling. However, a Butterworth filter is indispensable during the numerical simulation for the electrical feedback. This controversy questions the accuracy and applicability of the current calculation equation (4.62) in practice. Again, the piezoelectric effect is a very complicated process. Therefore, the current signal in reality might include other variables besides only the actuation force F_0 and the supplied voltage u. Each element in the current feedback control system remained unchanged during drilling. Results of the current feedback are presented in Figure 7.26.

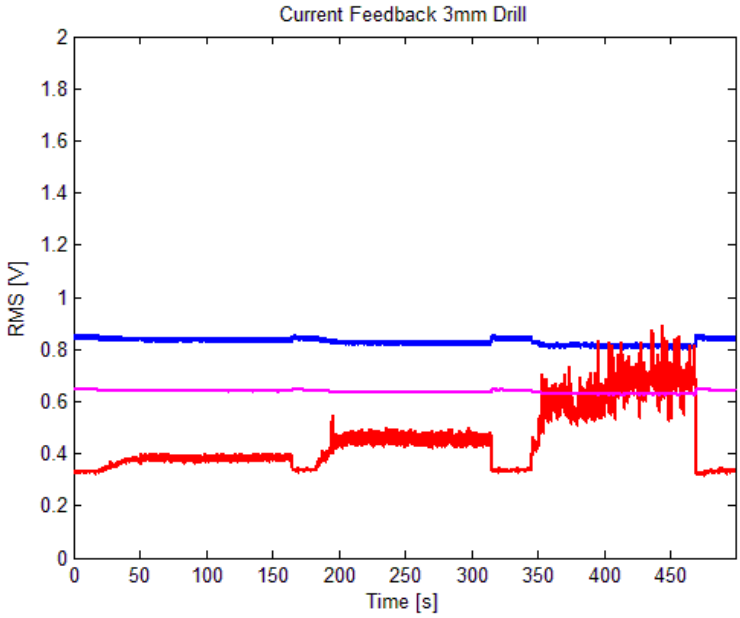

Figure 7.26 : Current feedback controlled 2nd step ultrasonic vibration, current and control effort

Figure 7.26 represents the oscilloscope readings of the drilling experiment with current feedback control system. Blue curve is the RMS of the 2nd step ultrasonic vibration x_2, pink curve stands for the RMS of the current i and red curve represents the RMS of the control

effort. A RMS of the 2nd step ultrasonic vibration x_2 value $0.85V$ was obtained with a RMS value of $0.33V$ for the control effort and a RMS value of $0.65V$ for the current i. Same as the mechanical feedback experiment, 3 different feed rates have been applied which were: 0.03mm/rev (at 15sec), 0.06mm/rev (at 185sec) and 0.09mm/rev (at 345sec). For all the 3 intervals when the feed was applied, the increase in the control effort was observed which seemed to rise proportionally. This increase in the control effort demonstrated the control system was working to compensate for the changes in the current sensor's output which was caused by the applied load. The current sensor's output, on the other hand, slightly dropped during drilling but could still be maintained at a desired level. This showed the efficiency of the control system as it was able to stabilise the amplitude of the 'signal to be controlled', in this case, current i. In terms of the inductive sensor's output, it demonstrated moderate decreases for 3 feed rates which implied a strong dynamic coupling between the current i and the mechanical vibration x_2 characteristic in reality. In a better interpretation, stabilising the ultrasonic vibration x_2 through keeping the current i was an effective method. Consequently, the reliability and convenience of the current feedback control was confirmed. The resonant frequency shift during the Ultrasonically Assisted Drilling (UAD) process was no more than $0.2KHz$ which indicated little phase change in the amplitude-phase characteristic of the current signal. Drilling depths for three feed rates were 3.0mm, 5.2mm and 7.5mm.

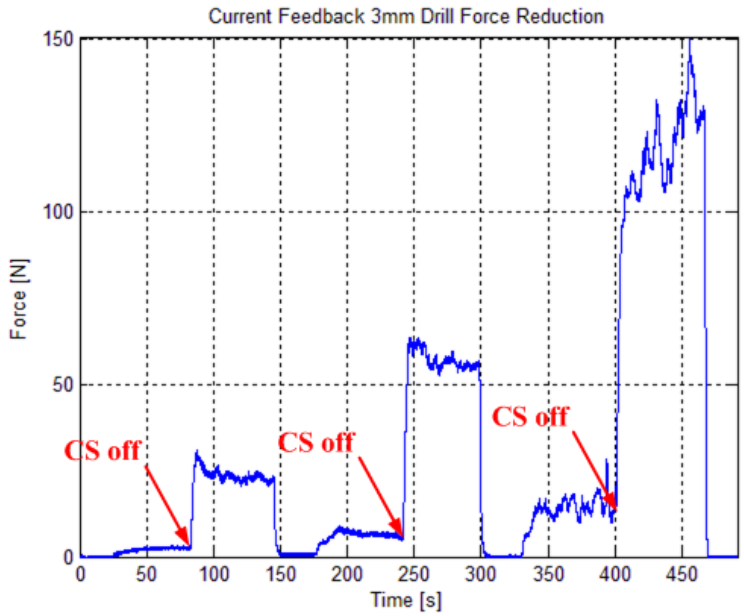

Figure 7.27 : Current feedback feed force reduction versus Conventional Drilling (CD)

The feed force reduction experiment from the Conventional Drilling (CD) to the current feedback controlled Ultrasonically Assisted Drilling (UAD) has been executed. Results are shown in Figure 7.27. 3 feed rates were executed with the autoresonant controlled ultrasonic vibration which happened at 25sec, 160sec and 330sec. When the Ultrasonic Assisted Drilling (UAD) process stabilised, the current feedback control system was turned off and these occurred at 80sec, 240sec and 400sec. As a result, the steady average feed force rose significantly to a higher level. Therefore, considerable feed force reduction from the Ultrasonically Assisted Drilling (UAD) to the Conventional Drilling (CD) for 3 feed rates indicated a strong ultrasonic vibration at the tip of the 3mm drill bit. Current feedback control worked efficiently to maintain the ultrasonic vibration on the tip of the 3mm drill bit during vibro-impact through stabilising the current signal and hence is a reliable autoresonant control strategy.

7.3.1.4 Power Feedback

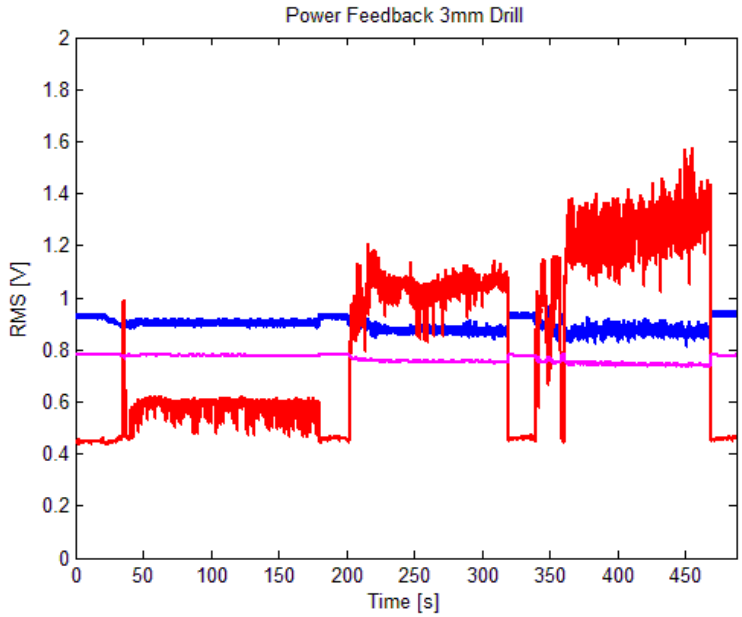

Figure 7.28 : Power feedback controlled 2nd step ultrasonic vibration, power and control effort

Power feedback employs a power sensor shown in Figure 7.7 (manufactured in the ultrasonic machining laboratory, Loughborough University) to measure the scaled instantaneous power and applies it as the 'signal to be controlled' in the negative feedback loop. Current flows through the piezoelectric transducer acts as the 'actuating signal' to form the positive feedback. This strategy aims at maintaining the 2nd step ultrasonic vibration x_2 which is in

proportion to the ultrasonic vibration on the tip of the 3mm drill bit at a constant level through stabilising power during drilling. The experimental procedure is the phase shifter and potential meter marked as $100K\Omega$ as well as $50K\Omega$ in Figure 7.7 were properly adjusted. The $50K\Omega$ potential meter in Figure 7.15 was tuned to the maximum to achieve the maximum gain and the other $50K\Omega$ potential meter was adjusted to reach power signal resonance which was designed to have a similar level of current RMS in the current feedback. Each element in the power feedback control remained fixed during drilling. Results of the power feedback are showed in Figure 7.28.

Blue curve represents the RMS of the 2nd step ultrasonic vibration x_2 measured by the inductive sensor, pink curve stands for RMS of the scaled instantaneous power measured by the power sensor and red curve is RMS the of control effort which is the output of the voltage-controlled amplifier. A RMS $0.95V$ of the 2nd step ultrasonic vibration x_2, a RMS $0.45V$ of the control effort and a RMS $0.78V$ of the instantaneous power were obtained initially. In this instance, 3 feed rates 0.03mm/rev, 0.06mm/rev and 0.09mm/rev were applied which took place at 35sec, 200sec and 340sec. The control effort can be clearly observed as it showed some difference from the mechanical feedback and the current feedback. RMS of the power sensor's output indicated a roughly constant level for low feed rate 0.03mm/rev which required a little increase in the control effort. In comparison, RMS of the power for high feed rates presented obvious drops which gave rise to the enormous increase in the control effort. In addition, high feed rates caused the control effort completely exceeded the linear operational range of the universal amplifier. Therefore the resultant supplied voltage would be partially truncated. This was not observed during mechanical feedback and current feedback whose control efforts were strictly within the linear zone.

In terms of the inductive sensor's output, there was a slightly more decrease for 3 feed rates than the other 2 feedbacks even though the control effort was tremendous. This implies a weakened dynamic coupling between the mechanical vibration characteristic and the instantaneous power signal than the current for the loaded ultrasonic vibrating system. Resonant frequency shift monitored during the power feedback controlled Ultrasonically Assisted Drilling (UAD) was no more than $0.2KHz$ which meant little change in the amplitude-phase characteristics of the power signal. Drilling depths for three feed rates were 2.9mm, 4.8mm and 7.8mm.

Feed force reductions from the power feedback controlled Ultrasonically Assisted Drilling (UAD) to the Conventional Drilling (CD) is illustrated in Figure 7.29. 3 feed rates 0.03mm/rev, 0.06mm/rev and 0.09mm/rev were examined which happened at 20sec, 220sec and 395sec. Power feedback controlled ultrasonic vibrating system was switched on initially and after certain depth of the Ultrasonically Assisted Drilling (UAD) with a stabilization of the Kistler dynamometer's output, control was turned off. As can be observed, tremendous feed force reduction indicated strong ultrasonic vibrations on the tip of the 3mm drill bit during vibro-impact for three feed rates. The ultrasonic vibration amplitude can be maintained through keeping the power at a constant level. Similar to the current feedback, this remote control strategy also emphasises the convenience and feasibility of the employment of the instantaneous power as a feedback signal.

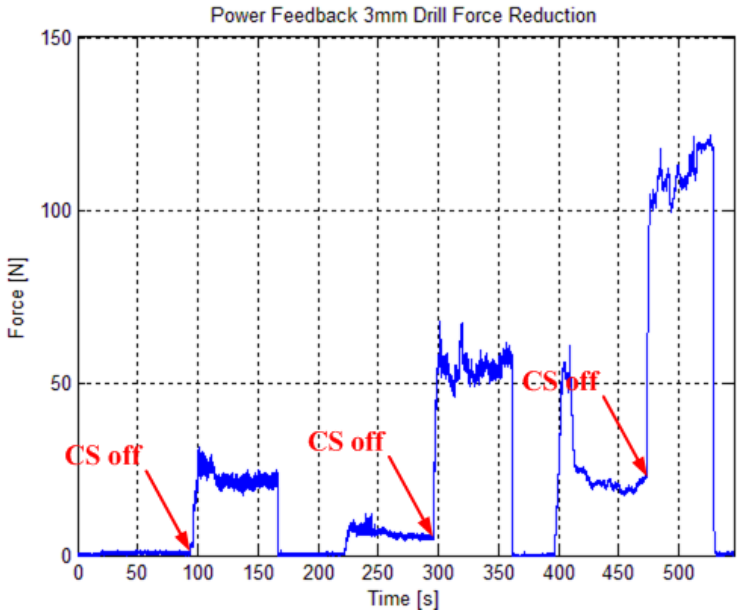

Figure 7.29 : Power feedback feed force reduction versus conventional drilling

7.3.1.5 Summary

In the above sections, the listed control strategies have been explored on a 2-step ultrasonic transducer attached with a 3mm drill bit shown in Figure 1.1. In order to analyse the results more thoroughly, the maximum deflection in the RMS of the 2nd step ultrasonic vibration x_2 from the desired levels, feed force reductions from the Ultrasonically Assisted Drilling (UAD) to the Conventional Drilling (CD) for each feed rate have been shown in Table 7.2 and Table 7.3.

As can be seen in Table 7.2, the frequency control seems lacking of ability to maintain the 2nd step ultrasonic vibration x_2 with a constant control effort as the maximal deviations from the desired levels present considerably large values. Therefore, no feed force reductions have been observed for 3 feed rates. With the help of the amplitude control system, the RMS of the 2nd step ultrasonic vibration x_2 with a low feed rate 0.03mm/rev can be maintained at a desired level with 7.5% deflection. Feed force reduction for the 0.03mm/rev feed rate is phenomenal which presents an 88.9% value shown in Table 7.3. For the high feed rates 0.06mm/rev and 0.09mm/rev, the amplitude control system generated huge control efforts against the considerable drops in the inductive sensor's output. However, the improvement in the RMS of the 2nd step ultrasonic vibration x_2 is small compared with frequency control. This is due to the high Q factor of the ultrasonic vibrating system where the resonant frequency shifted under significant applied load which resulted in a considerable amplitude drop in the frequency-amplitude characteristic. Moreover, even though huge control effort was produced by the negative feedback loop to the universal amplifier, no further benefit could be achieved from the increased control effort because it completely exceeded the linear zone. Reasonable feed force reductions 24% and 25.5% have been witnessed for high feed rates shown in Table 7.3. This can be ascribed to the huge control effort.

Table 7.2 : Maximum deflection in RMS of the 2nd step ultrasonic vibration of a 3mm drill bit application

Strategy / Deflection	Frequency Control	Freq+Amp control	Mechanical Feedback	Current Feedback	Power Feedback
0.03mm/rev	78.7%	7.5%	0.5%	1.2%	2.5%
0.06mm/rev	79.8%	56.9%	1.2%	2.4%	6.3%
0.09mm/rev	80.8%	58.1%	3.4%	3.7%	6.7%

For the 3 autoresonant control strategies, they are able to keep the nonlinear resonant mode of the oscillations in ill-defined and time changing conditions. A completed investigation on a 3mm drill bit application reveals that mechanical feedback shows an overall best performance

with a minimum deflection in RMS of the 2nd step ultrasonic vibration x_2 from the desired levels shown in Table 7.2 and the largest force reductions shown in Table 7.3 for 3 feed rates. This superior control can be ascribed to the fact that mechanical feedback employs the 2nd step ultrasonic vibration information x_2 as the 'signal to be controlled' and manipulates it directly as the location of the sensor reflects the true ultrasonic vibration information. In contrast, current feedback shows a slightly worse control in terms of the RMS of the 2nd step ultrasonic vibration x_2 deflection and feed force reduction for 3 feed rates. To this point, it can be concluded that the characteristic of the current i is physically and strongly coupled to the mechanical vibration x_2. Therefore, such indirect control strategy realises the remote control possibility for industrial use. Power feedback presents an overall worst performance compared with the other 2 strategies in the sense of maximal deviation in the RMS of the 2nd step ultrasonic vibration x_2 from the desired levels. This control strategy is debatable, because as the vibro-impact process continues, a drill bit penetrates deeper into the work piece and therefore larger power consumption from the piezoelectric transducer is required. However, the power feedback control is to maintain the RMS of the ultrasonic vibration x_2 through keeping the power at a constant level rather than increasing it. It is strongly recommended that the overall power should be increased in the power feedback control in order to stabilise the ultrasonic vibration level. In contrast, in current feedback, current signal is to be maintained at a desired level and this is done through increasing the supplied voltage (control effort) to the piezoelectric transducer. As a result, the overall power during the vibro-impact for the current feedback will be higher than a prescribed level.

Table 7.3 : Feed force reduction of a 3mm drill bit application

Strategy / Reduction	Freq+Amp control	Mechanical Feedback	Current Feedback	Power Feedback
0.03mm/rev	88.9%	90.2%	89.2%	96.2%
0.06mm/rev	24.0%	89.8%	88.4%	89.1%
0.09mm/rev	25.5%	88.4%	87.8%	84.4%

However, in terms of the feed force reduction, power feedback has a comparable level with the current feedback. For the low feed rate the feed force reduction is even superior over mechanical feedback. This is due to the higher level of control effort that the power feedback generated which can be seen in Figure 7.28. It should be mentioned that the control effort level entirely depends on the change in the 'signal to be controlled' (feedback sensor's output). Even though drops were more obvious in the RMS of the 2nd step ultrasonic vibration for 3 feed rates for the power feedback, considerable feed force reduction results prove it is still an efficient and valid control strategy. It should be re-emphasized that electrical feedback strategies need neither band-pass filters nor Butterworth filters which again highlights the difference between the piezoelectric transducer in theory and piezoelectric effect in practice.

Generally speaking, by observing the results shown in Table 7.2 and Table 7.3, improvement of using the autoresonant control from the frequency control even with the help of the amplitude control system is remarkable, especially in dealing with high Q factor oscillation systems. In order to explore which control strategy presents the overall best control, surface roughness examination will be presented later which is a direct informative reflection of the control.

7.3.2 A 6mm Diameter Standard Drill Bit

The 6mm drill bit used during Ultrasonically Assisted Drilling (UAD) experiments is a HSS-Co 8% tin coated heavy duty jobber drill bit. Point angle of such a 6mm drill bit is 135° and helix angle is 28°. The overall length is 93mm and the flute length is 57mm, it weighs 154 grams. The autoresonant control strategies and the frequency control were applied to the 2-step ultrasonic transducer shown in Figure 1.1 attached with a 6mm drill bit. Unfortunately, the 2-step ultrasonic transducer was not powerful to drive the 6mm drill bit during drilling. Therefore, a more powerful ultrasonic transducer is strongly recommended. A 4-piezoceramic rings transducer was available in the ultrasonic machining laboratory in Wolfson School of Mechanical and Manufacturing Engineering in Loughborough University and it was employed for the investigation of the autoresonant control on a 6mm drill bit application. The 4-piezoceramic rings powerful transducer structure and dimensions are shown in Figure 7.30.

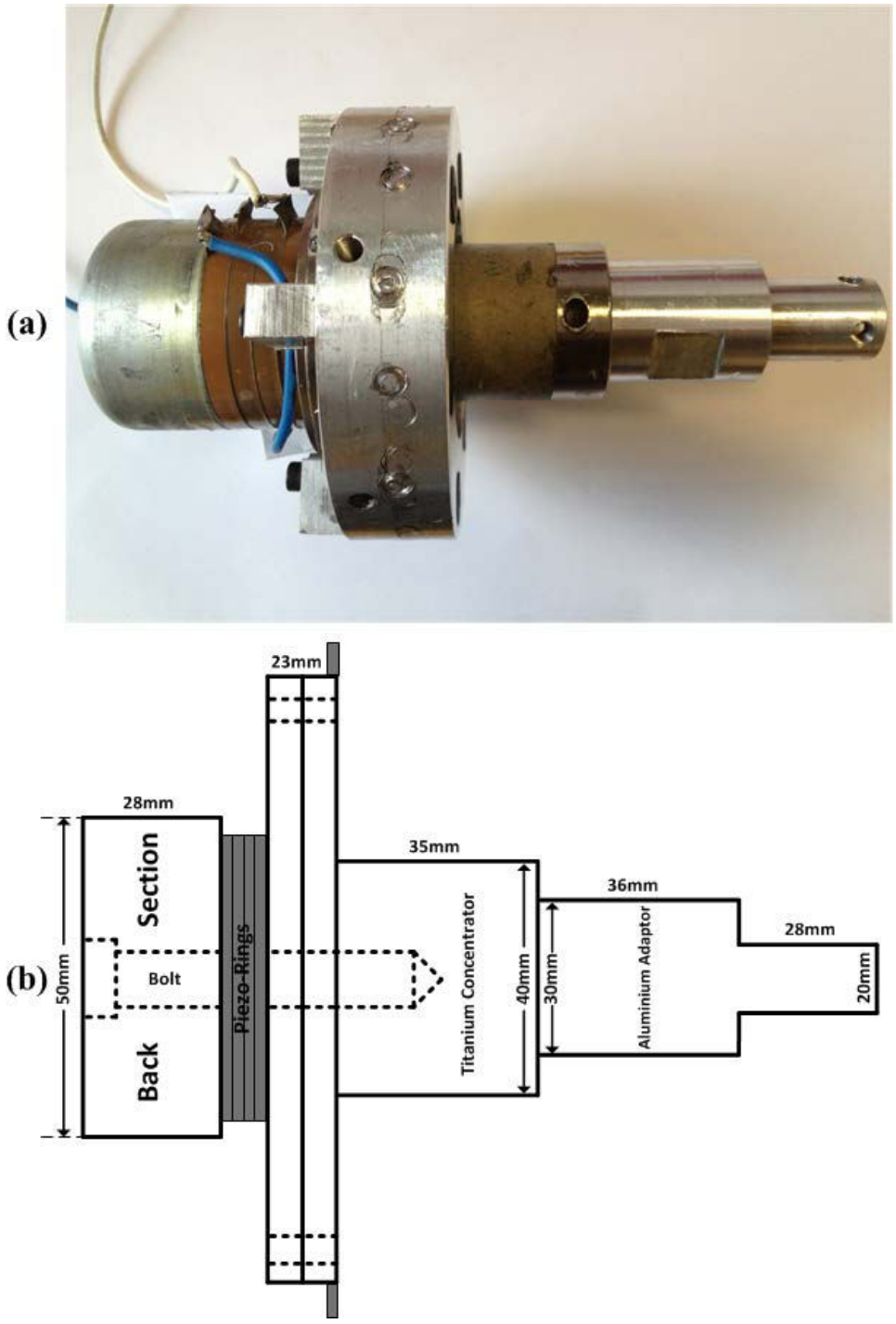

Figure 7.30 : 4-piezoceramic rings ultrasonic transducer: (a) structure, (b) dimensions

As can be seen, there are 2 pairs of piezoceramic rings connected together. The back section of the concentrator is made from steel and the concentrator material is titanium. The ultrasonic transducer was assembled with a tensioning bolt. In order to fix a 6mm drill bit to the ultrasonic transducer, a 2-step aluminium adaptor has been manufactured which was screwed to the titanium concentrator. At the end of the aluminium adaptor, 4 grub screws were used to hold a 6mm drill bit. As introduced in Figure 7.20, an application of a 6mm drill

bit to the ultrasonic transducer needs acoustical matching as such a diameter size should be treated as an additional step of the waveguide (concentrator).

7.3.2.1 A 6mm Drill Bit Proper Tuning

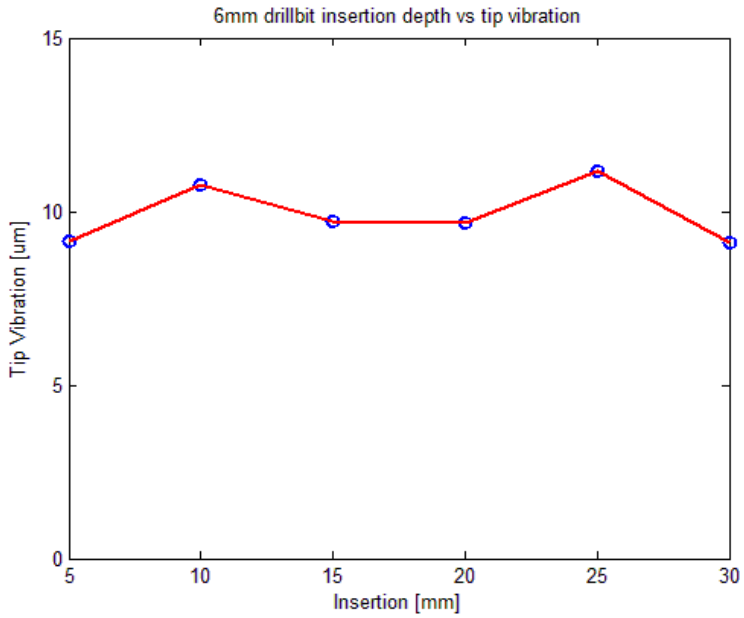

Figure 7.31 : A 6mm drill bit proper tuning

Theoretically, the waveform shown in Figure 7.20 for an appropriately adjusted ultrasonic vibrating system should be achieved. In practice, however, this is difficult to be realized due to the material difference, geometry complexity etc. Therefore, in order to properly tune the 6mm drill bit so as to enable it to match with the ultrasonic transducer acoustically, the following experiment has been performed. 30mm from the end of the shank of a 6mm drill bit was selected which was then divided into 6 equal segments with a marker. The drill bit was fixed to the ultrasonic transducer with the shank inserted to the following length: 5mm, 10mm, 15mm, 20mm, 25mm and 30mm. The resonant frequencies of different insertion depths of the 6mm drill bit of the ultrasonic vibrating system were explored with the help of the SFG-2110 synthesized function generator. A thin reflection film was attached to the tip of the 6mm drill bit in order to record the ultrasonic vibration magnitude at resonance. The insertion depth which generates the maximum vibration magnitude at the tip of the drill bit will be used for the investigation of the autoresonant control. Results are shown in Figure 7.31. Experiment revealed that an insertion depth of 25mm of the 6mm drill bit shank into the ultrasonic transducer was able to develop the largest vibration magnitude $11.2\mu m$ zero-to-

peak. Therefore, the 6mm drill bit was fixed with an insertion depth 25mm into the tool holder.

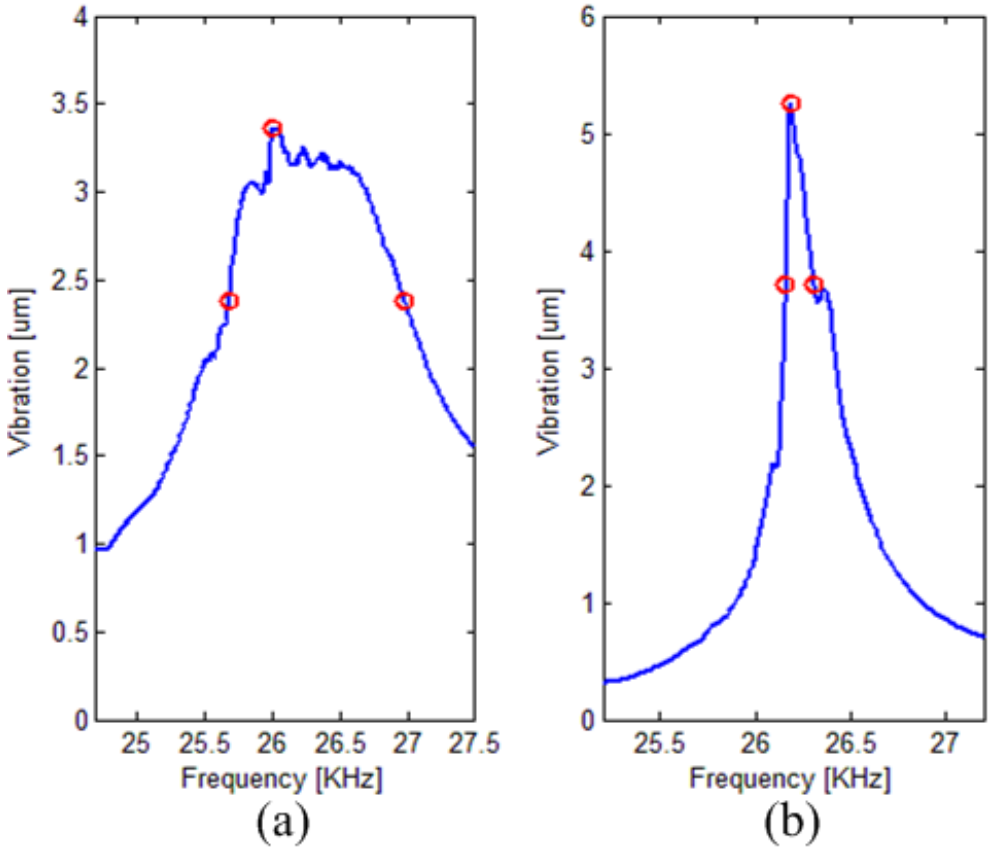

Figure 7.32 : Q factor of the powerful ultrasonic transducer: (a) no tool, (b) a 6mm drill bit

In order to study the difficulties that might be encountered during the investigation of the listed autoresonant control strategies, the Q factor of the 4-rings ultrasonic transducer shown in Figure 7.30 with and without the attachment of a 6mm drill bit was experimentally explored. Results are shown in Figure 7.32. (a) represents the frequency-amplitude characteristics of the 4-rings ultrasonic transducer. (b) shows the frequency-amplitude characteristics of the 4-rings ultrasonic transducer attached with a 6mm drill bit. As can be seen, a 6mm drill bit hardly shifts the resonant frequency of the 4-ring ultrasonic transducer; however, it considerably narrows down the half power bandwidth of the characteristic which results in a tremendous increase in Q factor value. Experiments data suggests a Q factor value of the 4-rings ultrasonic transducer without a 6mm drill bit attachment 20 (a). In comparison, a 178 Q factor value was obtained with a 6mm drill bit attached (b). Unsurprisingly, this Q factor with attachment of a 6mm drill bit exhibits a low value as research shows that a properly tuned ultrasonic transducer normally has a value 200-250 for the same sweep rate

[68]. In other words, the autoresonant control strategies might not be more superior over the frequency control provided with a sufficient driving voltage because a low Q factor system implies a moderate sloping peak in the frequency-amplitude characteristic.

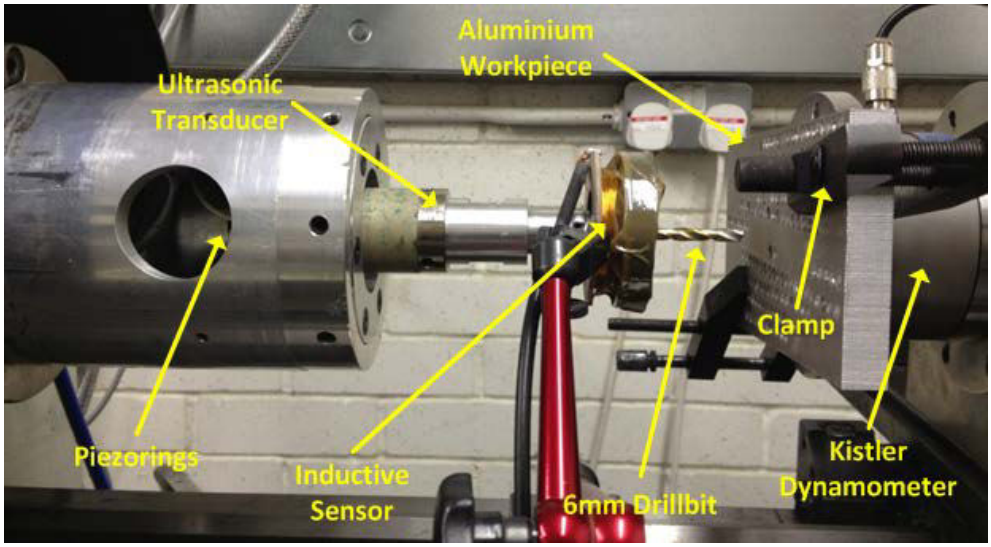

Figure 7.33 : Autoresonant control experimental setup for a 6mm drill bit application

Experimental setup for the investigation of the autoresonant control for a 6mm drill bit application is shown in Figure 7.33. 4 grub screws were used to clamp the 6mm drill bit at the end of the aluminium adaptor uniformly and tightly from 4 directions. The entire ultrasonic vibrating system was properly centred with the help of a centring gauge. The inductive sensor was placed at the end of the aluminium adaptor to capture the ultrasonic vibration information during machining. An aluminium work piece was clamped firmly to the vertical plane surface of the Kistler dynamometer which measures the axial feed force. The rotational speed of the spindle was fixed as 40rev/min. 2 feed rates 0.03mm/rev and 0.06mm/rev were applied.

7.3.2.2 Frequency Control

As can be seen in Figure 7.34, a RMS $0.38V$ and $26.20KHz$ actuating signal (red curve, also the control effort) was able to produce a RMS $2.75V$ of ultrasonic vibration signal at the end of aluminium adaptor (blue curve) in idle condition (no machining). In the beginning, the ultrasonic vibration was activated and the ultrasonic transducer developed 40sec without contact with the work piece. Since then, the initial contact started with a feed rate 0.03mm/rev and a 40rev/min rotation. The frequency control was able to deal with the vibro-

impact process until 110sec before the tip of the 6mm drill bit was completely engaged into the aluminium work piece even though certain drop was observed in the RMS of the ultrasonic vibration signal. After that RMS of the ultrasonic vibration dropped to an insignificant level $0.2V$ it led to a failure of frequency control. The 6mm drill bit and the aluminium work piece were separated at 105sec and then the ultrasonic vibration retrieved. Feed rate 0.06mm/rev was applied at 240sec, and this feed rate caused the RMS of the ultrasonic vibration decreased to a similar low level as the case of the 0.03mm/rev feed rate. Therefore control failed. For both feed rates, the control effort hardly changed. Due to the fact that the ultrasonic vibration at the end of the aluminium adaptor dropped significantly during the contact with the aluminium work piece, the ultrasonic vibrating system lost its benefits hence no obvious force reduction was witnessed. The ultrasonic vibration measured at the end of the aluminium adaptor was proportional to the ultrasonic vibration at the tip of the 6mm drill bit, since the ultrasonic vibration system conforms to certain waveform during resonance.

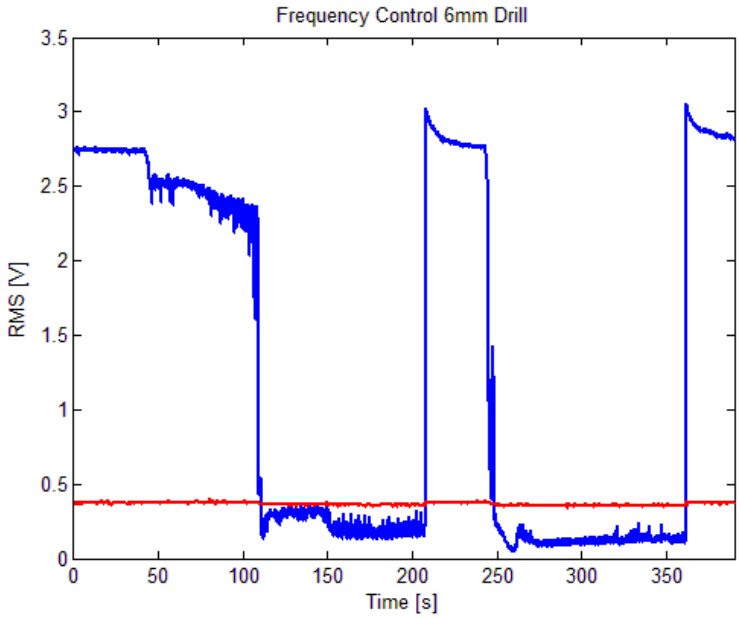

Figure 7.34 : Frequency controlled ultrasonic vibration and control effort

In order to explore whether the ultrasonic vibration can be maintained with the help of the amplitude control system, negative feedback loop shown in Figure 7.2 and Figure 7.3 was connected to the frequency controlled ultrasonic vibrating system. During this process, the SFG-2110 synthesized function generator's output signal with a pre-defined frequency ($26.20KHz$) acted as the 'actuating signal' and the inductive sensor's output (RMS of the

ultrasonic vibration) acted as the 'signal to be controlled'. The phase shifter was removed from loop and the output of the voltage-controlled amplifier was applied to the universal amplifier to drive the ultrasonic vibrating system. It should be emphasised that the negative feedback gain $50K\Omega$ shown in Figure 7.15 was adjusted to the minimum in this instance due to the drastic change in the inductive sensor's output with a 6mm drill bit application. Such a minimum feedback gain allows the voltage-controlled amplifier to work equally efficient with a low sensitivity since a high gain feedback might cause a sudden failure in the control system. Such sudden failure was observed during experiments occasionally. Results of the frequency control with the help of the negative feedback loop for 2 feed rates are shown in Figure 7.35.

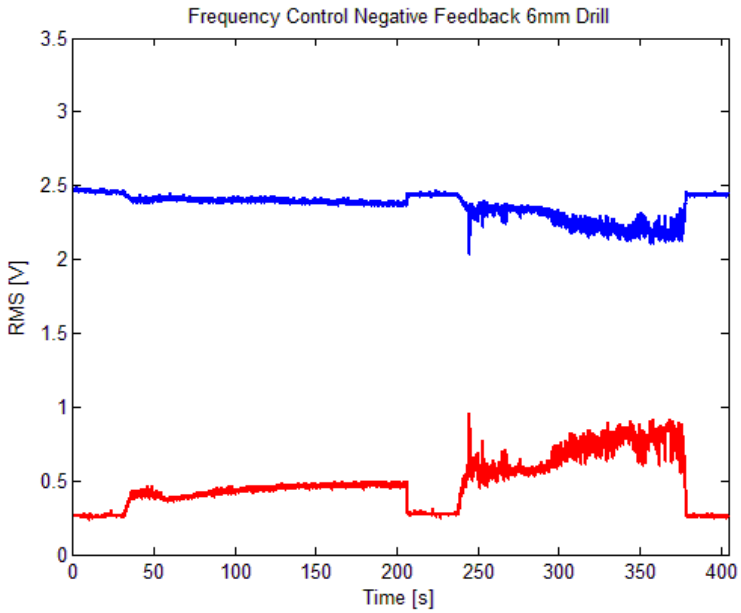

Figure 7.35 : Frequency control and amplitude control ultrasonic vibration and control effort

As can be seen, the initial contact between the 6mm drill bit and the work piece took place at 30sec with a spindle rotation 40rev/min and a feed rate 0.03mm/rev. RMS of the control effort increased against the moderate drop in the RMS of the ultrasonic vibration. This process implied the fast and accurate working principle of the negative feedback control which was designed to compensate for the drop in the RMS of the ultrasonic vibration signal. The drill bit and the work piece were separated at 205sec. Feed rates 0.06mm/rev was applied at 240sec. As a result, RMS of the ultrasonic vibration decreased more obviously and RMS of the control effort increased to make up for the drop in the 'signal to be controlled'. Drilling depths for the 2 feed rates were 3.5mm and 5.6mm.

Such an improved control result revealed the effectiveness of the negative feedback control. The voltage-controlled amplifier worked to react against the drop in the RMS of the ultrasonic vibration and provided the ultrasonic vibrating system with more voltage to compensate for the energy loss at the tip of the 6mm drill bit during vibro-impact. Nevertheless, such superior control results could be attributed to the low Q factor of the ultrasonic vibrating system as the resonant frequency shift during vibro-impact was small which implied little drop in the amplitude in the frequency-amplitude characteristic. In addition, nonlinearity was hardly developed with the application of a low feed rate and a low spindle rotation with a low Q factor oscillating system. The increased voltage supply to a 4-rings piezoelectric transducer was able to maintain the ultrasonic vibration at a desired level during machining.

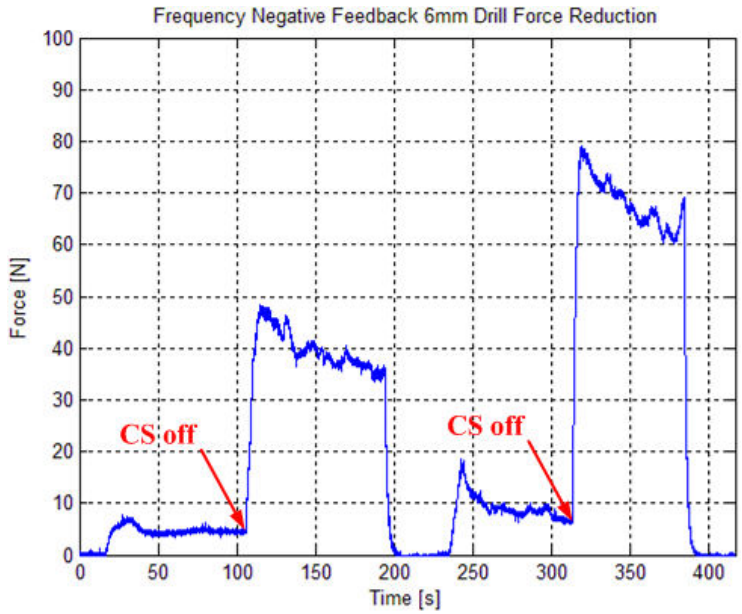

Figure 7.36 : Frequency control with amplitude control force versus conventional drilling

In comparison with the fixed frequency control, the ultrasonic vibrating system with the help of the amplitude control system was able to deal with both feed rates and considerable drilling depths. Therefore, remarkable force reductions during drilling for both feed rates were expected. Results are shown in Figure 7.36. The initial contact of the 6mm drill bit with the work piece happened at 15sec. Due to the participation of the amplitude control, Ultrasonically Assisted Drilling (UAD) lasted for 90secs with a 40 rev/min spindle rotation and a 0.03mm/rev feed rate. The steady thrust force during this process is less than $5N$. At 105sec, both the frequency generator and the negative feedback control system were switched

off and the ultrasonic vibration vanished. Steady feed force turned into nearly $40N$ as a result of the Conventional Drilling (CD). Control system was turned on after the separation of the drill bit and the work piece and a higher feed rates 0.06mm/rev was applied at 235sec. As soon as the Kistler dynamometer's output signal became stable, the control system was turned off. As a result, the thrust force immediately climbed up to a higher level $70N$. Such phenomenal force reductions for both feed rates seemed to correspond to the results shown in Figure 7.35. A strong ultrasonic vibration existence at the tip of the 6mm drill bit during drilling was implied. In addition, certain regular waveform of the 6mm drill bit during machining was confirmed. In other words, RMS of the ultrasonic vibration at the end of aluminium adaptor is a reliable observation point and can be treated as a 'signal to be controlled' source.

7.3.2.3 Mechanical Feedback

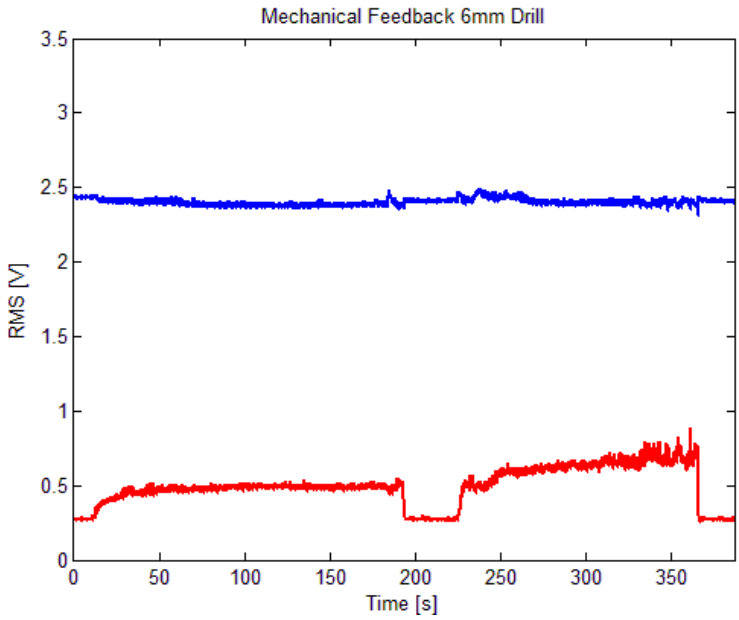

Figure 7.37 : Mechanical feedback controlled ultrasonic vibration and control effort

Mechanical feedback control employs the actual ultrasonic vibration measured by an inductive sensor as both the 'actuating signal' and the 'signal to be controlled'. The aim of this strategy is to maintain the ultrasonic vibration at the tip of a 6mm drill bit at a constant during drilling through keeping the ultrasonic vibration at the end of the adaptor constant based on the assumption that vibrations obtained from two positions are proportional. Since mechanical feedback measures and controls the mechanical vibration directly, it is supposed to present the overall best results. The operational procedure is that the phase shifter was

manually adjusted in order to bring the RMS of the ultrasonic vibration at the end of the aluminium adaptor to the resonance. After this the potential meter '$50K\Omega$' shown in Figure 7.15 connected between the negative port of the offset amplifier OP07 and the output 'U_{DC}' was tuned to the minimum. Such adjustments prevented the voltage-controlled amplifier's sudden failure due to the drastic change in the inductive sensor's output during drilling. Then the potential meter marked as '$50K\Omega$' connected between $12V$ and earth was adjusted until both the voltage-controlled amplifier's output (control effort) and the inductive sensor's output presented peak values. During drilling, the phase shifter and each element in the negative feedback were fixed. Results of the mechanical feedback control are shown in Figure 7.37.

The red curve represents the RMS of the control effort and the blue line stands for the RMS of the ultrasonic vibration measured at the end of the adaptor. An ultrasonic vibration level $2.45V$ was obtained with a control effort RMS $0.3V$. As can be seen, the initial contact between the 6mm drill bit and the work piece happened at 15sec with a 0.03mm/rev feed rate and a 40rev/min spindle rotation. As the drill bit penetrated deeper into the work piece, the ultrasonic vibrating system required more energy to deal with the energy loss on the 6mm drill bit tip. RMS of the control effort increased from $0.3V$ to $0.5V$. Meanwhile, RMS of the ultrasonic vibration was maintained perfectly at a constant. At 195sec, the drill bit and the work piece were separated with a recovery of both the RMS in the ultrasonic vibration and the control effort. At 225sec, a higher feed rate 0.06mm/rev was applied. Ultrasonically Assisted Drilling (UAD) lasted for 140secs with the control effort increased from $0.3V$ to $0.7V$ which was twice as high as the control effort of the previous feed rate. RMS of the ultrasonic vibration slightly decreased as the 6mm drill bit was engaged deeper into the work piece but still can be kept at a constant level. For both feed rates, the control effort climbed up gradually against the change in the inductive sensor's output. In comparison, mechanical feedback shows a superior control over the frequency control with the help of the negative feedback shown in Figure 7.35. This emphasised the importance of the employment of phase control rather than frequency control. For the same feed rate, the phase-amplitude characteristic presents a more gently sloping peak than the frequency-amplitude characteristic even though the Q factor of the ultrasonic vibrating system was reasonably low. It should be emphasised that the resonant frequency has been monitored; the maximal change in the resonant frequency was no more than $0.2KHz$ which hardly altered the phase in the phase-

amplitude characteristic of the ultrasonic vibrating system. Drilling depth for 2 feed rates were 3.7mm and 5.6mm.

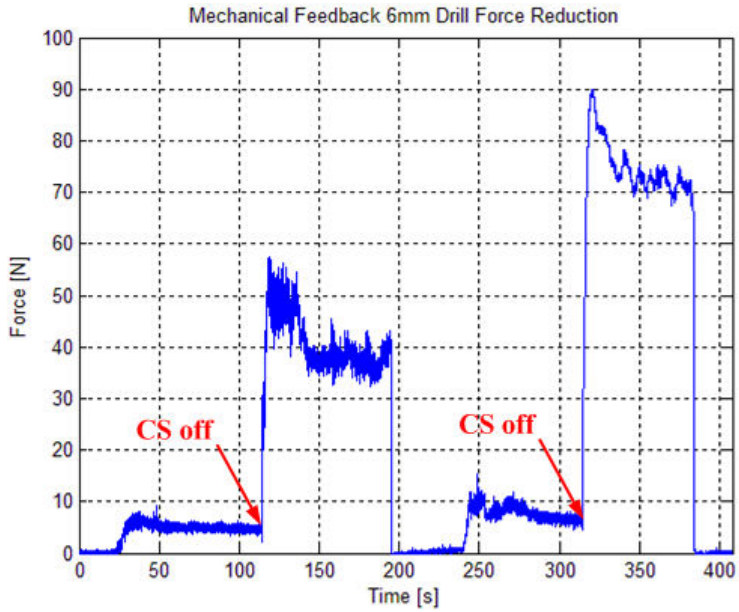

Figure 7.38 : Mechanical feedback force reduction versus Conventional Drilling (CD)

In order to examine the existence of the ultrasonic vibration on the tip of the 6mm drill bit during machining, the feed force was monitored and results are shown in Figure 7.38. The initial contact with a 0.03mm/rev feed rate and a 40rev/min rotation happened at 25sec and Ultrasonically Assisted Drilling (UAD) process lasted for 90secs until the feed force stabilised. The thrust force level during this process was around $5N$. At 115sec, the mechanical feedback control system was switched off which resulted in a sudden increase in the thrust force to $40N$. This process showed the transition from the Ultrasonically Assisted Drilling (UAD) to the Conventional Drilling (CD). The drill bit and the work piece were separated at 195sec and the control system was turned on. A higher feed rate 0.06mm/rev was applied at 240sec and feed force increased to $8N$. This Ultrasonically Assisted Drilling (UAD) process lasted until 315sec with a switch-off of the mechanical feedback control. As a result, Conventional Drilling (CD) took place which produced a nearly $75N$ feed force. Such tremendous force reductions from the Conventional Drilling (CD) to the Ultrasonically Assisted Drilling (UAD) for both feed rates proved a strong ultrasonic vibration at the tip of the 6mm drill bit.

7.3.2.4 Current Feedback

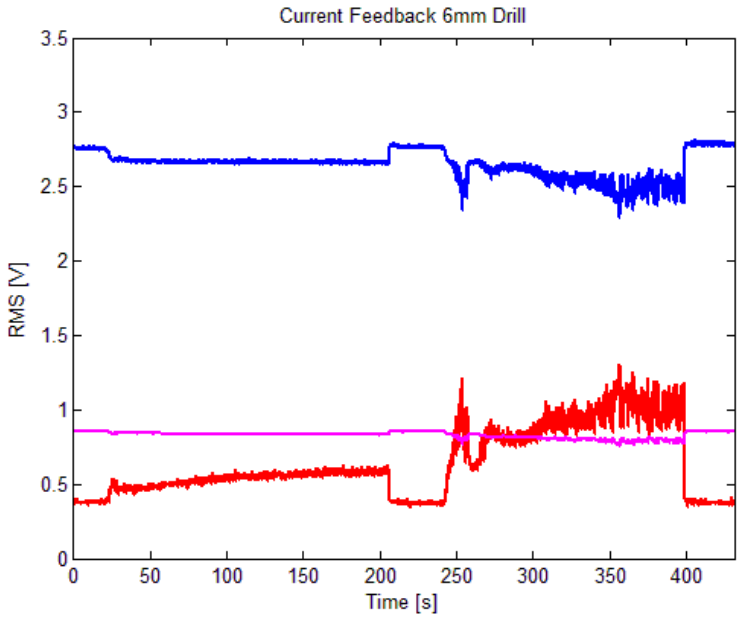

Figure 7.39 : Current feedback controlled ultrasonic vibration, current and control effort

Current feedback uses a current probe which is placed between the universal matchbox (transformer) and the ultrasonic transducer to measure the current i flowing through the pizeoceramic rings and considers it as both the 'actuating signal' and the 'signal to be controlled'. This strategy aims at maintaining the ultrasonic vibration at the end of the adaptor which is proportional to the ultrasonic vibration on the tip of a 6mm drill bit at a constant level during drilling. This is done through stabilising the current i. Since current feedback controls the mechanical vibration in an indirect way, the effectiveness of the control entirely relies on the dynamic coupling between the current and the mechanical vibration characteristics. The experimental procedure is the phase shifter was adjusted to reach the current resonance and then the potential meter marked as '$50K\Omega$' shown in Figure 7.15 was adjusted to allow the maximum gain (since the electrical characteristics are obtained at a distance from the machining zone therefore the changes are small) in the negative feedback loop. This negative feedback gain values depend on the change in the 'signal to be controlled'. It was experimentally found that the drop in the current signal was not as drastic as the ultrasonic vibration as the electrical parameters were located at a distance from the machining zone which was affect less than the mechanical characteristics. The other '$50K\Omega$' potential meter in Figure 7.15 was adjusted until both the output of the voltage-controlled amplifier (control effort) and the output of the current probe reached resonance. It should be emphasised, being similar to a 3mm drill bit application, neither a band-pass filter nor a

Butterworth filter was employed to tackle the ambiguity characteristic of the current signal during drilling. Each element in the current feedback remained unchanged during drilling. Results of the current feedback are presented in Figure 7.39.

Figure 7.39 presents the oscilloscope readings of the drilling experiment with the current feedback control system on a 6mm drill bit. Blue curve represents the RMS of the ultrasonic vibration, pink curve stands for the RMS of the current and red curve shows the RMS of the control effort. A RMS of the ultrasonic vibration $2.75V$ was obtained with a RMS of $0.38V$ for control effort and a RMS of $0.85V$ for current. Same as the previous experiment, 2 feed rates had been applied which were: 0.03mm/rev (20sec) and 0.06mm/rev (245sec). For the 2 intervals when the feed rates were applied, the increase in the control effort could be observed. This increase in the control effort demonstrated the control system was working to compensate for the changes in the current sensor's output which was caused by the applied load. Current sensor's output, on the other hand, slightly dropped during drilling but still could be maintained at a desired level. This showed the efficiency of the control system as it was able to stabilise the amplitude of the 'signal to be controlled'. In terms of the inductive sensor's output, it demonstrated obvious decreases especially for the high feed rate which implied a weakened coupling between the current and the mechanical vibration in reality for a 6mm drill bit application. In a better interpretation, although stabilising the ultrasonic vibration through keeping the current is still an effective method, current feedback worked not efficient as mechanical feedback. Instead, it has a comparable performance with the frequency control with help of the negative feedback control system. Resonant frequency shift during the Ultrasonically Assisted Drilling (UAD) process was no more than $0.2KHz$ which indicated little phase change. Drilling depth for 3 feed rates were 3.7mm and 6.4 mm.

The force reduction experiment for the current feedback has been executed. Results are shown in Figure 7.40. 2 feed rates were executed with current feedback which happened at 20sec and 230sec. When the Ultrasonic Assisted Drilling (UAD) process stabilised, the current feedback control was turned off which occurred at 110sec and 310sec. As a result, the steady feed force increased significantly to a higher level. Therefore, considerable force reductions for 2 feed rates indicated a strong ultrasonic vibration at the tip of the 6mm drill bit. Current feedback control worked efficiently to maintain the ultrasonic vibration on the tip

of the 6mm drill bit during vibro-impact through stabilising the current and hence is a reliable control strategy.

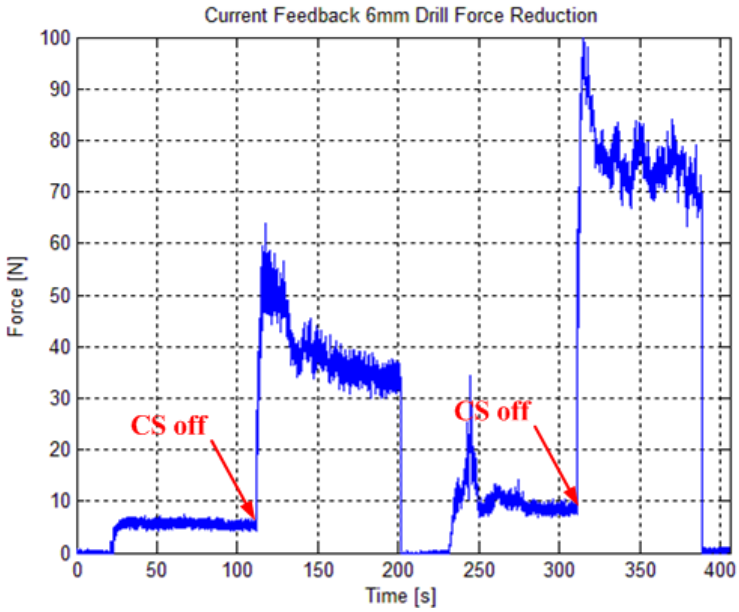

Figure 7.40 : Current feedback force reduction versus Conventional Drilling (CD)

7.3.2.5 Power Feedback

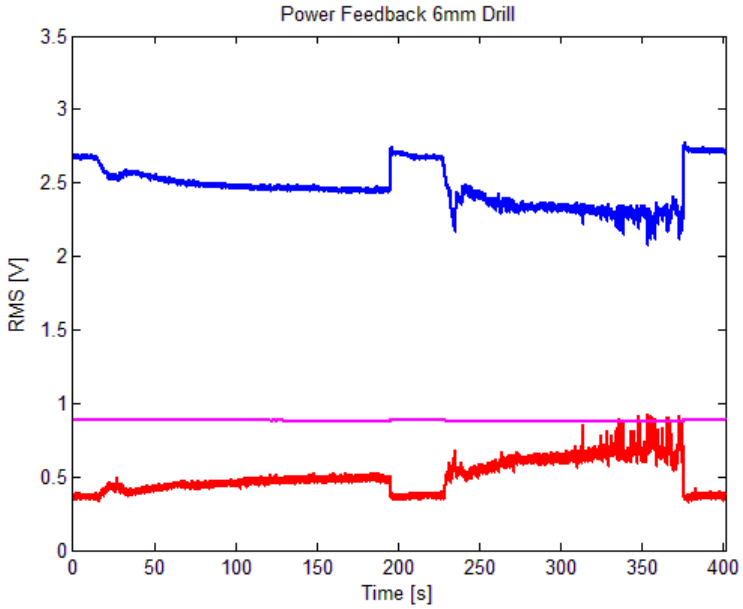

Figure 7.41 : Power feedback controlled ultrasonic vibration, power and control effort

Power feedback employs a power sensor shown in Figure 7.7 (manufactured in the ultrasonic machining laboratory, Loughborough University) to measure the scaled instantaneous power and applies it as the 'signal to be controlled' in negative feedback loop. Current flows through the piezoelectric transducer still acts as the 'actuating signal' to form the positive

feedback. This strategy aims at maintaining the ultrasonic vibration at the end of the adaptor which is in proportion to the ultrasonic vibration on the tip of the 6mm drill bit at a constant level through stabilising power. The experimental procedure is the phase shifter and potential meter marked as $100K\Omega$ and $50K\Omega$ in Figure 7.7 were properly adjusted. The $50K\Omega$ potential meter shown in Figure 7.15 had been tuned to achieve the maximum gain (since the electrical characteristics are obtained at a distance from the machining zone therefore the changes are small) and the other $50K\Omega$ potential meter was adjusted to reach the power resonance which was designed to have a similar level as the RMS of the current in the current feedback. Each element in the power feedback system remained fixed during drilling. Results of the power feedback are showed in Figure 7.41.

Blue curve represents the RMS of the ultrasonic vibration measured by an inductive sensor, pink curve stands for the RMS of the scaled instantaneous power measured by a power sensor and red curve is the RMS of the control effort which is the output of the voltage-controlled amplifier. A RMS $2.7V$ of the ultrasonic vibration, a RMS $0.38V$ of the control effort together with a RMS $0.89V$ of the instantaneous power was obtained initially. In this instance, 2 feed rates 0.03mm/rev and 0.06mm/rev were applied which happened at 15sec and 230sec. Control effort can be clearly observed which indicated that the power feedback control was working to compensate for the decrease in the RMS of the instantaneous power. RMS of the power sensor's output indicated a nearly constant level for both feed rates which required a little increase in the control effort. In terms of the inductive sensor's output, there were more obvious decreases for 2 feed rates than the other 2 feedbacks. This implies a weaker coupling between the mechanical vibration characteristic and the instantaneous power signal than the current signal. Resonant frequency monitored during the power feedback controlled Ultrasonically Assisted Drilling (UAD) showed no more than $0.2KHz$ which meant little change in the phase in phase-amplitude characteristics. Drilling depth for 2 feed rates were 3.6mm and 5.9mm.

Force reductions for the power feedback are illustrated in Figure 7.42. 2 feed rates 0.03mm/rev and 0.06mm/rev were examined which happened at 20sec and 220sec. Power feedback controlled ultrasonic vibrating system was switched on initially and after certain depth of Ultrasonically Assisted Drilling (UAD) with a stabilisation of the Kistler dynamometer's output, control system was turned off. As can be observed, tremendous force

reductions indicated strong ultrasonic vibrations on the tip of the 6mm drill bit during vibro-impact. The ultrasonic vibration amplitude can be kept through keeping the RMS of the instantaneous power at a constant level. Being similar to the current feedback, this remote control strategy also emphasises the convenience and feasibility of the employment of the instantaneous power as a feedback signal, although this remote control strategy might not be as effective as the mechanical feedback.

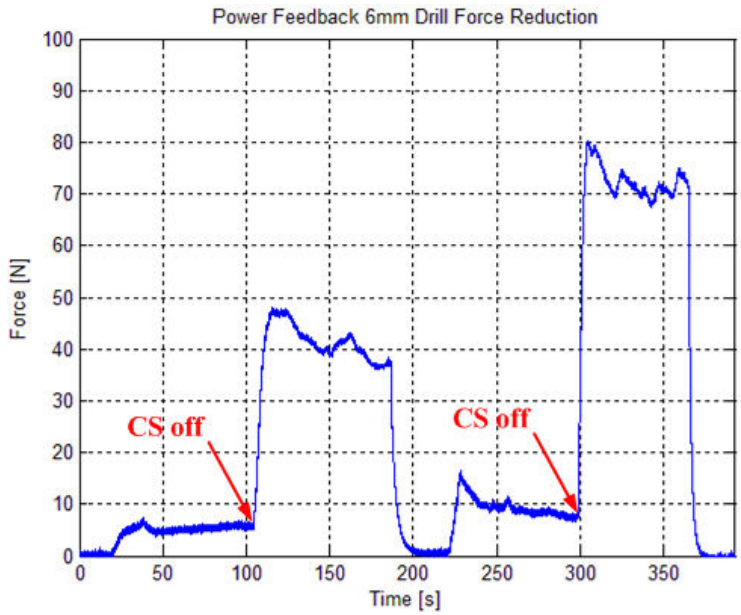

Figure 7.42 : Power feedback force reduction versus Conventional Drilling (CD)

7.3.2.6 Summary

Being similarly to the investigation of a 3mm drill bit application, in order to analyse the efficiency of different control strategies more clearly, the maximum deflection in RMS of the ultrasonic vibration from the desired levels, drilling force reductions for each feed rate for a 6mm drill bit application have been shown in Table 7.4 and Table 7.5.

As can be seen in Table 7.4, maximum deflection of the RMS of the ultrasonic vibration presents tremendously large values for both feed rates for the fixed frequency control which indicates a failure. Therefore, no force reduction was observed. With the help of the amplitude control system, RMS of the ultrasonic vibration at the end of the transducer can be maintained at a desired level even though a high feed rate 0.06mm/rev shows a greater deflection. Consequently, force reduction for both feed rates is phenomenal shown in Table 7.5. The improvement of the control with the help of negative feedback indicates a low Q

factor of the ultrasonic vibrating system. In other words, sufficient voltage supply is able to keep the ultrasonic vibration at a desired level during vibro-impact regardless of a small resonant frequency shift.

Table 7.4 : Maximum deflection in RMS of the ultrasonic vibration of a 6mm drill bit application

Strategy / Deflection	Frequency Control	Freq+Amp control	Mechanical Feedback	Current Feedback	Power Feedback
0.03mm/rev	93.4%	3.7%	2.5%	4.0%	8.2%
0.06mm/rev	95.7%	11.6%	0.1%	11.0%	17.3%

Table 7.5 : Feed force reduction of a 6mm drill bit application

Strategy / Reduction	Freq+Amp control	Mechanical Feedback	Current Feedback	Power Feedback
0.03mm/rev	89.3%	88.0%	86.3%	86.0%
0.06mm/rev	88.2%	90.7%	88.0%	87.7%

For 3 autoresonant control strategies, experiments reveal that mechanical feedback shows an overall best performance with a minimum deflection in the RMS of the ultrasonic vibration from the desired levels shown in Table 7.4. Meanwhile, considerable force reductions shown in Table 7.5 for 2 feed rates are observed for mechanical feedback. This superior control can be ascribed to that mechanical feedback employs the ultrasonic vibration at the end of the transducer as the 'signal to be controlled' and controls it directly. In contrast, current feedback shows a worse control in terms of the deflection in the RMS of the ultrasonic vibration at the end of the transducer and the force reduction for 2 feed rates. To this point, it can be concluded that the characteristic of the current is related to the ultrasonic vibration. However, compared with the application of a 3mm drill bit, an increased sized drill bit seems

to have more effect on the current feedback control. Therefore, such an indirect control strategy still realises the remote control possibility for the industrial use but not efficient as the mechanical feedback. Power feedback presents an overall worst performance compared with the other 2 strategies in the sense of the maximal deviation in the RMS of the ultrasonic vibration. Again, this control strategy's principle is debatable since the target of negative feedback is to increase the supplied power to the ultrasonic vibrating system rather than stabilise it. It's strongly suggested a modification is executed to increase the supplied power during power feedback control. Nonetheless, considerable force reductions of the power feedback show it has a comparable control to the current feedback.

Generally speaking, by observing the results shown in Table 7.4 and Table 7.5, the improvement of using autoresonant control from the fixed frequency control is remarkable, especially dealing with high Q factor oscillating systems. In order to explore which control strategy presents the overall best performance, surface roughness examination which is a direct informative reflection of control will be presented.

7.4 Holes Surface Roughness Examination

In order to explore the impact of different control strategies impose on the aluminium plates, holes have been produced for both diameters of drill bit 3mm and 6mm with several feed rates (0.03mm/rev and 0.09mm/rev for a 3mm drill bit, 0.06mm/rev for a 6mm drill bit) and a fixed spindle rotation 40 rev/min. Theoretically, a number of measurements can be executed on the specimens in order to evaluate the holes quality, including roundness, burr formation, tool wear, surface roughness etc. However, for such handmade ultrasonic vibrating systems, circularity measurement is not able to reveal the advantages and the disadvantages of each control strategies because it needs a high precision ultrasonic vibrating system setup. Instead, surface roughness reflects the direct information of the ultrasonic drilling with different control strategies. Therefore, the surface roughness experiments have been carried out.

The aluminium specimens have a thickness 15mm, 2 diameters of drill bits were used to produce through holes with different control strategies. After that, holes have been milled through the middle and the inner surface quality of the grooves was measured. A TALYSURF CLI 2000 machine [84] was available in the Metrology Laboratory in Loughborough University which was used to perform the surface roughness test. It should be

noted that the measurement length for each groove was 12 mm and for each case the measurement settings remain same for each set of experiment. Surface roughness results for a 3mm drill bit and a 6mm drill bit can be seen in the following.

7.4.1 A 3mm Drill Bit Surface Roughness

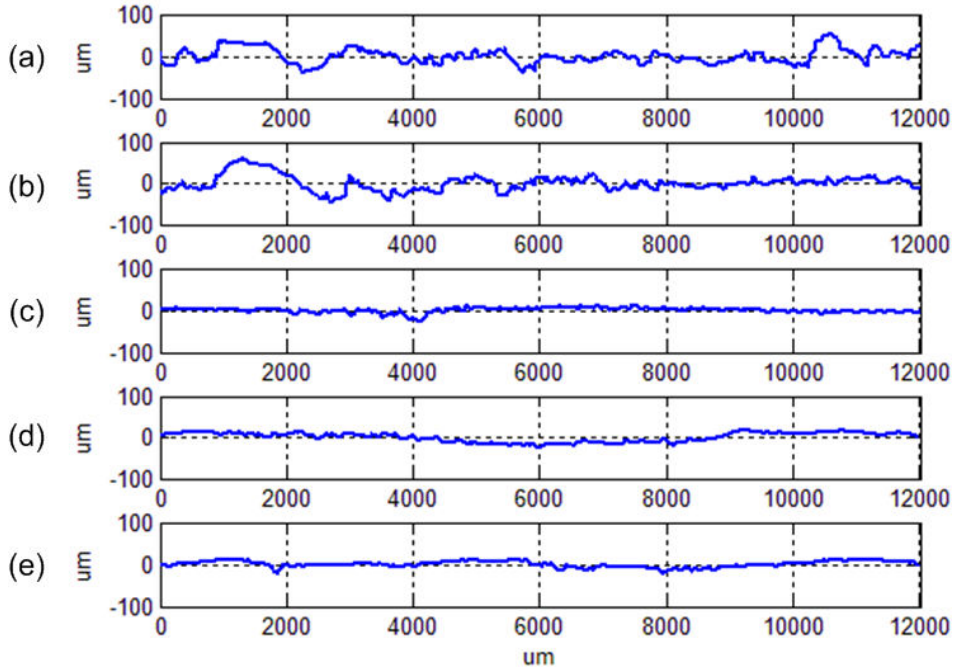

Figure 7.43 : Surface roughness of a 3mm drill bit with a 0.03mm/rev feed rate

Table 7.6 : Surface roughness test with a 0.03mm/rev and a 40rev/min of a 3mm drill bit application

Strategy	$R_a\ (\mu m)$	$R_t\ (\mu m)$	$R_p\ (\mu m)$	$R_v\ (\mu m)$	$R_q\ (\mu m)$	$R_z\ (\mu m)$
Conventional	**5.527**	46.543	12.585	13.695	6.5487	26.28
Frequency Control	**4.7738**	49.565	12.413	12.679	5.9565	25.093
Current Feedback	**1.9024**	22.905	5.3005	6.7074	2.4411	12.008
Power Feedback	**1.7453**	15.087	4.3032	4.6882	2.1402	8.9914
Mechanical Feedback	**1.5337**	21.218	3.7739	5.8589	2.0575	9.6328

Figure 7.43 shows the holes surface roughness profiles deviations from their ideal surfaces produced by a 3mm drill bit with a feed rate 0.03mm/rev and a rotation 40rev/min with different control strategies. (a) represents the surface roughness of the Conventional Drilling

(CD) (non-ultrasonic), (b) shows the fixed frequency control, (c) demonstrates the current feedback, (d) stands for the power feedback and (e) is the mechanical feedback. Horizontal axis is the groove length and vertical axis is the surface profiles. As can be seen, the surface roughness profiles were considerably improved with an application of the autoresonant control as the curves show smaller deviations. Parameters of the surface roughness for the holes produced by different control strategies can be seen in Table 7.6.

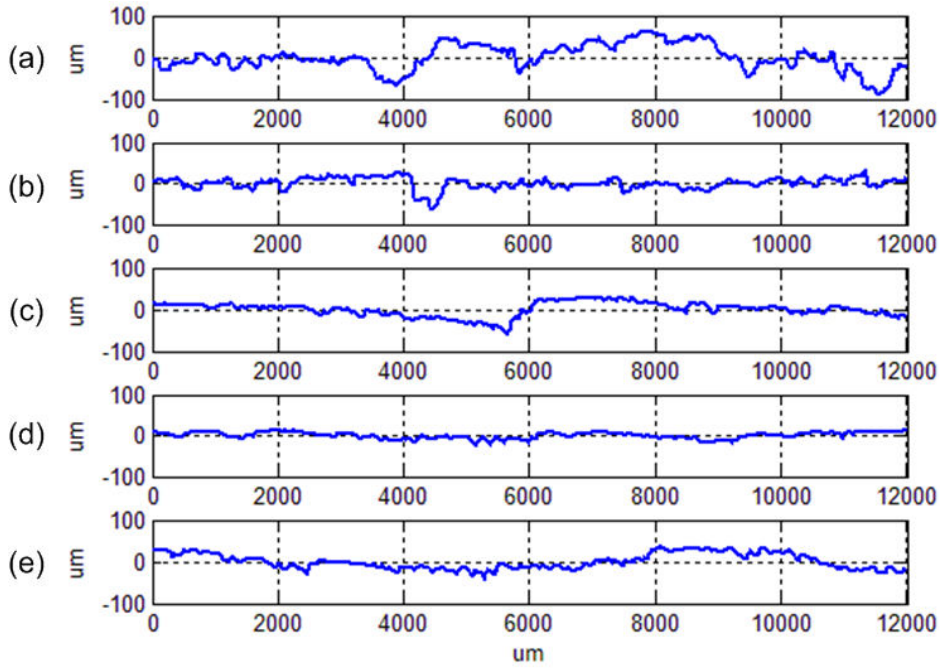

Figure 7.44 : Surface roughness of a 3mm drill bit with a 0.09mm/rev feed rate

$\boldsymbol{R_a}$ means the arithmetic average of the absolute values which is the most commonly used measurement parameters. R_t is the range of the collected roughness data points. R_p is the maximum peak height and R_v is the maximum valley depth. R_q is the root mean squared values of evaluated data points. R_z is the average distance between the highest peak and lowest valley each sampling length. All the measurement parameters have units μm. As can be seen, the most commonly used parameter $\boldsymbol{R_a}$ indicates an overall maximum deviation of data points for the Conventional Drilling (CD) and a minimum deviation for the mechanical feedback control. Current feedback and power feedback show a slightly larger deviation, but improvement of the autoresonant control produced holes quality is remarkable.

Figure 7.44 shows the surface roughness profile of a 3mm drill bit produced holes with different control strategies for a 0.09mm/rev feed rate and a 40rev/min rotation of the spindle.

(a), (b), (c), (d) and (e) have the same meanings as the 0.03mm/rev feed rate. As can be seen in Table 7.7, the power feedback shows an overall smallest deviation $\boldsymbol{R_a}$ where Conventional Drilling (CD) exhibits the maximum. The current feedback and the mechanical feedback seem slightly worse than the power feedback in the surface roughness evaluation however still show superiority over the Conventional Drilling (CD) and the fixed frequency control. This emphasises the advantages of the employment of the autoresonant control even with a high feed rate.

Table 7.7 : Surface roughness test with a 0.09mm/rev and a 40rev/min of a 3mm drill bit application

Strategy	$\boldsymbol{R_a}$ $(\boldsymbol{\mu m})$	R_t (μm)	R_p (μm)	R_v (μm)	R_q (μm)	R_z (μm)
Conventional	**6.0497**	58.745	13.86	15.859	7.4142	29.719
Frequency Control	**4.9983**	53.675	12.632	15.032	6.3811	27.664
Current Feedback	**2.8994**	33.697	7.5257	9.0908	3.7056	16.616
Power Feedback	**2.1256**	24.319	5.026	7.9691	2.7001	12.995
Mechanical Feedback	**3.4921**	27.499	7.6466	10.362	4.2895	18.008

7.4.2 A 6mm Drill Bit Surface Roughness

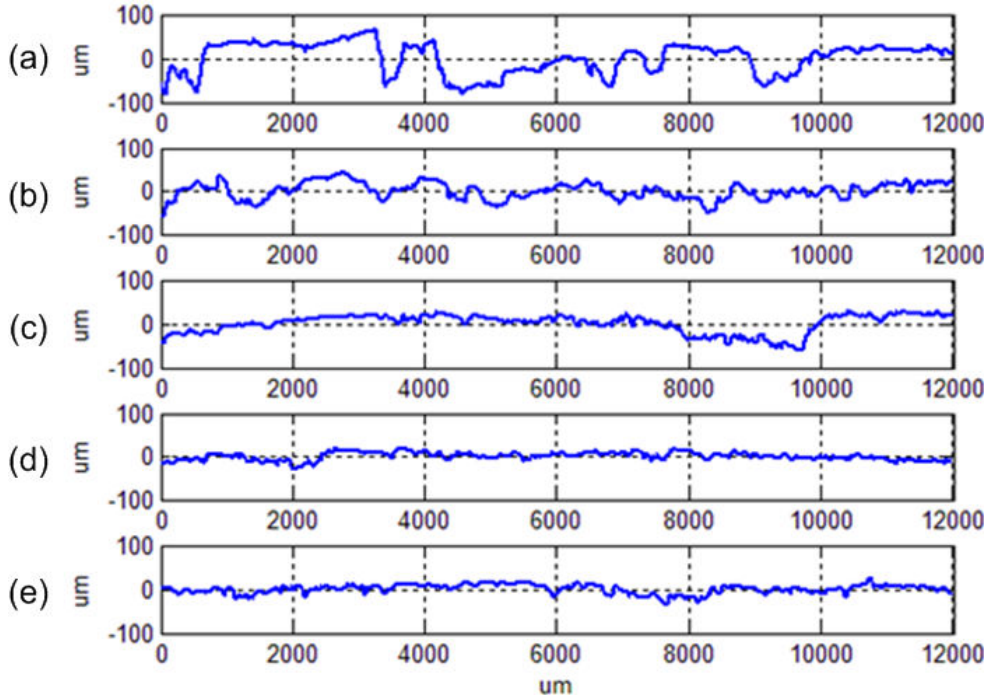

Figure 7.45 : Surface roughness of a 6mm drill bit application with a 0.06mm/rev feed rate

Figure 7.45 shows the surface roughness profile of a 6mm drill bit produced holes with different control strategies for a 0.06mm/rev feed rate and a 40rev/min rotation of the spindle. (a), (b), (c), (d) and (e) represent the control strategies same as Figure 7.43 and Figure 7.44. As can be seen in Table 7.8, mechanical feedback, current feedback and power feedback show a comparable deviation $\boldsymbol{R_a}$ where the Conventional Drilling (CD) or even the fixed frequency control exhibits a several times larger value. This emphasises the advantages of the employment of the autoresonant control even with an increased diameter drill bit.

Table 7.8 : Surface roughness test with a 0.06mm/rev and a 40rev/min with a 6mm drill bit

Strategy	$\boldsymbol{R_a}$ $(\boldsymbol{\mu m})$	R_t (μm)	R_p (μm)	R_v (μm)	R_q (μm)	R_z (μm)
Conventional	**8.0287**	95.593	18.396	22.926	10.158	41.322
Frequency Control	**6.5282**	48.596	15.039	14.351	7.7196	29.39
Current Feedback	**3.4254**	35.18	9.3441	11.896	4.4622	21.24
Power Feedback	**3.3696**	27.542	8.8707	10.097	4.2268	18.968
Mechanical Feedback	**3.4742**	35.105	8.2785	13.167	4.507	21.445

Chapter Eight Conclusions and Future Work

Ultrasonically Assisted Drilling (UAD) has won recognition in industrial applications due to its prominent advantages over Conventional Drilling (CD), i.e. tremendous force reduction, burr elimination, shorter chip formation, surface roughness and circularity improvement, strong ability to machine difficult-to-cut materials etc. Analysis on the dynamics of a distributed parameter model suggests a simplified 2-DOF model which consists of 2 sets of spring-mass-damper as a replacement of a 2-step electromechanical ultrasonic transducer used in experiments. Despite resonant frequencies of the 2-step electromechanical transducer and the 2-DOF model are different, an agreement of the ultrasonic vibration amplitude at the end of the 2^{nd} step concentrator confirms the feasibility and possibility to employ such a simple 2-DOF model in numerical simulation. In order to complete an ultrasonic vibrating system, an applied load model with a Kelvin-Voigt form has been developed, parameters have been computed and confirmed according to a vibro-impact experiment performed on an Ultrasonically Assisted Broaching (UAB) experiment. Consistency of the simulation results and the experimental results verifies the accuracy of the applied load model.

An autoresonant control feedback system which combines the phase control and the amplitude control has been created in Matlab-Simulink. 3 feedback control strategies namely mechanical feedback control, current feedback control and power feedback control have been executed and compared. A Butterworth filter with a proper bandwidth has been selected to perform the current feedback and the power feedback. By changing the applied load parameters, mechanical feedback shows an overall best result over current feedback and power feedback. However, the difference between these three feedback control strategies remains small. The explanation for such little difference could be that the drill bit effect is ignored during numerical simulation. Frankly speaking, efficiency of the electrical feedback control entirely depends on the dynamic coupling between the electrical parameters and the mechanical vibration characteristics. Currently, formulae which describe the electrical current and the mechanical state are only available in piezoceramics supplier's technical specification. The linear operational interval of the piezoelectric transducer might be changed in reality depending on the piezoceramic material etc. This implies a simplified process of the piezoelectric transducer in numerical simulation. Nonetheless, the autoresonant controlled ultrasonic vibration level during change in the applied load presents a superior performance

in comparison with the fixed frequency control and the non-ultrasonic machining which react sensitively to the applied load. It should be emphasised that in numerical simulation a tool is not attached due to a complex dynamics and geometry of a drill bit creates during the applied load which will complicate the simulation process.

In order to verify the numerical results and investigate the drill bit effects on the autoresonant control, experiments have been performed. A prototype autoresonant control system has been designed and manufactured and 2 dimensions of drill bits 3mm and 6mm in diameter were employed to execute the Ultrasonically Assisted Drilling (UAD) experiments. Different feed rates in combination with a fixed spindle rotation speed were applied to 3 control strategies. A completed investigation reveals that the mechanical feedback shows the overall superior control over the other 2 feedback control strategies. This emphasises the importance and efficiency of using the direct ultrasonic vibration information which is obtained by a mechanical sensor placed in the machining zone. 2 dimensions of drill bits applications on the autoresonant control present the highest efficiency of maintaining the RMS of the ultrasonic vibration in the mechanical feedback. Although the ultrasonic vibration at the tip of a drill bit is unavailable during machining, it has been experimentally proved that the ultrasonic vibration at the end of the concentrator is proportional to the vibration at the tip of a drill bit due to a regular waveform of an ultrasonic vibrating system. In industrial applications, the inductive sensor could be effectively employed as a replacement of the laser vibrometer due to its low cost. In order to ensure the persistency and safety of the Ultrasonically Assisted Drilling (UAD) process, the inductive sensor can be placed anywhere (apart from the nodal point) along the direction of the waveguide where is far from the machining zone. The ultrasonic vibration level on the tip of the drill bit could be maintained through keeping the inductive sensor's output stable due to the fact that the ultrasonic vibrating system conforms to a regular waveform at resonance.

In comparison, electrical feedback use a current sensor or a power sensor to measure the electrical characteristics of the piezoelectric transducer then employ them as the 'actuating signal' and the 'signal to be controlled' in the feedback loop. Therefore, electrical feedback reflects the mechanical vibration in an indirect way which inevitably worsens the control accuracy of the ultrasonic vibration. Furthermore, the electrical parameters are less affected by the machining zone compared with mechanical characteristics which also explains the reduced efficiency of the electrical feedback control during maintaining. Ultrasonically

Assisted Drilling (UAD) experiments showed that the power feedback exhibited a slightly worse control than the current feedback and this deterioration was aggravated as the diameter of a drill bit increased. Generally speaking, power feedback shows the lowest efficiency in keeping the ultrasonic vibration level and the explanation is the ultrasonic vibrating system requires more power during vibro-impact process. However, power feedback is designed to keep the power at a constant level which is debatable. It is therefore strongly recommended that more power should be produced in the power feedback control in order to compensate the the energy loss and stabilise the mechanical vibration. Current feedback, on the other hand, aims to stabilise the current by increasing the control effort which results in an overall power increase. It should be emphasised that being contrary to the numerical simulation, the electrical feedback required no Butterworth filters to tackle the 'confusion' problem (one phase corresponds to several vibration regimes). This conflict reveals the difference between the theory and the practice. The piezoelectric effect is a complicated process in reality which can be affected by many factors. Whereas, a formula describes the mechanical state and the electrical current has been employed in the numerical simulation which essentially simplify the piezoelectric effect. Surface roughness profiles for a 3mm drill bit and a 6mm drill bit generally conforms to the experimental results except certain particular feed rates.

The limitation of the autoresonant control technology is the driving power of the ultrasonic vibrating system. As explained that a 2-piezoceramic rings transducer used for the application of a 3mm drill bit was insufficient to drive a 6mm drill bit. Therefore, a more powerful transducer with 4-piezoceramic rings acting as the actuating elements was employed for the application of a 6mm drill bit. Even though, a feed rate higher than 0.06mm/rev in combination with a spindle rotation 40rev/min led to a failure in control. The acoustic power handling capacity of a radiating transducer is limited by several factors including the dynamic mechanical strength of the ceramic, the reduced efficiency due to the dielectric loss and the mechanical loss, the depolarisation of the ceramic which disable the piezoelectric rings to benefit more vibrations from increased supplied voltage and therefore results in saturation.

One of the possible solutions to tackle the power limitation of the piezoelectric transducer is to add more piezoceramic rings to drive the ultrasonic transducer. However, it's been explored in experiment that a 4-ring piezoelectric transducer does not indicate a doubled power compared with a 2-ring piezoelectric transducer. Alternatively, more powerful piezoceramic rings can be employed to such as PZT-8. Ideally, an increased voltage supply to

the actuation elements should generate stronger ultrasonic vibrations at the tip of a tool. Therefore, it is strongly recommended the linear operation voltage interval of a piezoelectric transducer should be extended. In order to achieve this, another option is to replace the universal amplifier and the universal matchbox (transformer) with a valve amplifier which allows operating at a higher voltage without any waveform distortion. As introduced before, the universal amplifier's linear operational zone is $\pm 70V$ and any signal output exceeds this range will be truncated. According to experiments, such a narrow zone limits the effective control efforts supplied to the universal matchbox (transformer). The autoresonant control realises the possibility of maintaining the nonlinear resonant mode of oscillations caused by the applied load in ill-defined and time changing conditions where the fixed frequency control or even an adjusted frequency control seems insufficient. In order to show the high efficiency of the autoresonant control technique, a high Q factor ultrasonic vibrating system is strongly recommended.

In addition to the limitation of the supplied power to the piezoelectric transducer, an improved design of a drill bit is suggested. The drill bits used in the autoresonant control during Ultrasonically Assisted Drilling (UAD) are conventional, standard, heavy duty drill bits with regular helix angles and high point angles which have stronger cutting edges and produce narrow chips, such drill bits are used in materials that have been hardened or extremely tough. Such drill bits were able to develop a considerable force reduction during autoresonant control on the specimens of aluminium with hardness 77HV. However, it was explored that when the hardness of the aluminium alloy was increased or different materials were applied, the autoresonant control was not so efficient. This is partially due to the limitation on the supplied power to the ultrasonic transducer and the changed material properties, i.e. hardness etc. Another important reason is the geometry of the drill bits. Therefore, it is also a subject of interest to investigate different geometry of drill bits to examine the tool effect on the autoresonant control. A successful design of a drill bit could improve the efficiency and robustness of an autoresonant control system.

An optimization on the universal matchbox for the application of a 6mm drill bit on a 4-piezoring ultrasonic transducer has been executed and the results are promising and interesting. The idea of the optimization process is to increase the gap between 2 ferrite cores until the maximal ultrasonic vibration amplitude is achieved with a fixed input signal to the universal amplifier. Experimental results indicate that an air gap $\Delta = 2.5mm$ is the optimal

gap distance which develops the largest ultrasonic vibration, a nearly $\frac{\pi}{2}$ phase shift between the voltage and the current across the universal matchbox (transformer), maximal voltage and maximal current as well as a peak power. Analysis shows that the optimal air gap is able to cancel the phase different between the voltage and the current in an LC circuit which is a simplified form of the universal matchbox (transformer) and the ultrasonic transducer. Therefore, a maximal energy transfer from the source to the piezoelectric transducer is achieved. This enables the ultrasonic transducer to work at the most efficient regime at resonance.

For each ultrasonic vibrating system, the universal matchbox (transformer) optimization process is critical and indispensable as the effective inductance of the universal matchbox (transformer) will change considerably as the air gap develops which will inevitably change the behaviour of the ultrasonic vibrating system in terms of resonant frequency, vibration amplitude, driving voltage etc. It should be mentioned that at the end phase of the project, a more powerful amplifier module MF450 was purchased to replace the defected MF200 module. The new amplifier module proves to deliver extremely powerful signal to the ultrasonic transducer. The driving voltage for the ultrasonic transducer easily exceeds 3000 volts peak-to-peak. As a result, the piezoceramic rings seems not to reject such a high voltage as observed in experiments. Therefore, it is strongly recommended to explore a bigger size drill bit for the autoresonant control. Moreover, it is also worth to explore the maximal working voltage of the piezoceramic rings.

References

[1] Abboud, N.N., Wojcik, G.L., Vaughan, D.K., J. Mould, D.J. Powell and L. Nikodym (1998). *Finite Element Modelling for Ultrasonic Transducers.* Proceedings – SPIE the international society for optical engineering. Issue 3341: pp. 19-42.

[2] Alam, K., Mitrofanov, A.V. and Silberschmidt, V.V. (2011). *Experimental investigations of forces and torque in conventional and ultrasonically assisted drilling of cortical bone.* Medical Engineering & Physics. **Vol.33:** pp. 234-239.

[3] Anton, H. and Rorres, C. (2000). *Elementary Linear Algebra.*(Applications Version), 8th Edition, John Wiley. (Chpater 7, hard copy)

[4] Azarhoushang, B. and Akbari, J. (2007). *Ultrasonic-assisted drilling of Inconel 738-LC.* International Journal of Machine Tools&Manufacture 47: pp. 1027-1033.

[5] Astashev, V.K. (1981). *Calculation of rod concentrators with a nonlinear load.* Soviet Physics-Acoustics 27(6).

[6] Astashev, V.K. and Babitsky, V.I. (1998). *'Ultrasonic cutting as a nonlinear (vibro-impact) process'.* Ultrasonics **Vol. 36** (n. 1-5): pp. 89-96.

[7] Astashev, V.K. and Babitsky, V.I. (2000). *Dynamics and Control of Machines*. Berlin, Springer, ISBN: 3540637222.

[8] Astashev, V.K. and Babitsky, V.I. (2007). *Ultrasonic Processes and Machines – Dynamics, Control and Applications*. Berlin, Springer, ISBN: 978-3-540-72060-7.

[9] Astashev, V.K. and Sakayan, A.R. (1967). *Experimental investigation of the dynamics of the vibrating system of an ultrasonic lathe.* Mashinovedenie.**Vol.4** (n.3-n.7). (in Russian)

[10] Babitsky, V.I. (1992). *Some Applications of Autoresonant Strongly Nonlinear Vibratory Systems.* Machine Vibration **Vol.1** (n.2): pp. 110-119.

[11] Babitsky, V.I. (1995). *Autoresonant mechatronic systems.* Mechatronics. **Vol.5**: pp. 483-495.

[12] Babitsky, V.I. (1998). *Theory of Vibro-Impact Systems and Applications.* Berlin, Springer. Revised translation from Russian, Moscow, Nauka, 1978.

[13] Babitsky, V.I. (2009). *Autoresonant excitation and control of nonlinear vibration modes*. Physcon, Catania, Italy.

[14] Babitsky, V.I., Astashev, V.K. and Kalashnikov, A.N. (2004). *Autoresonant control of nonlinear mode in ultrasonic transducer for machining applications.* Ultrasonics 42: pp. 29-35.

[15] Babitsky, V.I., Astashev, V.K. and Meadows, A. (2007). *Vibration excitation and energy transfer during ultrasonically assisted drilling.* Journal of Sound and Vibration 308: pp. 805-814.

[16] Babitsky, V.I., Kalashnikov, A.N. and Molodtsov, F.V. (2004). *Autoresonant control of ultrasonically assisted cutting.* Mechatronics, **Vol. 14** (n.1): pp. 91-114.

[17] Babitsky, V.I. and Sokolov, I.J. (2002). *Autoresonance Control of Vibratory Systems.* The sixth international conference on Motion and Vibration Control. Saitama, Japan. Japan Society of Mechanical Engineers: pp. 643-648.

[18] Babitsky, V.I. and Sokolov, I.J. (2007). *Autoresonant homeostat concept for engineering application of nonlinear vibration modes.* Nonlinear Dyn 50: pp. 447-460.

[19] Balamuth, L. (1964). *Ultrasonic vibrations assist cutting tools.* Metalwork. Prod. 108(24): pp. 75-77.

[20] Bogomolov, S. and Simson, E. (1981). *Optimal design of ultrasonic concentrators.* Acoustical Journal. **Vol.27** (4) (in Russian)

[21] Brehl, D.E. and Dow, T.A. (2008). *Review of vibration-assisted machining.* Precision Engineering, **Vol.32** Issure 3: pp. 153-172.

[22] Bruce, T. (1984). 'Energy Methods'. *Advanced Dynamics for Engineers.* HRW Series in Mechanical Engineering. United States of America: CBS College Publishing. ISBN 0-03-063366-4.

[23] Chern, G.L. and Liang, J.M. (2007). *Study on boring and drilling with vibration cutting.* International Journal of Machine Tools&Manufacture 47: pp. 133-140.

[24] Chew, E.K (1988). *Response of a rotating machine supported on nonlinear springs.*

[25] Clifton, D., Imal, Y. and Mc-Geough, J.A. (1993). *Some ultrasonic effects on machining materials encountered in the offshore industries*. In: Proceedings of the 30th International MATADOR Conference: pp. 119-123.

[26] Day, R.A. (1996). *PVDF and Array Transducers.* Lawrence Livermore National Laboratory.

[27] Devine, J. (1985). *Ultrasonically assisted metal removal.* Source Book: American Society for Metals, Fabrication of Composite Materials.

[28] Farago, F.T. (1980). *Abrasive Methods Engineering.* Industrial Press.**Vol.2:** pp. 480-481.

[29] Farrer, J.O. (1948). *USM.* English Patent No. 602801

[30] Fuller, C.R., Elliott, S.J. and Nelson, P.A. (1996). *Active Control of Vibration.* Academic Press INC, ISBN:0-12-269440-6.

[31] Gary, F.B. (1987). *Book on Non-Traditional Manufacturing Processes.* Marcel Dekker, nc, New York: pp. 67-86 Chap 6.

[32] Ghahramani, B. and Wang, Z.Y. (2001). *Precision ultrasonic machining process: a case study of stress analysis of ceramic (Al_2O_3).* International Journal of Machine Tools & Manufacture.**Vol.41**: pp. 1189-1208.

[33] Gilmore, R. (1990). *Ultrasonic machining of ceramics.* SME Paper.MS90-346 (12).

[34] Harlow, J.H. (2004). *Electric power transformer engineering.* CRC Press: pp.2-216. ISBN 9780849317040.

[35] Kennedy, D.C. and Grieve, R.J. (1975). *Ultrasonic machining – a review.* Prod. Eng. 54(9): pp. 481-486.

[36] Kikuchi, Y. (1969). *Ultrasonic transducers.* Corona.

[37] Kremer, D. (1991). *New developments on ultrasonic machining.* SME Technical Paper MR91-522: pp. 13.

[38] Kumabe, J. (1979). *Vibratory Cutting.* Jikkoyo Publisher, Tokyo(in Japanese).

[39] Kuo, K.L. (2009). *Ultrasonic vibrating system design and tool analysis.* Transactions of Nonferrous metals Society of China. s225-s231.

[40] Lacalle, L.D. and Norberto, L. (2008). *Ultrasonic assisted machining.* SciTopics.

[41] Li, Z.C., Jiao, Y., Deines, T.W., Pei, Z.J. and Treadwell, C. (2005). *Rotary ultrasonic machining of ceramic matrix composites: feasibility study and designed experiments.* International Journal of machine Tools & Manufacture. **Vol.45:** pp. 1402-1411.

[42] Liang, Z.Q., Wu, Y.B., Wang, X.B. and Zhao, W.X. (2010). *A new two-dimensional ultrasonic assisted grinding (2D-UAG) method and its fundamental performance in*

monocrystal silicon machining. International Journal of Machine Tools&Manufacture 50: pp. 728-736.

[43] Madan, V.P., submitted by Dolph, C.L. (1969). *On Longitudinal Vibrations of a Semi-Infinite Voigt-Kelvin Rod with Non-Uniform Viscoelastic Properties.*Journal of Mathematical Analysis and Applications 28, 88-92.

[44] Module 9, Non-conventional machining. Lesson 36 Ultrasonic Machining (USM). Version 2 ME, IIT Kharagpur.

[45] Neppiras, E.A. (1956). *Report on ultrasonic machining.* Metalworking Prod. **Vol.100** : pp. 1283-1288,1333-1336,1377-1382,1420-1424,1464-1468,1554-1560,1599-1604.

[46] Neppiras, E.A. (1964). *Ultrasonic Machining and Forming.* Ultrasonics for industry.

[47] Neugebauer, R. and Stoll, A. (2004). *Ultrasonic application in drilling.* Journal of Materials Processing Technology 149.

[48] Newcomb, C.V and Flinn, I. (1982). *Improving the Linearity of Piezo-electric Ceramic Actuators.* Electronic Letters 18. No. 11: pp. 442-444.

[49] Nishimura, G. (1954). *Ultrasonic machining – Part I.* J.Fac. Engg. Tokyo University.**Vol.2 (**n.3): pp. 65-100.

[50] Pei, Z.J. and Ferreira, P.M. (1997). *Modelling of ductile-mode material removal in rotary ultrasonic machining.* International Journal of Machine Tools & Manufacture.**Vol.38:** pp. 1399-1418.

[51] Pei, Z.J., Ferreira, P.M., Kapoor, S.G. and Haselkorn, M. (1994). *Rotary Ultrasonic Machining for Face Milling of Ceramics.* International Journal of Machine Tools & Manufacture.**Vol.35.No.7:** pp. 1033-1046.

[52] Perkins, J. (1972). *An outline of power ultrasonics.* Technical Report by Kerry Ultrasonics: pp. 7.

[53] PIEZOELECTRICITY. By Brush Clevite Europe's leading manufacturers of Piezoelectric Ceramics. BRUSH CLEVITE, THORNHILL SOUTHAMPTON.

[54] Rong, H.W, Wang, X.D, Xu, W and Fang, T (2010). *Resonant response of a non-linear vibro-impact system to combined deterministic harmonic and random excitations.* International Journal of Non-Linear Mechanics.

[55] Rozenberg, L.D. and Kazantsev, V.F. et al (1964). *Ultrasonic cutting.* Consultant Bureau, New York.

[56] Samir, L. and Nermina, Z.U..*Recognition of Vibration Mode Shapes Using 3D Computer Visualisation.*

[57] Scab, K.H.W. (1990). *Parametric studies of ultrasonic machining.* SME Tech. Paper MR90-294: PP. 11.

[58] Seah, K.H.W., Wong, Y.S. and Lee, L.C. (1993). *Design of tool holders for ultrasonic machining using FEM.* Journal of Materials Processing Technology.**Vol.37**: pp. 801-816.

[59] Shaw, M.C. (1956). *Ultrasonic grinding.* Microtechnic 10(6): pp. 257-265.

[60] Sokolov, I.J. and Babitsky, V.I. (2001). *'Phase control of self-sustained vibration.'* Journal of Sound and Vibration **Vol.248** (n.4): pp. 725-744.

[61] Sokolov, I.J., Babitsky, V.I. and Halliwell, N.A. (2007). *Autoresonant vibro-impact system with electromagnetic excitation.* Journal of Sound and Vibration 308: pp. 375-391.

[62] Soundararajan, V. and Radhakrishnan, V. (1986). *An experimental investigation on the basic mechanisms involved in ultrasonic machining.* Int. J. MTDR. **Vol.16**(5): pp. 307-321.

[63] Thoe, T.B., Aspinwall, D.K. and Wise, M.L.H. (1998). *Review on ultrasonic machining.* Int. J. Mach. Tools Manufacturing.**Vol.38**(n.4): pp. 239-255.

[64] Thomas, P.N.H. (2008). *Modelling of an Ultrasonically Assisted Drill Bit.* Journal of Sound and Vibration.

[65] Thomas, P.N.H. and Babitsky, V.I. (2007). *Experiments and simulations on ultrasonically assisted drilling.* Journal of Sound and Vibration 208: pp. 815-830.

[66] Tooley, M.H. (2006). *Electronic circuits: fundamentals and applications.* Newnes: pp. 77-78. ISBN 9780750669238.

[67] Voronina, S., Babitsky, V.I. and Meadows, A. (2007). *Modelling of autoresonant control of ultrasonic transducer for machining applications.* Proc. IMechE **Vol.222** Part C: J. Mechanical Engineering Science.

[68] Voronina, S., Biabitsky, V.I and Meadows, A. (2008). *Modelling of Autoresonant Control of an Ultrasonic Transducer for Machining Applications.* Journal of Mechanical Engineering Science. **Vol. 222**(n.10): pp. 1957-1974.

[69] Weller, E.J. (1984). *Non-traditional machining processes(2nd edn.).* Soc of Manuf. Engineers: pp. 15-171.

[70] Wang, L.P., Wang, L.J., He, Y.H. and Yang, Z.J (1998). *Prediction and computer simulation of dynamic thrust and torque in vibration drilling.*

[71] Amplifier modules. http://www.bkelec.com/Modules/Amplifiers.htm

[72] ANALOG DEVICES. Integrated Circuit True RMS-to-DC Converter AD536A. http://pdf1.alldatasheet.com/datasheet-pdf/view/48036/AD/AD536A.html

[73] ANALOG DEVICES. UltralowOffset Voltage Operational Amplifier OP07. http://pdf1.alldatasheet.com/datasheet-pdf/view/225183/AD/OP07.html

[74] Burr-Brown Products from Texas Instruments. High Gain Adjust Range, Wideband, Voltage-Controlled Amplifier VCA810. http://pdf1.alldatasheet.com/datasheet-pdf/view/86944/BURR-BROWN/VCA810.html

[75] Faraday's law of induction. http://en.wikipedia.org/wiki/Faraday%27s_law_of_induction#Faraday.27s_law

[76] Filter Circuits.LABORATORY ELECTRONICS II. http://www.niu.edu/~mfortner/labelec/lect/p575_07a.pdf

[77] Inductance. http://en.wikipedia.org/wiki/Inductance

[78] Lissajous curve. http://en.wikipedia.org/wiki/Lissajous_curve

[79] LM148,LM248,LM348 QUADRUPLE OPERATIONAL AMPLIFIERS. Texas Instruments. http://www.ti.com/lit/ds/symlink/lm348.pdf

[80] Low Cost Analog Multiplier AD633. ANALOG DEVICES. http://pdf1.alldatasheet.com/datasheet-pdf/view/48102/AD/AD633AN.html

[81] Permeability. http://en.wikipedia.org/wiki/Permeability_(electromagnetism)

[82] Permeability. http://en.wikipedia.org/wiki/Permeability_(electromagnetism)

[83] PIEZOELECTRIC CERAMICS. MorganElectroCeramics. ELECTRO CERAMICS SOLUTIONS. http://www.morganelectroceramics.com/resources/literature/

[84] Talysurf CLI 2000. http://taylor-hobson.virtualsite.co.uk/talysurf2000.htm

[85] UA741 GENERAOL PURPOSE SINGLE OPERATIONAL AMPLIFIER. ST. http://www.datasheetcatalog.org/datasheet/stmicroelectronics/5304.pdf

Appendix I Optimization of a Universal Matchbox

As described in Chapter Seven that a matchbox is an important equipment used to step up a voltage from a universal amplifier to a higher value in order to excite an ultrasonic transducer, this research is dedicated to a thorough investigation of the gap distance between 2 ferrite cores effect on the mechanical vibration, inductance, resonant frequency, phase difference between the supplied voltage and the current and the average active power of an ultrasonic vibrating system together with the gap optimization of the universal matchbox (transformer). First of all, the basic working principle of a transformer will be explained. After that, experimental measurements together with elaborate analyses will be presented.

I.1 Universal Matchbox Structure and Working Principle

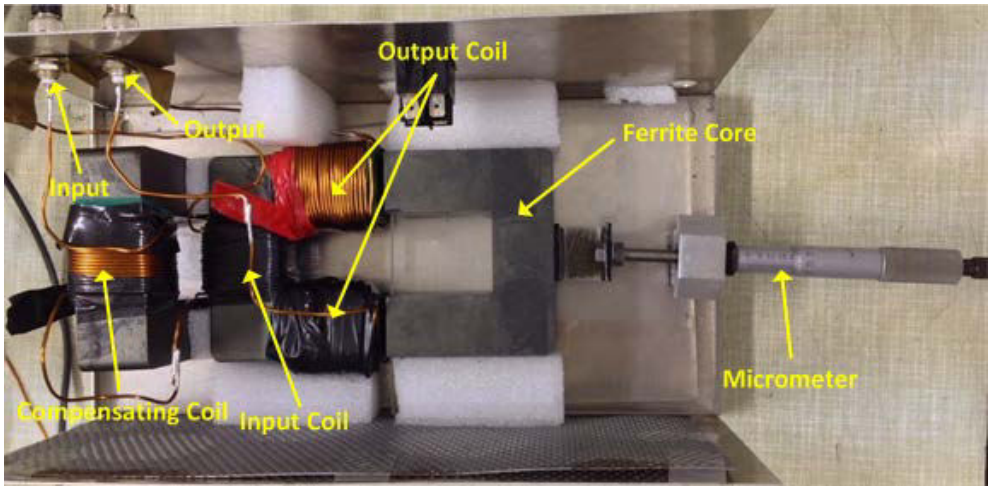

Figure I.1 : Internal structure of a universal matchbox and experimental setup

The internal structure of the universal matchbox is shown in Figure I.1. As can be seen, the input signal is connected to an independent compensating coil with an inductance $100\mu H$ wound on a vertical ferrite core in order to shunt the ultrasonic transducer's capacitance. After this, the signal is applied to a transformer consisting of an input coil set and an output coil set wound around a flat ferrite core. Another ferrite core which is placed on the right hand side of the picture is attached with a Micrometre and appropriately aligned parallel with the wall of the universal matchbox (transformer) in order to make sure the movement is purely horizontal during the increase of the gap. In order to understand the detailed connection of the compensating coil with the input coil set and output coil set, Figure I.2 has been illustrated.

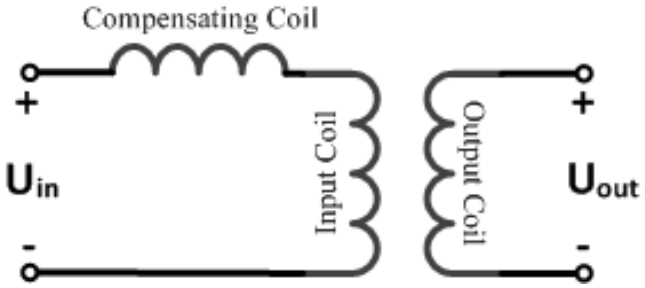

Figure I.2 : Detailed connection of the universal matchbox

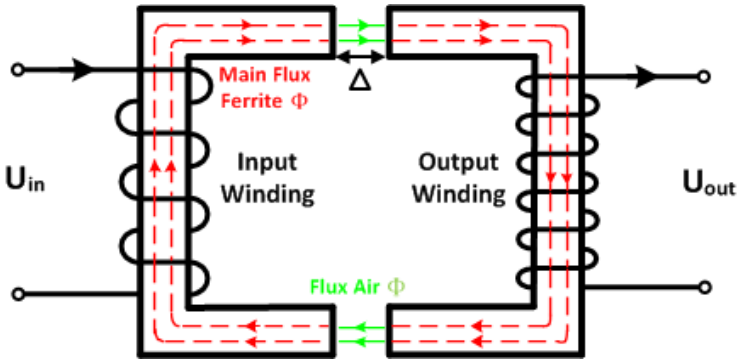

Figure I.3 : Ideal transformer and induction law

Figure I.3 illustrates an ideal transformer and the induction law together with the introduction of an air gap in the cores. The input AC voltage is U_{in}, the output AC voltage is U_{out}, the input winding has N_{in} turns, the output winding has N_{out} turns, an air gap distance between 2 ferrite core is Δ, the magnetic flux through the cores is denoted as Φ, L means the inductance, I is the current. A varying current produced by the input AC voltage U_{in} creates a varying magnetic flux in the ferrite core and thus a varying magnetic flux through the output winding is produced. This varying magnetic flux induces a varying voltage U_{out} in the output core. Due to the fixed ratio between the input and the output windings, the input and the output voltages are in proportion. According to the Faraday's law of induction [75] and the definition of inductance [77]:

$$U = -N\frac{d\Phi}{dt} = -L\frac{dI}{dt} \tag{I.1}$$

Re-arranging equation (I.1) gives:

$$L = N\frac{d\Phi}{dI} \tag{I.2}$$

Figure I.4 presents 2 idealized B-H loops for a ferrite core with and without an air gap. The steep slope is for a core without an air gap which means a high permeability. The more gradual slope loop represents the same core with a small gap which refers to a low permeability. Vertical scale means the flux density B and horizontal scale represents the magnetizing force H. The relation between the magnetic flux density B and the magnetizing force H can be described with the help of the material permeability [81]:

$$B = \mu H \tag{I.3}$$

Where the permeability of the ferrite material can be up to $8 \times 10^{-4} H/m$ and the permeability of the air is $1.26 \times 10^{-6} H/m$. Therefore, it is expected that the electrical characteristics of the universal matchbox (transformer) will be affected significantly by introducing a small air gap as the permeability of the ferrite and the permeability of the air vary nearly several hundred times.

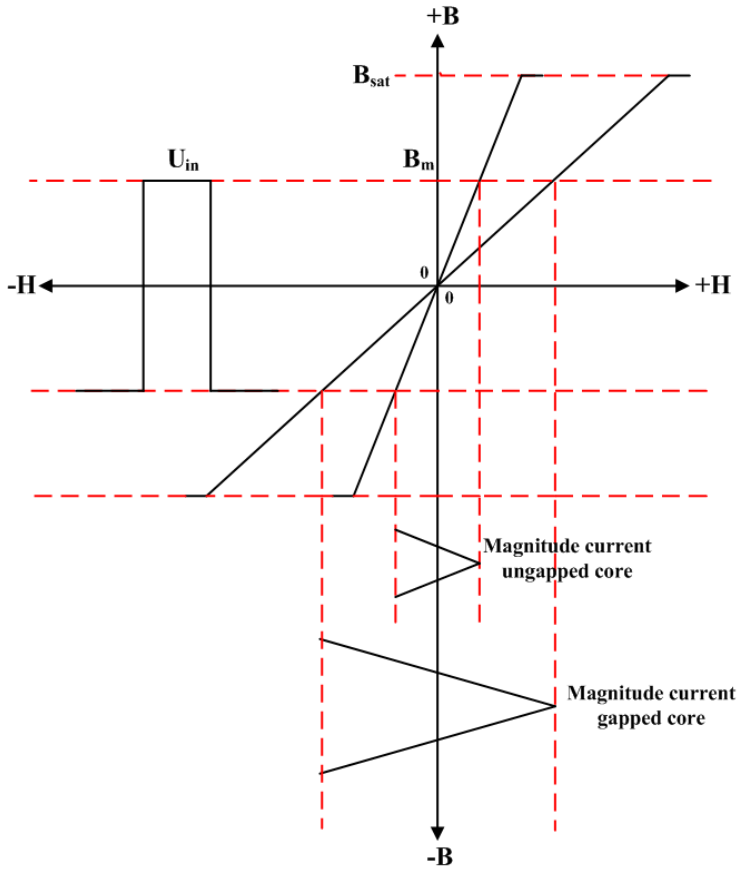

Figure I.4 : Two idealized B-H loops for a ferrite core with and without an air gap

As can be seen in Figure I.4, the flux density B is proportional to a time invariant square input voltage U_{in}. The peak value B_m is projected right so as to intersect with the non-gapped and gapped B-H loops and the margin between the peak working point B_m and the saturation B_{sat} remains the same with or without an air gap. The magnetizing force H is proportional to the induced current. The increase in the magnetizing current between the non-gapped and the gapped cores is clearly shown in the projection. Therefore, if the input voltage to the transformer is fixed, which results in an invariance of flux density B, an increase in the magnetizing current I in the core will give rise to a decrease in the core inductance L according to equation (I.2). This change in inductance during the increase in the air gap Δ will inevitably affect the performance of the universal matchbox (transformer) and further influence the whole ultrasonic vibrating system. In order to explore the effect, experimental measurements are presented.

I.2 Experimental Measurements

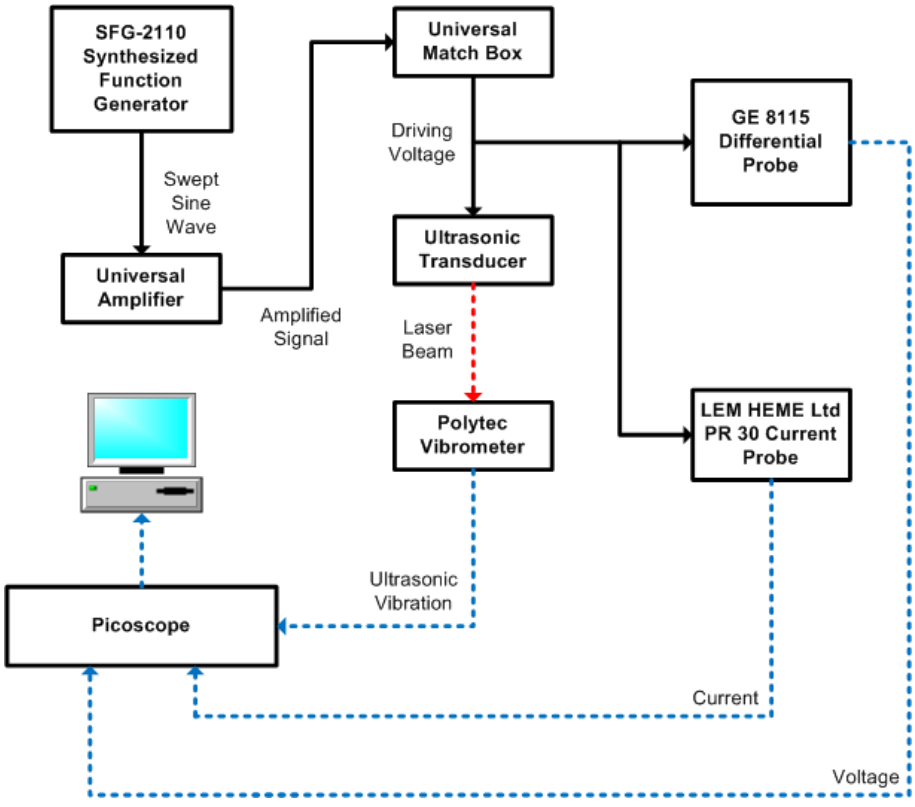

Figure I.5 : Schematic diagram of an ultrasonic vibrating system for the investigation of the universal matchbox

The schematic diagram of the ultrasonic vibrating system to investigate the universal matchbox (transformer) effect is illustrated in Figure I.5. A model number SFG-2110 synthesized function generator generates a swept sine wave with fixed amplitude (the frequency generator does not run at its maximal power) to a universal amplifier. It should be mentioned that due to the age of the 200W MOSFET amplifier module MF200, a more powerful 450W MOSFET amplifier module MF450 [71] has been purchased as a replacement. It has been experimentally explored that the linear working voltage interval of the MF450 amplifier module is $\pm 180V$ where the MF200 is only able to handle a voltage level within $\pm 70V$. The output of the amplifier module is applied to the universal matchbox (transformer) which is shown in Figure I.1. After that, a high voltage signal is developed to drive the ultrasonic transducer. The transducer with a 6mm drill bit attached used to act as a dynamic loading which has 4-piezoceramic rings and its structure is shown in Figure 7.30. The procedure of the investigation on the universal matchbox (transformer) is to move one ferrite core gradually and precisely away from the other one wound around with the input and the output coils, and then adjust the excitation frequency of the ultrasonic vibrating system for each gap in order to bring the ultrasonic vibrating system to a new resonant regime. Simultaneously, the mechanical characteristics and electrical characteristics are measured and recorded. It has been experimentally determined that the change in the air gap is $\Delta \in \{0mm \sim 10mm\}$ with an increment of $0.5mm$ with the help of a Micrometer shown.

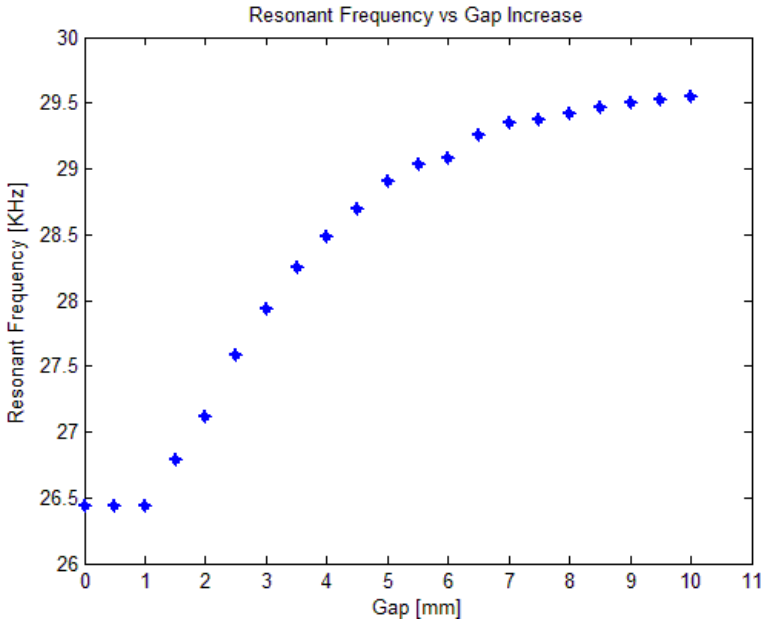

Figure I.6 : Resonant frequency change during increase the air gap

Figure I.6 illustrtes the change in the resonant frequencies as the increase in the air gap Δ. As can be seen, the resonant frequency has increased from $26.5KHz$ to $29.5KHz$ and gradually saturates. The slope of the change in the resonant frequency as the air gap Δ increases shows the steepest when the gap distance $\Delta = 2.5mm$. When the gap is increased furthermore, the resonant frequency seems to increase less drastically. Generally speaking, the change in the resonant frequencies is a result of the appropriate adjustment of the entire ultrasonic vibrating system as the ultrasonic transducer is an active dynamic loading.

Figure I.7 shows the change in the matchbox inductance as the increase in the air gap Δ. As can be seen that the inductance is nearly $50mH$ when zero gap. However, it drops immediately to less than $5mH$ when a small gap is developed. The inductance value L seems to react sensitively to the change in air gap Δ which is consistent with analysis in section I.1. Due to the essential differences in the permeability of the ferrite and the air, even if a tiny gap is introduced, the effective inductance L will be affected drastically. Moreover, when the gap reaches up to $2.5mm$, the inductance L seems to saturate which implies the air gap permeability dominates where the permeability of the ferrite becomes less important.

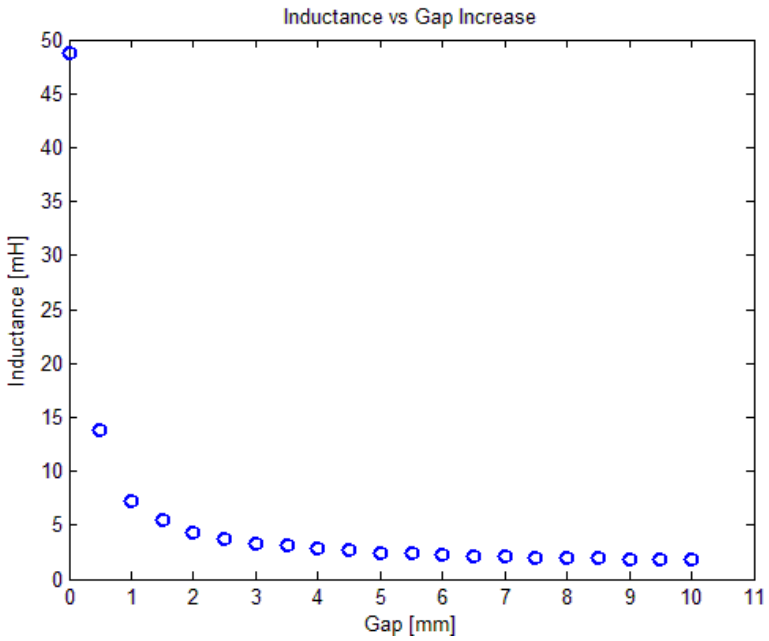

Figure I.7 : Matchbox inductance change during increase the air gap

Figure I.8 shows the change in mechanical vibration level at end of the ultrasonic transducer measured by a laser vibrometer as the air gap Δ increases. As can be seen, interestingly, the

ultrasonic vibration is extremely low when zero gap and it increases aggresively to the maximal over $7\mu m$ zero to peak when an air gap $\Delta = 2.5mm$ is developed. After that, the ultrasonic vibration level drops down and stabilizes to less than $5\mu m$. The remarkable increase in the ultrasonic vibraiton level from zero gap to $2.5mm$ gap seems to be inversely proportional to the drop in the matchbox inductance shown in Figure I.7.

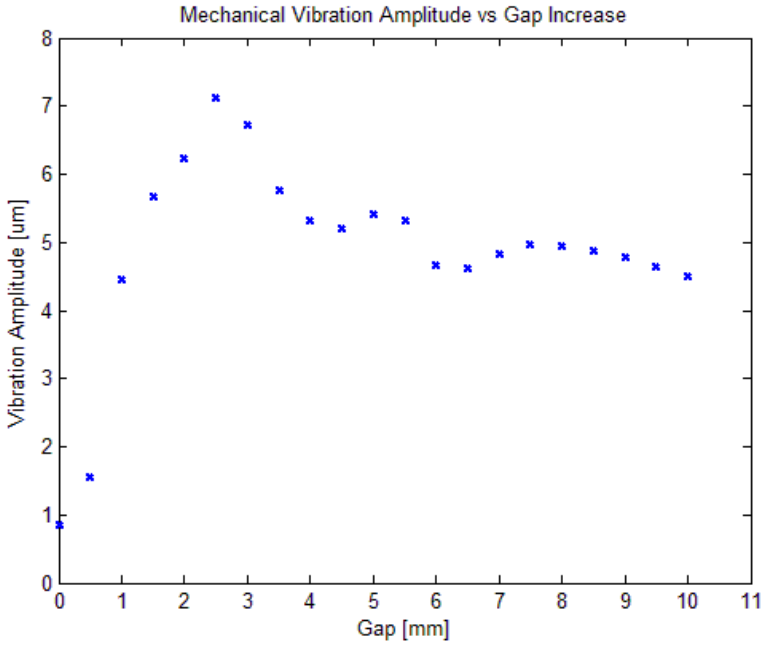

Figure I.8 : Ultrasonic vibration at end of transducer during increase the air gap

In order to better understand the effect of the increased gap between 2 ferrite cores on the ultrasonic vibrating system, the output voltage (actual driving voltage of the piezoeelctric transducer) of the matchbox and the current have been recorded for each air gap Δ. In Figure I.9, the Lissajous curves [78] with horizontal scale the current and vertical scale the voltage have been drawn for each air gap Δ. As can be seen, the circles are enlarging drastically as the air gap Δ increases from zero to $2.5mm$ which indicates an increase in both the voltage and the current. This is consistent with the observation in the increase in ultrasonic vibration amplitude in Figure I.8. Amazingly, at air gap $\Delta = 2.5mm$, the voltage generated by the universal matchbox has a nearly $3000V$ peak-to-peak value even if the ultrasonic vibrating system is not full powered by the synthesized function generator. The current level also climbs to a nearly $5A$ peak-to-peak. This powerful signal will definitely develop a dominant ultrasonic vibration at the end of the ultrasonic transducer which is proved in Figure I.8. However, the voltage drops when an air gap $\Delta > 2.5mm$ and eventually arrives at $1000V$

peak-to-peak with a $3A$ current peak-to-peak. This gradual decrease in both current and voltage with a more visible gap is also consistent with ultrasonic vibration drop in Figure I.8.

Another function of the Lissajous curves is to observe the phase difference between 2 signals. As can be seen in Figure I.9 that all the curves for each gap are rotating anti-clockwise, and the curves have positive slopes. These voltage and current Lissajous curves resemble the curves shown a phase shift $\delta \in \{-45° \sim -90°\}$ shown in Figure I.10, where the voltage (vertical scale) lags the current (horizontal scale). This indicates that the dynamic loading (ultrasonic transducer) acts as a purely capacitor at resonance where the voltage lags current by 90° for an idea capacitor..

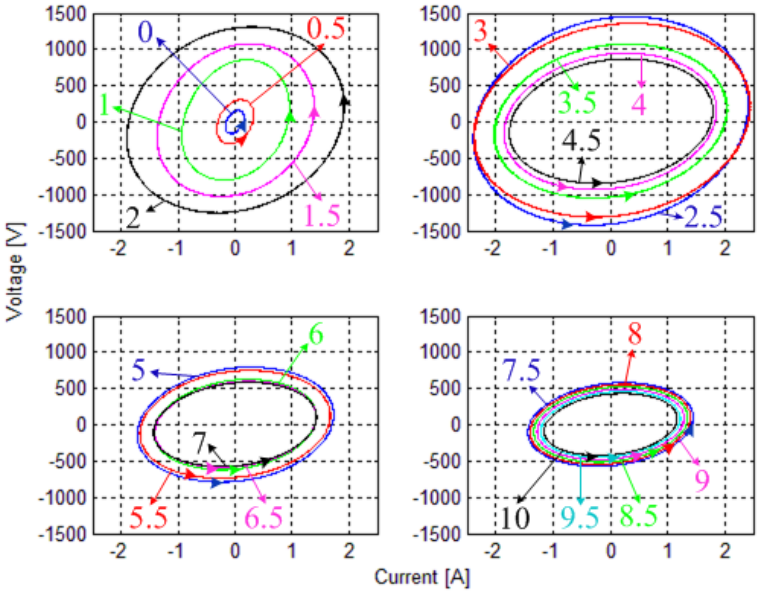

Figure I.9 : Lissajous curves of ultrasonic transducer driving voltage and current for each air gap of ferrite cores in matchbox

However, it is difficult to calculate the exact phase different between the current and the voltage for each gap Δ by observing the Lissajous curves shown in Figure I.9. Therefore, the phase shift for each air gap Δ has been precisely calculated by capturing the current signal and the voltage signal in time domain. Results are shown in Figure I.11. As can be seen, the voltage lags the current by only less than 0.38π when zero gap. However, when the air gap distance Δ gradually increases to 2mm, the phase shift turns to over 0.46π which is very close to 0.5π which indicates the dynamic loading is dominant and acts nearly as a pure capacitor at resonance. If the air gap distance is further increased, the phase shift has a slight decrease but slowly stabilises to 0.45π. This phase shift trend seems to be inversely proportional to the change in effective inductance L of the unviersal matchbox in Figure I.7.

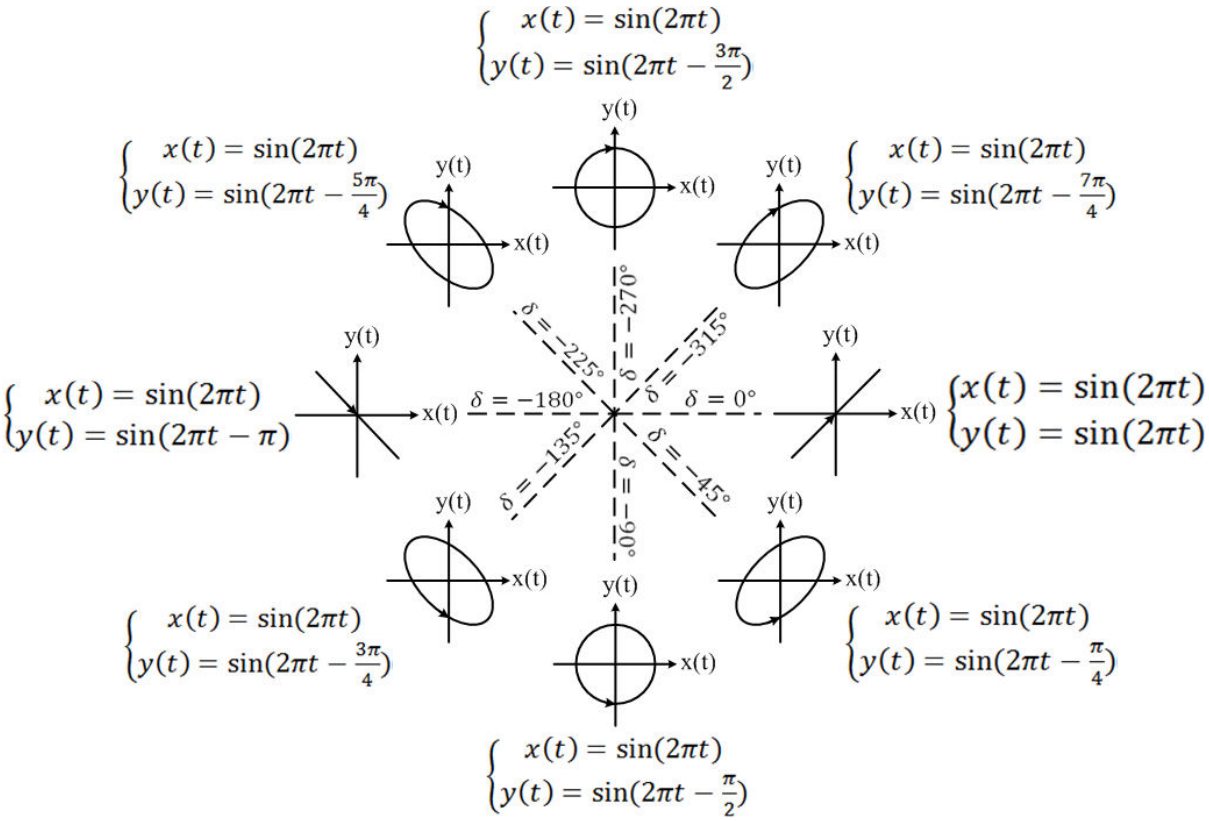

Figure I.10 : LTI Lissajous figures with the same frequency, eccentricity and direction of rotation determined by phase shift

Reproduced and Revised from [78]

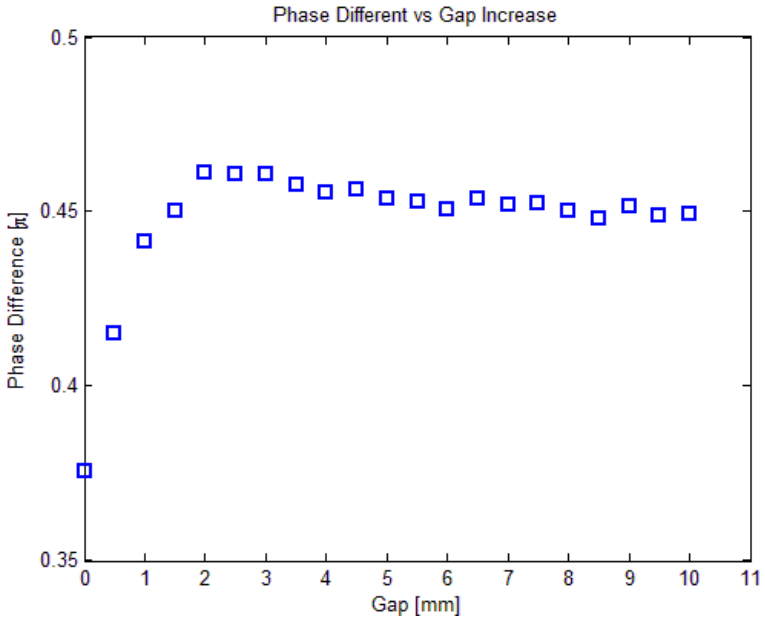

Figure I.11 : Phase shift between voltage and current during increase the air gap

The average (active) power developed by the universal matchbox has been calcualted for each air gap Δ according to equation (I.4). Results of the average (active) power are shown in Figure I.12. As can be seen that at air gap $\Delta = 2.5mm$ the average power (active power) develops to nearly $1.6KW$ where the power increase from zero gap to $2.5mm$ gap is remarkable. If the gap is further increased, the average delivered power (active power) drops quickly and stabilizes to $200W$. It has been confirmed that higher power is able to develops larger vibration magnitudes and the piezoceramics can sustain $1500V$ zero-to-peak or even higher voltages on the 4-piezoceramic rings powerful ultrasonic transducer.

$$P = \frac{1}{2} UIcos(\varphi) \tag{I.4}$$

Where U and I are the voltage and the current magnitudes respectively. φ is the phase difference between the current and the voltage.

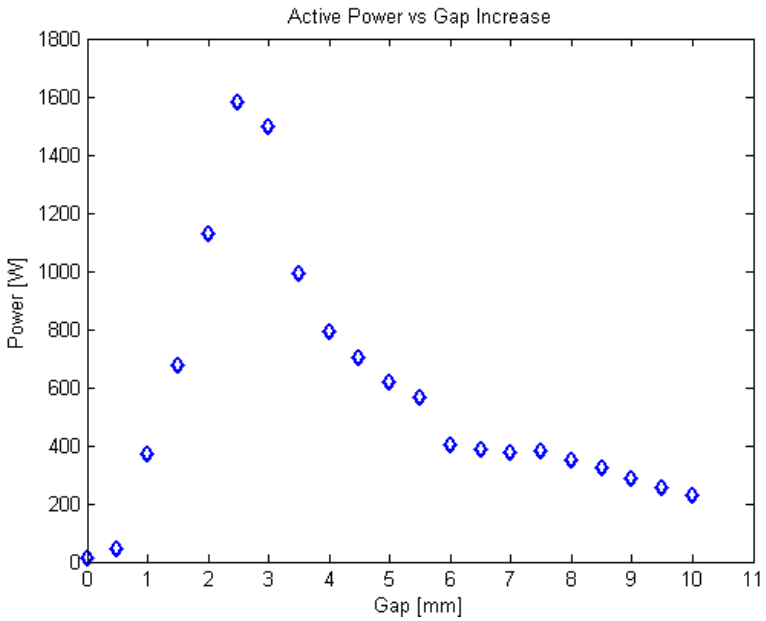

Figure I.12 : Average power (active power) developed in the universal matchbox during increase the air gap

I.3 Summary

In order to explore the whole process deeply, Figure I.13 is illustrated which describes the connection between the universal matchbox and the ultrasonic transducer. As can be seen, L represents the series inductance, i.e. the effective inductance of the universal matchbox values which are shown in Figure I.7 for each air gap distance Δ. C is the static capacitance of

the ultrasonic transducer shown in Figure 7.30 and the value has been measured by an 'Atlas LCR' meter as $15.17nF$. The static capacitor is connected parallel with an impedance of the resonant mechanical system, i.e. the ultrasonic transducer impedance during resonance because the electrical impedance of a piezoelectric device is more complicated in reality than a simple capacitor. During resonance, the impedance of the ultrasonic transducer may become a resistance of relatively low value and it is shunted by a static capacitor [53]. The static capacitance is undesirable because it acts as a load on the active part of the ultrasonic transducer and reduces the electrical output. In a better interpretation, this static capacitor limits the supplied power from the amplifier to the ultrasonic transducer since the voltage is lagging current 0.5π across the capacitance. Therefore, the static capacitance C is 'neutralized' by employing a shunt or series inductor L chosen to resonate with the static capacitance at the operating frequency [53].

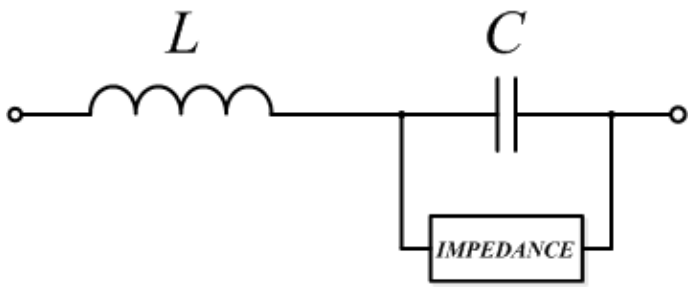

Figure I.13 : Resonant piezoelectric device with static capacitance 'neutralized' by an inductor [53]

The compensating coil with value $100\mu H$ shown in Figure I.1 was originally and specially designed to act as the shunting inductor L. Ideally, for different ultrasonic transducer applications, this compensating coil should be optimized until the LC circuit delivers the maximal power to the resonant mechanical device. In other words, the LC circuit is designed to minimize the phase difference between the voltage and the current. One of the options to execute the optimization is to change the air gap distance Δ in order to adjust the effective inductance of the universal matchbox L which has been shown. Another possible solution is to change the effective inductance of the universal matchbox L electrically through a connection with an external DC voltage power supply. By controlling the input current to the compensating coil is able to realize the change in the effective inductance thus achieve the optimization.

In conclusion, for the application of a 6mm drill bit on a 4-piezorings powerful ultrasonic transducer, an air gap $\Delta = 2.5mm$ develops the largest vibration amplitude $7.13\mu m$ zero-to-peak at a resonant frequency $27.59KHz$. The effective inductance of the matchbox is $L = 3.696mH$. With this optimal inductance value, the voltage lags the current by $82°$ which indicates the ultrasonic transducer is almost working as a pure and dominating capacitor at resonance. Amazingly, the developed voltage has a $1453V$ zero-to-peak value and the developed current has a $2.43A$ zero-to-peak value. Such current and voltage signals generate an overall $1.58KW$ for the ultrasonic transducer even if the synthesized function generator is not operated at its maximal power. During autoresonant control, phase will be slightly tuned together with the air gap until the maximum ultrasonic vibration amplitude is achieved. However, phase will not change as considerably as frequency since the phase-amplitude characteristic is more gently sloping and always linear compared with frequency-amplitude characteristic. Once the phase and the optimal gap has been developed, they will be fixed for the machining process as a drill bit penetrates into the work piece at a slow rotation and a low feed rate.

Appendix II

- ## Derivation of equation (4.17):

Taking the expression of 2nd step concentrator displacement shown in equation (4.15) into account and applying the boundary condition of the 2nd step concentrator shown in equation (4.16) gives:

$$B_1 k\cos(kx) - B_2 k\sin(kx)|_{x=L} = 0 \tag{II.1}$$

Therefore, the relationship between B_1 and B_2 can be obtained:

$$B_2 = B_1 \frac{\cos(kL)}{\sin(kL)} \tag{II.2}$$

Replacing the expression of B_2 into the expression of 2nd step concentrator displacement $D_2(x)$ in equation (4.15) produces:

$$D_2(x) = B_1 sin(kx) + B_1 \frac{\cos(kL)}{\sin(kL)} \cos(kx) \tag{II.3}$$

$$D_2(x)\sin(kL) = B_1 sin(kx)\sin(kL) + B_1 \cos(kx)\cos(kL) \tag{II.4}$$

Consequently, the expression of displacement of the 2nd step concentrator can be obtained:

$$D_2(x) = B\cos[k(x - L)] \tag{II.5}$$

Where $B = \frac{B_1}{\sin(kL)}$. Equation (II.5) is same as equation (4.17).

- ## Derivation of Figure 4.3:

As can be seen in Figure II.1 (which is the copy of Figure 4.3), there are two expressions of the longitudinal wave equations for the 1st step and 2nd step concentrator respectively. The equations are shown in (4.18). Obviously, at the origin point when $x = 0$, we have:

$$Asin(kx)|_{x=0} = 0 \tag{II.6}$$

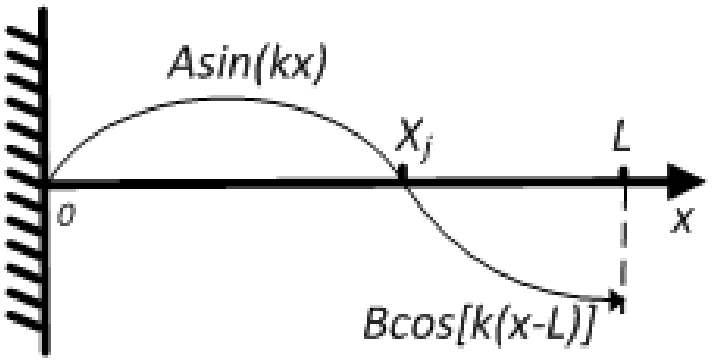

Figure II.1 : Possible vibration mode of the 2-step concentrator

In the middle of the 1st step concentrator, the absolute displacement of the 1st step is supposed to arrive at its maximal:

$$D_1\left(\frac{x_j}{2}\right) = Asin(k\frac{x_j}{2}) \tag{II.7}$$

Where A is the vibration amplitude, k is the wavenumber shown in equation (4.12). Taking the values of ρ, E, x_j shown in Table 4.1 and the resonant frequency f_2 in equation (4.25) into account, the displacement of D_1 in (II.7) can be calculated:

$$D_1\left(\frac{x_j}{2}\right) = Asin\left(\sqrt{\frac{2700\times(2\times\pi\times21300)^2}{0.7\times10^{11}}}\times 0.06\right) = Asin(90.36^{\circ}) \approx A \tag{II.8}$$

At the connection coordinate x_j between the 1st step and 2nd step concentrator, a nodal point is identified at the resonant frequency shown in equation (4.25) when the 1st step and 2nd step concentrator vibrate in anti-phase.

Therefore, at the connection coordinate x_j, the 1st step concentrator longitudinal vibration has an expression:

$$D_1(x_j) = Asin(kx_j) \tag{II.9}$$

Where A is the vibration amplitude, k is the wavenumber shown in equation (4.12). Taking the values of ρ, E, x_j shown in Table 4.1 and the resonant frequency f_2 in equation (4.25) into account, the displacement of D_1 in (II.9) can be calculated:

$$D_1(x_j) = Asin\left(\sqrt{\frac{2700\times(2\times\pi\times21300)^2}{0.7\times10^{11}}}\times 0.12\right) = Asin(180.716^{\circ}) \approx 0 \qquad \text{(II.10)}$$

Similarly, at the connection coordinate x_j, the 2nd step concentrator longitudinal vibration has an expression:

$$D_2(x_j) = Bcos[k(x_j - L)] \qquad \text{(II.11)}$$

Where B is the vibration amplitude, k is the wavenumber shown in equation (4.12). Taking the values of ρ, E, x_j shown in Table 4.1 and the resonant frequency f_2 in equation (4.25) into account, the displacement of D_2 in (II.11) can be calculated:

$$D_2(x_j) = Bcos\left(-\sqrt{\frac{2700\times(2\times\pi\times21300)^2}{0.7\times10^{11}}}\times 0.06\right) = Bcos(-90.36^{\circ}) \approx 0 \qquad \text{(II.12)}$$

As can be seen in Figure II.1, the calculated displacement of the 1st step concentrator and the 2nd step concentrator shown in equation (II.10) and (II.12) both equal 0 which confirms the physical nodal point at the connection coordinate x_j. At the end of the 2nd step concentrator, the longitudinal vibration is supposed to achieve its maximal value:

$$D_2(L) = Bcos[k(L - L)] = B \qquad \text{(II.13)}$$

Appendix III

Root-Mean-Square

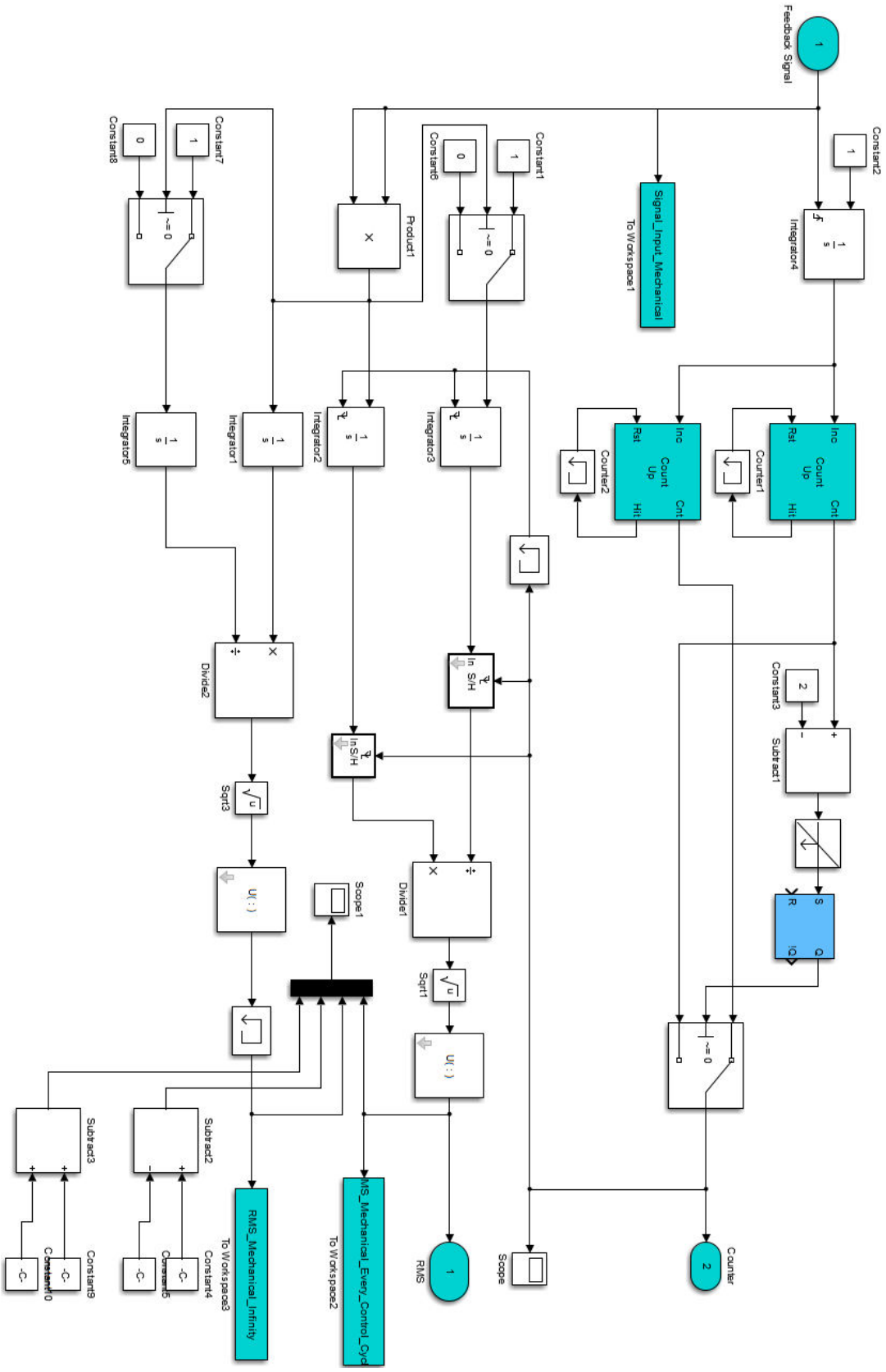

Phase Control

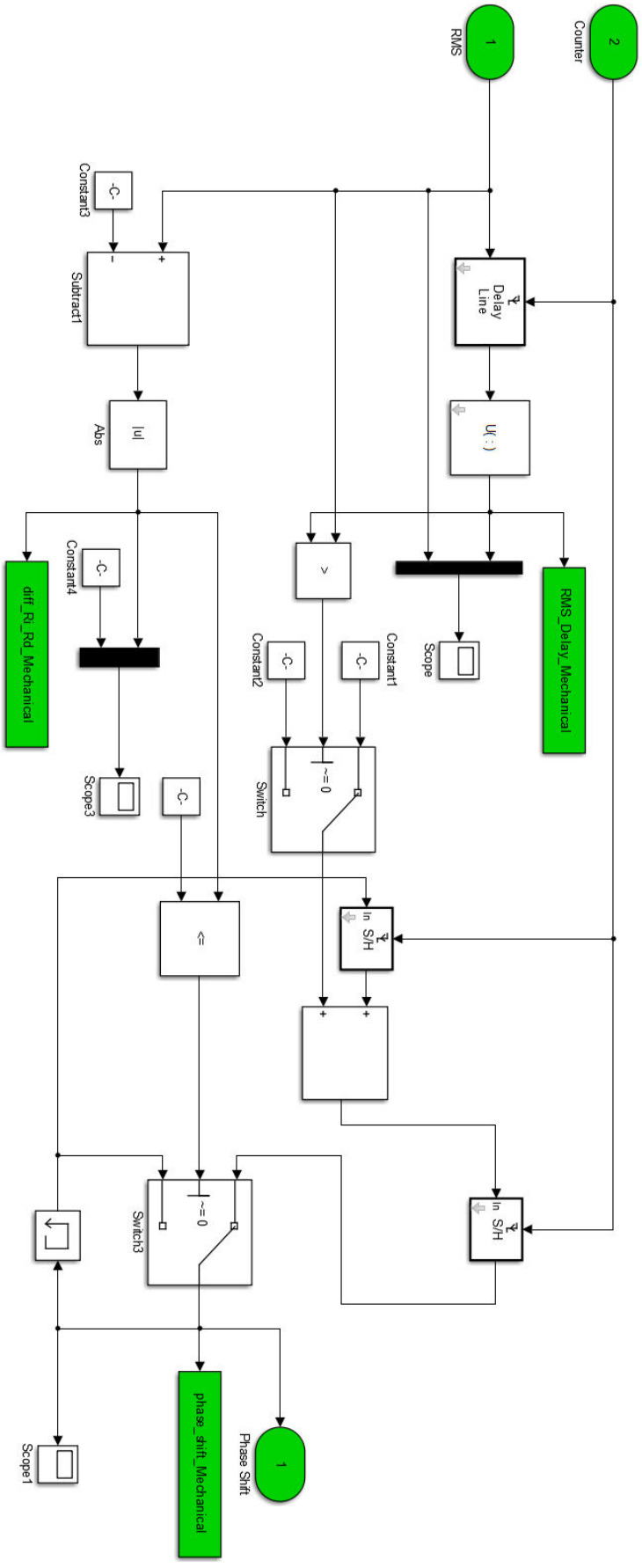

Amplitude Control

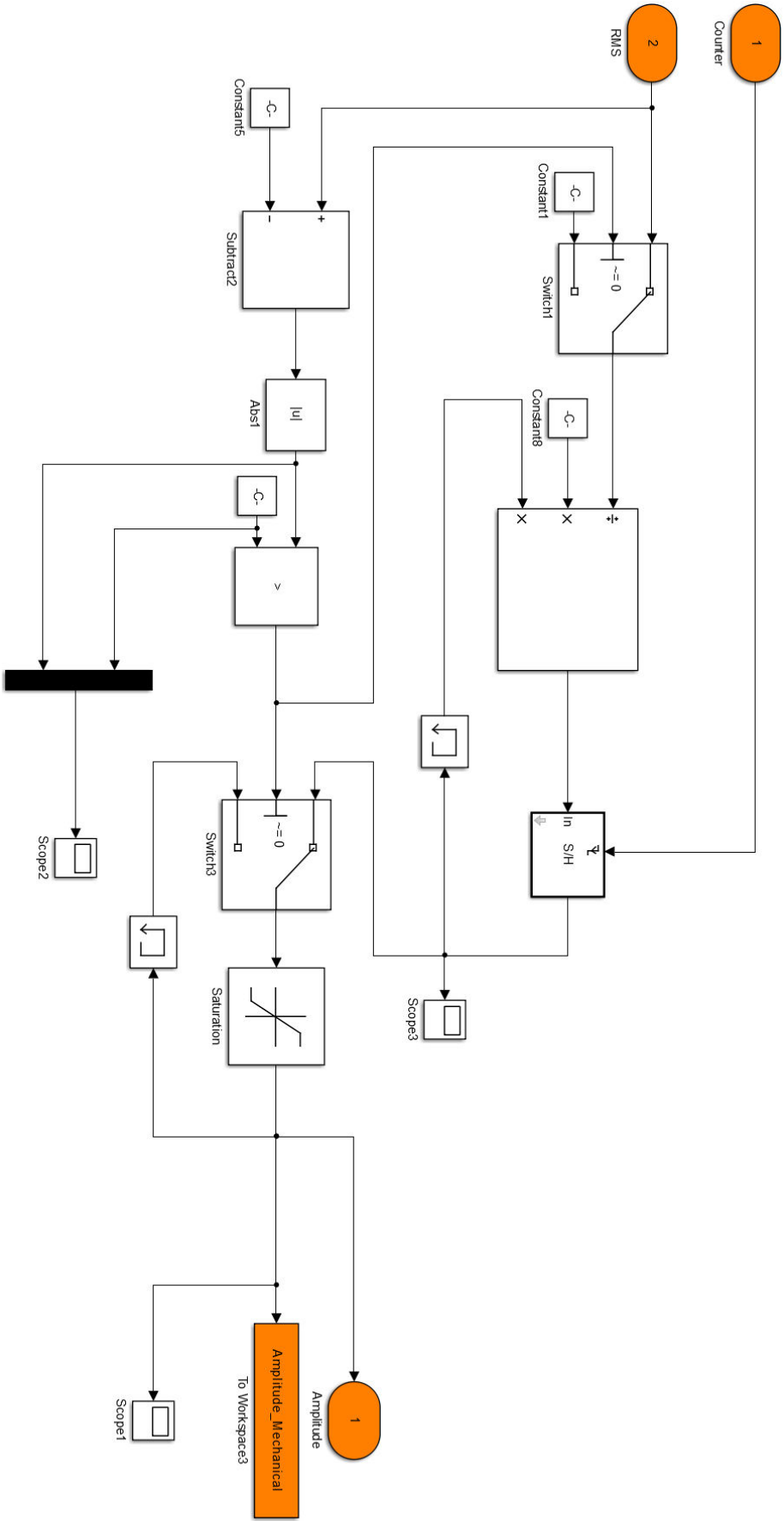

Mean Value

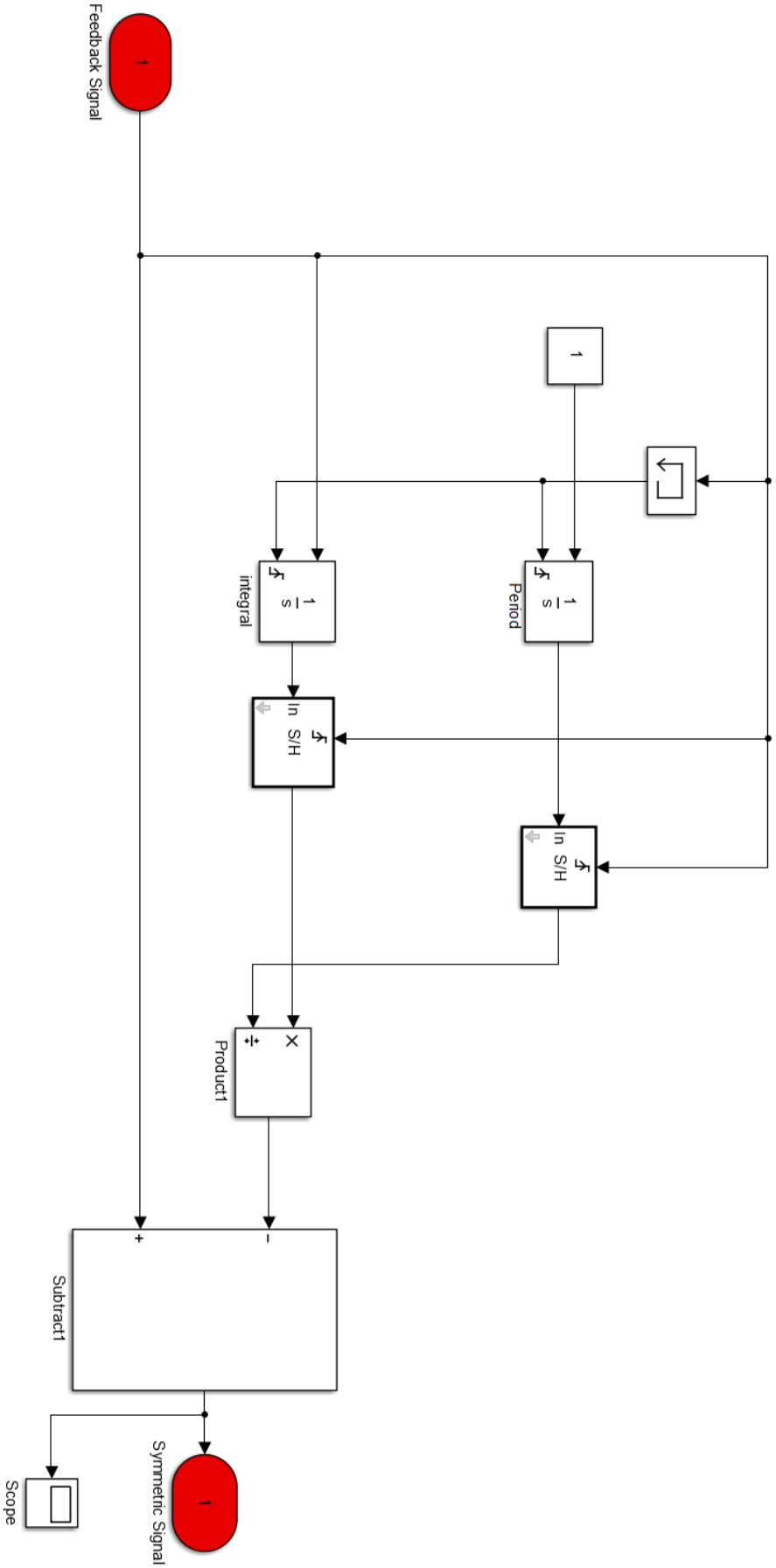
Feedback Signal
1
1
integral
Period
In S/H
In S/H
Product1
+
-
Subtract1
Scope
Symmetric Signal
1

Phase Shifter